Single particle tracking of G protein-coupled receptor – β-arrestin interactions

by

Jak Grimes

A thesis submitted to the University of Birmingham for the degree of

DOCTOR OF PHILOSOPHY

Institute of Metabolism & Systems Research

College of Medical & Dental Sciences

University of Birmingham

July 2022

UNIVERSITY OF
BIRMINGHAM

University of Birmingham Research Archive

e-theses repository

This unpublished thesis/dissertation is copyright of the author and/or third parties. The intellectual property rights of the author or third parties in respect of this work are as defined by The Copyright Designs and Patents Act 1988 or as modified by any successor legislation.

Any use made of information contained in this thesis/dissertation must be in accordance with that legislation and must be properly acknowledged. Further distribution or reproduction in any format is prohibited without the permission of the copyright holder.

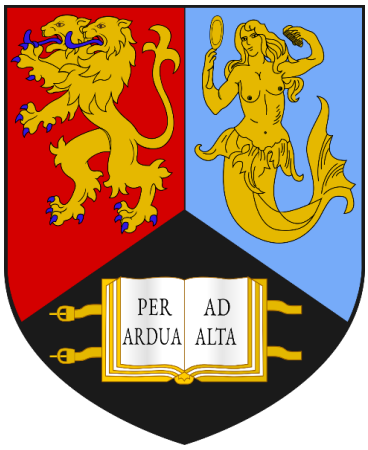
PER
ARDUA
AD
ALTA

ABSTRACT

Following activation by an agonist, G protein-coupled receptors (GPCRs) recruit β-arrestins, which mediate rapid signal desensitisation and receptor internalisation. β-arrestins can also activate non-classical signalling pathways, distinct from those triggered by G proteins. The mechanisms that govern receptor–β-arrestin interactions in the complexity of a living cell, however, remain poorly understood.

Classically, β-arrestins are thought to exist in the cytoplasm and form stable complexes with activated GPCRs at the plasma membrane, diffusing together with GPCRs to clathrin-coated pits (CCPs). Recent biophysical data has brought this model into disrepute, suggesting that transient interactions govern signalling, to meet the everchanging needs of the cell.

Here, a dynamic characterisation of GPCR–β-arrestin interactions is presented, at the plasma membrane of living cells with single-molecule resolution. β-adrenergic receptors were used as a prototypical GPCR family, given their crucial roles in cardiac physiology and pathologies dominated by aberrant β-arrestin signalling. βArr2 was shown to spontaneously bind to the plasma membrane, where it transiently interacts with β_2ARs via lateral diffusion. Following receptor interaction, the plasma membrane stabilises βArr2 in a membrane-bound, active-like conformation, allowing it to reach clathrin-coated pits (CCPs) without the activating receptor.

A major lipid-anchoring site in the C-edge of βArr2 and a novel role of the finger loop region were identified – independent of a bound receptor. These results shed new light on the complex sequence of events involved in β-arrestin interaction with GPCRs and its activation, revealing a critical role for β-arrestin interactions with the lipid bilayer.

Given the importance of β-adrenergic receptors in the development and treatment of chronic heart failure, single particle tracking methodologies were then used to generate assays which would enable the imaging of endogenous receptors and their signalling proteins in physiologically relevant cells, where they exert their effects. Fluorescent ligands were employed to image adult mouse cardiac myocytes, so that the diffusion and spatial localisation of GPCRs could be observed in a complex cell model. This pushes the capabilities of single-molecule microscopy techniques to their current limits, providing insights into endogenous plasma membrane receptors in live, beating heart cells.

LIST OF MANUSCRIPTS SUBMITTED DURING THIS THESIS

Grimes J*, Koszegi Z*, Lanoiselée Y*, Miljus T, O'Brien S, Stepniewski, T, Medel-Lacruz B, Baidya M, Shukla A, Selent J, Hill S, Calebiro D. Plasma membrane binding drives β-arrestin lateral diffusion and activation. *Under review in Cell*. (2022)

Benkel T, Zimmerman M ,Zeiner J , Bravo S , Merten N, Liu V ,Matthias E , Drube J, Monteleone M, **Grimes J** , Koszegi Z, Lanoiselée, Y , O'Brien, S , Inoue, A , Nikolaev, N , Calebiro D, Chevigné A , Schulz S, Hoffmann C, Kolb P , Waldhoer M , Simon K , Gomeza J, Kostenis E. How Carvedilol activates β2 adrenergic receptors. *In revisions at Nature Communications*. (2022)

Calebiro D, **Grimes J**, Tripp E, Mistry R. GPCR Signaling in Nanodomains: Lessons from Single-Molecule Microscopy. *GPCRs as Therapeutic Targets. Wiley & Sons* (2022)

Lanoiselée Y, **Grimes J**, Koszegi Z, Calebiro D. Detecting transient trapping from a single trajectory: a structural approach. *Entropy*. doi: 10.3390/e23081044. (2021)

Calebiro D, **Grimes J**. G Protein-Coupled Receptor Pharmacology at the Single-Molecule Level. *Annu Rev Pharmacol Toxicol*. doi:10.1146/annurev-pharmtox-010919-023348 (2020)

Buenaventura T, Bitsi S, Laughlin W, Inoue A, Hanyaloglu A, **Grimes J**, Koszegi Z, Calebiro D, Rutter G, Bloom S, Jones B, Tomas A. Agonist-induced membrane nanodomain clustering drives GLP-1 receptor responses in pancreatic beta cells. *PLoS Biol*. doi:10.1371/journal. pbio.3000097 (2019)

Grimes J, Desai S, Charter N, Moita Santos R, Mason A, Wolfe L, Green A, Bridges A, Dalmas Wilk D, Brown AJ. MrgX2 is a promiscuous receptor for basic peptides causing mast cell pseudo-allergic and anaphylactoid reactions. *Pharmacol Res Perspect*. doi:10.1002/prp2.547 (2019)

Brown AJ, **Grimes J**, Desai S, et al. The mast cell receptor MrgX2 and drug-induced anaphylaxis. *J Pharmacol Toxicol Methods*. doi:10.1016/j.vascn.2019.05.084 (2019)

ACKNOWLEDGEMENTS

First, I would like to thank my primary supervisor Prof. Davide Calebiro. Without you, I'd have never had the opportunity to work on such exciting research and meet such amazing people. You helped me develop beyond a bench scientist into a critical thinker, for which I'll always be grateful. I'd also like to thank Prof. Steve Hill, my second supervisor, who took the chance on me and suggested to Davide that I'd be a good fit for the Calebiro Lab. I've always loved GPCRs and pharmacology, and Steve has only enhanced that 7-fold (one for each helix; sorry H8).

Zsombor and Yann; each of us had a part to play in this project, but together we made it whole. Thank you both for the time you put into training me, answering any questions I had and challenging any new ideas with a healthy dose of cynicism. Zsombor, I'll really miss running over to each other's microscope sessions in excitement after testing a new mutant. Yann, I was hopeless at mathematics and programming before I started my PhD. I can now confidently say that I am only mostly hopeless at it.

Shannon, you are a BRET expert, whether you like it or not. You also kept me sane throughout the PhD with daily canteen trips, laughs and support. I'd say I'll miss you, but I really won't as I know we'll continue to see plenty of each other. To the Calebiro group, thank you for being such a great group of people, inside and outside of the lab.

To Nina, I genuinely couldn't have done this without you. Thank you for moving back to Birmingham with me, even if I did sweeten the deal with a tiny, white cat. You and Tizzy made these years some of the best of my life, and the walk back from work was always filled with excitement, knowing you'd be at home. You've been with me every step of the way, and I can't wait to get married and buy our first home this year – to continue walking that road with you.

Mum, you've supported me through the last two decades or so of education – from my first day of school to the last day writing this. Thank you for always having an unrealistic belief in my abilities, it really boosted my ego and made me consider crazy stuff like doing a PhD. Dad, the last few years have been tough, but the strength you've shown through it has made this all seem like a walk in the park.

A massive shout-out goes to my D&D boys who have laughed through my frustrations, listened to my rambling talks on science and provided some well-needed breaks from reality.

Lastly, I'd like to thank the planet Saturn and of course, all of its rings.

“I'd almost forgotten the excitement of not knowing, the delights of uncertainty.”

Jon Osterman

TABLE OF CONTENTS

LIST OF FIGURES

LIST OF ABBREVIATIONS

AKAP	A-kinase-anchoring protein
AMP	Adenosine monophosphate
AP	Action potential
AR	Adrenergic receptor
ATP	Adenosine triphosphate
BODIPY	Boron difluoride pyrromethene
BRET	Bioluminescence resonance energy transfer
CCP	Clathrin coated pit
CHO	Chinese hamster ovary
CI	Confidence interval
CICR	Calcium induced calcium release
CM	Cardiac myocyte
CNS	Central nervous system
COPD	Chronic obstructive pulmonary disease
CRISPR	Clustered regularly interspaced short palindromic repeats
DAG	Diacylglycerol
DMEM	Dulbecco's modified eagle medium
DNA	Deoxyribonucleic acid
EC	Electron coupling
ECL	Extracellular loop
EDTA	Ethylenediaminetetraacetic acid
ELA	Extended lipid anchoring
EM	Electron microscopy
EMCCD	Electron multiplying charge coupled device
ERK	Extracellular signal-regulated kinases
FBS	Foetal bovine serum
FCCS	Fluorescence cross correlation spectroscopy
FCS	Fluorescence correlation spectroscopy
FDA	U.S food and drug administration
FLR	Finger loop region
FRAP	Fluorescence recovery after photobleaching
FRET	Fluorescence resonance energy transfer
GABA	Gamma aminobutyric acid
GAP	GTPase activating protein
GDP	Guanosine diphosphate
GEF	Guanine nucleotide exchange factor
GFP	Green fluorescent protein
GIRK	G protein coupled inwardly rectifying potassium channel
GPCR	G protein-coupled receptor

GRK	G protein-coupled receptor kinase
GTP	Guanosine triphosphate
HBSS	Hanks buffered salt solution
HEK	Human embryonic kidney
HEPES	4-(2-hydroxyethyl)-1-piperazine ethane sulfonic acid
HF	Heart failure
ICL	Intracellular loop
IP3	Inositol triphosphate
KO	Knockout
LB	Lysogeny broth
LC	Liquid chromatography
LTCC	L-type calcium channels
MAPK	Mitogen-activating protein kinase
MOA	Mechanism of action
MSD	Mean square displacement
NA	Numerical aperture
PAFR	Platelet-activating factor receptor
PALM	Photoactivated localisation microscopy
PAR	Protease-activated receptor
PDB	PubMed database
PBS	Phosphate buffered saline
PCR	Polymerase chain reaction
PDE	Phosphodiesterase
PED	Performance enhancing drugs
PIP2	Phosphatidylinositol 4,5-bisphosphate
PKA	Protein kinase A
PLB	Phospholamban
PLC	Phospholipase C
PM	Plasma membrane
PMID	PubMed identification
PTX	Pertussis toxin
RET	Resonant energy transfer
RNA	Ribonucleic acid
RNP	Ribonucleoprotein
RyR	Ryanodine receptors
SEM	Scanning electron microscopy
SERCA	Sarco/endoplasmic reticulum calcium ATPase
SMALP	Styrene-maleic acid lipid particles
SMM	Single-molecule microscopy
SPT	Single particle tracking
SR	Sarcoplasmic reticulum
SSRI	Selective serotonin reuptake inhibitors
STED	Stimulated emission depletion
STORM	Stochastic optical reconstruction microscopy
TAMSD	Time-averaged mean square displacement

TEM	Transmission electron microscopy
TIRF	Total internal reflection fluorescence
TM	Transmembrane
YFP	Yellow fluorescent protein

STATEMENT OF CONTRIBUTIONS

CHAPTER 1

This chapter was written entirely by me, to introduce the thesis. Figures were all generated by me in Chapter 1, with some inspired by the literature and annotated as such. Figure 1.3 was adapted from the published book chapter, Figures 1.8 and 1.9 were inspired by Theakston et al. [1] and Figure 1.15 was adapted from Calebiro & Grimes [2].

CHAPTER 2

The custom-built TIRF microscope had recently been implemented into the Calebiro lab, set up by Zsombor Koszegi and Davide Calebiro. I was involved in the regular maintenance, repair and use of the system, and built a prototype hypoxic imaging chamber, which was further developed and used for imaging experiments. BRET experiments were conducted by me, with training provided by Shannon O'Brien on the PheraStar. MATLAB workflows were already implemented by Davide Calebiro, many of which were altered by me, Zsombor Koszegi and Yann Lanoiselée to meet the requirements of the new single-molecule study. Yann Lanoiselée generated new models of diffusion, trapping, interaction, and Markov Chain analysis, for which I was an end-user – running scripts and implementing my own experimental data as needed.

CHAPTERS 3 & 4

All single-molecule microscopy experiments were conducted by me and Zsombor Koszegi, which was required - to generate the large number of datasets in this body of work. All figures were generated by me, with many adapted from an upcoming publication. Markov Chain and History plots were generated in MATLAB by Yann Lanoiselée. Molecular Dynamics (MD) simulations were performed solely by the group of Jana Selent, with mutational data for their use provided by me and Tamara Miljus. The content of these chapters is under revision by Cell for a joint first author publication – shared in authorship between me, Zsombor Koszegi and Yann Lanoiselée.

CHAPTER 5

All single-molecule microscopy experiments, BRET, optimisation, and cardiac myocyte microscopy experiments were conducted by me. Adult mouse hearts and cardiac myocytes were isolated by Daniel Johnson from the lab of Davor Pavlovic. I was additionally trained to isolate myocytes, taking PILA/B training courses for a home office license. Fluorescent ligands used in this chapter were from the labs of my co-supervisor, Steve Hill, and were previously used in the referenced studies.

1 INTRODUCTION

1.1 OVERVIEW

G protein-coupled receptors (GPCRs) comprise the largest protein family, mediating a plethora of effects in response to a wide range of extracellular stimuli, such as: hormones, ions, neurotransmitters and photons [3]. Considering GPCRs' paramount role in physiological processes such as neuronal transmission, endocrine signalling, inflammation, heart contraction and vision – this is perhaps not surprising. In fact, 30-40% of US Food and Drug Administration (FDA)-approved drugs have a GPCR as their target [4].

Pioneering experiments initiated in the 1950s by Sutherland and Rall [5], followed by half a century of extensive efforts across the world have clarified the major biochemical steps in GPCR signalling. In simplified terms, the binding of a ligand to a plasma-membrane located GPCR causes a conformational change in the receptor, which is followed by GPCR activation. GPCR activation involves the recruitment of a heterotrimeric guanine nucleotide binding protein (G proteins) and subsequent modulation of effector enzymes by the G protein subunits [6]. After early observations, it became clear that upon prolonged stimulation, GPCRs lose sensitivity to activation [7,8]. It was found that GPCRs became phosphorylated after stimulation by G protein-coupled receptor kinases (GRKs), leading to the binding of so-called 'arrestin' molecules. Arrestins were found to desensitise GPCRs to G-protein signalling and internalise GPCRs via the endocytic pathway [9-11].

In the last decade, our understanding of the molecular mechanisms of GPCR signalling has been deepened in the solving of three-dimensional (3D) structures at atomic resolution [12-14]. We now possess structures of over 80 different GPCRs [15], obtained via X-ray crystallography and more recently, cryogenic electron microscopy (cryo-EM) [16-18]. These include structures of receptors

bound to agonists [14,19,20], antagonists [16,21,22], G proteins [18,23-25] and arrestins [26,27]. In combination with biophysical approaches on purified proteins, these results reveal that GPCRs are highly dynamic and can assume multiple conformations [28-30]. These findings have led to a re-imagining of the classical model, in which GPCRs are viewed as simple 'on/off switches. Instead, GPCR signalling is dependent on the context of the cell and effector proteins available, where the activation of varying signalling pathways fine tunes a biological response.

In spite of considerable progress, fundamental questions remain in the underlying mechanisms of GPCR signalling specificity. It is well known that activation of GPCRs by selective ligands produces highly specific pharmacological effects *in vivo*. How this is achieved on a cellular level is less clear, especially since the hundreds of unique GPCRs in a single cell membrane converge on only a few signalling pathways [31]. Possible explanations reside in the spatiotemporal profile of the signals produced in GPCR activation, which may differ along receptors, dependent on the available proteins in the local microenvironment. Interestingly, there is growing evidence that signals produced by receptor activation remain highly organised in space and time, thus only impacting downstream molecular pathways only in their proximity [32,33].

Not only are the effects induced by GPCR activation often highly specific, but they are dependent on the ligand treatment used. The concept of 'biased signalling' postulates that activation of the same receptor by different agonists can elicit distinct pharmacological responses [34,35]. To explain this, it has been suggested that ligands stabilise a range of receptor conformations, which would preferentially couple the GPCR to specific G protein isoforms or β-arrestins. This is supported by growing evidence obtained from biophysical and structural data obtained in the presence of 'biased' ligands [36-38]. In order to further our basic understanding and improve drug discovery platforms - whose high attrition rates lead to vast costs and medicines with

adverse side effects - we need to characterise the complex machinery that controls receptor signalling as best we can.

As our knowledge of the physical mechanisms governing pharmacology deepens, it is becoming evident that investigations in live cells are required, with the capability to observe proteins in real-time and with high resolution. In this context, single-molecule microscopy approaches - which can characterise complex populations with millisecond and nanometre precision - are emerging as powerful tools to study GPCRs on the spatiotemporal scale in which they operate.

1.2 G PROTEIN-COUPLED RECEPTOR SIGNALLING IN LIVE CELLS

1.2.1 GPCR evolution

GPCRs play multiplex roles in human physiology, requiring a broad range of receptors to maintain function in response to diverse stimuli. Evolving from a common seven transmembrane (7TM) receptor, more than 800 GPCRs have now been identified, making them the largest protein superfamily in nature [39]. On the successful completion of the Human Genome Project, many putative GPCRs were further identified, based on sequences suggestive of a 7TM structure [40,41].

From an evolutionary standpoint, GPCR signalling emerged early in eukaryotes, conserved from yeast to mammals [31], with some prokaryotes sharing structural features of GPCRs. Fascinatingly, this signalling machinery predates the development of the nervous system and evolution of multicellular organisms, with even amoebae displaying GPCRs on their membrane [42].

1.2.2 GPCR structure and classification

The common molecular architecture of GPCRs comprises seven membrane-spanning α-helices, which are connected by alternating intracellular loops (ICLs) and extracellular loops (ECLs), an amino extracellular terminus (N-terminus) and amphipathic eighth helix (TM8) connected to a carboxyl intracellular terminus (C-terminus) (**Figure 1.1**)

. Since the first successful crystallisation of Bovine Rhodopsin (bRho) at a resolution of 2.8Å [12], the structures of pharmacologically important receptors soon followed. This included the β_2–adrenergic receptor (β_2AR) [13], the A_{2A}-adenosine receptor (A_{2A}R) [43] and the M_2-muscarinic receptor (M_2R) [44].

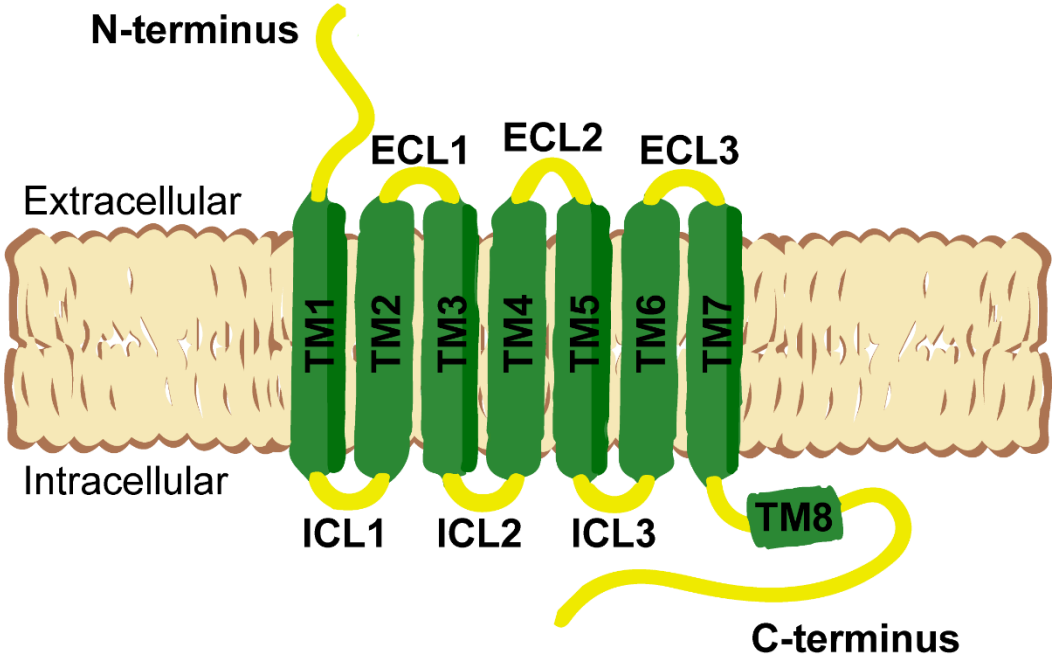

Figure 1.1 General structure of a G protein-coupled receptor (GPCR). Schematic of a generic GPCR structure containing an amino N terminus which emanates from the extracellular face of the plasma membrane, 7 helical transmembrane domains (TM1-7) which alternate intracellular loops (ICL1-3) and extracellular loops (ECL1-3) between the helices. This is followed by a smaller helix 8 (TM8) which sits on the intracellular leaflet of the membrane and ends with the carboxyl C-terminus.

Interestingly, these structures share little sequence homology, despite a common structural topology. Greatest similarity is observed in the TM regions, with the ICL/ECL regions having greater diversity, even amongst closely related receptors [13]. The presence of reserved motifs and residues was used to divide GPCRs into families (Families A-F), which are subdivided in humans as: Class A (rhodopsin-like), Class B (secretin-like), Class C (glutamate), adhesion receptors and frizzled [39]. Family A are the largest and most diverse subfamily, representing over 90% of all GPCRs. These receptors bind a heterogeneous group of small-molecule ligands, including proteins, nucleotides, fatty acids and biogenic amines, which bind mostly in the 7TM bundle. Family A GPCRs account for around 80% of all GPCRs and comprise the major hormone and neurotransmitter receptors, which have important roles in major physiological pathways.

1.2.3 G protein signalling

The G protein mostly interacts with the GPCR on ICL2, ICL3 and the C-terminus [45]. The coupling of a G protein to the GPCR causes the catalytic exchange of GDP → GTP in the Gα subunit, which in turn catalyses the GTP-bound complex to dissociate from the βγ-subunit (**Figure 1.2**). Residues are exposed in the G protein which were previously inaccessible to effector enzymes, allowing them to freely interact with target proteins and to initiate signalling cascades. G proteins have intrinsic GTPase activity, leading to GTP hydrolysis and re-association of the subunits, limiting signalling. This is further facilitated by a family of GTPase activating proteins (GAPs) which further increase the enzymatic hydrolysis [46].

After binding to a ligand, receptor conformations are adopted which are more likely to form productive interactions with membrane-associated heterotrimeric G proteins, consisting of α, β- and γ- subunits. The human genome contains 33 genes encoding G proteins, for which Gα has

4 broad subtypes: $G\alpha_i$, $G\alpha_s$, $G\alpha_q$ and $G\alpha_{12/13}$ [47]. 16 total α-subunits exist, in addition to 5 β-subunits and 12 γ-subunits [48]. $G\alpha_s$ was the first protein isolated, based on its direct interactions with adenylyl cyclases [49,50], which stimulates cAMP production. Conversely, $G\alpha_{i/o}$ proteins generally inhibit the activity of adenylyl cyclases.

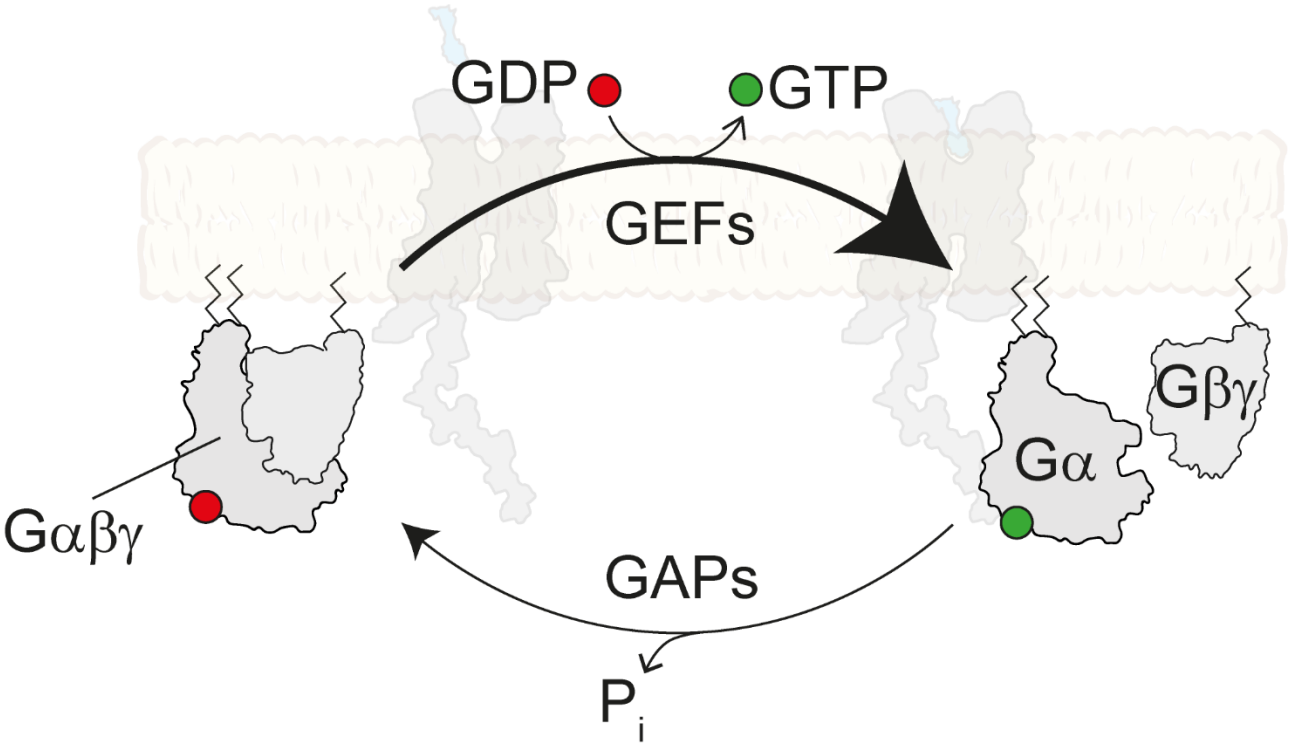

Figure 1.2 Control of G protein activation by GPCRs and associated proteins. Coupling of G proteins to GPCRs leads to conformational changes which propagate catalytic exchange of GDP → GTP on the Gα subunit, catalysed by guanine nucleotide exchange factors (GEFs). This causes G protein dissociation and is a reversible process, by which GTPase activating proteins which catalyse dephosphorylation of GTP → GDP, which promotes re-formation of the complex.

Interestingly, some groups have found that prolonged $G\alpha_i$ activity can increase cAMP production [51], demonstrating the dynamic nature of these proteins. $G\alpha_{q/11}$ activates the β-isoforms of phospholipase C (PLC-β), catalysing the synthesis of inositol 1,4,5-triphosphate (IP_3) and diacylglycerol (DAG) from phosphatidylinositol 4,5-biphosphate (PIP_2). IP_3 in turn stimulates the release of intracellular Ca^{2+} stores and subsequent activation of protein kinase C

(PKC) via DAG. $G\alpha_{12/13}$ proteins modulate the activity of Rho guanine nucleotide exchange factors (RhoGEFs) [52], which activate Rho family GTPases and regulate the activity of actin dynamics.

The β and γ isoforms were initially thought to have the same function once assembled into the Gβγ dimer and were thought of as an accessory to Gα signalling. This rhetoric has been re-evaluated in recent years and Gβγ subunits are now known to bind directly to a plethora of proteins, including G protein-dependent inwardly rectifying K+ (GIRK) channels [53], G protein-coupled receptor kinases (GRKs) [54,55], mitogen-activated protein kinases (MAPKs) [56], voltage-gated Ca^{2+} channels [57-59] and PLC-β [60]. GPCRs were originally thought to couple only one type of G protein, activating one downstream pathway. It is now well established that GPCRs are promiscuous and can signal via multiple G protein pathways.

Since the discovery of the central components of GPCR signalling machinery, multiple hypotheses and models have been postulated as to rationalise how the proteins interact to mediate their effects. Eventually, the ternary complex model prevailed as a basic descriptor of GPCR – G protein interactions [61,62], which posits that receptors exist in an equilibrium of active and inactive conformations. These conformations can be stabilised by the binding of agonist ligands, which shifts the equilibrium towards receptors adopting active conformations, increasing the likelihood of downstream signalling proteins such as G proteins.

1.2.4 Structural understanding of GPCR activation

Over the last decade, remarkable progress has been made in the study of GPCR structures, revealing previously unknown complexities in conformation and signalling modalities. As a prototypical GPCR with clinical significance and one of the most well-characterised signalling

pathways, β_2AR reports many high-resolution 3D structures in complex with ligands and adaptor proteins. An active conformation of β_2AR bound to the agonist BI-167107 and in complex with Gαs first showed the extensive interactions of GPCR with the G protein C- and N-terminus [63,64]. Of note, significant conformational changes are observed in the receptor after agonist activation, including: an extension of the intracellular portion of TM5 towards the cytoplasm, a major outward shift in TM6 and an opening of the intracellular loop 3 (ICL3) interface to interact with the C-terminus of Gαs [65], which itself undergoes a major rotation of the helical domain to become active (~127° rotation) (**Figure 1.3**). Additional studies have additionally highlighted a shift in the N-terminus of helix 8, which is suggested to dock G protein receptor kinases (GRKs) for receptor phosphorylation and arrestin recruitment [10,66]. More recent studies using cryo-EM with a host of GPCRs from different families reveal a similar receptor-G protein interface, suggesting a conserved mechanism of activation among GPCRs.

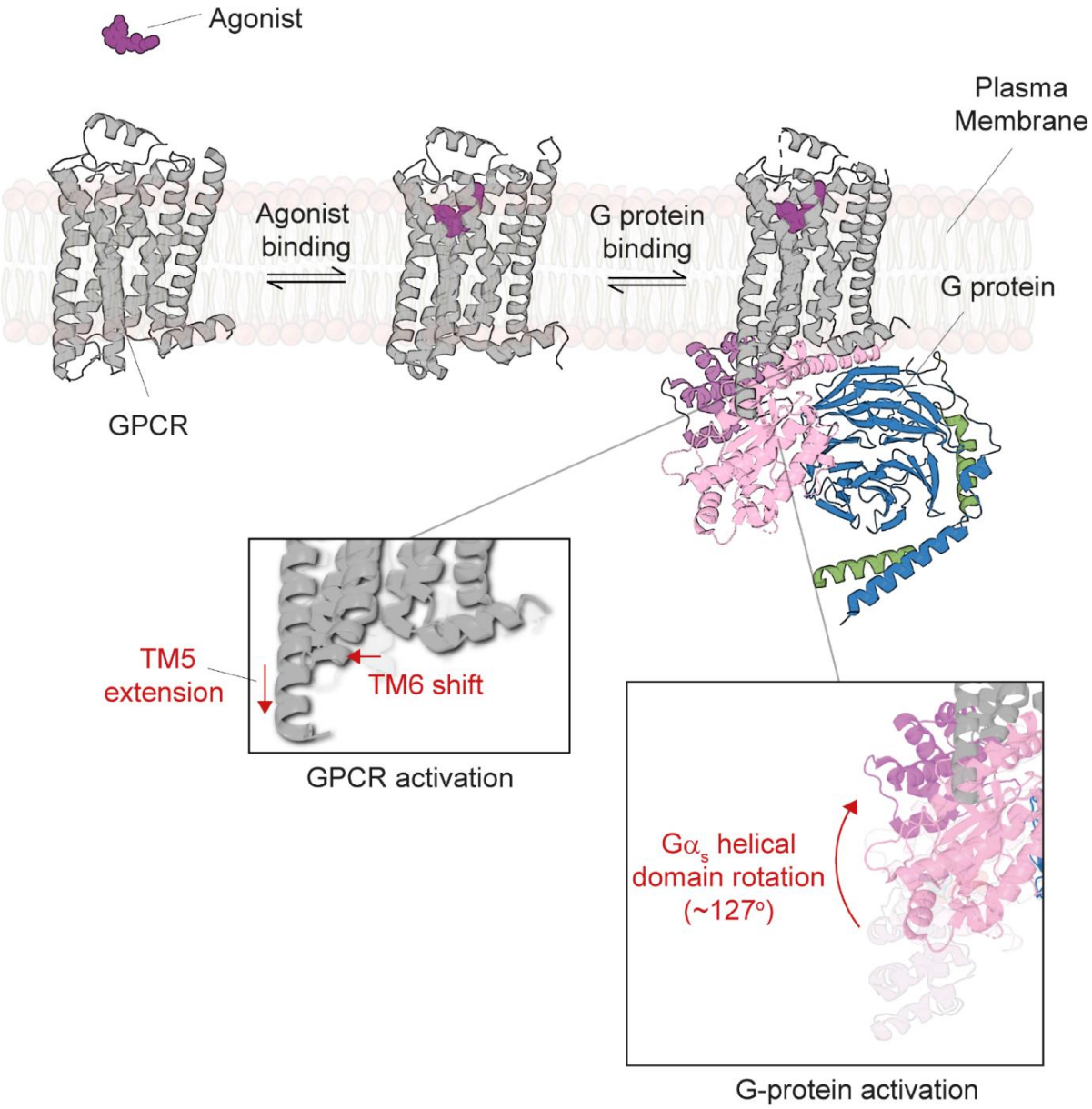

Figure 1.3 Conformation changes during GPCR and G protein activation. GPCRs exist in dynamic equilibrium between conformational states even prior to ligand binding. Upon binding of an agonist, a series of conformational changes shift this equilibrium towards active-like receptor conformations, which reveals an intracellular binding pocket more likely to interact with G proteins. The agonist-bound conformation represents an intermediate state in the GPCR activation process, with full activation requiring both agonist and G protein binding. The fully active state is characterised by a major, outward movement of transmembrane-domain 6 (TM6) in the receptor, and a major rotation in the helical domain of the Gα subunit in the G protein. PDB reference for the combined GPCR-G protein complex (7WU9).

1.3 β-ADRENERGIC RECEPTORS

1.3.1 Adrenergic receptor family

Adrenergic receptors act as the signalling pathway for the hormones adrenaline and noradrenaline. By stimulating adrenergic receptors across the body, these molecules have long been known to play a pivotal role in the regulation of sympathetic control of neural, cardiac and pulmonary physiologies [67-69]. After either endocrine release from the adrenal glands or synthesis in neuronal axons in the CNS, activation of adrenergic receptors results in a multitude of effects, including the modulation of heart rate, smooth muscle relaxation and the fight-or-flight response. Three subtypes of adrenergic receptors exist: α_1, α_2 and β [70,71]; with further sub-classifications expanding the receptor families based on differences in ligand pharmacology, G protein selectivity and sequence divergences uncovered by molecular cloning [72].

1.3.2 Adrenergic receptor signalling

α_1-adrenoreceptors are found mainly in vascular smooth muscle and presynaptic nerve ganglia, mediating submucosal vasoconstriction. In humans, α_2-adrenoreceptors consist of 3 highly homologous proteins (α_{2A}, α_{2B}, α_{2C}) that mainly activate Gαi/o proteins in the central nervous system, where a negative feedback loop is maintained in the presynaptic ganglia through the inhibition of cAMP production. When noradrenaline is released from an adrenergic neuron, vesicular resorption feeds back to α_2 receptors, depolarising the pre-synapse.

The β-adrenoreceptors are perhaps one of the most common therapeutic drug targets , due to their adverse pathophysiology in heart disease. Much like α-adrenoreceptors, they are

endogenously activated by adrenaline and noradrenaline. The β_1AR is distributed throughout cardiac tissue and the kidney, primarily coupling to Gαs; promoting cAMP production through adenylyl cyclase and activation of Protein Kinase A (PKA). This regulates a multitude of downstream functions, ultimately leading to an increase in blood vessel relaxation and a modest increase in contractility in cardiac myocytes [73]. The β_2AR exerts similar cardiac functionality to β_1AR, but also signals through Gαi after receptor phosphorylation [74], through a signalling class switch mediated by PKA activation. It was recently confirmed that β_1ARs are present in all cardiac myocytes [75], whereas β_2AR is frequently absent, being expressed more densely in non-myocyte cells in the endothelium.

Interestingly, excessive β_1AR signalling has been shown to promote apoptosis of cardiac myocytes due to excessive cAMP signalling, whereas β_2AR signalling has cardioprotective effects due to Gαi-mediated signalling [76-79]. Less well characterised than its β_1 and β_2 counterparts, β_3AR is mostly involved in the regulation of lipolysis and thermogenesis in brown adipose tissue and skeletal muscle through Gαs stimulation [80-82].

1.4 β-ARRESTINS

1.4.1 β-arrestin discovery

Arrestins were described in the 1980s for visual rhodopsin, acting as an adaptor for rhodopsin kinase and desensitising receptor signalling via steric hindrance of the G protein [83,84]. With an evolutionary lineage as old as GPCRs [85], the coordinated actions of arrestins and associated kinases are critical for GPCR downregulation and the attenuation of G protein-dependent signalling. The protein family was expanded beyond visual arrestin after the discovery of two

homologous proteins that desensitised GPCR signalling in non-retinal tissue [7]. The so-called β-arrestin1 and β-arrestin2 share approximately 78% sequence homology in humans and are expressed ubiquitously throughout our tissues [86]. In mice, knockout of not one but both β-arrestin isoforms results in embryonic lethality [86-88]. This suggests that one β-arrestin isoform rescues the phenotype of the other - but at least one is required for normal development and physiology.

Although the above framework describes the most basic actions of arrestin, it does not account for all phenotypes observed in live cells. Indeed, liquid chromatography (LC) tandem mass spectrometry experiments of Angiotensin II type 1 receptor (AT_1R)-activated β-arrestin1/2 identified over 100 interacting proteins which are involved in signalling, cytoskeletal organisation and nuclear transcription [89].

1.4.2 G protein-coupled receptor kinases

Agonist-induced activation of GPCRs, subsequent G protein signalling and 2nd messenger generation occurs on the timescale of milliseconds, with differential kinetics observed depending on the cell and receptor employed [90]. After G protein dissociation, GRKs phosphorylate serine/threonine residues on the receptor C-terminus (tail) and ICLs (core) [91-93]. Traditionally, β-arrestin is thought to arrive from the cytoplasm to bind these phosphorylated residues, providing an interface with the receptor that precludes further G protein interaction (**Figure 1.4**).

Among the 7 GRK isoforms, GRK 1 and 7 expression is sequestered in the eyes to modulate visual Rhodopsin [94], GRK4 is limited to the testes [92] and GRKs 2, 3, 5 and 6 are found

ubiquitously [95]. Initial verification of the desensitisation mechanism of arrestin included the finding that increasing GRK2 concentrations in reconstituted GPCR systems reduced G protein binding only in the presence of β-arrestin [91]. By occupying the receptor core in which the G protein occupies, arrestins are thought to sterically hinder their binding, preventing further signalling [96].

GRKs induce a variety of phosphorylation patterns on the GCPR C-tail. The 'Barcode Hypothesis' was developed in response to the finding that ligand choice influenced the phosphorylation state, thus determining the downstream arrestin function [27,97] (**Figure 1.4**). By analysing the ligand-induced phosphorylation states of prototypical GPCRs, the relationship between different GRKs and their cellular functions were determined. For the V_2 vasopressin receptor (V_2R), AT_1R and β_2AR, it was found that GRK2/3 mediated most phosphorylation and were responsible for arrestin recruitment and internalisation. For β_2AR, the ligand Carvedilol has been found to stimulate phosphorylation only at GRK6-specific sites, resulting in both arrestin recruitment and the activation of extracellular signal-regulated kinases (ERK) [98].

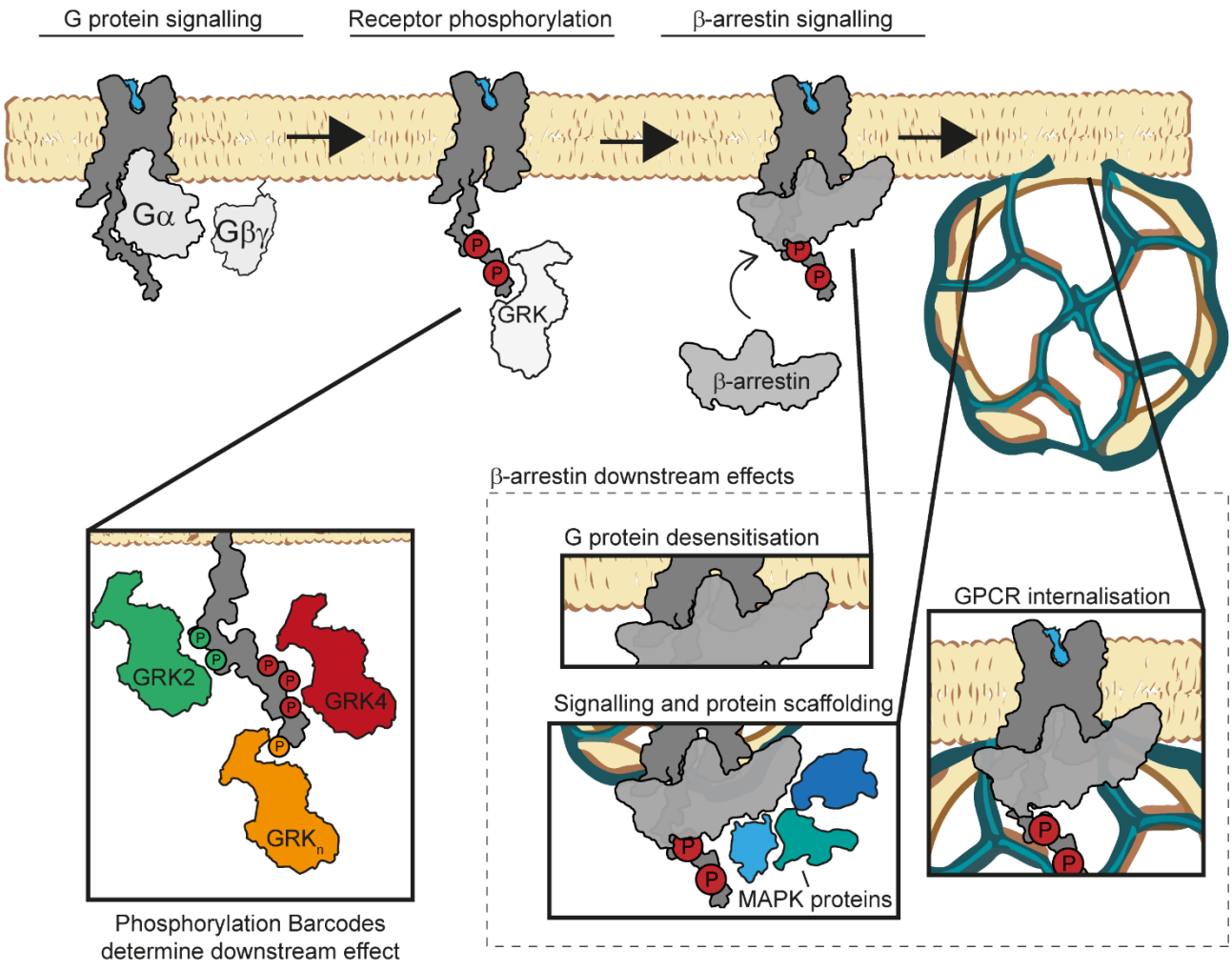

Figure 1.4 Expanded classical view of β-arrestin signalling. Broadly, GPCR signalling is thought to occur in two major phases: G protein signalling and β-arrestin signalling. After dissociation of the Gα subunit and dependent on G protein subtype, GRKs are recruited to the receptor C tail and phosphorylate residues to provide docking sites for β-arrestins. After GRK dissociation, β-arrestin - which is classically thought to occupy the cytoplasm close the plasma membrane - can now recognise the receptor C tail and bind to the receptor, dependent on the phosphorylation barcode present. Physical binding of the arrestin provides a competitive inhibition site for the G protein, desensitising the response and GPCR-arrestin complexes are thought to migrate or act as sites of clathrin-coated pit (CCP) formation for GPCR internalisation. Additionally, β-arrestin is known to signal via scaffolding of MAPK proteins such as ERK, Raf and Src kinases on CCPs.

1.4.3 Receptor internalisation at CCPs by β-arrestins

Two decades ago, Benovic and colleagues identified a new modality of β-arrestin signalling, through high-affinity interactions with components of the clathrin-mediated endocytosis (CME) pathway [99,100]. By binding directly to β_2-adaptin (AP2) and the clathrin heavy chain [101,102], β-arrestins play an important role in facilitating receptor recycling. This sequestration provides a platform to attenuate the signalling response, by recycling the receptors through endosomes. Years of research have found the role of arrestin-clathrin interactions to be essential in GPCR trafficking [102-106] and research has shown that overexpression of a dominant negative β-arrestin can inhibit β_2AR internalisation [107].

Purified β-arrestin has been shown to specifically bind clathrin with a similar K_d to AP2 [99]. Laporte et al. verified with mutant β-arrestin 2 that lacked either the AP2 or clathrin binding sites that AP2 interaction was a necessary step for β_2AR clustering at CCPs [108], whereas mutating direct interactions with clathrin still resulted in translocation of receptor and arrestin to CCPs. Interestingly, this study also showed that β-arrestin can bind to clathrin and AP2 independent of a colocalising receptor [102].

Clathrin has 3 heavy chains and 3 light chains; each heavy chain has a globular amino terminus group and terminates at a triskelion core. The light chains are associated with each heavy chain and stabilise the legs [99]. Each heavy chain has a binding site for AP2. These interactions allow the formation of the clathrin-arrestin-AP2 complex , which targets arrestin-bound GPCRs to sites of clathrin-coated pit biogenesis. The clathrin triskelions form a cage structure which has a stable icosahedral symmetry and has been visualised recently by cryo-EM [109]. The formation of triskelion cages invaginates the plasma membrane, forming vesicles that are excised to internalise plasma membrane proteins, which can disassemble after membrane scission.

Clathrin-coated pit (CCP) biogenesis is initiated by the interaction of AP2 with phosphatidylinositol 4,5-bisphosphate (PIP2) on the plasma membrane and furthered by the recruitment of clathrin triskelions to AP2. These interactions can occur independent of GPCRs, arrestins and other adaptor proteins, providing a platform for protein scaffolding and recycling of membrane lipids. GPCR-β-arrestin complexes enhance the formation of clathrin-AP2-PIP2 complexes through the direct interactions with β-arrestin described by *Laporte et al.* [101]. Here, it was demonstrated that upon agonist stimulation of β_2AR with the full-agonist isoprenaline, complex formation between β_2AR, β-arrestin 2 and AP2 enhanced receptor internalisation. β-arrestin then provides the ability to cluster, enhancing growth of existing CCPs and initiate formation of CCPs (**Figure 1.5**). Recruitment of more AP2, arrestin and clathrin stabilise the CCP and have been shown to occur in higher concentrations after agonist activation of GPCRs [103,110]. CCP formation is finalised by the recruitment of dynamin proteins, which are upregulated by β-arrestin signalling [111] (**Figure 1.5**). Dynamin proteins and the combined efforts of cortical actin cytoskeleton mature to CCP prior to scission from the membrane and uncoating of the cargo from the newly formed vesicle [112-114].

Class A receptors, such as β_2AR, are so named for weaker binding to arrestin, and are thought to dissociate from arrestin during CCP internalisation [115]. Conversely, Class B receptors, such as the vasopressin-2 receptor (V_2R), are thought to internalise with β-arrestin and continue to signal inside the cell [10,116]. Ubiquitination seems to play a role in determining whether arrestin-GPCR interactions are Class A or Class B, with Class A receptors displaying ubiquitination barcodes that promote fast degradation of βArr2 and recycling of endosomes [111,117,118].

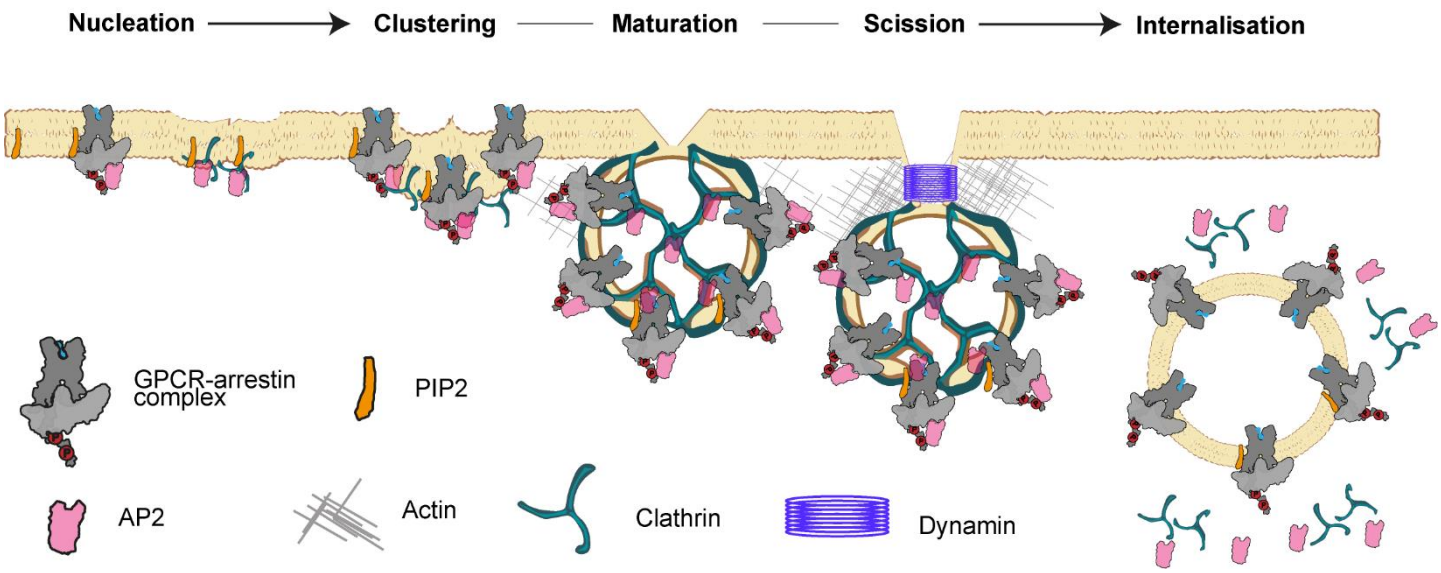

Figure 1.5 Simplified overview of clathrin-coated pit (CCP) formation. Schematic of CCP formation from nucleation of AP2-clathrin-GPCR-arrestin complexes through clustering and maturation with cortical actin on the membrane to form a clathrin cage, scission of the invaginated membrane leaflet through dynamin and uncoating and internalisation of the GPCR complexes as an intracellular vesicle.

The importance of phosphoinositide interactions for β-arrestin mediated receptor internalisation at CCPs was recently investigated by Jung et al. [119]. Using the protease-activated receptor 2 (PAR2), which is known to undergo rapid desensitisation and extensive endocytosis, the authors found that β-arrestin activation after agonist stimulation of the receptor led to stable binding of PAR2 and β-arrestin at CCPs. They found that although G protein (Gαq) signalling via PLC depleted the phosphoinositide, PIP2, which is crucial in the formation of clathrin-coated pits (CCPs); β-arrestin signalling led to recruitment of the PIP2 synthesis enzyme (PIP5K) to the plasma membrane. Phosphorylation of membrane PIP → PIP2 was required for receptor endocytosis and overexpression of PIP5K led to increased binding of both β-arrestin and PAR to CCPs [119], inducing local PIP2 gradients that promote receptor endocytosis. These results were supported by high-resolution structures published via cryo-

EM in lipid nanodiscs [120-122], where residues in β-arrestin have been found to bind at the interface of PIP2 and the Neurotensin-1 receptor (NSTR1) [120], which has been supported by biophysical studies of visual arrestin [123].

Janetzko et al. [124] most recently found that plasma membrane PIP2 stabilises an active conformation of arrestin and that promotes GPCR-arrestin complex formation. Essentially, the authors suggest that PIP2 acts as an allosteric modulator of GPCR and arrestin interactions, adding a further layer of complexity to arrestin signalling beyond receptor phosphorylation by GRKs.

1.4.4 β-arrestin signalling mechanisms

In addition to the classical roles of G protein desensitisation and GPCR internalisation, β-arrestins are now known to act as signal transducers, capable of G protein-independent activation of GPCR signalling [10,11], including regulation of the mitogen-activated protein kinase (MAPK) pathway [74,125,126]. This is intrinsically linked to the phosphorylation of kinases, such as ERK1/2, Src and p38, resulting in β-arrestin mediated effects on transcriptional regulation, cellular senescence and apoptosis [118,127,128]. The promotion of these mitogenic responses, independent of G proteins, were first reported for the AT_1R [129] - where arrestin plays a crucial role in promoting cell division.

In studies utilising dominant-negative mutants of β-arrestin, it has been found that β_2-adrenergic receptor (β_2AR) internalisation was required for ligand-dependent activation of ERK1/2 [129,130], suggesting that internalised GPCRs are still able to signal from endosomes, challenging the classical view that GPCR signalling occurs exclusively on the plasma membrane.

Furthermore, subsequent studies suggest that there are two independent phases of ERK signalling. The first phase is a transient activation via G proteins at the plasma membrane which leads to localised ERK accumulation and nuclear ERK translocation. The second phase is sustained, triggered by GPCRs and β-arrestin in endosomal compartments, so that signalling in discrete cytoplasmic nanodomains can prolong signalling outcomes [128,131].

The topic of G protein independent β-arrestin signalling remains contentious, and the above studies have been challenged. Using small interfering RNAs (siRNA) to silence β-arrestin, O'Hayre et al. found that although β-arrestin is required for β_2AR internalisation, it is dispensable for ERK activation [132]. Additionally, Grundmann et al. used genome-edited cells lacking either endogenous Gα protein or β-arrestin and found that only the absence of G protein abrogated ERK signalling by GPCRs [133]. It is likely that both arguments have merit and that the cellular response is dynamic; with choice of cell line, ligand choice and environmental factors impacting observed signalling outcomes. Combined with studies that implicate β-arrestin in phosphoinositide 3-kinase (PI3K) signalling [134-136] and epigenetics [137,138], it is clear that this once 'simple' protein has an array of complex functions.

With arrestins and their interacting partners emerging as proteins in control of major signalling pathways, identifying the mechanism by which arrestin interacts with other proteins is of keen interest. Additionally, increasing our understanding of arrestin-mediated effector activation might lead to the development of new therapeutic approaches targeting these pathways. Advanced techniques are required, beyond the scope of traditional pharmacology, to fully understand the role β-arrestin plays in biology - at resolutions where we can observe the action of single molecules.

1.4.5 Structural biology of β-arrestin-GPCR interactions

β-arrestin has been resolved to near atomic resolution in the last decade, with a multitude of crystal structures, EM grids and *in silico* docking poses existing in multiple conformations; including arrestin bound to GPCRs with various ligands and conjugated to nanobodies [27,45]. Arrestin is composed of N- and C-domains which are rigid at rest and have rotational flexibility during arrestin activation. Arrestin activation is triggered on binding of the phosphorylated receptor C-tail [36,45,139,140] which involves disruption of the polar core by phosphates binding to residues in β-strand I [45], which disrupts the polar core. Displacement of the arrestin C-tail leads to inter-domain rotation of the two domains by ~20°, relative to each other. This interaction also displaces the arrestin finger-loop region (FLR), which becomes mobilised for binding to the receptor core, forming a fully engaged complex (**Figure 1.6**).

The FLR is a flexible loop region in the β-arrestin central crest and has a high affinity for multiple TM domains in the GPCR core; proposed to stabilise interactions between arrestin and GPCR. *Cahill et al.* found that signalling-deficient β-arrestin mutants, which were unable to mediate the GPCR core interaction, could still signal via ERK and internalise GPCRs [27]. Interestingly, these arrestins were defective in their ability to desensitise GPCRs to G protein signalling, suggesting that the tail and core interactions have differing functions in cells. In particular, this suggests that activated β-arrestin FLR competes for the G protein binding cleft, acting as competitive inhibition to desensitise signalling.

More recent studies have further probed this mechanism, finding that the arrestin FLR adopts an active-like conformation after the N domain of arrestin inserts in the C-terminal tail of the GPCR and displaces it [141]. This brings the arrestin C domain into close contact with the receptor

and the plasma membrane, where it is suggested to interact further with adaptor proteins, structural elements and perhaps membrane phospholipids.

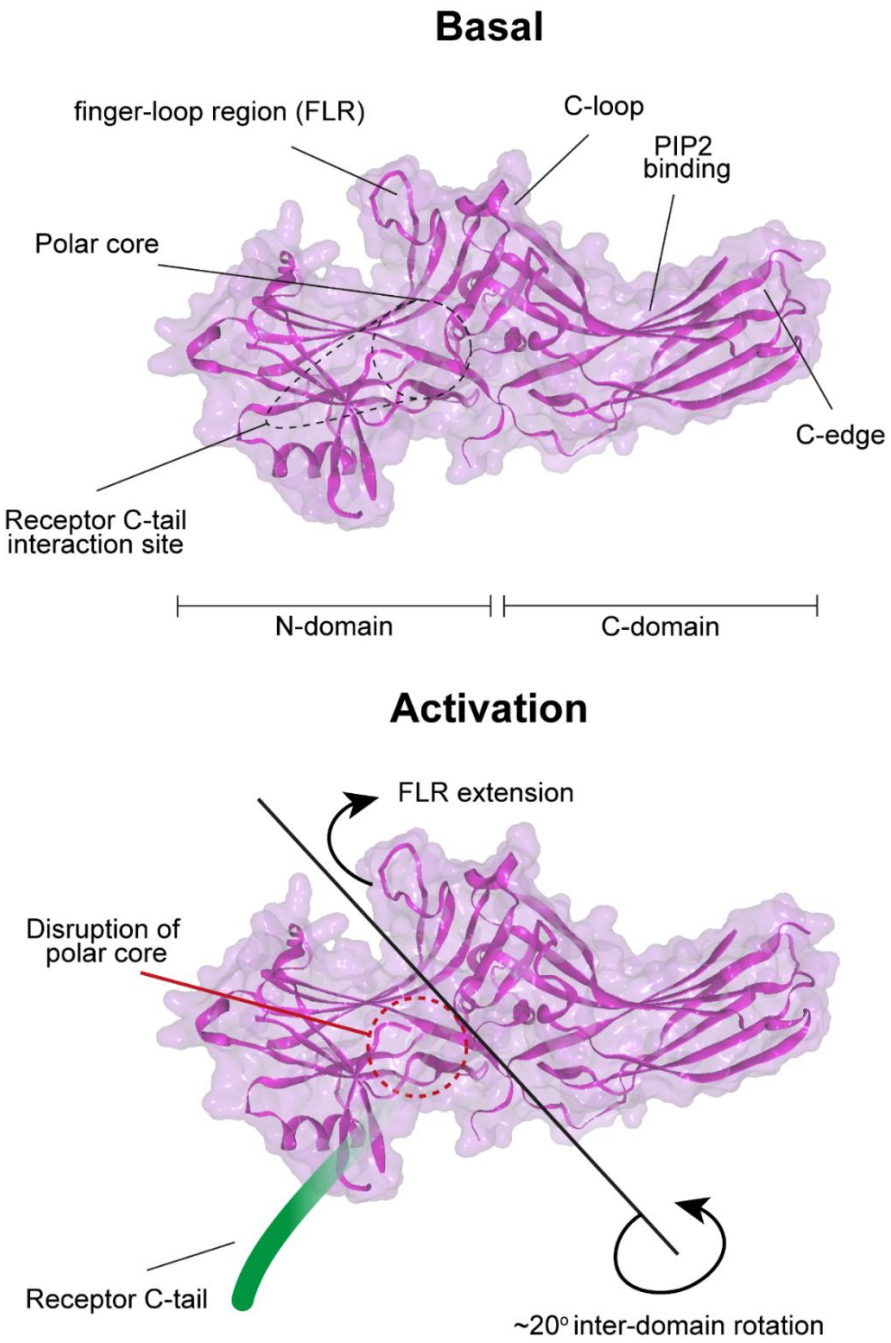

Figure 1.6 β-arrestin structure with activation mechanism. Structure of inactive β-arrestin2 is shown (PDB ID:1G4M), with major structural elements labelled. Below, major structural changes are highlighted, after disruption of the arrestin polar core by GPCR C-tail phosphates. This includes an interdomain rotation between the N- and C- domains and extension of the FLR – which inserts into the GPCR core.

By studying a chimeric β_2AR with the C-terminus replaced by the C-terminus of V_2R, which has a higher affinity for arrestin whilst maintaining the same pharmacological properties as β_2AR, *Shukla et al.* found two distinct interaction poses of GPCRs and β-arrestins [45]. They found that β-arrestin1 was bound to the receptor C-terminus alone in ~60% of interactions, whereas the other ~40% are engaged through both C-terminus and through transmembrane and ICL2/3 associations, via the arrestin FLR (**Figure 1.7**). This led to the nomenclature of two key binding motifs that mediate arrestin binding to GPCRs, named the 'tail' and 'core' interactions [140]. The proposed binding model is that an inactive β-arrestin binds to the phosphorylated receptor C-tail via the N-terminal domain of arrestin ('tail interaction'). Stabilisation of this semi-engaged complex displaces arrestins C-edge towards the receptor, where the β-arrestin finger loop region (FLR) binds to the GPCR transmembrane bundle ('core interaction') (**Figure 1.7**).

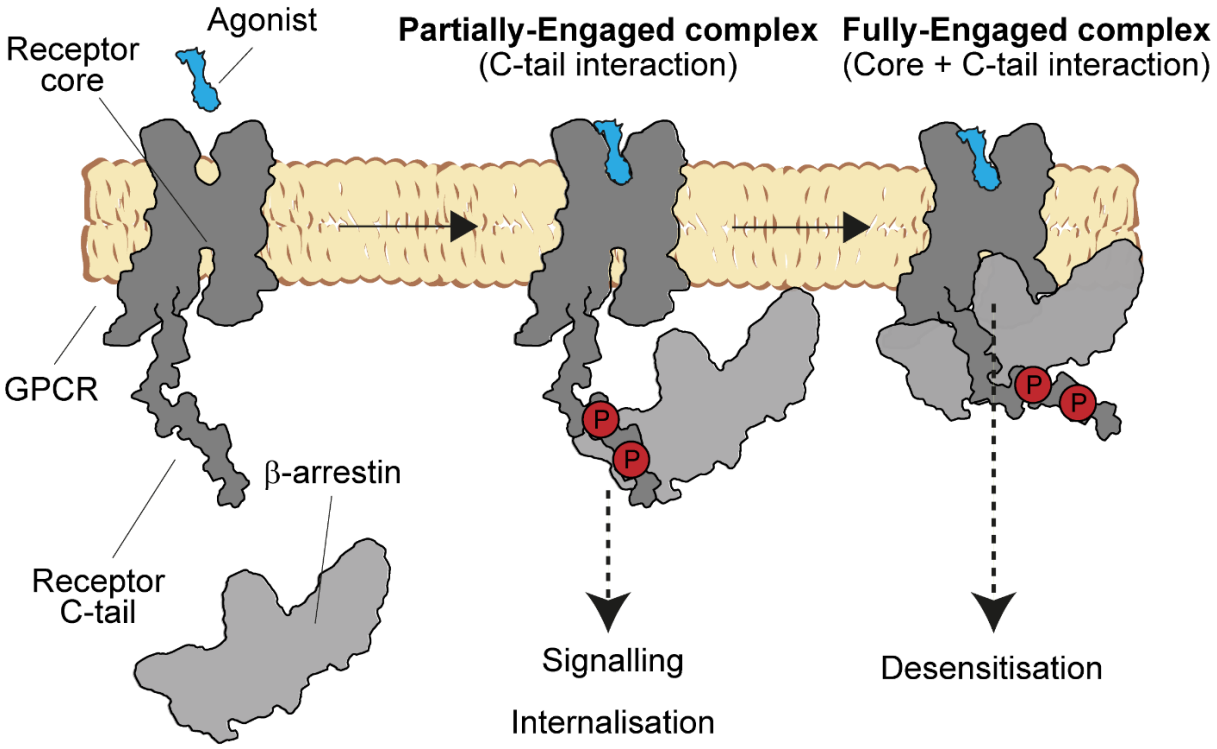

Figure 1.7 Predicted binding modes of β-arrestin to GPCRs. The schematic illustrates the two-way binding mode by which GPCRs can activate β-arrestin. After ligand binding to the extracellular GPCR pocket, conformational changes lead to GPCR signalling which culminates in phosphorylation of the receptor C-tail by GRKs (not shown). By β-arrestin binding to the phosphorylated receptor C-tail (C-tail interaction), GPCRs are thought to be targeted to clathrin-coated pits for internalisation. After the tail interaction, in which the β-arrestin is hanging, a secondary interaction with the GPCR core and the arrestin finger loop region is proposed to desensitise G protein signalling by blocking the binding site.

Although β-arrestin has only two domains, it has complex structural domains which mediate specific interactions with a multitude of downstream effectors [9]. Clathrin interactions mediate GPCR internalisation by tethering the arrestin-GPCR complex to the clathrin heavy chain, and the AP2 binding motif allows AP2 to bind and scaffold proteins at the CCP. Phosphoinositide binding sites are required for trafficking β-arrestin to CCPs and the plasma membrane [103,142], highlighting the requirement for interactions with lipids as well as proteins to maintain β-arrestin function. How these interactions lead to the defined phenotypes that occur on the

timescale of single receptor-arrestin interactions in the cell remains to be seen, and current methods have relied heavily on static pictures of the complexes garnered by structural biology.

1.5 β-ADRENERGIC RECEPTORS IN CARDIAC SIGNALLING

1.5.1 Cardiac Myocytes

Mammals contain three groups of muscle tissue: skeletal muscle, cardiac muscle and smooth muscle. The major function of all groups is to provide contractility in response to stimuli. Cardiac Myocytes (CMs) are the large, multinucleated cells responsible for the contraction of cardiac tissue and are long-lived cells that contract from foetal development until death. Due to their high metabolic demand, CMs contain high concentrations of mitochondria, which are responsible for supplying the ATP required for continued contractions. In humans, CMs can be hundreds of micrometers in length and tens of millimeters in diameter, making them one of the largest single cells in the body. The plasma membrane of CMs is topologically uneven and forms deep invaginations through the cell, known as transverse tubules (t-tubules). These long protrusions provide a large surface area for membrane proteins, providing an extensive architecture for signalling to occur fast and efficiently. The sarcoplasmic reticulum (SR) is another specialised structure in CMs, the membrane of which ruffles, to provide an even larger surface area inside the cells. The purpose of the SR is to store calcium ions within the cell, providing an ionic gradient crucial for contraction (**Figure 1.8**).

Cardiac myocytes are broadly organised into two groups, based on their location in the heart. Atrial CMs have a different ultrastructure when compared to ventricular CMs, in addition to differences in gene expression patterns regarding membrane proteins, ion channels and transcription factors [143]. In particular, t-tubules are present mostly in ventricular myocytes [144]

and are found only in adults – with neonatal myocytes lacking these specialised structures entirely [145]. This is perhaps due to the size of neonatal cardiac myocytes, where a much-decreased size means that Ca^{2+} release is sufficient to synchronously activate cells. In adult cells, increased size comes from an increased lengthening of the myofibrils, so that diffusion of calcium is no longer sufficient to rapidly depolarise the cell without specialised structures.

Advances in microscopy, in particular of super resolution imaging and transmission electron microscopy (TEM), have shown that t-tubules are regularly spaced in ~2μm intervals along the cardiac myocyte [146]. Additionally, changes in t-tubule diameter have been linked to differences in β-adrenergic receptor signalling [147-149]. Lastly, diseases such as chronic heart failure have decreased expression of GPCR signalling proteins such as β-arrestin, which leads to altered membrane expression and signalling of β-adrenergic receptors – the impact of which is discussed in 1.6.6.

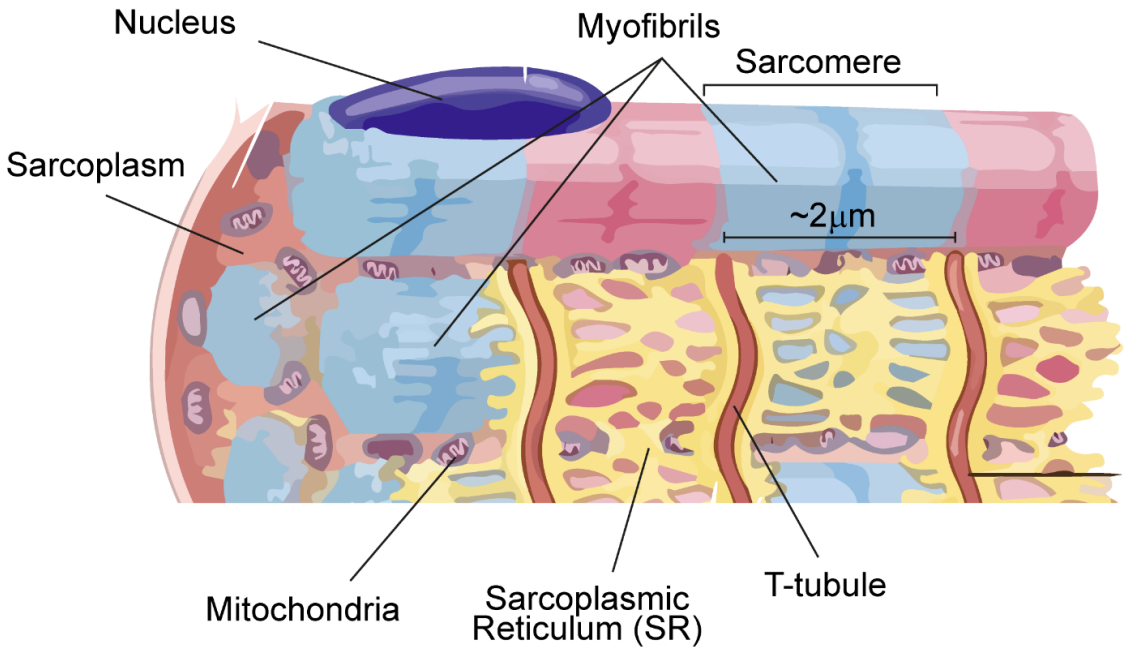

Figure 1.8 Specialised structure of a cardiac myocyte. Cross section of a cardiac myocyte showing the specialised structures that maintain a large surface area, high energy landscape for signalling and contractile units (~2μm diameter).

1.5.2 β-adrenergic maintenance of contractility

β_1AR makes up approximately 70% of the total β-adrenergic receptor population within the heart. Signalling via Gαs in the heart catalyses adenylyl cyclase 5 and 6 (cardiac isoforms) production of cAMP [150]. After cAMP production and PKA activation, the excitation-contraction (EC) coupling response is generated through ion gradients, leading to heart contractility through action potentials. Action potentials (AP) in the heart vary based on location, time and function. They represent a change in membrane potential of the cell through the coordinated opening and closing of ion channels. Action potentials can be recorded with a microelectrode inserted into the cardiac myocyte and can be described through phases of depolarisation and repolarisation of the ion gradient, which generates a shift in electric potential and contraction. A short lag proceeds the AP to restrict excessive signalling, which would otherwise over-excite the cells and lead to cardiomyopathies. The effects of β-adrenergic receptors on EC-coupling are described below.

After PKA activation through β_1AR, targets for PKA include Phospholamban (PLB), Ryanodine receptors (RyR) and L-type Ca^{2+} channels (LTCC) [151], all of which enhance release of calcium stores from the sarcoplasmic reticulum (SR) – a type of smooth endoplasmic reticulum present in smooth muscle cells, such as cardiac myocytes. PLB becomes phosphorylated on Ser16 by PKA, reducing its affinity for sarco/endoplasmic reticulum Ca^{2+} ATPase (SERCA) inhibition. This reduced association eliminates ATP hydrolysis and Ca^{2+} translocation across the SR membrane from the cytosol. This leads to so-called calcium-induced calcium release (CICR), first described in cardiac myocytes by Fabiato and Fabiato [152,153], where a positive-feedback loop consistently recycles Ca^{2+} across the SR membrane into the cytosol [154,155], providing a

sustained and greater force of contraction. Without the action of PLB, the ionic gradient is too slow and diffuse to dissipate effective signalling (**Figure 1.9**).

1.5.3 Compartmentalisation of β-adrenergic receptors in cardiac myocytes

Although β_1AR and β_2AR share a common signalling pathway through cAMP production, stimulation in the same cell produces different reactions, with many contributing factors exerting effects on signalling, spatial localisation and temporal activation of receptors. Firstly, only β_2AR couples through Gαi, which is enhanced by PKA-mediated receptor phosphorylation, leading to a decreased affinity for the Gαs protein. For β_1AR, PKA-induced receptor phosphorylation instead acts to increase PLB and troponin I activation, further inducing Ca^{2+} release [156,157]. These set a precedent for negative feedback mechanisms in β_2AR, but not β_1AR; where G protein signalling relies more on β-arrestin and other mechanisms to downregulate signalling.

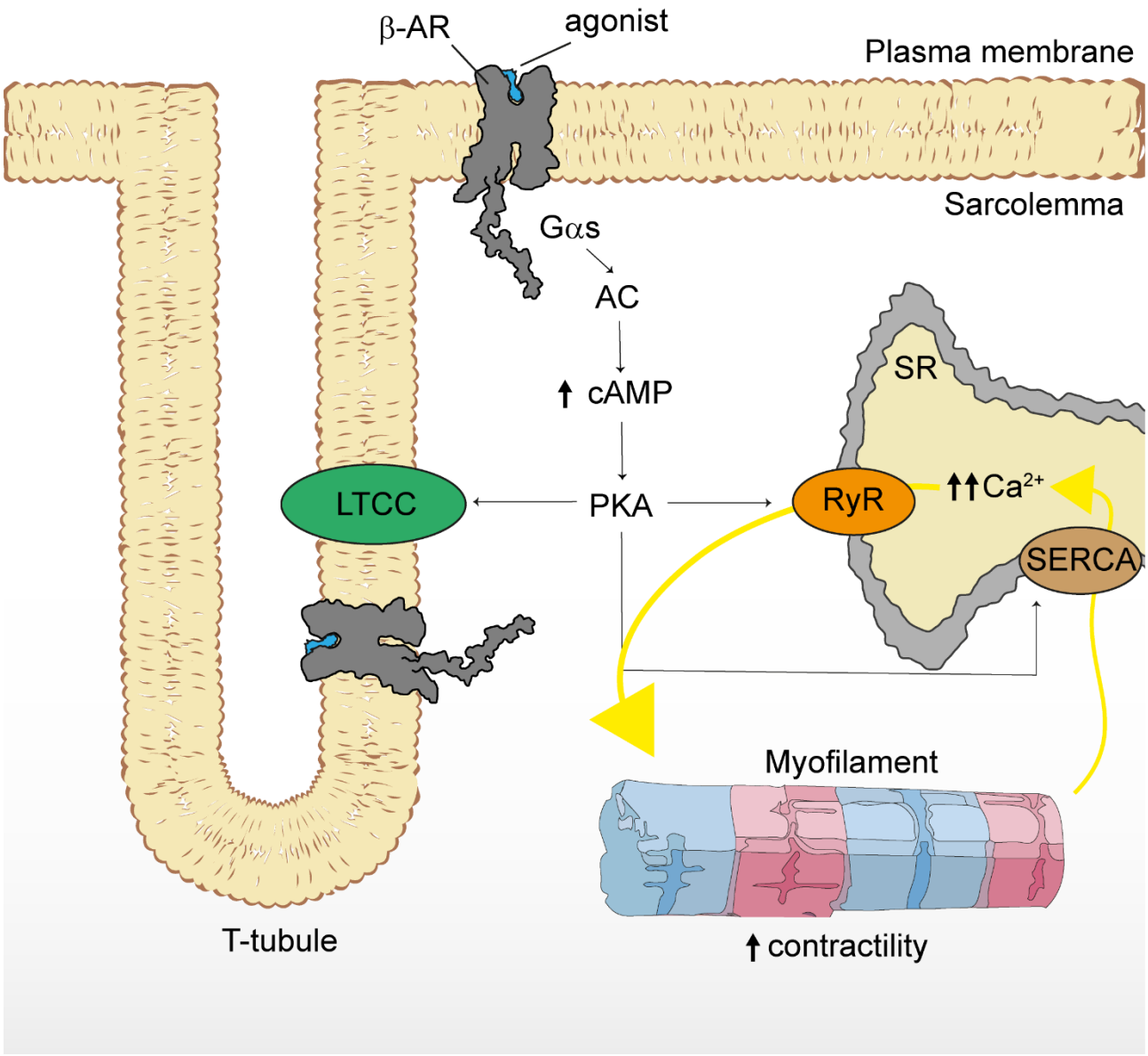

Figure 1.9 β-adrenergic control of cardiac myocyte contractility. Contractility is induced after stimulation of β-adrenergic receptors by endogenous catecholamines, such as adrenaline. Adrenergic-receptor signalling increases cAMP levels by activation of G proteins (Gαs) and downstream adenylyl cyclase (AC). cAMP activates protein kinase A (PKA), leading to phosphorylation and activation of L-type calcium channels (LTCCs) and Ryanodine receptors (RyR) at dyadic junctions, connecting the T-tubules to the sarcoplasmic reticulum (SR), respectively. Activation of RyR leads to Ca^{2+} leakage from the SR and PKA activation of SERCA induces a positive feedback loop in calcium release from the SR - stimulating myofilaments to contract in the myocyte.

Compartmentalisation of β_2AR is well established [158,159], however the extent of receptor compartmentalisation in β_1AR signalling is less well understood. In addition to β_2AR, β_1AR has

been detected in lipid rafts and the concentration of receptor localised in lipid rafts and cholesterol rich domains is increased after isoprenaline stimulation [160,161]. Wypijewski et al. found that stimulation of β_1AR with a specific agonist increased local concentrations of signalling proteins such as cavin-1 in caveolae [162]. Caveolae are small, balloon-shaped invaginations of a cell membrane, composed mostly of cholesterol and sphingolipids [163]. That act as scaffolds for protein signalling and act as endocytic vesicles [164,165]. Cavin-1 is crucial in stabilising caveolae and in mouse models of cavin-1 KO, cardiac muscle exhibits an almost complete loss of caveolae [166,167]. These studies suggest a role for β_1-adrenergic receptor signalling compartmentalisation in specialised structural domains.

β_2AR produces a smaller cAMP signal in the heart when compared to β_1AR [78,168,169], however β_2AR signalling has the ability to couple both inhibitory and stimulatory cAMP G proteins and has a higher affinity for β-arrestin. In contrast to β_1AR, which is expressed ubiquitously across cardiac myocytes [75], β_2AR localisation has been contested in the last decade. Some groups suggest that β_2AR is primarily expressed in non-caveolar t-tubule membranes [170], whereas others find functional roles primarily in caveolae across the sarcolemma [171]. More recent studies find that the localisation is dependent on the ligand, disease state and cell type; finding that β_2AR expression is altered between the t-tubules and sarcolemmal crest (basement membrane) after stimulation and that this action is disrupted in disease states [159,172].

1.5.4 Compartmentalisation of β-AR signalling molecules in cardiac myocytes

In cardiac muscle, after noradrenaline activation of Gαs through β-adrenergic receptor signalling, adenylyl cyclase is upregulated. As such, the localisation of adenylyl cyclases and cAMP is tightly regulated in cells, so that signalling can occur with high localisation efficiency

and speed. Phosphodiesterases (PDE) catalyse the hydrolysis of the phosphodiester bond in cAMP, generating AMP and attenuating cAMP signalling. There are 11 PDE families in mammals, which act to hydrolyse both cAMP and another cyclic nucleotide, cGMP [173]. After β-AR activation and signalling, PDE4 is recruited to sites of receptor activation and thus, cAMP production, acting to control sarcoplasmic Ca^{2+} by downregulating PKA signalling [174].

Zaccolo et al. demonstrated this using genetically encoded FRET-based biosensors, where β-AR stimulation in neonatal rat cardiac myocytes elicited only local concentrations of cAMP, proximal to the receptor [175]. This production of cAMP was disrupted but not abolished by PDE activity[175,176]. Using simulations, Yang et al. found that PDE activation alone in cardiac myocytes was not enough to compartmentalise the cAMP signal [177]. Sufficient cAMP gradients were only induced by PDEs on the introduction of anatomical barriers in the simulation models, suggesting that spatial compartmentalisation is required in addition to activation-based compartmentalisation. These described mechanisms are in place to control the localisation, duration and amplitude of adrenergic receptor and cAMP signalling.

Agonist-dependent desensitisation occurs through GRKs, which phosphorylate GPCRs and lead to increased binding of arrestins. GRK2 and GRK5 are the most abundant isoforms in cardiac tissue [93,178], with GRK2 knockout leading to embryonic lethality of mice - due to underdeveloped cardiac tissue . In healthy cardiac myocytes, physiological β-adrenergic receptor desensitisation through β-arrestin acts to reduce catecholamine-induced stimulation, reducing Gαs signalling. This acts as a negative feedback mechanism to uncouple G protein signalling after chronic stimulation, resulting further in receptor downregulation on the plasma membrane by internalisation [179-181].

βarr2 been suggested to have a cardioprotective role in adults [182,183]. This is due to a decrease in cardiac myocyte function, preventing chronic catecholamine stimulation and reducing the likelihood of tachycardia or apoptotic cell death [183]. In disease states, the actions of β-arrestins are less well understood, as signalling is a multifaceted process and depends on the arrestin isoform, receptor and cellular model investigated.

Lastly, the occurrence of adrenergic compartmentalisation has been studied in models of heart failure, suggesting a role in the proliferation of this disease. In chronic heart failure, Wright et al. found that β_2ARs redistributed from t-tubules to the basement membrane, which disrupts the formation of functional signalling units with adaptor proteins [184]. This reorganisation means that an insufficient cAMP gradient was maintained, due to a lack signalling in proximity to the SR and myofibrils. Confocal microscopy and immunoblotting elucidated remodelling changes in the rat cardiac myocytes 8-16 weeks post myocardial infarction. This included a decrease in t-tubule number and depression of adenylyl cyclase activity [184]. As such, cAMP production was suppressed, further decreasing the contractive output of the cells, which could not be recovered with *in vivo* gene therapy. These results suggest that localisation of the β_2AR is empirical in physiological cardiac function, and that changes in their distribution can have long-term, potentially irreversible effects on health.

1.6 β-ADRENERGIC RECEPTORS IN HEART FAILURE

1.6.1 Heart Failure

Defined as the inability of the heart to reach sufficient cardiac output to meet physiological metabolic demands, Heart failure (HF) describes a plethora of diseases and is a leading cause of death in the modern world. The British Heart Foundation estimates that 1-2% of the

population suffers from chronic heart disease [185], with males over age 65 being the predominantly affected group. The causes of HF vary, ranging from hereditary mutations, lifestyle risk factors such as obesity and co-morbidities such as hypertension. Heart disease often goes undocumented until a major event, such as a myocardial infarction, results in hospitalisation and the underlying causes are noted. Infarctions can lead to tissue necrosis, remodelling and impaired function of the heart and surrounding vasculature.

Secondary features of HF include sympathetic hypersensitivity, in an attempt to maintain equilibrium. Here, the adrenal medulla secretes excess catecholamines (such as adrenaline) in response to the reduced capability induced by the primary cause of HF [186]. Excess catecholamine release also leads to structural remodelling of the cardiac myocytes, as a compensatory mechanism to signal more efficiently.

Excessive β-AR stimulation induced by chronic catecholamines is often the driving force behind these effects, as its activation induces transcriptional changes in morphology, apoptosis and metabolism [187,188]. To combat these changes, β-blockers (β-AR antagonists) are commonly used to inhibit the remodelling changes induced in HF and are one of the most commonly used drugs in the world [189,190]. The mechanism of many β-blockers is still not fully understood, however the principle is to reverse the changes induced by HF. Mammalian models of heart failure have been particularly enhanced in recent years by the advent of super resolution microscopy, as the pathophysiology can be visualised with a spatial resolution enough to identify the nanoscale changes in protein clustering, t-tubule geometries and calcium signalling [191,192].

1.6.2 β-adrenergic receptors in Heart Failure

β-ARs are a vital receptor family in cardiac tissue with complex signalling capabilities, so present many opportunities for failure. HF is indeed characterised by dysregulation of β-AR signalling pathways and decreasing contractility, which is mediated by a reduction in β_1AR density on the membrane [193-195], loss of signalling localisation and chronic receptor desensitisation [196]. The increased decoupling from G proteins after chronic stimulation of β-ARs leads to increased GRK2 expression in cardiac myocytes, through arrestin-mediated MAPK signalling and binding of proteins to nuclear transcriptional regulators [93,197,198]. This finding has been reported in patients with long-term HF [196], leading to a reduction in Gαs signalling and subsequent cAMP production and PKA activation and ultimately a reduction in myocyte contraction (**Figure 1.10**). This has been confirmed in mouse models of HF, where cardiac myocyte-restricted overexpression of GRK2 significantly decreased β-AR signalling and myocyte contraction [55,199]. GRK2 inhibition has been suggested as a potential therapy for treating HF and studies in rats and dogs have further suggested this may be viable [200-204].

Increased β-arrestin activity means increased receptor internalisation and subsequent targeting by ubiquitin ligases for receptor degradation. For chronic β_1AR stimulation, the degradation pathway seems to take precedence [205], perhaps to reduce the continuous Gαs signalling. Overexpression of β_1AR in cardiac tissue during HF has adverse consequences, exacerbating catecholamine-induced hypersensitivity and further decreasing contractility [170,206,207]. β_2AR signalling changes in HF are often confounded due to studies finding contradictory results. This furthers the concept that β-AR signalling can be complex, and those studies' experiment design, cell type and environment should be taken into consideration.

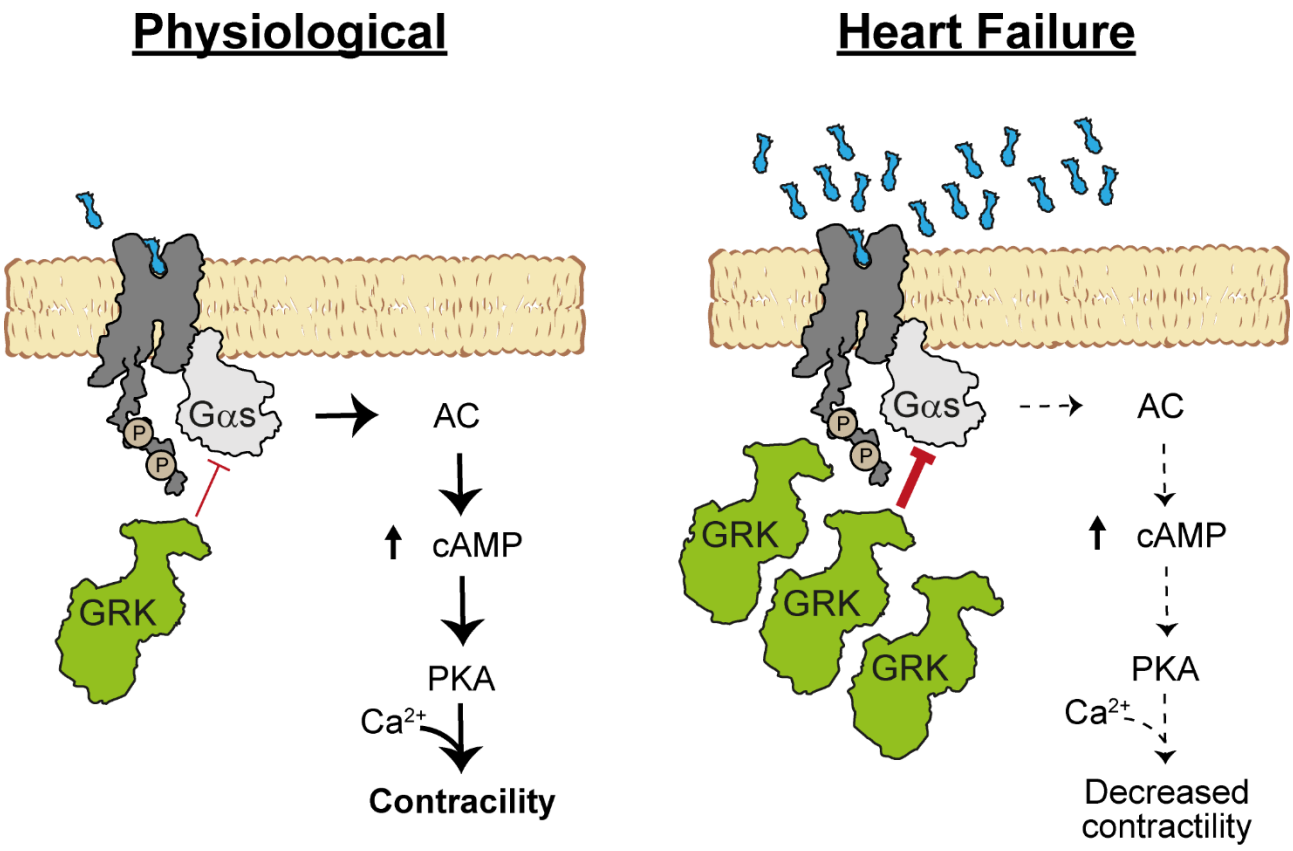

Figure 1.10 β-adrenergic heart failure. Under physiological conditions, catecholamines activate β-adrenergic receptors, resulting in Gαs activation - stimulating adenylate cyclase (AC) to produce cAMP. cAMP then activates protein kinase A (PKA) and regulates different intracellular substrates, exerting contractility via inotropy and chronotropy. GRKs regulates G protein signalling and heart contractility by phosphorylating receptors and increasing β-arrestin signalling, which suppresses the G protein response to basal levels. During heart failure, increased circulating catecholamines (blue) lead to hyper-activation of β-adrenergic receptors and excessive upregulation of GRKs – thus causing excessive G protein desensitisation and a chronic decrease in contractility.

A consistent finding is that β_2AR signalling is altered during HF, and that there is a relocation of the β_2ARs in the t-tubules of cardiac myocytes to the sarcolemmal crest, where a diffuse cAMP response is generated across the cell, causing a loss of the more specific activation observed at calcium dyads in tubules [150]. It is still debated whether β_2AR overexpression in the cardiac tissue is cardioprotective or not, with some groups reporting amelioration of HF symptoms in transgenic mice expressing high β_2AR levels in cardiac myocytes [202,208,209]. Rengo et al. even

found evidence that gene delivery of β_2AR improved contractility and corrected maladaptive programming in heart, promoting angiogenesis [202]. Inversely, β_2AR overexpression has led to spontaneous cardiac dysfunction and has been associated with higher mortality by other groups [210-212]. The patient context is important in all of these studies, as aged human populations find associated comorbidities more frequently with HF than in healthy animals and younger adults [210].

1.6.3 β-blockers

The initial elucidation of β-ARs in decreased heart contractility led to therapeutic interventions with agonists such as adrenaline and dobutamine, in an effect to increase inotropy. These attempts were quickly curtailed when it was found that stimulating receptors exacerbated symptoms [213], furthering arrythmias and hypertension . Synthetic agonists for β-ARs, such as isoprenaline, are instead used for the treatment of bradycardia (slow heart rate) or heart arrest, due to their mimicking of natural catecholamines such as adrenaline.

Blocking β-ARs has been achieved pharmacologically since the 1960s, with propranolol and pronethalol being used in the treatment of angina and tachycardia [214]. β-blockers equilibrate β-AR signalling in preventing chronic GPCR activation by adrenal catecholamines, providing an excess of available, high-affinity antagonist to compete with the cognate receptor binding pocket. The reduction in receptor signalling is achieved by blocking the deleterious effects of chronically-activated G protein in the heart, reducing receptor phosphorylation by GRKs and downstream receptor down-regulation [215].

Functionally, β_1-selective blockers act to reduce cAMP production and are known as cardio-selective β-blockers since their primary location of effect is the heart. In reducing the receptor availability by competing with agonists, a decrease in adrenergic tone is achieved. This reduces chronotropy and inotropy by decreasing the cAMP production of Gαs [215]. β_1-blockers also have action in the renal system, due to high levels of β_1AR expression in the kidneys. This aids in antagonism of cardiac output, as renin release and creation of angiotensin II is dependent on cAMP signalling [216,217]. In antagonising this, β_1-blockers reduce stroke volume and decrease cardiac load.

β_2-selective blockers are often associated with increased side-effects, due to the more ubiquitous expression of β_2AR in the body. They work similarly to β_1-blockers but block the effects of catecholamines systemically, which has indirect effects on multiple physiologies. By preventing sufficient smooth muscle relaxation in the lungs, underlying diseases such as asthma and COPD can be exacerbated [190]. In the CNS, β_2-blocking decreases the sympathetic acute stress responses ('fight-flight-freeze') - which has been shown to decrease anxiety and tremors [218]. This however also decreases sympathetic control of hypoglycaemia, which has contraindications with diseases such as diabetes. As such, β_2-blockers such as metoprolol have been used as performance-enhancing drugs (PED) in sports that require a lowered heart rate and steady hand, such as snooker or archery and have been banned in competitions such as the Olympics [219,220].

1.6.4 Alternative β-AR treatments for HF

Instead of treatments that interfere directly with β-adrenergic receptor pharmacology, some treatments intervene in HF by targeting downstream signalling cascades of β-ARs. β-blockers are effective in treating HF; however, β-blockers are associated with long-term side effects and have less impact on reversing the remodelling changes seen in the heart. Thus, they act more to stabilise the underlying pathophysiology of low receptor number and excess GRK2, not correct it.

Of note, paroxetine, a selective serotonin reuptake inhibitor (SSRI), has micromolar affinity for GRK2 and has been shown to improve ventricular contraction with chronic HF [221], independent of its SSRI functionality. Although paroxetine is a non-ideal drug candidate due to its use its treatment of depression and treatment of neuropsychological conditions, small molecule agents are in development to produce selective GRK2 inhibitors for the treatment of HF [222,223].

For targeting GRK2 directly, more recent studies are using RNA aptamers, single-stranded RNA (ssRNA) molecules which bind to complementary targets with high affinity conjugated to small-molecule drugs, to target the pathway [73,224]. Additionally, gene therapies are being developed for βARK-ct, a kinase which binds to Gβγ and also acts as a GRK2 peptide inhibitor [225]. In transgenic mice, those that expressed βARK1 showed enhanced contractility and sensitivity to acute adrenergic stimulation , whereas an increase in transgenic GRK2 decreased contractility and furthered HF. GRK2 inhibition upregulates receptors by removing the desensitisation/ internalisation stimulus and has been shown to resensitise receptors [203,204].

Some groups have shown that the co-treatment of β-blockers and GRK2 inhibitors improves tertiary symptoms of HF, such as insulin resistance [150,201]. It remains that those pharmacological treatments are most effective in treating HF once it has reached critical levels, but lifestyle

choices are likely to have similar if not greater impact on the prevention, treatment efficacy and future prognosis of the disease. De Lucia et al. found that long-term caloric restriction increased β_1AR density on the plasma membrane and improved inotropy in animal models of HF [150]. Additionally, healthy lifestyle changes are well-known to reduce the likelihood of HF [226-229].

With high attrition rates in drug discovery and associated costs, new therapeutic approaches are needed, but should be approached with caution. We still have much to learn about how these receptors signal with downstream proteins in the cell. Therapeutic avenues should be co-researched with new, advancing methodologies that can study GPCRs in live cells on the spatial and temporal resolutions where they exert their effects. Here, direct visualisation of protein-protein interactions and localisation of signalling nanodomains might offer new therapeutic targets in addition to better describing the landscape on which new drugs exert their effects.

1.7 OPTICAL METHODS TO STUDY β-ADRENERGIC RECEPTOR DYNAMICS

1.7.1 Fluorescence

Fluorescence is a term used to describe the vibrational relaxation of an excited-state fluorophore. A fluorophore is an organic molecule that has the ability to absorb and re-emit photons at different wavelengths. When a fluorophore absorbs a photon of particular wavelength and energy, electrons in atoms of the fluorophore absorb the energy and are excited from a ground state to an excited state, which lasts on the order of nanoseconds [230]. Energy dissipates through the molecule which can lead to re-emission of the photon with lower energy, which can be visualised as a fluorescent signal as the molecule returns to the ground state. The transfer of energy between excitation and emission to the fluorophore results in a longer wavelength photon emitted. Fluorophores can cycle excitation-emission sequences repeatedly

and the quantum yield describes the efficiency that a fluorophore emits absorbed photons as fluorescence.

The quantum yield is equal to the emitted photons relative to absorbed photons and thus has an upper limit of 1. Fluorophores cycle this process until they are photobleached or become quenched and fluorescence is not detected. Quenching occurs as a result of interactions of the fluorophore with its local molecular environment, such as a plasma membrane or buffer, which can lower the quantum yield. Photobleaching describes the process whereby a fluorophore interacts with oxygen or other surrounding molecules that cleave covalent bonds, photochemically altering the fluorophore into a non-fluorescent substrate [231-235].

1.7.2 Resonant Energy Transfer (RET) methods

Whereas pharmacological and biochemical methods have been instrumental in dissecting the basic mechanisms of GPCR signalling, they typically require membrane disruption and cannot be applied in live cells to study GPCR dynamics [236]. An important advance in the field was the introduction of biosensors based on fluorescence resonance energy transfer (FRET), which is now used routinely to monitor GPCR signalling in living cells, with ensemble and single-molecule resolution [48,65].

Often described as a 'spectroscopic ruler', FRET is a physical phenomenon that consist of the non-radiative transfer of energy between a 'donor' and an 'acceptor' fluorophore located in close proximity, generally less than 10nm [237,238]. Besides a short distance, many other conditions mut be met for FRET to occur, including: a favourable orientation between the fluorophores, a sufficient overlap between their emission and excitation spectra and external excitation with a laser. Bioluminescent resonance energy transfer (BRET) is the bioluminescent

equivalent of FRET, which utilises modified luciferase enzymes to generate light through oxidation of a specific substrate [239-241]. Given the short proximity required for RET, it can be exploited to provide accurate measurements of protein-protein interactions as well as conformational changes in a protein of interest. For GPCR signalling, RET methods have been used to monitor key steps in GPCR signalling in live cells, from ligand binding through to activation of downstream effectors like PKA [240,242-250]. In fact, these experiments were crucial in evidencing our understanding of cAMP compartmentalisation after GPCR stimulation [170,251].

1.7.3 Single-molecule microscopy; vs. ensemble methods

Single-molecule microscopy (SMM) describes a broad range of advanced microscopy techniques that offers several advantages over ensemble methodologies. An important limitation of FRET and BRET is that they often require overexpression of the investigated molecules, which can alter their pharmacological profile [252]. Secondly, ensemble methods measure the average behaviour of potentially millions of molecules. Since they are not synchronised, it precludes direct estimation of kinetic rates [253]. In contrast, SMM can directly visualise and interrogate individual fluorescent molecules at physiological concentrations; this allows estimation of kinetic parameters such as association and dissociation rates. Moreover, the capture of rare and transient events is often hidden in ensemble measurements, yet these events may be crucial in the pathophysiology of disease and early detection of biomarkers. With a spatial resolution of tens of nanometres, the nanoscale organisation of proteins of interest can be studied. SMM does suffer from drawbacks too, such as the requirement of complex and time-consuming computational analyses.

1.7.4 Single-molecule FRET (smFRET)

The use of FRET to study single molecules was first reported in 1996 by Ha et al. [254], who proposed its application to study rotational and conformational changes in DNA. Since then, single-molecule FRET (smFRET) has been applied to study a variety of biological systems with purified fluorescent proteins *in vitro*. In a typical smFRET experiment, purified receptors or other proteins of interest are labelled at two distinct sites via insertion of a suitable pair of small, organic fluorophores or fluorescent proteins (FP). The proteins are then immobilised on a glass coverslip and conformational dynamics can be monitored in real-time by monitoring FRET changes between the fluorophores [255].

smFRET has elucidated some interesting mechanisms of β_2AR activation. Conformational states of β_2AR were found to exist in dynamic equilibrium between at least two configurations, that extended to three distinct states only upon full-agonist addition [256]. This finding was expanded in the last decade using β_2AR reconstituted in phospholipid nanodiscs labelled with an environmentally sensitive fluorophore (Cy3) on TM6 [257]. In the absence of G protein and ligands, receptors were found to occupy mostly inactive states, but sporadically alternate into short-lived active states. Stimulation with isoprenaline, a full agonist, shifted receptors into the active state, with inactive states sporadically entered for short periods of time. An analysis of these dwell times in the two FRET states revealed complex transition kinetics, in which ligands act to stabilise the active state long enough for G protein to bind [257].

Gregorio et al. placed fluorophores on the cytoplasmic ends of TM4 and TM6 of β_2AR, to determine the effect of Gαs binding to conformational receptor dynamics with purified proteins [258]. In the absence of G protein, agonists with increasing efficacy were found to cause a reduction in FRET proportional to their efficacy; with a 4 Å shift of TM6 from TM4 observed

from activation with full agonists. The addition of Gαs stabilised this shifted state, lengthening the time that this low FRET state was occupied, supporting our understanding of G proteins acting to maintain active GPCR conformations [258].

These experiments can capture rare and transient states missed by ensemble approaches and provide good quantification of the temporal and rotational changes in proteins. They do however often lack a cellular context – which is crucial for membrane protein biology. Much like X-ray crystallography, smFRET takes proteins out of the membrane; this disrupts key lipid and inter-protein bonds that occur in nature, meaning that states observed by smFRET may have less relevance in live cells. To combat this, many groups are employing techniques to solubilise proteins in native annular lipids [259-262].

Accurate distance measurements in smFRET can be perturbed by the fluorophore used and orientation of the dyes. More important in smFRET is studying the changes between different states that a GPCR can occupy. Additionally, further biochemical modifications are often required to immobilise molecules for smFRET measurements, often via biotinylating, meaning that comparisons to native proteins remain contentious. Lastly, in order to obtain accurate statistics from these measurements, lots of photons are required, which means a high laser intensity and phototoxicity to the species of interest. As such, smFRET is less well suited to probe kinetic events longer than the average lifetime of the fluorescent dyes.

1.7.5 Fluorescence correlation spectroscopy

Fluorescence correlation spectroscopy (FCS) measures the intensity fluctuations as fluorescent species diffuse across a small, confocal detection volume. Obtained data is used to perform a time-dependent autocorrelation, providing quantitative information about the average

number, diffusion speed and dwell time of fluorescent molecules in the detection volume. This allows quantification of the concentration, stoichiometry and diffusion of heterogenous protein mixtures. An extension of FCS is fluorescence cross-correlation spectroscopy (FCCS), which measures multiple emission channels and finds important application in the study of protein-protein interactions. These methods have been employed to investigate various aspects of β-AR signalling, including an approximation of β_2AR diffusion heterogeneity on the PM [263-265]. Photon-counting histograms are also utilised in FCS to estimate the size of protein complexes. This has been employed to identify transient dimers and higher-order oligomers of β-adrenergic receptors [265].

The formation of lipid nanodomains has been contested in live cells, and FCS has been crucial in determining their existence. By combining FCS with stimulated emission depletion (STED) microscopy, a super resolution technique which employs a secondary depletion beam to overcome the diffraction limit, increasing resolution; researchers were also able to monitor the diffusion of sphingolipids and GPI-anchored proteins with nanometre precision [231]. It was found that these molecules were trapped in nanodomains on the membrane of <20nm diameter, residing there for ~10-20ms. Cholesterol is suggested to play a role in the formation of these nanodomains, as it is depleted from them and present only on the boundaries [231]. This data is consistent with the proposal that the plasma membrane is composed of discrete, transiently diffusing lipid-protein complexes as opposed to stable domains, which was initially described in the fluid mosaic model.

As fluctuations are detected by molecular diffusion, FCS is not suitable for studying immobile species and as such, complementary biophysical techniques to study receptor dynamics. This is important given the observations of molecular trapping and GPCR immobility in determining

signalling outcomes [253,266,267]. The high temporal resolution (<10μs) and efficiency at low, endogenous expression levels make FCS an ideal technique to study GPCR oligomerisation and ligand-binding at physiological concentrations in real time. Particularly, this technique has contributed extensively to our understanding of ligand-GPCR kinetics [264]. Lastly, although FCS measures diffusion through a small confocal pinhole, it is not strictly a single-molecule technique, as autocorrelation analyses build ensemble measurements from the single fluorescent species. As such, rare and transient events can be lost amongst the averaging.

1.7.6 Single-molecule microscopy; Self-labelling dyes

Richard Feynman first proposed the idea of directly observing single molecules over half a century ago. In 1976, Hirschfield et al. attached fluorescent proteins to a single γ globulin molecule in solution, proving that the concept was possible [268]. In 1989, Moerner and Kador detected the absorption spectra of single pentacene molecules organised in *p*-terphenyl crystals [269]. Over the last three decades, the development of sensitive cameras, the synthesis of brighter, photostable fluorophores and advances in image analysis platforms have made visualising and manipulating individual molecules more accessible to the research community. Due to these improvements, we are now not limited to studying biological processes in solution but can importantly image in living cells and tissues [270].

Many labelling strategies exist for SMM, including incubation of proteins of interest with fluorescently labelled antibodies, tagging them with fluorescent ligands or genetically encoding fluorescent proteins onto them. A major advance in the field was the introduction of so-called self-labelling tags, such as SNAP, CLIP and Halo; which are genetically fused to a protein and react enzymatically with small, organic substrates that fluoresce upon this catalysis. SNAP is a

20kDa protein tag derived from the human DNA repair enzyme O^6-alkylguanine-DNA alkyltransferase, which forms irreversible adducts with fluorescent benzylguanine derivatives [271].

CLIP was further engineered from SNAP and can label fluorophore-conjugated benzylcytosine derivatives [272], to allow orthogonal labelling with two different fluorophores. The Halo protein is a mutant of a bacterial dehalogenase that removes halogens from aliphatic hydrocarbons. A fluorescent molecule can be tagged to a chloroalkane linker and will form a covalent bond with the Halo tag. A schematic of how self-labelling proteins work can be found in **Figure 1.11**. Compared to other methods of protein labelling, self-labelling proteins allow for a broad choice of fluorescent dyes to conjugate, providing flexibility in experimental design. Additionally, the organic fluorophore substrates have a high fluorescence intensity and photostability compared to fluorescent proteins like GFP. Fluorescence is also initiated only when the label is added, giving temporal control and specificity.

1.7.7 Single-molecule microscopy; Single-molecule localisation microscopy (SMLM)

Single-molecule localisation techniques, such as direct stochastic optical reconstruction microscopy (dSTORM) and photoactivated localisation microscopy (PALM), rely on the temporal segregation of fluorophores obtained by stochastically activating only a subset in a given time window. dSTORM exploits the spontaneous blinking of suitable organic fluorophores [273,274]. Under favourable environmental conditions, these fluorophores randomly switch between a dark and a fluorescent state. Since only a small fraction of fluorophores are visible at any given frame of an image sequence, their position can be determined with high

accuracy by 2D Gaussian fitting. This process is repeated thousands of times, resulting in the reconstruction of high-resolution images.

dSTORM has been successfully employed to investigate the organisation of GPCRs in cells and tissues. For instance, Szalai et al. employed dSTORM to investigate corticotropin-releasing hormone type 1 receptors in the mouse hippocampus [275]. More recently, our group applied dSTORM to study the nanoscale organisation of metabotropic glutamate receptors in the mouse cerebellum [276]. This approach revealed that mGluR4s are localised in small nanodomains within pre-synaptic active zones, where they are found in close proximity to voltage-dependent Cav2.1 channels and Munc18-1, a component of the secretory machinery. This tight spatial organisation seems to be regulated to enable fast inhibition of glutamate release by mGluR4 at the synapse.

PALM is based on a concept similar to that of dSTORM, but utilizes photoswitchable or photo-convertible probes instead. These probes can be activated by excitation with low-intensity near-UV light [234]. The molecules carrying the probes are then localised and rapidly brought to a dark state, usually via photobleaching. PALM has been employed to analyse GPCR clustering on the plasma membrane in a study by Scarselli et al. [277]. This study showed that β_2ARs form pre-associated clusters on the membrane of cardiac myocytes with the participation of the actin cytoskeleton [277].

The described features make SMLM particularly useful for imaging densely packed cellular structures such as the cytoskeleton. Since image acquisition typically takes several minutes to hours, SMLM have only limited temporal resolution and, as a result, are often applied to fixed samples. Additionally, the stochastic nature of dSTORM often results in molecules being

counted multiple times, complicating quantitative analyses on determining oligomeric status of proteins.

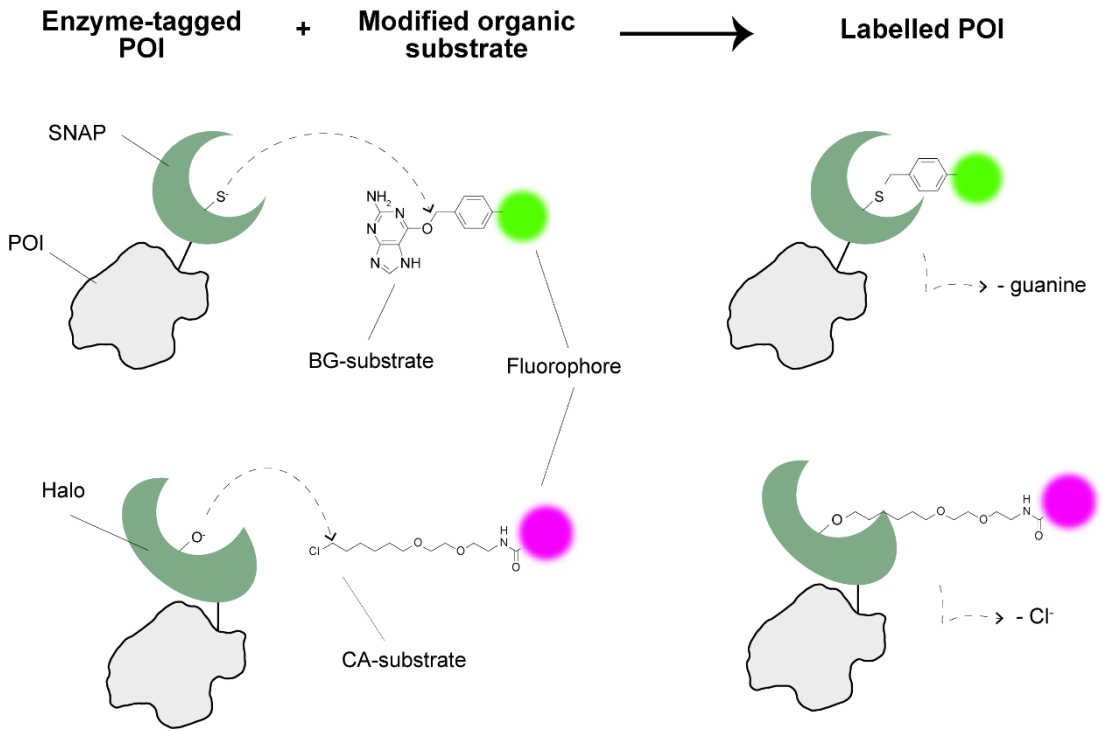

Figure 1.11 Covalent labelling of proteins of interest (POI) with self-labelling dyes. This schematic shows the fluorescent labelling of a POI with either benzylguanine (BG) or chloramine (CA) -conjugated fluorophores.

1.8 SINGLE PARTICLE TRACKING

1.8.1 Resolution

Microscopy is dependent on a characteristic known as the point spread function (PSF), which represents an image generated from a point source of light. The image produced by a microscope can be described as a convolution between the real object and the point spread function, defining how much the image becomes blurred in the microscopy experiment. In real experiments, the PSF can become locally distorted by imperfections in the imaging setup. The

PSF needs to be determined for experiments to account for these aberrations. In 2D, this is known as the airy disc. The airy disc can be fitted with a Bessel function of wave propagation from the intensity maxima, which is most often approximated by a Gaussian distribution [278].

Conventional optical microscopy is limited in its resolution by the diffraction limit of light. Resolution is described as the minimum distance between two objects that would allow them to be visualised as two distinct objects. Generally, resolution in optical systems is approximately half of the wavelength of light used for illumination, which approaches ~200nm dependent on the optical setup [279,280]. Many metrics can be used to equate resolution, including those of Sparrow, Rayleigh and Abbe, yet all agree that a larger numerical aperture lens and shorter wavelength yield higher resolution. Indeed, the radius of the airy disk radius (δ) can be approximated by these factors and is often considered as the standard resolution limit:

$$\delta = 0.61 \frac{\lambda em}{NA}$$

Where λem is the wavelength of the emitted light and NA is the numerical aperture of the objective. If point sources of light are separated below the airy disk radius, they appear too blurred to be defined as separate sources of light, by traditional methods.

1.8.2 Total internal reflection fluorescence microscopy

In a single-molecule experiment for detecting proteins which are expressed on or near the plasma membrane, total internal reflection fluorescence (TIRF) illumination is often the most effective methodology. This was originally detailed for microscopy in the 1950s [281], but demonstrations to observe the plasma membrane of live cells was accomplished decades later [282]. By totally reflecting a beam of light between two media that have different refractive indices,

an evanescent excitation field is generated. When collimated light propagates from one medium through another, incident light at the interface is either refracted through, at a deflected angle, or reflected from the interface.

Total internal reflection (TIR) only occurs when the propagating light encounters greatly different refractive indices, governed by Snell's Law (dependent on the two refractive indices and angle of light incidence at the interface). When light approaches the interface of the two materials at a sufficiently high angle (critical angle), the refraction direction becomes parallel to the interface and angles above the critical angle of light are reflected entirely (**Figure 1.12**). Although no light passes into the second medium in this case, the reflected light generates an electromagnetic field adjacent to the interface, into the lower index medium. The field is evanescent and decays exponentially in intensity with distance to the interface.

For live cell experiments, the evanescent field from TIRF extends ~100nm into the specimen media (lower refractive index) from the glass (high refractive index). Thus, only fluorophores within the evanescent field are excited, assuming they are in the spectral range excited by the wavelength of the illumination beam. Due to a lack of excitation in the bulk of the cell, TIRF confines the background fluorescence to a smaller area and achieves a higher signal-to-noise ratio (S:N ratio) than conventional epifluorescence (**Figure 1.12**). These features make TIRF an ideal choice to detect single molecules on the plasma membrane. Imaging is further enhanced by using a high numerical aperture (NA) objective lens, which has a high angular acceptance of incoming light, increasing the prospective resolution. Beneficial, also for single-molecule TIRF, is a detector which is capable of detecting low photon counts whilst minimising background noise, such as an electron-multiplying charge-coupled device (EMCCD).

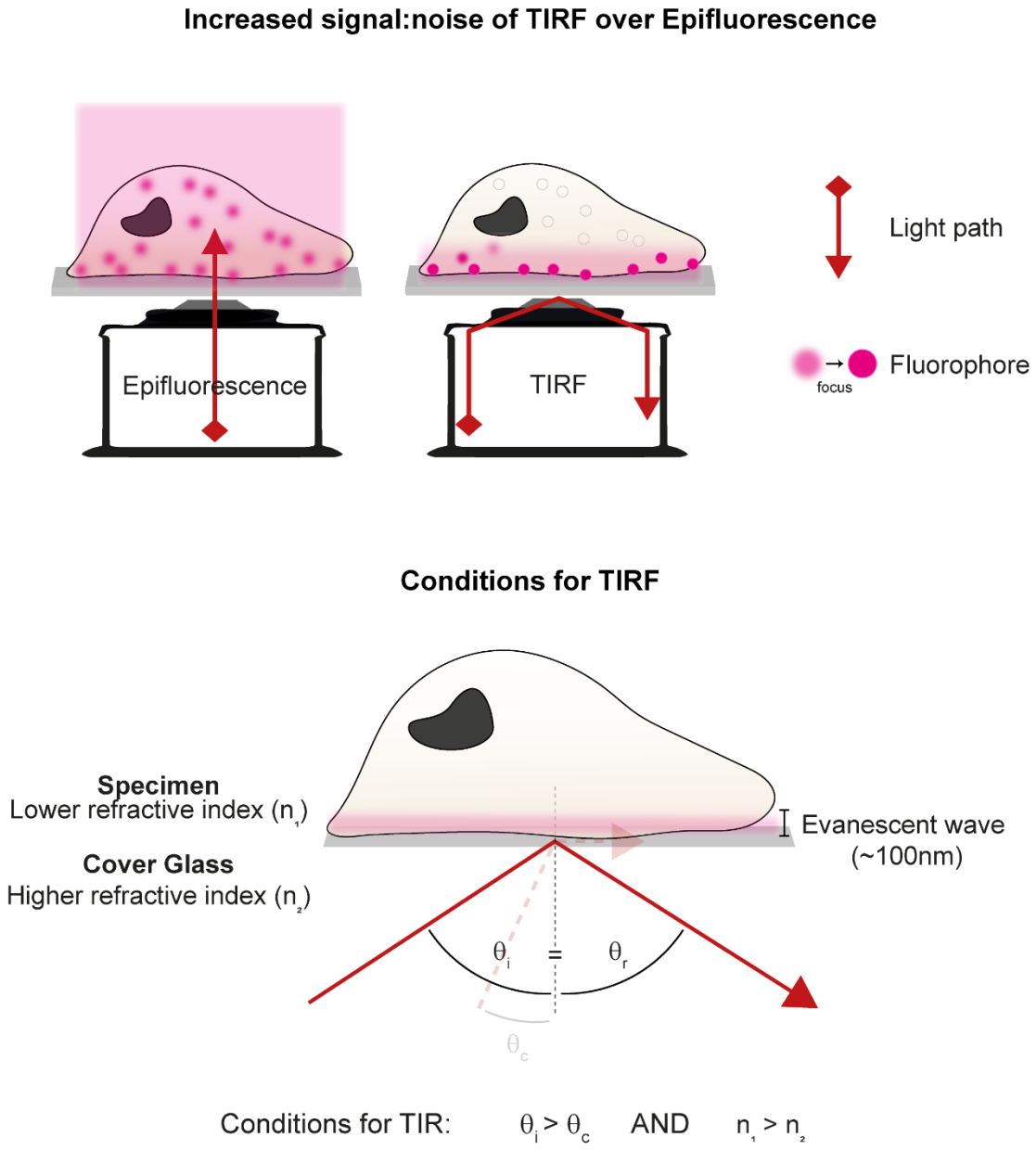

Figure 1.12 Total Internal Reflection Fluorescence (TIRF). (Top) Epifluorescence vs TIRF illumination for cells transfected with fluorescent proteins. Epifluorescence illuminates the whole sample via collimated light passing transverse to the imaging plane, which leads to excitation of all fluorophores in the light path. TIRF produces an evanescent excitation field, which excites only fluorophores ~100nm from the interface between the coverslip and the sample. This gives a superior signal-to-noise ratio, facilitating the study of membrane molecules. (Bottom) TIRF occurs at the interface between two media with differing refractive indices. When light of incident angle (θ_i) is greater than the critical angle (θ_c) the reflected light (θ_r) is totally internally reflected. This results in an evanescent electromagnetic field generated from the interface, with the intensity of the field decreasing exponentially with the distance from the interface.

1.8.3 Single-particle tracking (SPT)

Resulting images from single-molecule TIRF acquisitions contain fluorescently labelled proteins of interest, which appear as diffraction-limited spots. Image acquisition often represents only the first step in analysis and automated computer algorithms are used to detect the position of diffraction-limited spots below the diffraction limit. Although the spots appear much larger (~200nm dependent on wavelength and laser intensity) than the proteins of interest (~2-4nm for GPCRs), their position can be determined with nanometre precision by further localising the intensity maxima.

This is achieved by assuming, as theoretically described, that the light emanating from a point source decays according to a Gaussian distribution, as described in section 1.8.1. By fitting pixel intensities with a two-dimensional Gaussian distribution (**Figure 1.13**), accurate localisation of a single molecule can be determined. This is dependent on multiple factors, including the wavelength of the emitted light and the signal to noise ratio (S:N ratio) achieved with the microscopy setup. Theoretically, there is no limit to the localisation precision that can be achieved using this methodology, but values of ~10-30nm in space are typically attained for available fluorophores and technology [283].

This is around 10 times the resolution limit of conventional fluorescence microscopy methods like confocal, but also around 10 times the size of membrane proteins. As such, a limitation of this fitting is that molecules can only be localised at sufficiently low concentrations, typically < 1molecules/μm^2, as higher concentrations mean overlapping emission patterns and an inability to distinguish spots apart [2,253] (**Figure 1.13**).

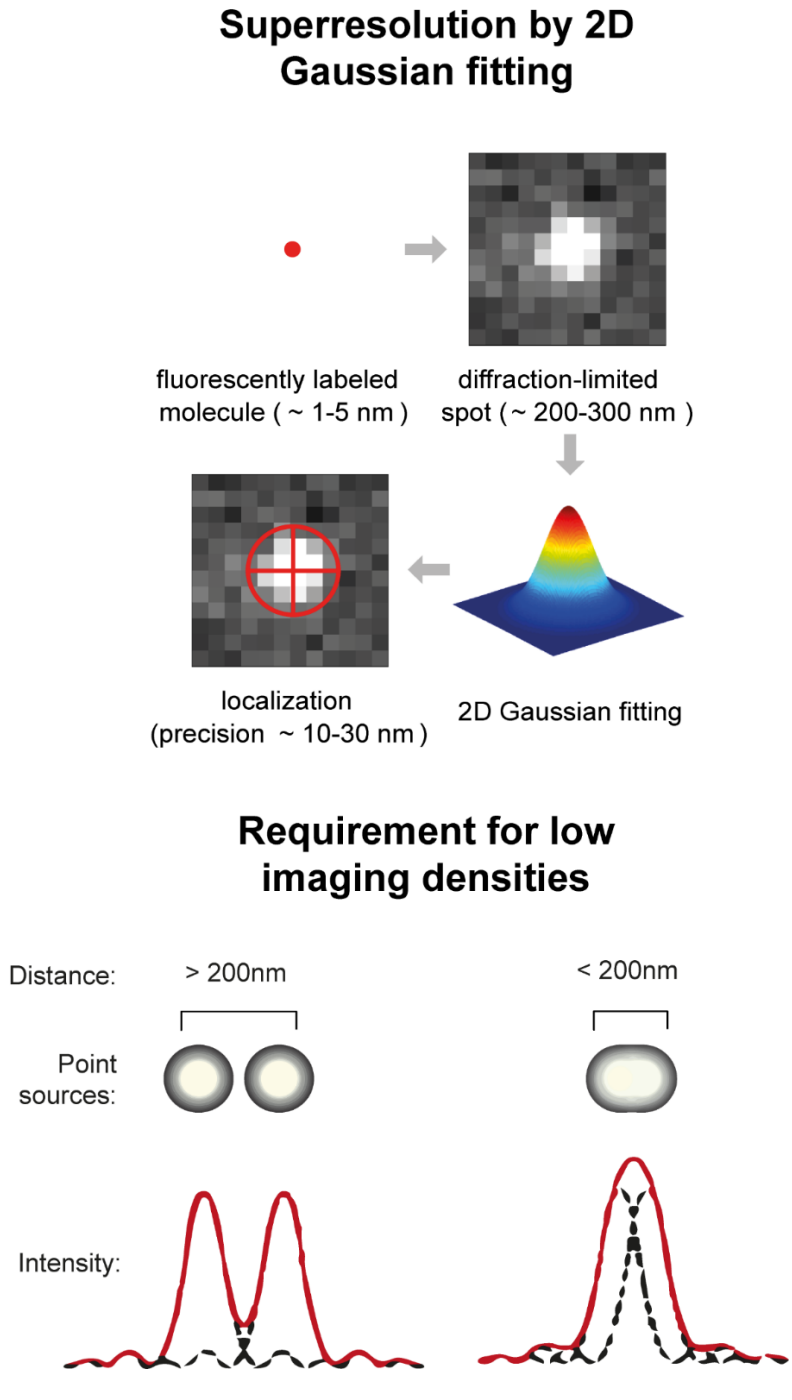

Figure 1.13 Localisation of single molecules for SPT experiments. (Top) Due to the diffraction of light, point sources of light appear as spots sized ~200-300nm on the plasma membrane, dependent on the numerical aperture (NA) of the system and wavelength of light. The location can be localised with higher precision by fitting a 2D Gaussian distribution over the spot. This principle is at the basis of many super-resolution microscopy methods and offers the opportunity to resolve objects to around ~20nm in space. (Bottom) Two diffraction-limited objects cannot be separated if their distance is less than approximately half their emission wavelength. This limits the resolution of conventional fluorescence to around the size of a diffraction-limited spot and requires point sources to be adequately spaced for super-resolution localisation methods to localise with high precision.

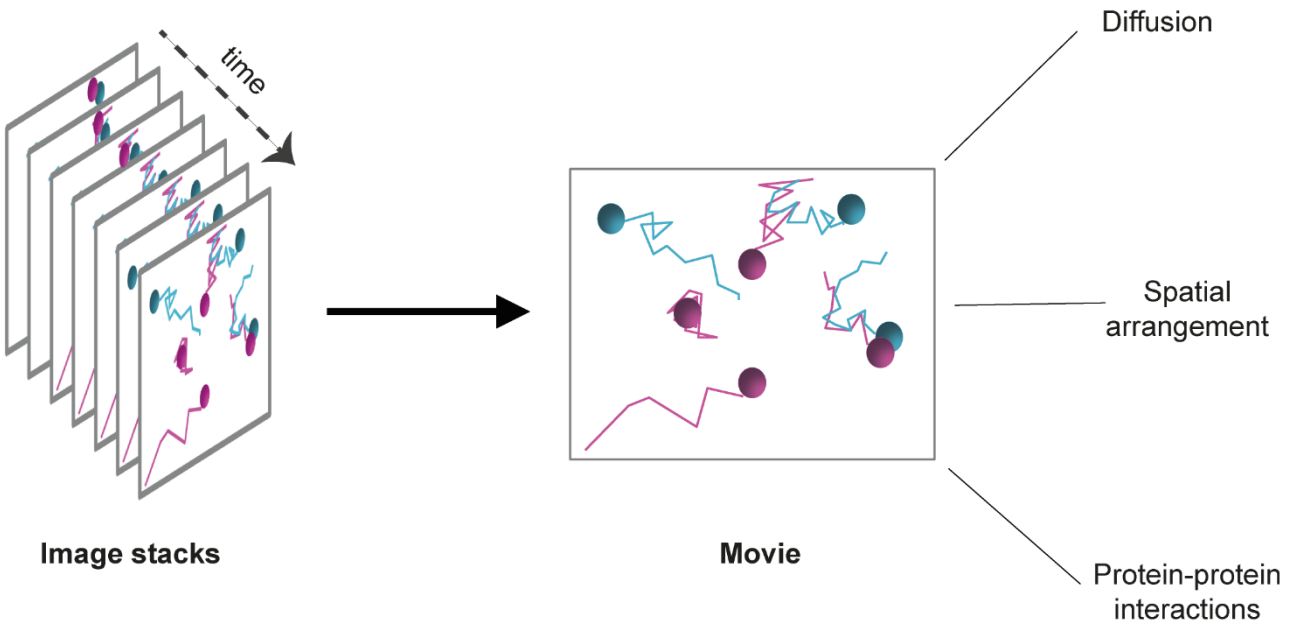

Figure 1.14 Single particle tracking. Workflow of the computational analyses in single-molecule TIRF imaging. After stacking images in time, automated single particle detection and tracking algorithms are used to follow fluorescently labelled molecules as diffuse on a live cell plasma membrane. Obtained trajectories can be further analysed to elucidate information about their diffusion, spatial arrangement or interactions with other molecules.

For live cell imaging, automated SPT algorithms are used to link all detected particles in an image sequence and reconstruct their trajectories over time (**Figure 1.14**). Perhaps the most powerful approach is multiple hypothesis tracking, which assigns a cost to possible events that a particle can undertake in a given frame [283]. This calculates a trajectory, given events such as: particles appearing, disappearing, merging and splitting of multiple particles and fluorophores blinking. By minimising the sum of all costs, a global solution with the highest probability is selected. As particle densities increase in SPT data, mathematically ideal tracking routines become computationally difficult. With increasing molecular densities, tracking a trajectory with high confidence becomes difficult, due to permutations becoming very large. To combat this, the minimisation of cost in SPT algorithms is not global over the whole image sequence, but instead works on a moving time window over the trajectory (~10 frames), so that any

inaccuracies in detection caused by overcrowding or other external factors are minimised. Obtained trajectories from SPT can be further analysed to elucidate information about their diffusion, spatial arrangement or interactions with other molecules.

1.8.4 Plasma membrane structure as it relates to SPT

In its most crude form, the plasma membrane (PM) is a phospholipid bilayer, which organises amphiphilic lipids to form a barrier for the cell. In reality, the PM is a complex architecture of lipids, laterally diffusing membrane proteins, axially diffusing adaptor proteins, cytoskeletal compartments and specialised membrane topologies [284,285]. These components are organised in space and time in accordance with cellular requirements to accommodate signalling, trafficking and cellular migration. The fluid mosaic model describes the membrane as a 2-dimensional viscous fluid with freely diffusing, randomly distributed particles . This model is now considered as vastly oversimplified [286]. Advanced optical and electron microscopy methods have visualised the membrane in 4 dimensions (x,y,z,t) with incredible precision in real-time, finding that proteins and lipids are organised into tightly regulated domains [285,287]. As such, models of the PM need to be widely adopted, which integrate these advanced imaging and mathematical approximations for diffusional properties and spatial organisation.

One of the first biological applications of single-molecule microscopy was to study the diffusion of GPCR diffusion on the PM. Suzuki et al. followed the diffusion of individually tagged μ-opioid receptors with gold nanoparticles at speeds of 25μs in a study now considered a historical milestone [287]. This study was empiric in developing the fence-and-picket model, which postulates that subcortical actin cytoskeleton and integral membrane proteins partition the PM into nanodomains of 40-300nm, acting to transiently trap diffusing membrane proteins and

lipids. Researchers found that receptors exhibit rapid hop diffusion as they jump between these small membrane compartments. The hypothesis is that the resulting segregation forms barriers for signalling molecules, increasing their spatial and temporal interaction probabilities, making signalling more effective.

Besides the cytoskeleton, previously described lipid nanodomains such as lipid rafts, clathrin-coated pits and caveolae are known to localise membrane proteins in nanodomains [288,289]. Lipid rafts are sphingolipid and cholesterol rich domains identified due to their resistance in detergent extractions [290,291]. On examination, these fractions were found to contain dense populations of membrane proteins such as the β_2AR and Gαs [161,162,277,292]. The existence of these domains in live cells remained a matter of debate for a long time, with confocal microscopy studies failing to visualise stable lipid domains on the PM [293]. A possible explanation for these findings is that lipid nanodomains are smaller and more dynamic than previously thought, meaning that optical methods which extend beyond the diffraction limit of light are required for their study [294].

Particularly important for GPCR signalling, clathrin-coated pits (CCPs) are invaginations of membrane phospholipids which are scaffolded by clathrin triskelion cages and cargo proteins. Much like caveolae in cardiac myocytes, these are important sites for GPCR signalling, but also act as primary endosomes for GPCR internalisation and trafficking [107,295-297]. These domains are now considered a novel site for GPCR signalling and especially for β-arrestin, however more advanced optical methods are required to fully elucidate their mechanism of action.

1.8.5 Diffusion

The orchestrated arrangement and diffusion of membrane proteins is required to convey signalling that is rapid, selective and specific to the needs of the cell. Brownian motion is the fundamental model for random motion of a molecule, due to thermally driven collisions, with surrounding molecules that exhibit an isotropic Gaussian distribution of displacements that spreads over time proportionally to the square-root of time. For a fluorescently labelled GPCR in the plasma membrane, collisions with water and membrane lipids lead to a continuous motion. Other proteins in the membrane and structural elements with affinities for the GPCR lead to departures from ideal Brownian motion due to their interactions [298,299]. This may lead to tethering, through covalent bonds, which leads to immobilisation or the formation of protein complexes. The cortical actin cytoskeleton is known to corral diffusion which leads to partial confinement, with proteins less likely to escape the actin mesh [300]. Although diffusion within a corral may be normal (scaling with sqrt[1]), the requirement to hop between them means that particles will explore space less effectively than if the boundaries were not there, in a process known as sub-diffusion.

The mean squared displacement (MSD) of a molecules position is often used to study their diffusion [301]. This is plotted as a function of a given time lag (Δt), which for microscopy is a multiple of the exposure time. For a given time lag, the squared displacements are averaged over the trajectory, to provide an average behaviour. For Brownian motion, where the trajectory has an ability to explore space in each direction equally, the MSD will increase linearly with time. If the MSD behaves linearly within the time window, a diffusion coefficient can be determined by fitting the slope of MSD as a function of Δt. These diffusion coefficients

are often not the most reliable measure of a molecules true motion, as they often occur on a not entirely flat surface (cell membranes are heterogeneous and can have invaginations).

Additionally, molecules are in constant motion - but only captured frames are observed - so a sufficiently high framerate (~30-40fps) is required to omit disparate lags in space. In a living cell, it is most likely that the diffusion of a single molecule does not have a linear relationship between MSD and time but rather a power relationship t^{alpha} where alpha is the 'anomalous exponent' for which the term of 'anomalous diffusion' has been coined. The slope of the MSD indicates either a restriction in movement (alpha<1), perhaps due to confinement in membrane nanodomains and also the presence of immobile molecules, or an active diffusion process (alpha>1) where molecules explore space more effectively. This could either represent a molecule undergoing sub-diffusion through an active mesh (alpha<1) or a protein travelling along a microtubule (alpha>1).

1.8.6 Protein-protein interactions

Another important application of single-particle tracking is the study of the stoichiometry of protein complexes. Two main approaches are commonly used for this purpose, the first of which is based on analysing the distribution of the intensities of the detected particles. In the case of a mixture of monomers, dimers and/or oligomers, the relative abundance of the individual components is estimated by mixed Gaussian fitting [267]. The number of fluorophores present in each spot can also be estimated by following their photobleaching over time. Since the photobleaching of each individual fluorophore produces a characteristic step in the intensity profiles, the initial number of fluorescent molecules can be estimated by counting the

number of bleaching steps. Appropriate controls, including individual fluorophores as well as monomeric and dimeric proteins, are usually used to calibrate and validate these analyses [267].

In addition, single-particle tracking is emerging as a powerful method to precisely characterise dynamic protein-protein interactions, such as those occurring among receptors and other membrane proteins. Since this approach allows researchers to simultaneously estimate the density of the labeled molecules and both the frequency and duration of their interactions, it can be used to derive microscopic association and dissociation rate constants [253]. A possible complication of this approach is the simultaneous occurrence of random colocalisations. However, it has been shown that a method based on the deconvolution of the observed colocalisation durations with those due to random colocalisations can be used to correct for this factor and efficiently estimate the durations of the underlying interactions [253].

1.9 SINGLE PARTICLE TRACKING STUDIES OF GPCRS

1.9.1 SPT studies of GPCR oligomerisation

In vitro studies of GPCRs, using smFRET, have been crucial in elucidating the dimerisation states, G protein binding and ligand kinetics. These studies however rely on the use of solubilised proteins. It is likely that local concentrations of signalling molecules, membrane lipids and cytoskeletal elements have impacts on signalling in the cell. By expressing GPCRs in native membranes and allowing complex interactions with their surrounding micro-environment in live cells, we can begin to understand how these proteins might interact naturally in our bodies.

Hern et al. first successfully applied SPT to investigate GPCR dimerisation in live cells, expressing muscarinic (M_1) receptors in Chinese hamster ovary (CHO) cells and labelling with

a high affinity fluorescent antagonist. They found that M_1 receptors were diffusing in the plasma membrane of CHO cells and that ~30% of receptors formed transient and reversible dimers, with an average lifetime of 500ms at room temperature [302]. A similar approach showed that N-formyl peptide receptors formed transient dimers in live cells and this study also characterised the association and dissociation rates of the receptor complexes. They found that ~41% of receptors existed as transient dimers, associating with a new receptor on average every 150ms and interacting for around 90ms [303].

Our group previously applied SPT approaches to the single-molecule visualisation of three prototypical GPCRs: β_1AR, β_2AR and $GABA_B$ [267]. Similar to previously described receptors, β_1- and β_2AR rapidly associate and dissociate – forming transient dimers and even higher-order oligomers. β_2AR had a higher dimerisation frequency than β_1AR, but neither receptor stoichiometry was affected by the addition of agonist, suggesting that the monomer-dimer equilibrium is governed separately to activation. Both receptors' lateral mobility was found to decrease after agonist activation, which may be concomitant with binding to signalling molecules, structural elements and scaffolding proteins. A higher density of receptors becoming immobile makes sense when thinking about the amplification of signalling, as efficiency can be increased by increasing concentrations of signalling molecules local to activated receptors.

In this study, consistent with previous observations [304,305], $GABA_B$ was found to consist of $GABA_{B1}$-$GABA_{B2}$ heterodimers, forming tetrameric and even octameric complexes. These were largely immobile on the plasma membrane at rest and organised in rows along the actin cytoskeleton through a known interaction maintained by $GABA_{B1}$. Agonist activation of $GABA_B$ increased the lateral mobility of the complexes [267]. This supports the view that $GABA_B$ tunes

synaptic signals - diffusing between synapses after activation to maintain desensitisation between inhibitory synapses [148,306]. Together, these studies shed important light on the nature of receptor dimerisation in live cells, providing direct evidence for highly dynamic receptor-receptor interactions.

In fixed cells, SMM can be applied without the requirement of tracking the proteins of interest. Although fixation can introduce artefacts, it allows experimentation under environmental conditions not compatible with live cells such as cryogenic freezing, which has beneficial photophysical properties [307]. By imaging at temperatures of liquid helium (~4.3K) and under near-vacuum pressure, fluorophore photostability is increased due to a decrease in oxidation. Combined with a decrease in blinking, more photons can be detected from a single fluorophore, enhancing spatial resolution and thus localisation precision.

Tabor et al. studied the dimerisation of SNAP-tagged dopamine D_2 receptors in fixed CHO cells, reporting a spatial resolution of <10nm [307]. D_2 receptors were imaged with enough resolution to measure distances between two receptors within a dimer, which was estimated to be ~9nm, consistent with an appropriate distance for physical interaction between the two proteins. This was confirmed in living cells years later, finding that although these D_2 interactions are transient in nature, they are true interactions critical for signalling [308].

1.9.2 SPT studies of GPCR nanodomain organisation

GPCR organisation goes beyond the intermolecular receptor interactions described in 1.5.3. GPCRs interact with a multitude of signalling proteins and structural elements, many of which have been shown to sequester GPCR signalling in nanodomains on the plasma membrane. Recently, our group used single particle tracking to image individual GPCRs and G proteins to

study diffusion and protein-protein interactions in live cells [253]. In this study, SNAP-tagged adrenergic receptors (α_{2A}AR and β_2AR) and cognate CLIP-tagged G proteins (Gαi and Gαs respectively) were imaged simultaneously with fast, multicolour TIRF microscopy at a resolution of 20nm and 30ms in space and time. Experiments were performed in CHO cells and primary human endothelium, so that diffusion and interaction comparisons could be made in cells where α_{2A}AR and β_2AR exert their physiological roles.

An unexpected heterogeneity and complexity was revealed, in both the diffusion of receptors and G proteins. Molecules were found to alternate phases of immobility, confined motion and free diffusion [253]. The immobility and confinement could be explained by transient trapping of GPCRs and G proteins in defined sites on the plasma membrane. This was supported by PALM imaging of the cortical actin cytoskeleton, which revealed that the trapping was at least partially due to barriers provided by actin, in agreement with the fence-and-picket model of the plasma membrane [284,285]. These sites were coined as 'hot spots', which act as dense sites of proteins where signalling molecules can preferentially scaffold and interact [253]. A nanobody-based biosensor that recognises active Gαs protein (Nb37) confirmed that active G protein accumulates in these 'hot spots' [309,310], suggesting that they are important for signalling.

Localisation was also altered upon stimulation, where α_{2A}AR was found to have low levels of transient binding to clathrin-coated pits (CCP) at rest, consistent with low-levels of constitutive receptor phosphorylation and recruitment to CCPs. After agonist stimulation, a higher fraction of receptors occupied CCPs, likely as a result of β-arrestin activation. These findings help explain the high specificity, speed and efficiency observed in GPCR signalling. Despite the fact that hundreds of GPCRs are expressed in a typical cell, cells could easily converge on a relatively

small number of signalling pathways, if GPCR signalling is sequestered into defined sites on the membrane (**Figure 1.15**).

A novel mathematical model was reported in this study, to estimate the kinetic rate constants of protein-protein interactions based on apparent single-molecule colocalisation times. An estimation of association (k_{on}) and dissociation (k_{off}) rate constants were determined for GPCR-G protein interactions after interrogation with a panel of ligands. Under basal conditions, low levels of basal interactions were observed between GPCR and G protein (k_{on}=0.015 μm^2 $molecule^{-1}$ s^{-1} for α_{2A}AR-Gαi interactions), which lasted for ~1-2 seconds on average (k_{off}=0.5-1 s^{-1}). Agonists increased the association rate constant up to 10-fold and a positive correlation was found between efficacy and association rate constants for GPCR and G protein, similar to results observed by Gregorio et al. on purified proteins with smFRET [258]. α_{2A}AR-Gαi had ~10-fold higher k_{on} values than β_2AR-Gαs when comparing interactions with different G proteins, which is consistent with the understanding that Gαi signalling is more efficient than Gαs [311,312]. The kinetic differences between these two receptor systems might also explain why only Gαi proteins are capable of efficiently activating GIRK channels, even though both Gαs and Gαi trigger G$\beta\gamma$ release [313].

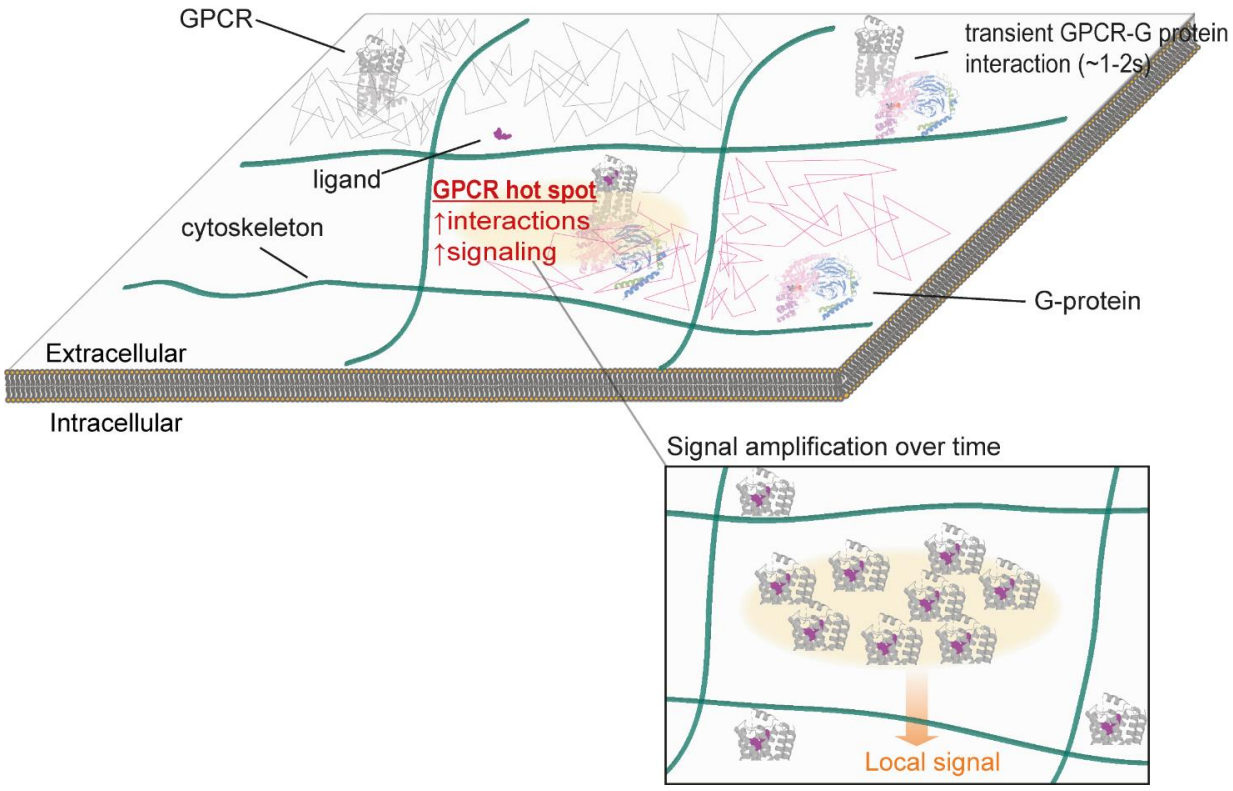

Figure 1.15 Hot spots for GPCR signalling. Important contributions of barriers provided by the cytoskeleton and associated proteins leads to the preferential accumulation of receptors and G proteins in small nanodomains on the plasma membrane (hot spots), where they preferentially interact and signal. Figure is adapted from Calebiro & Grimes [2], based on work conducted by Sungkaworn et al. [253].

Interestingly, only minor changes were observed in the length of interactions after stimulation. Combined with the increase in k_{on} after agonist interrogation, this suggests that the number of interactions is important in mediating signal amplification, rather than the duration of individual interactions. This again supports a model where the membrane is organised, to increase the likelihood of productive interactions occurring. These investigations of GPCR-G protein interactions have shed new light on the debate of whether G proteins are pre-coupled to receptor in the absence of agonists [66]. The interactions that were observed were transient, with most only lasting for a matter of seconds, ruling out the occurrence of stable, pre-formed complexes. Basal GPCR-G protein interactions instead appear to represent transient

constitutive activity, since basal activity was prevented by addition of inverse agonists or inactivation of Gαi with PTX [253]. Transient interactions and diffusional barriers provided by the cytoskeleton likely contribute to maintaining receptor and G protein populations in close proximity, allowing rapid response upon agonist-induced receptor activation. Similarly, the occurrence of transient rather than stable interactions allows a single receptor to catalytically activate multiple G proteins in a nanodomain, furthering signal amplification. The duration of receptor-G protein interactions estimated by SPT (~1-2s) is significantly shorter than the time required to activate downstream effectors, such as GIRK channels and adenylyl cyclase, which can occur within 100ms of agonist stimulation [314] - though further studies are required to elucidate the importance of these interaction durations.

1.9.3 SPT studies of β-arrestin signalling

Few studies exist that probe the dynamics of GPCRs and β-arrestins on a single-molecule scale. Eichel et al. recently used TIRF microscopy to study the localisation of β-arrestin and β-adrenergic receptors on the plasma membrane of live cells [106,315]. They found that β-arrestin was enriched at CCPs with receptors after agonist-induced receptor activation, but also found that β-arrestin was enriched at CCPs lacking GPCRs. Additionally, the authors reported most often that β-arrestin molecules laterally diffused without an accompanying receptor. Taken together, these results combat the classical view of β-arrestin signalling, where the arrestin binds directly to GPCRs and then translocates as a complex to CCPs. The authors only reported indirect evidence of events, as they were unable to resolve a full trajectory where β-arrestin arrived on the membrane, interacted with a receptor transiently and then migrated and immobilised on a CCP alone.

It was reported that the amino acids proximal to the finger loop region (FLR) of β-arrestin, a region known to be important for mediating β-arrestin activation upon GPCR binding, mediated GPCR-independent β-arrestin signalling. By using a mutant which transiently engaged the GPCR core without the C-tail interaction, as confirmed by structural studies, it was suggested that β-arrestin could be catalytically activated and diffuse to CCPs alone after receptor engagement [315]. The authors were again unable to confirm this, due to photobleaching, as β-arrestin spent much longer on the plasma membrane than the average fluorophore bleaching time.

These results suggest that β-arrestin likely engages other effector molecules on the plasma membrane to enable its trafficking to CCPs without a GPCR, as β-arrestin has no known intrinsic membrane-anchoring linker. By mutating a residue in β-arrestin known for binding to membrane phosphoinositides [142], ligand-induced trafficking of β-arrestin to the plasma membrane and CCPs was eliminated [315].

By mutating residues responsible for β-arrestin interactions with clathrin and AP2, both crucial in the formation of and signalling at CCPs, the authors significantly reduced β-arrestin enrichment at CCPs, but found ubiquitous enrichment of β-arrestin across the rest of the plasma membrane [106]. It is important to note that photobleaching is a major concern in these experiments, as GPCR-independent β-arrestin at CCPs may reflect unlabelled or photobleached GPCRs in complex. Based on the above results, a model is proposed in which transient engagement of GPCRs by β-arrestin catalyses the diffusion and enrichment of both β-arrestin and the GPCR in CCPs, by interactions which are stabilised by non-GPCR partners. Lastly, CCPs containing only β-arrestin were found to have higher levels of ERK expression [315], which may provide a framework for signalling without the requirement for a bound GPCR.

Using super resolution imaging, including SPT and dSTORM, Jung et al. presented a working model for β-arrestin binding to CCPs, which is dependent on the maintenance of β-arrestin on the membrane by interactions with phosphoinositides [119]. Two binding modes of arrestin to CCPs were identified. The authors found that β-arrestin/GPCR complexes could bind to the outskirts of mature CCPs, forming stable interactions in a donut shaped cluster around their boundary. They suggest that newly formed CCPs, for which the membrane is less invaginated, act as sites for the stable binding of β-arrestin and GPCRs. Both described interactions were stabilised by the recruitment of PIP5K and maintenance of PIP2, which promote GPCR endocytosis. It was also found phosphoinositide depletion from the plasma membrane reduced the recruitment of β-arrestin to CCPs. It is postulated that these two motifs might mediate different mechanisms of β-arrestin activity in cells, with the CCP-boundary arrestins acting to scaffold signalling cascades and the arrestin clustered inside of CCPs mediating endocytosis. Although SPT is used in this study, β-arrestin and GPCR are not considered separately, so it provides no evidence for or against the canonical model of arrestin recruitment.

1.9.4 SPT studies of β-adrenergic signalling in cardiac myocytes

The diffusion of β_1AR and β_2AR has been studied in H9c2 cardiomyocyte-like cells, labelling the receptors with quantum dots (QD) [316]. It was found that β_1AR and β_2AR had both mobile and immobile fractions in H9c2 cells, with the authors finding that immobile receptors were often tethered to scaffolding proteins. This immobilisation contributes to spatial segregation of βARs and means they can act as scaffolds for signal transduction components. Additionally, it contributes to the specificity of cardiac signalling, as the authors found that it was either β_1AR or β_2AR that were found in the immobile complexes, not both [316].

Recently, fluorescence spectroscopy and SPT was used to image βARs in isolated cardiac myocytes with a non-specific βAR fluorescent antagonist [317], so that the localisation of endogenous receptors could be quantified. It was found that β_2AR was confined to the t-tubular network in healthy cells, as opposed to the β_1AR, which diffused also on the basement membrane in addition to t-tubules. After overexpressing β_2AR, mimicking the excess catecholamine stimulation observed in chronic HF, the authors found that β_2AR segregation was lost, and receptors diffused also on the basement membrane [317].

M_2 muscarinic receptors, which are responsible for acetylcholine signalling and contribute to the propagation of action potentials in cardiac tissue, have also had their diffusion and spatial organisation studied in primary cardiac cells [318]. Diffusion of M_2R in CHO cells was similar to the diffusion seen in primary isolated cardiac myocytes. Interestingly, M_2R diffusion in cardiac tissue slices was found to be increased 4-fold when compared to primary, adherent cells; emphasising the importance of the cellular background chosen for study. Compared to studies on βARs, M_2R was expressed mostly homogenously across the plasma membrane of tested cell types, with differences in density on the membrane observed in aging mice. M_2R was found to form transient dimers as they diffused in the plasma membrane, as seen in previous SPT studies of Class A GPCRs [267].

1.10 SCOPE OF THESIS

β-arrestin is a fundamental regulator of GPCR signalling [236]. Following GPCR activation by an agonist and phosphorylation by G protein coupled receptor kinases (GRKs), β-arrestin translocates from the cytoplasm to the active receptors at the plasma membrane. By interfering

with G protein binding, this interaction mediates rapid GPCR desensitisation [84,180,319]. Moreover, β-arrestin triggers receptor internalisation via interaction with the adaptor protein 2 (AP2) and clathrin [3]. Besides these 'classical' functions, β-arrestin has been proposed to mediate 'non-classical' G protein-independent effects [74], providing a mechanism for biased signalling [320].

The recent determination of high-resolution structures of arrestins in complex with GPCRs [26,120,122] has provided important molecular insights into receptor-arrestin interactions. Moreover, intriguing new mechanisms have been hypothesised for β-arrestin activation [315]. Despite these recent advances, the mechanisms that enable β-arrestin to interact with GPCRs, maintain active conformation(s) and participate in GPCR signalling in living cells remains elusive. Fundamental and presently unanswered questions remain, such as: How do GPCRs and β-arrestins meet on the plasma membrane? How long do they interact? How is β-arrestin stabilised in an active conformation at the plasma membrane to mediate G-protein independent signalling? How do β-arrestins and receptors reach clathrin coated pits (CCPs) to mediate G protein independent signalling as well as GPCR internalisation?

Despite considerable efforts, answering these questions has been hampered by important limitations of the conventional approaches, such as biochemical and ensemble biophysical methods, commonly used to investigate GPCR signalling. A first limitation of current methodologies to probe these questions is insufficient spatiotemporal resolution, which precludes a detailed investigation of protein–protein interactions on the plasma membrane. These typically occur on the scale of tens of nanometers and milliseconds [321]. A second important limitation is that ensemble methods only report the average behaviour of thousands or millions of generally unsynchronised molecules, precluding a direct estimation of kinetics parameters or the analysis of complex sequences of events.

To circumvent these limitations, an innovative single-molecule approach is used here, which our group previously used to investigate receptor–G protein interactions [253]. This allows the simultaneous visualisation of individual β-arrestin and receptors as they diffuse and interact at the surface of living cells, with unprecedented spatial (~20nm) and temporal (~30ms) resolution. As an initial model, we chose β-arrestin2 (βArr2) and the β_2-adrenergic receptor (β_2AR), utilising this family-A GPCR that controls numerous physiological processes including heart contractility and smooth muscle tone as a model system [319]. Furthermore, two additional receptors were studied: the β_1-adrenergic receptor (β_1AR) and a chimeric β_2AR–vasopressin V_2 receptor (β_2V_2), which have been extensively used as models of weak and strong β-arrestin interactions, respectively [140].

Unexpectedly, results show that, contrary to the current widely accepted model, β-arrestin does not directly translocate to receptors from the cytoplasm, but rather spontaneously inserts into the plasma membrane via hydrophobic interactions mediated via its C-edge. It is also found that this pre-association is critical for β-arrestin to meet receptors on the membrane via lateral diffusion. Moreover, results reveal that receptor – β-arrestin interactions are much more dynamic than previously thought, lasting on average only approximately 0.7 s, a time insufficient for receptors and β-arrestins to reach clathrin coated pits together, as currently assumed. Finally, they uncover a previously unknown potential interaction of the finger loop domain of β-arrestin with the plasma membrane, which appears to play a critical role in stabilising β-arrestin in a membrane-bound, active-like conformation after transient interaction with a receptor.

2 MATERIALS and METHODS

2.1 MATERIALS

2.1.1 Cell Lines

Chinese Hamster Ovary (CHO)-K1 cells and Human Embryonic Kidney (HEK)-293 cells were from ATCC. CHO-K1 CRISPR KO β-arrestin 1/2 cells were generated in house (see section 2.2.4) and HEK293 CRISPR KO β-arrestin 1/2 cells were a kind gift from the lab of Asuka Inoue [133,322]. Competent *E. coli* (TOP10) were from ThermoFisher Scientific. Adult murine ventricular cardiac myocytes were obtained from the lab of Davor Pavlovic, after isolation from 8-week-old C57BL/6 mice (see section 2.2.16).

2.1.2 Cell culture media and supplements

Dulbecco's Modified Eagle's Medium (DMEM), DMEM/F-12 without phenol red (#21041025) and with phenol red (#11320033), reduced serum medium (Opti-MEM) (#31985070), Fluorobrite phenol-red free medium (A1896701), Hanks Balanced Salt Solution (HBSS) (#14025092), Foetal Bovine Serum (FBS) (A4736401), 0.25% Trypsin/EDTA (25200056), L-Glutamine (#25030149) and Phosphate buffered Saline (PBS) (#10010023) and Penicillin/Streptomycin (P/S) (#15140122) were from Gibco.

2.1.3 Fluorescent Dyes

SNAP-Surface 549 (S9112S), SNAP-Surface 649 (S9159S), SNAP-Cell 647-SiR (S9102S), CLIP-Surface 547 (S9233S) and CLIP-Surface 647 (S9234S) were from New England Biolabs (NEB).

Halo-Janelia 549 (GA1110), Halo-Janelia 646 (GA1120) and Halo-R110 (G3221) were from Promega.

2.1.4 Reagents

Lipofectamine© 2000 transfection reagent (#11668030) and TetraSpeck fluorescent beads (T7279) were from ThermoFisher. Cas9 protein and RNAs were purchased from Integrated DNA technologies. Ultraclean glass coverslips were obtained as described in Calebiro et al. [267]. Lysogeny Broth (LB) and LB agar was made according to the Lennox formulation. Ultraclean glass coverslips (#631-1584) were obtained as previously described [267].

2.1.5 Ligands

The high-affinity β_2AR agonist Isoprenaline (Isoproterenol) (#1747), the non-specific β-AR antagonists Propranolol (#0624), Metoprolol (#3256) and Alprenolol (#2806), the β_2AR-specific inverse agonist ICI 118,551 (#0821) were from Tocris Bioscience. The β-AR antagonist, Carvedilol, was provided by Evi Kostenis from the University of Bonn as part of a collaboration. The fluorescent ligands Propranolol-BODIPY 630/650, Propranolol-BODIPY FL, Alprenolol-BODIPY 630/650 and ICI 118,551-BODIPY 630/650 were provided by the laboratories of Steve Hill and Barrie Kellam at the University of Nottingham (see [323] for synthetic pathway and validation of Propranolol-BODIPY 630/650 and [265] for ICI-BODIPY 630/650).

2.1.6 Plasmids

Plasmids encoding N-terminally SNAP-tagged human β_1AR (SNAP-β_1AR), β2AR (SNAP-β_2AR) and CD86 (SNAP-CD86) were previously generated and verified to be functional [267]. A plasmid encoding N-terminally SNAP-tagged human β_2AR carrying the vasopressin V_2 receptor C-tail (SNAP-β_2V_2) was generated by replacing the C-tail in the SNAP-β_2AR construct with that of V_2 (ARGRTPPSLGPQDESCTTASSSLAKDTSS). Plasmids encoding N-terminally SNAP-tagged human β_2AR with a deletion in the third intracellular loop (SNAP-β_2AR-ΔICL3) or lacking the entire C-tail (SNAP-β2AR-ΔC-tail) were generated by PCR using standard procedures. A plasmid encoding C-terminally Halo-tagged bovine β-arrestin 2 (βArr2-Halo) was generated by replacing CFP with the Halo tag in a previously described βArr2-CFP construct [324]. A plasmid encoding C-terminally Halo-tagged bovine βArr2 carrying mutations that interfere with binding to both clathrin (L373A/I374A/F376A) and AP2 (R393A/R395A) [101,102] (βArr2-CCPAP2-Halo) was generated by PCR mutagenesis. Similar procedures were used to generate plasmids encoding C-terminally Halo-tagged bovine βArr2 with a deletion of the arrestin finger loop (YGREDLDVLGLSFRK) (βArr2-ΔFLR-Halo) [27] or carrying mutations (K233Q/R237Q/K251Q) that interfere with PIP2 binding (βArr2-PIP2-Halo) [103]. An additional βArr2-Halo construct carrying a panel of mutations (R189Q/F191E/L192S/M193G/T226S/K227E/T228S/K230Q/K231E/K233Q/R237E/K251Q/K325Q/K327Q/V329S/V330D/R332E) was designed to prevent plasma membrane interactions (βArr2-ELA-Halo), by PCR mutagenesis of the βArr2-PIP2-Halo construct, followed by Gibson assembly. A plasmid encoding human β_2AR containing NanoLuciferase (Nluc) fused to its C-terminus (β_2AR-Nluc) was previously generated by Kilpatrick et al. [325]. Plasmids encoding β_1AR, β_2V_2, β_2AR-ICL3 and β_2AR-C-tail with Nluc fused to their C-termini were cloned

from the β_2AR-Nluc construct by replacing the β_2AR coding sequence with those of the corresponding receptor constructs. A plasmid encoding K-Ras with Nluc fused to its N-terminus was kindly provided by Kevin Pfleger [326]. A plasmid encoding N-terminally GFP-tagged clathrin light chain was kindly provided by Emanuele Cocucci and Tom Kirchhausen [327]. A plasmid encoding N-terminally CFP-tagged clathrin light chain was cloned by replacing GFP in GFP-CCP using PCR and Gibson assembly. A plasmid encoding Lifeact-YFP was generated by replacing GFP with YFP in a previously described Lifeact-GFP construct (kindly provided by Antje Gohla) [253]. A plasmid encoding N-terminally Nluc-tagged clathrin light chain was obtained by gene synthesis at Twist Bioscience. A plasmid encoding C-terminally Halo-tagged ScFV30 (SCFV30-Halo) was generated by replacing the YFP sequence with Halo in a previously described ScFv30-YFP construct (kindly provided by Arun Shukla) [140].

2.2 CELLULAR ASSAYS

2.2.1 Plasmid Amplification

For plasmid amplification, chemically competent *E. coli* (TOP10) were used. 50µl competent cells, stored at -80°C, were incubated on ice for 20 minutes and 100ng plasmid DNA was added. Mixture was equilibrated on ice for 20 minutes and heat shocked for 30 seconds in 42°C water. 500µl LB medium was added, followed by a 1-hour incubation at 37°C with 220rpm horizontal shaking. 100µl was inoculated on LB agar plates doped with appropriate antibiotic, namely either ampicillin at 0.1mg/ml or kanamycin at 0.04mg/ml. Agar plates were incubated for 14-16 hours at 37°C to obtain transformed colonies. A single colony was picked the next day and inoculated into 2ml LB medium supplemented with antibiotic as previously described. The mixture was then incubated 14-16 hours at 37°C with 220rpm horizontal shaking before DNA purification using the Qiagen MIDI plus kit, following the manufacturer's protocol. Plasmid DNA

was stored in 100µl ddH_2O and DNA concentration and purity was measured on a NanoDrop 2000 (ThermoFisher Scientific) before storing at -20°C.

2.2.2 Continuous cell culture

Chinese Hamster Ovary (CHO)-K1 cells were cultured in phenol red-free DMEM/F12, supplemented with 10% FBS, 100U/ml and 0.1mg/ml P/S at 37°C, 5% CO_2. Cells were routinely passaged at ~90% confluency by washing in PBS, detaching for 2min with Trypsin/EDTA and resuspension in fresh medium. HEK293 cells were cultured similarly, in complete DMEM supplemented with 10% FBS, 2mM L-Glutamine and 0.1mg/ml P/S. All cells were routinely tested for mycoplasma contamination and cultured using aseptic technique.

2.2.3 Generation of β-arrestin CRISPR knockout CHO cells

To generate the cell line, β-arrestin 1 & 2 were sequentially knocked out in CHO cells using a ribonucleoprotein (RNP) mediated CRISPR-Cas9 system. Cas9 protein and RNAs were purchased from Integrated DNA Technologies. Guide sequences to target both β-arrestin 1 & β-arrestin 2 for CRISPR-Cas9 mediated knockout were designed using the CHOPCHOP webtool (https://chopchop.cbu.uib.no) [328]. Designed sequences were 5'-ATCGACCTCGTGGACCCTGTGGG -3' and 5'- GCGCGACTTTGTAGACCACCTGG -3', for exon 3 of the ARRB1 gene and exon 3 of the ARRB2 gene respectively. Guide sequences were synthesised as CRISPR RNA (crRNA), which were annealed to a trans-activating CRISPR RNA (tracrRNA) to form single guide RNAs (sgRNAs) for each gene. Knockout of ARRB2 was carried out first by incubating the ARRB2 sgRNA with Cas9 protein to form the functional RNP complex, which was then transfected into CHO cells using Lipofectamine CRISPRMAX (ThermoFisher Scientific)

according to the manufacturer's instructions. After 48 hours, cells were diluted and seeded in 96-well plates at a density of 0.5 cells/well to generate monoclonal cell populations. Once confluent, genomic DNA (gDNA) was extracted from each monoclonal population using QuickExtract DNA Solution (Cambio) and the gDNA used in PCR reactions using the following primers: 5'- GTCTTCAAGAAGTCGAGCCCTA -3' and 5'- GAATTCCTTCTTCTTCCTGCCT -3'. PCR fragments were sequenced, and clones containing indels in both copies of ARRB2 were kept. One clone was selected and used in the knockout of ARRB1 by transfecting cells with the RNP specific for ARRB1 in an identical method to above. Selection of clones was carried out as described for ARRB2 knockouts, with the PCR reactions being carried out using the following primers: 5'-GCTCCCTGCCTAGTTCAGAGT A-3' and 5'–TATTCTGCAGTGTACCTGGTGG–3'. Knockout of both β-arrestin 1 and 2 was verified by Western blotting using a rabbit polyclonal antibody for pan-β-arrestin (ThermoFisher Scientific, PA1-732).

2.2.4 Transfection

Single-molecule microscopy (SMM): CHO cells were seeded on 25mm ultraclean coverslips (2.2.2) the night before transfection at a density of $6x10^5$ cells per well in 6-well plates. The next morning, 500μl Opti-MEM medium was incubated with relevant plasmid DNA (up to 2μg) and 500μl Opti-MEM was incubated with 6μl Lipofectamine© 2000 for each well. After 5 minutes, the two mixtures were combined and incubated for 20 minutes at room temperature. Whilst incubating, cells were washed with PBS and then 1ml fresh DMEM/F12 medium without FBS was added. 1ml transfection mixture was then added dropwise on top of medium and lightly agitated to mix and plates were incubated for 3.5-4 hours (unless stated otherwise) to obtain low physiological expression levels prior to labelling and imaging.

BRET: HEK293 cells were seeded at $3x10^5$ cells per well in 6-well plates. The next morning, 100µl Opti-MEM medium was incubated with relevant plasmid DNA (up to ~400ng) and 100µl Opti-MEM was incubated with 3µl Lipofectamine© 2000 for each well. After 5 minutes, the two mixtures were combined and incubated for 20 minutes at room temperature. Whilst incubating, cells were washed with PBS and then 1.5ml fresh DMEM medium supplemented with 10% FBS. Transfection mixtures were then added dropwise on top of medium and lightly agitated to mix and moved to the incubator. After 24 hours, transfection mixture was removed and cells were resuspended in Fluorobrite phenol-red free medium supplemented with 4mM L-glutamine, 5% FBS at a density of $1x10^5$ cells per well in poly-D-lysine coated 96-well white polystyrene Nunc microplates (Sigma) and incubated for a further 24 hours prior to protein labelling and experimentation (48-hour total transfection).

2.2.5 BRET assays

48-hours post transfection, as detailed in 2.2.4, culture medium was replaced with 60µl HBSS supplemented with 10mM HEPES and 100nM Halo R110 ligand; the plates were incubated for 1 hour at 37°C. After labelling, 500nM furimazine was added and incubated in the dark at room temperature for 5 minutes before reading running on a PheraStar (BMG Labtech) plate reader. Cells transiently transfected with proteins of interest and labelled with HaloTag ligands and Furimazine (2.2.4/2.2.5) were read on a PheraStar plate reader (Promega) capturing bioluminescence of Nluc donor and R110 acceptor emission with band pass filters (430-485nm; 500-550nm) (**Figure 2.1**). BRET measurements were taken every 30 seconds at 37°C and following 4 baseline readings, cells were treated with vehicle or 10µM ligand (Isoproterenol unless stated otherwise). The BRET signal observed between interacting proteins was

normalised by subtracting the background BRET ratio as follows: the acceptor/donor emission readout for a well sample treated with vehicle was subtracted from the same ratio for a concomitant well sample treated with ligand. Vehicle and ligand treated wells were assayed in triplicate wells for each independent experiment and three biological replicates were obtained unless stated otherwise.

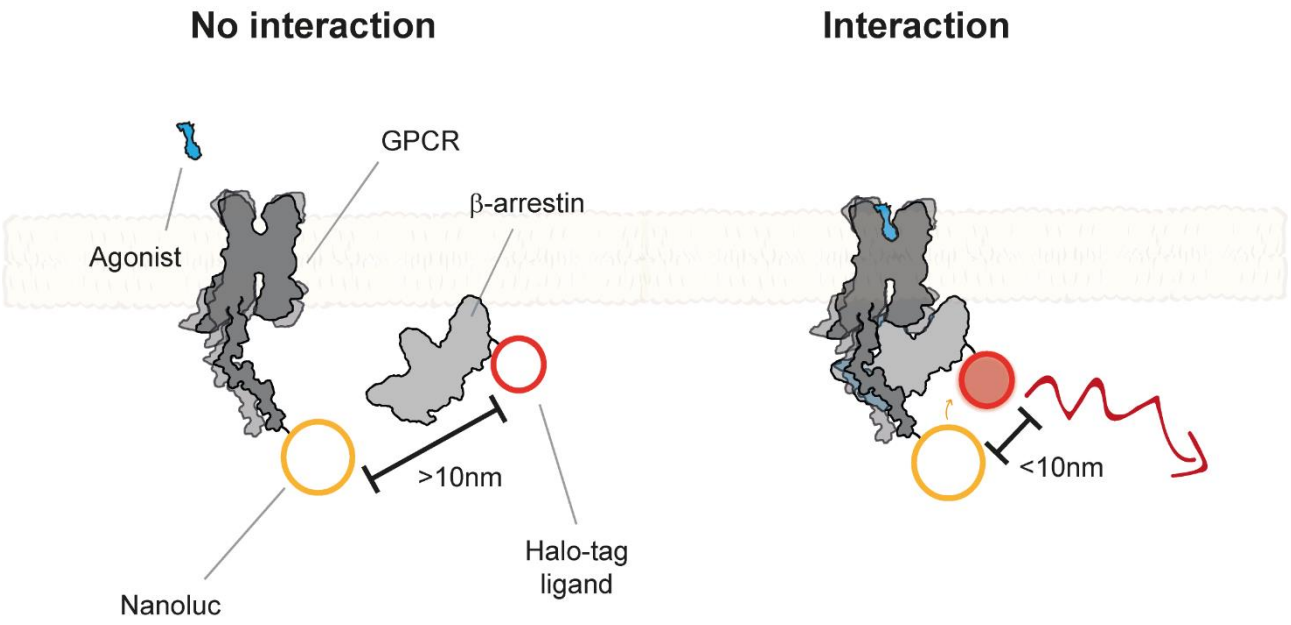

Figure 2.1 BRET schematic. Schematic of BRET-detected interactions between β2AR-Nanoluc and Halo-βarrestin 2 after isoproterenol-mediated GPCR activation. BRET is sensitive at distances <10nm, and resonant energy transfer occurs from a donor (Nanoluc) to an acceptor (Halo) fluorophore after addition of the Nanoluc substrate (furimazine) and Halo-dye (R110) and stimulation with isoproterenol.

2.2.6 Live cell protein labelling

Self-labelling dye labelling: Transfected cells containing a SNAP-, CLIP- or a Halo-tag were labelled accordingly prior to imaging. Optimal dye concentration for labelling was determined by saturation binding with titration experiments in cells. In cases of known optimal concentration [253,267], literature-suggested concentrations were used. For labelling, cells were first washed twice in PBS. The dye was then solubilised in culture medium at final assay

concentration and applied to cells which were then incubated for 20 minutes at 37°C, 5% CO_2. Cells were then washed three times with complete culture medium without FBS and incubated for 5 minutes. This washing process was repeated 4 times prior to imaging of the cells.

Fluorescent ligand labelling: for high-affinity β-AR fluorescent ligands, optimal ligand concentration for experimentation was determined by serially diluting fluorescent ligand in culture medium to obtain a binding curve. Transfected cells were first washed twice in PBS and then washed three times in complete culture medium without FBS. Cells were incubated with the ligand solution for 10 minutes and mounted directly into imaging chambers for movie collection, without the requirement of further washing.

2.2.7 Isolation of adult mouse ventricular cardiac myocytes

For isolation of cardiac myocytes for single-molecule imaging, surgery was performed by a trained member of Davor Pavlovic's lab, with whom the collaboration was mediated (using methods described in [329]). The chest cavity of an anaesthetised adult mouse was opened to expose the heart. Haemostatic forceps were used to clamp ascending aorta and perfused with EDTA buffer into the right ventricle after clearing blood. Hearts were excised by snipping the descending aorta and removing from the cavity. Surgically removed hearts were then submerged in 60 mm sterile petri dishes containing EDTA. Solutions of 1x 10ml EDTA, 1x 3ml Perfusion, 1x 10ml Collagenase and 1x 3ml Collagenase buffer was prepared for dissociation of cardiac myocytes in petri dishes and syringes. For a 37°C digestion, which has the best yield of viable cells, syringes were kept on a heated mat. After locating the left ventricle, which is the largest and forms the apex at the bottom of the heart, EDTA was perfused at a rate of 2ml/min

into it. This step inhibits contraction and washes any blood and connective tissue from the coronary circulation, preventing coagulation.

Hearts were then transferred to perfusion buffer and similarly perfused, in the same injection site, removing excess EDTA and neutralising the pH for optimum survivability. Hearts were then transferred to petri dishes containing collagenase buffer and injected similarly, at a rate of 1-2ml/min. Buffer was recycled to further digestion of hearts until completely dissociated. Signs of complete digestion include loss of injection pressure, loss of shape, pale appearance and ejection of myocytes into the buffer. After digestion, the heart is separated into chambers using scissors and forceps. The left ventricle and isolated in the final collagenase buffer (3ml in petri dish). Here, manual dissociation of the ventricle is performed by gently tearing it into 1mm x 1mm pieces and cells are homogenised by gentle pipetting, using a wide-bore tip to reduce agitation stress. 5ml Stop buffer was then added to inhibit collagenase activity [329].

2.2.8 Purification of cardiac myocytes by gravity settling

Under sterile conditions in a biosafety cabinet, the cell solution is passed through a 100μm strainer, to remove cellular debris and undigested tissue. Filters were then washed with stop buffer. 100μm filters enable collection of isolated myocytes but do not allow myocyte clusters to pass, which would be unsuitable for imaging. Cells were then gravity settled for 20 minutes, where myocytes will settle in a pellet and non-myocytes remain mostly in solution. Gravity settling avoid damage introduced to the fragile membranes by centrifugation. 3 sequential rounds of 10-minute gravity settling were then done in perfusion buffer, with the myocyte pellet being retained each time. Cells were finally resuspended in 2ml DMEM/F12. Microscopic examination should reveal a high number of rod-shaped myocytes in suspension. Large

numbers of contracted and rounded myocytes indicates a poor isolation. Cells can be stored at room temperature for up to 2 hours in suspension.

2.3 MICROSCOPY

2.3.1 Hypoxic imaging chamber

Photobleaching is the loss of fluorescence which occurs stochastically after a fluorophore emits photons and is dependent on a multitude of parameters which need to be optimised to reduce its effect, including laser power, fluorophore choice and exposure time. For single-molecule experiments, photobleaching means the loss of information on particles which are still diffusing on the membrane but invisible to detection systems, hindering the ability to accurately form conclusions in downstream analyses. Researchers are constantly looking for ways to reduce photobleaching and for fixed cells, hypoxic conditions and oxygen scavengers are widely used. Oxygen is suggested to shorten the fluorophores triplet-state lifetime (the state in which it fluoresces), so reducing available O_2 in the cellular environment is a suggested mechanism to reduce photobleaching. Until recently, this approach has not been used in live cells for the detrimental effects hypoxia can have on cell viability.

Tsunoyama et al. developed an experimental procedure which reduces photobleaching and blinking, that does not significantly affect cell viability and vastly increases the fluorophore lifetime for single-particle tracking (SPT) experiments in live cells [330]. The authors found that approximately 2% O2 improved fluorescence lifetime by between 200-800% dependent on the fluorophore. Reactive oxygen species detrimental to cell health were only identified after hours of exposure to this condition, which suggests that for SPT experiments, where sample are recorded for 20-30 minutes, cell viability should not be a concern.

A reduced oxygen environment (2-4% O_2) was generated in the TIRF imaging chamber to decrease photobleaching without increasing cytotoxicity, using a mixture of nitrogen and air in a home-built gas mixing and humidifying system as previously described [330] (**Figure 2.2**). Oxygen concentration in the imaging solution was measured in real-time using a needle-type oxygen sensor connected to an OXY-1 microsensor (PreSens, Germany).

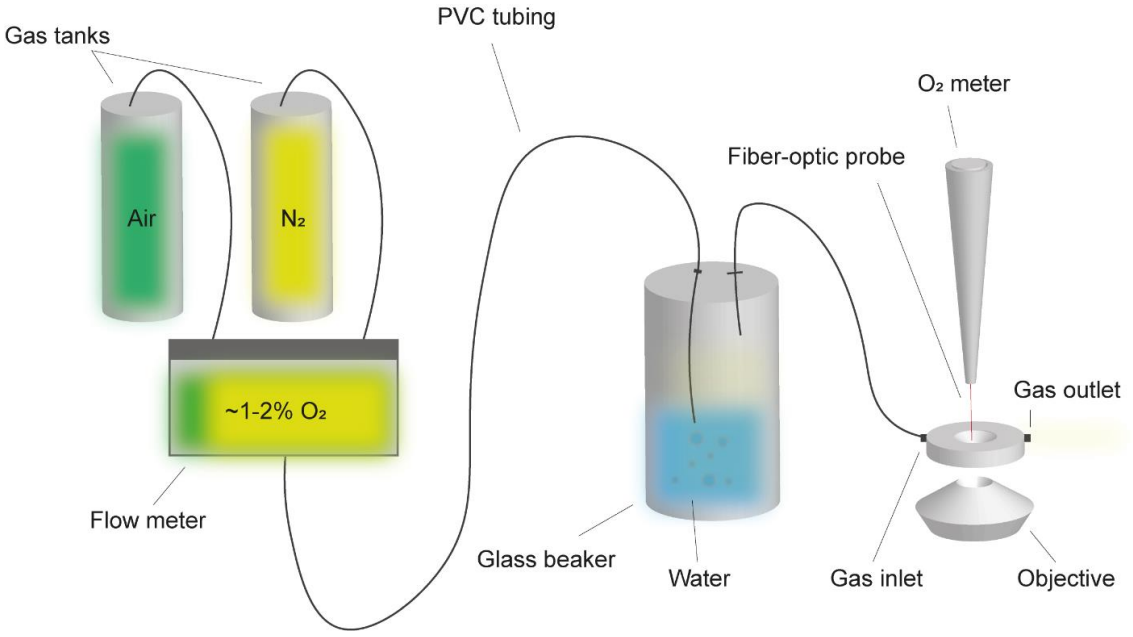

Figure 2.2 A custom-built hypoxia setup for TIRF imaging. Hypoxic imaging chamber generated, based on Tsunoyama et al. setup [330], where a 1-2% O_2 atmosphere reduces phototoxicity, enhancing fluorophore lifetime.

2.3.2 4-camera custom-built TIRF microscope

SMM experiments were performed using TIRF illumination on a custom-built system based on a Nikon Eclipse Ti2 microscope frame, equipped with:- a 100x oil-immersion objective (CFI SR HP APO TIRF NA 1.49, Nikon), 405, 488, 561, 637nm diode lasers (Coherent, Obis), an iLas2 TIRF illuminator (Gataca Systems) for 360º homogenous TIRF illumination, a quadruple band excitation and dichroic filter-set to achieve minimal delay among channels (<1ms switching time), a quadruple beam splitter, a 1.5x tube lens, four EMCCD cameras (iXon Ultra 897, Andor),

hardware focus stabilisation and a temperature-controlled enclosure (**Figure 2.3**). The sample and objective were maintained at 37°C throughout the experiments. Multi-colour single-molecule image sequences were acquired simultaneously on synchronised EMCCDs at a rate of one image every 33ms, in frame transfer mode using Andor Solis software for acquisition and Metamorph software (Molecular Devices) for illumination control.

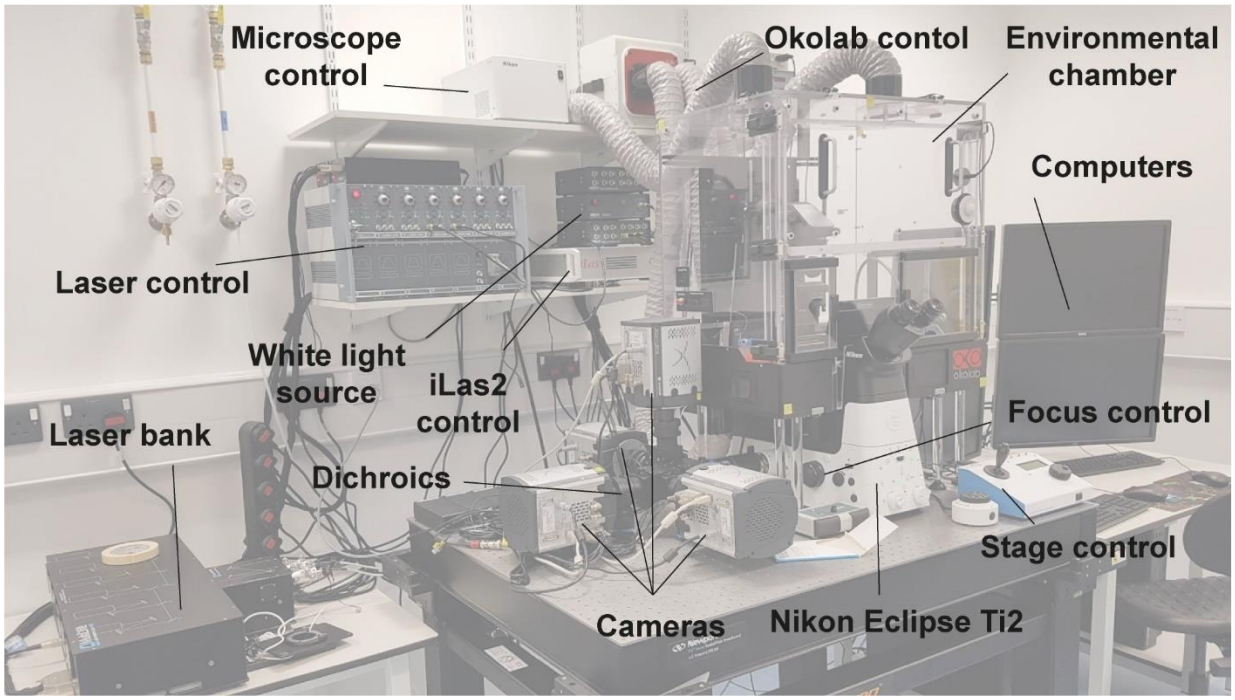

Figure 2.3 A custom-built multi-colour TIRF microscope for single-molecule microscopy.

2.3.3 Software control

Andor Solis was used for camera and acquisition control (Andor), with Metamorph (Molecular Devices) being used for laser control of illumination. Parameters regarding exposure time, readout mode (frame transfer), EM gain, laser choice, chip display size, TIRF angle (controlling the penetration depth of the evanescent field) filter selection, time interval of acquisition were maintained for basal and stimulated conditions alike.

2.3.4 Preparation of ultraclean coverslips

25mm glass coverslips were placed in a custom metal holder, which was then placed in a beaker. Coverslips were then submerged in chloroform and sonicated for 30 minutes. Afterwards, he holder was allowed to air dry prior to submersion in 5M NaOH and further sonicated for 30 minutes. Coverslips were then washed 3 times with ddH_2O and stored in absolute ethanol (ThermoFisher Scientific).

2.3.5 Coating glass coverslips for cardiac myocyte imaging

Given that primary cells, such as cardiac myocytes, adhere less to glass than plastic – surfaces were coated to maintain adherence in imaging. 25mm ultraclean glass coverslips were coated with laminin (Thermo), at a final concentration of 5 μg/ml in phosphate buffered saline (PBS), for 1 h at 37°C, or overnight at 4°C. Coverslips were used on the day of coating, but can be sealed and stored at 4°C for up to 4 days [329]. Before plating cardiac myocytes, excess laminin solution was aspirated and coverslips were washed 1x with PBS.

2.3.6 Single-molecule TIRF microscopy

After labelling proteins of interest (described in 2.2.5), coverslips were mounted into a custom imaging chamber and washed three times in 400μl HBSS supplemented with 10mM HEPES, pH 7.5. All experiments were conducted on the microscope setup described in 2.2.7. Laser power was kept as low as possible when searching for cells of interest, to minimise photobleaching. Basal images of cells expressing transfected proteins of interest were acquired for 1000 frames (~33 seconds); positions were marked with Metamorphs in-built software feature, so that epifluorescence or post-stimulation movies could be acquired when needed. Ligands were

loaded into syringes and injected into the imaging chambers dropwise and movies were acquired 2 minutes post-stimulation until 20 minutes post-stimulation.

2.3.7 Post-processing of TIRF image sequences

Image sequences with low expression levels, good focus and a high signal-to-noise ratio were considered for further analysis. After TIRF microscope acquisition, selected movies were further processed in ImageJ/Fiji (https://imagej.net/software/fiji/), to prepare them for automated particle detection and tracking in MATLAB. First, 512x512 images were cropped to 256x256 to reduce unnecessary computation in addition to a binary mask being drawn around the membrane of the cell. The movies were then analysed with custom scripts, based on multiple-hypothesis testing algorithms developed previously [267,283].

2.3.8 Super-resolution radial fluctuation (SRRF) imaging

For actin imaging experiments, super-resolved Lifeact-GFP images acquired alongside receptor and β-arrestin, with image sequences being analysed using the super-resolution radial fluctuations (SRRF) algorithm implemented in the NanoJ-SRRF ImageJ plugin [331]. In overlaid images, the coordinates of single-molecule trajectories were rescaled to match the higher resolution SRRF images.

2.3.9 Single molecule calibration with fluorescent beads

Fluorescent bead controls were generated on each experiment day, based on reference points taken with multi-colour fluorescent beads (100nm, TetraSpeck). Calibration samples were

prepared by spotting 50μl of 1:10000 diluted beads in DMSO on 25mm ultraclean coverslips. TIRF image sequences were acquired as described in 2.2.9 with the same imaging parameters. Sample areas which had well-separated diffraction-limited spots that bleach in a single step were chosen. Detection and tracking analysis were performed for each channel, and image sequences from different channels were registered against each other using a linear piecewise transformation algorithm [267]. The inter-channel localisation precision after coordinate registration was calculated as <20nm.

2.4 SPT ANALYSIS

2.4.1 Automated particle detection and tracking

Particles from processed TIRF movies were detected and tracked using custom algorithms in the MATLAB work environment. Subpixel location and intensity over background of diffraction-limited particles are calculated by fitting a 2D Gaussian distribution over local intensity maxima, with a standard deviation of the microscope point spread function. This is performed over all frames in the image sequences prior to linking of trajectories between frames. Tracking is performed on the multiple-hypothesis testing approach [283], which calculates the individual probability that a particle in one frame corresponds to a given particle in the next frame. For each particle at each frame, a cost is assigned to each potential event (e.g. Particle blinking, appearing, disappearing, merging and splitting) and the solution which minimises the cost is selected. As such, this allows tracking of a particle beyond a blinking event, which is not possible with other tracking methods. The tracking analysis outputs the position and intensity of each particle at each frame as well as information about merging and splitting events. Intensities are expressed as the amplitude of the 2D Gaussian fit and allows spot

number analysis for multiple particles, even when they are very close. Purpose-built MATLAB algorithms to study diffusion and interactions of single molecules were used further after detection and tracking.

2.4.2 Time-averaged mean squared displacement (TAMSD) analysis

Diffusion coefficients of single particles can be calculated from a time-averaged mean squared displacement (TAMSD) of trajectories from their origin position for a given time interval (Δt), which is averaged along the trajectory [298,332]. A linear dependence between MSD and Δt indicates Brownian motion, while a plateau in the curve is indicating confined diffusion. TAMSD data were fitted to the equation describing anomalous diffusion for the ensemble averaged TAMSD of an anomalous ergodic process:

$$TAMSD(\Delta) = 4D\Delta^{\alpha} + 4\sigma_{err}^{2}, \qquad \text{(Eq.1)}$$

where Δ indicates lag time between the two positions taken by the particle used to calculate its squared displacement, α is the anomalous diffusion exponent and σ_{err} is a constant, which accounts for localisation error. σ_{err} was estimated experimentally by tracking fluorophores immobilised on ultraclean glass coverslips and found to be ~40nm. Only trajectories lasting at least 100 frames were included in TA-MSD analysis, to increase the reliability in accurately measuring a diffusion coefficient, at the cost of a decrease of overall trajectory numbers analysed. Since this analysis revealed heterogeneity among particles, trajectories were then categorised according to the diffusion parameters D and α. Particles with $D < 0.01\mu m^2 s^{-1}$ were considered to be confined/trapped. For anomalous diffusive states, normal diffusion was assigned to particles that had $D \geq 0.01\mu m^2 s^{-1}$ and $0.75 \leq \alpha \leq 1.25$. Sub and super-diffusion were

assigned to particles with D ≥ 0.01μm^{2}s^{-1} and α <0.75 or α >1.25, respectively. These cut-offs were obtained from results generated by Sungkaworn et al. based on results obtained with simulated particles [253].

2.4.3 Sub-trajectory TAMSD analysis

The output of TAMSD is a single diffusion coefficient and exponent value for a trajectory. An issue with this is that cell membranes are non-ideal thermodynamic systems and molecules transition between multiple states of complex diffusion. The TAMSD averages over all points across a trajectory so transitions between diffusive states are obscured. Given that molecules can exhibit complex diffusion, a sub-trajectory TAMSD analysis was used, so that distributions of freely diffusing and trapped diffusion could be approximated [333]. Segments characterised by free diffusion were fitted using (Eq. 1). Eq. 1 cannot effectively approximate plateaus, which would be reported for molecules whose displacement does not change over time steps, and thus another method is required to accurately fit these events. Segments characterised by confinement/trapping were fitted using the equation describing diffusion of a molecule inside a harmonic potential [334,335]:

$$TA-MSD(\Delta) = \frac{4D}{\lambda(1-e^{-\lambda\Delta})} + (r_0^2 - D/\lambda)\left(1-e^{-\lambda\Delta}\right)^2 \frac{1-e^{-2\lambda(N-\Delta)}}{\lambda(N-\Delta)} + 4\sigma_{err}^2, \qquad \text{(Eq.2)}$$

where r_0^2 is the squared distance from the centre of the trap at the beginning of the diffusive process and λ is the mean reverting rate. From this, the approximate confinement/trap diameter (d) was deduced as $d = 2\sqrt{2D\lambda}$.

2.4.4 Spatial confinement analysis

Spatial confinement of trajectory segments characterised as confinement/trapping was further assessed using our recently published algorithm [333]. For each trajectory, a recurrence matrix (M_{ij}) containing information about the distances between each pair of points in a trajectory was computed:

$$M_{ij} = \exp\left(-\frac{1}{2}\left|\boldsymbol{x_i} - \boldsymbol{x_j}\right|^2/\lambda^2\right), \qquad \text{(Eq.3)}$$

where *i* and *j* denote different steps of the trajectory, *x* is the position of the particle and λ is the test length scale of the analysis. M_{ij} approaches 1 if the distance between $\boldsymbol{x_i}$ and $\boldsymbol{x_j}$ is smaller than λ. To minimise the effects of localisation error and possible mis-detected outliers, M_{ij} was smoothened by local averaging and thresholded to obtain a binary matrix (B), where $B_{ij} = 1$ if $M_{ij} > e^{-1}$ or zero otherwise. Trapped portions of the trajectory appear in B as square blocks of ones along the matrix diagonal (**Figure 2.4**). To detect these blocks, three quantities were calculated: block time ($t_|(n)$), neighbouring time ($t_\perp(n)$) and persistence time ($t_\parallel(n)$), from which the invariant quantity $v(n)$ was computed:

$$v(n) = \frac{t_|(n)}{t_\parallel(n) + t_\perp(n) - 1} \qquad \text{(Eq.4)}$$

In the idealised case of a perfect squared box of ones it is easy to verify that $v(n)$ = 1. In practice, blocks are never perfect squares so a cut-off of v_n = ¾ was used to identify blocks corresponding to potential confined trajectory segments. A statistical test based on the probability of detecting a bigger block by chance for a particle with 2D fractional Brownian

motion (fBM) and P value = 0.05 is then applied to decide if the detected block is a real confinement event.

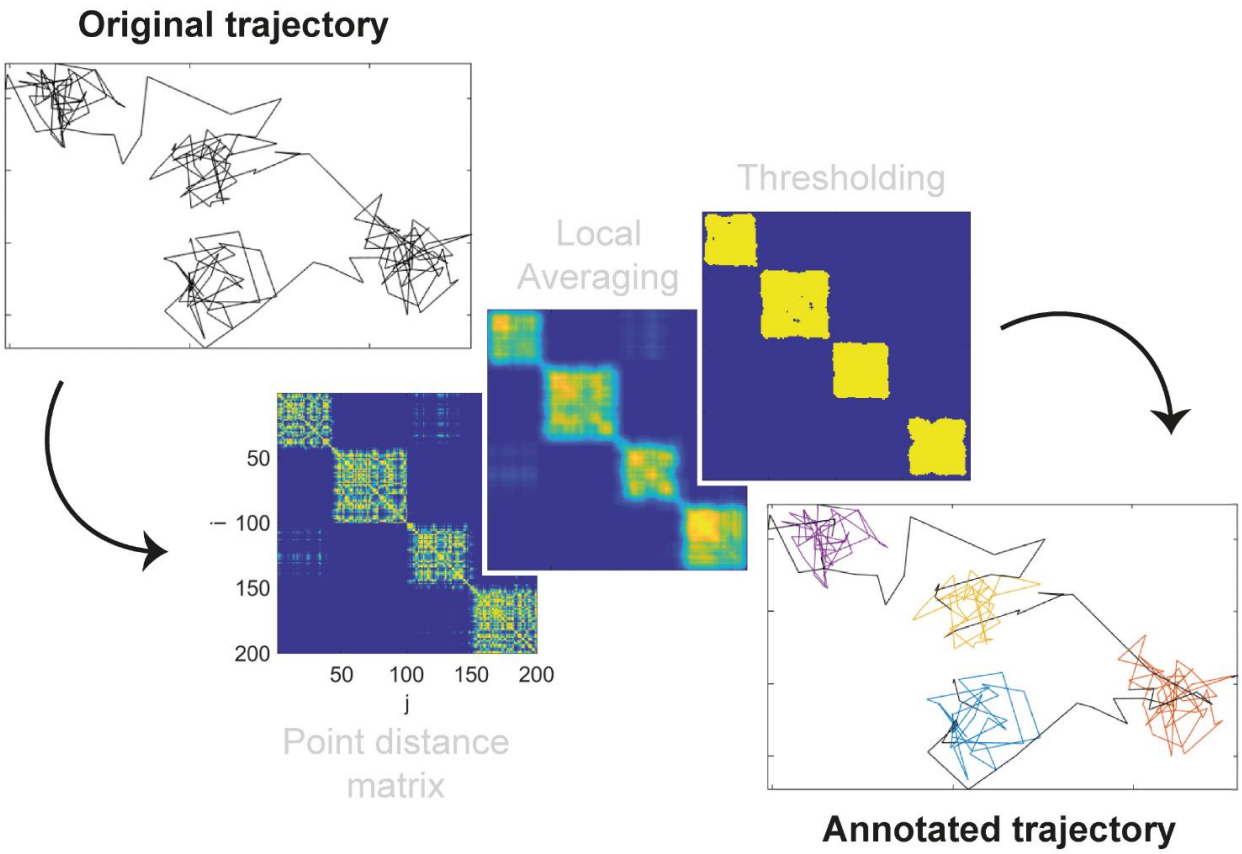

Figure 2.4 Schematic of spatial confinement analysis. Detection of spatially confined trajectory segments. Simulated trajectory alternating phases of free and confined diffusion (top-left), corresponding recurrence matrices point distances between a pair of points *i, j* after local averaging and thresholding (middle) and result of segmentation (bottom-right). Segments characterised by free diffusion are shown in black, whereas confined ones are highlighted in different colours.

2.4.5 CCP detection

Clathrin-coated pits (CCPs) could be detected from images by applying a frame-by-frame binary mask to CCP-GFP data. Image sequences were pre-processed to remove local background and enhance contrast, using a bottom and top-hat filter with a disk-shaped structuring element of

11-pixel diameter ('imtophat' and 'imbothat' functions in MATLAB). A temporal Kalman filter with low gain (0.1) was applied to reduce noise. The image sequences were then deconvolved with the theoretical point spread function (PSF) of the system using the Lucy-Richardson algorithm [336,337]. Binary masks corresponding to CCPs were then obtained by thresholding the image sequences with a value corresponding to the mean plus standard deviation of each frame. Only pixels persisting at least 45 consecutive frames (~ 1.5 s) were included in the final CCP masks.

2.4.6 Single-molecule interaction analysis and estimation of k_{on} and k_{off}

Single-molecule interactions were analysed using an algorithm developed previously [253], to extract information regarding real interactions between particles in two channels from total interactions (i.e. real interactions plus random colocalisations). Receptor and β-arrestin movies were aligned as previously described (see section 2.3.9). For each particle in channel 1 at a given frame, particles in channel 2 within a defined search radius (R_0= 150nm) were considered colocalising. The search radius was approximately 4 times the localisation error, which enables interaction of a particle at the far-left of the error localisation window with the far-right. For each colocalisation event, a start and termination frame were obtained to determine the length of colocalisations. Each observed colocalisation time (Δt_{obs}) corresponds to the average duration of true interactions (Δt_{true}) plus the average duration of random colocalisations (Δt_{random}).

A Monte Carlo approach was used to link colocalisation events that were prematurely terminated, due to uncertainty in the assignment of trajectory segments after a splitting event. The distribution of observed colocalisation times can be seen as a convolution of the

distribution of true interaction times with those random colocalisations. To estimate the true interaction times from this, expected random colocalisations were first estimated in cells expressing SNAP-CD86 labelled with SNAP-AF647, βArr2-Halo labelled Halo-JF549 and unlabelled wild-type β_2AR, since CD86 has no known interactions with arrestin. The distributions of true interaction times were estimated by deconvolving the observed distributions of colocalisation times with those obtained for the non-interacting control pair (CD86-βArr2), using Lucy-Richardson algorithms [336,337].

To estimate the dissociation rate constant of particle-particle interactions (k_{off}), normalised relaxation curves obtained from the distributions of deconvolved interaction times were fitted to an exponential decay function:

$$F_r(t) = F_{true} e^{-(k_{off}+k_{loss})t} \quad \text{(Eq.5)}$$

Where $F_r(t)$ is the fraction of surviving interactions at time t, $F_{true}(\leq 1)$ is the fraction of true interactions (out of total interactions) at t= 0. k_{loss} is a correction factor, accounting for the premature termination of interactions due to photobleaching, and loss of particles due to detection and tracking errors. k_{loss} was estimated based on simulated image sequences of randomly diffusing particles which existed as obligate dimers and could not dissociate.

Association rate constant (k_{on}) values are related to F_{true} and the rate of new colocalisations per unit of area $d[C]_\rho/dt$ were determined by the following equation:

$$\frac{d[C]_\rho}{dt} \cdot F_{true} = k_{on}[R]_\rho[A]_\rho, \quad \text{(Eq.6)}$$

where $[\ ]_\rho$ denotes density and $[R]_\rho$ and $[A]_\rho$ are the densities of free receptor and β-arrestin molecules, which can in turn be derived by subtracting the estimated density of receptor-β-

arrestin complexes ($[RA]_\rho$) from the total densities measured in channels 1 $[Ch1]_\rho$ and 2 $[Ch2]_\rho$. Finally, $[RA]_\rho$ can be deduced based on the balance between association and dissociation rates at equilibrium using the formula:

$$[RA]_\rho = \frac{1}{k_{off}} \frac{d[RA]_\rho}{dt} \cdot F_{true} \qquad \text{(Eq.7)}$$

These relationships allowed an estimation of k_{on} from using following formula:

$$k_{on} = \frac{\frac{d[RA]_\rho}{dt} \cdot F_{true}}{\left([Ch1]_\rho - \frac{1}{k_{off}} \frac{d[RA]_\rho}{dt} \cdot F_{true}\right)\left([Ch2]_\rho - \frac{1}{k_{off}} \frac{d[RA]_\rho}{dt} \cdot F_{true}\right)} \qquad \text{(Eq.8)}$$

k_{on} was estimated separately at each frame and the presented values were obtained by averaging over the analysed frames.

2.4.7 Markov chain analysis

Every β-arrestin at each frame was labelled with binary denominators describing the presence/absence of spatial confinement, CCP localisation, and colocalisation with a receptor. Considering all possible combinations and discarding the physically irrelevant ones, such as freely diffusing molecules on a CCP or colocalisation between a freely diffusing and a confined molecule, a set of 6 unique states plus a dummy state corresponding to molecules before or after their detection on the plasma membrane to account for movements between the cytosol and the plasma membrane, as well as disappearance due to fluorophore photobleaching were obtained (**Table 1**). When the diffusion state of the colocalising partner was different to the molecule of interest, they were considered not colocalising and instead passing each other (random colocalisation). Forward Markov chains were built by gathering state information

from all trajectories. Only states lasting at least 10 frames (0.33 s) and their transitions were considered.

#	State	Confined	Inside CCP	Colocalisation with receptor	Colocalising partner confined
0	Absent				
1	Free	0 0 0	0 1 0	0 0 1	 1
		0	1	1	1
2	Codiffusion	0 0	0 1	1 1	0 0
3	Confined	1 1	0 0	0 1	 0
4	Co-confined	1	0	1	1
5	Trapped alone in CCP	1 1	1 1	0 1	 0
6	Co-trapped in CCP	1	1	1	1

Table 1 β-arrestin states for Markov Chain analysis. Table representing the quadruplets corresponding to each assigned state. 'Confined' is determined from spatial confinement analysis, inside CCP is derived from CCP mask and colocalisation is obtained by checking the presence of a molecule on the on the other channel within a 150nm search radius. In the case when a molecule is within search radius the colocalising molecule is checked for trapping.

2.4.8 History plots

Plots displaying all the possible sequences of events before and after a given target state were generated in several steps. First, trajectories containing the target state were collated. Then, for each trajectory, the gathered *h* states were separated, preceding and following the target state. This information was used to build two separate tree graphs before and after the target state (past and future), where the branches represent all observed sequences of events. Taking advantage of graph theory, a branch number of each history in either graph was assigned using to the following formula:

$$branch\ number = \sum_{i=0}^{h} n_i \times N^i, \qquad \text{(Eq.9)}$$

where i iterates over all states in the sequence (from the target state i=0 to the furthest state from present to be accounted for i=h) with $n_i$being the state number of the state i, and N is the number of distinct states (including the absent state, $N = 7$). Finally, histories were sorted according to their branch number. Graphic representations were obtained by stacking all histories, each represented by a thin horizontal line; which were colour coded according to the contained states.

2.4.9 Statistics

Statistical analyses were conducted in MATLAB. Differences between three or more groups were assessed by a non-parametric Kruskal-Wallis test followed by unpaired two-tailed t-test with Bonferroni correction. Differences were considered significant for $P < 0.05$. Single-molecule data were analysed by automated scripts with no user intervention during the analysis. Individual statistical parameters are reported in the figure legends.

2.5 MOLECULAR DYNAMICS

2.5.1 Simulations

The initial conformation of βArr2 was modelled with MODELLER [338,339], using the structure of β-arrestin in complex with the muscarinic M2 receptor [PDB code: 6U1N] [120]. This template was selected as the C-edge is resolved in a conformation that exposes hydrophobic residues towards the membrane interface, which is expected to promote membrane interaction [123].

The inactive conformation of the finger loop was obtained from the inactive structure of βArr2 [PDB code: 3P2D] [340]. To study spontaneous association to the plasma membrane, the structure was placed in proximity to the lipid bilayer. To mimic the experimental conditions, the membrane composition of CHO cells was used in simulations [341], incorporating the five most abundant membrane components into the simulation setup: 10% cholesterol, 38% palmitoyl-oleoyl-phosphatidylcholine, 28% dioleoyl-phosphatidylcholine, and 24% dioleoyl-phosphatidylethanolamine.

Simulations were performed with the ACEMD3 package. Parameters for system components were obtained from CHARMM36m and CHARMM36 force fields [122]. To generate the βArr2 lipid-mutant, the involved modifications were introduced with the CHARMM-GUI server. To study spontaneous membrane entry of βArr2, 50 x production runs of 50 ns were carried out, starting from a conformation of βArr2 in the vicinity of the membrane. Afterwards, 4 x additional simulations were performed, each amounting to 600 ns, starting from a C-edge anchored conformation of βArr2 observed in the previous simulations.

2.5.2 Contact analysis

To study the strength and stability of βArr2–membrane interactions, 3 production runs of 1 μs each were carried out, starting from the conformation obtained in spontaneous association experiments with βArr2 anchored to the lipid bilayer. To quantify the interactions, the distance from the membrane of reference amino acids in the finger loop (A61-D79), C-loop (A240-Q251) and C-edge (T188-H199, N224-E231, S329-V336) were monitored. By using this approach, quantification of the coordination number for each of the residues studied can be analysed, which is directly related with the strength of the interaction between βArr2 and the lipid bilayer. The coordination number is calculated for each residue in each frame for the 3 accumulated μs to posteriorly calculate its mean value for the selected finger loop, C-loop and the C-edge residues. To simplify the comparison between wild-type and mutant βArr2, total coordination numbers for the finger loop, C-loop and C-edge were calculated by summing up the coordination numbers of each of the residues in each region.

2.5.3 Inter-domain rotation angle

To study the impact of membrane anchoring on the conformation of βarr2, 3 additional 1-μs runs with βArr2 in solution were carried out. The rotation angle between βArr2 N- and C-domains was computed as previously described [342]. The utilised scripts were kindly provided by Naomi Latoracca [141]. To evaluate the ability of Fab30 to recognise the observed active-like conformation of the fully membrane engaged βArr2, the conformations obtained in MD simulations with that of the structure of Fab30 in complex βArr2 were compared [PDB code: 4JQI] [45].

3 βArr2 laterally diffuses on the plasma membrane without an accompanying GPCR

3.1 PREFACE

β-arrestin is classically thought of as a cytosolic protein, which desensitises GPCRs to G protein signalling and leads to receptor internalisation at clathrin-coated pits (CCPs). Structural studies over the last decade have revealed a dynamicity previously unexpected of arrestin. Although *Eichel et al.* have initiated single-molecule TIRF investigations into β-arrestin and β-adrenergic receptors [106,315], finding evidence that arrestin can accumulate at CCPs without an accompanying receptor, multi-colour single particle tracking and elucidation of the sequence of events in an arrestins lifetime on the plasma membrane remain to be seen. Experimentally, single-molecule TIRF forms an ideal system to investigate GPCR signalling, offering a high signal-to-noise ratio around the plasma membrane and requiring expression of low, physiological densities of molecules. The arrestins, GPCRs and structural elements were studied together, in real-time and with spatiotemporal resolution sufficient to answer questions regarding β-arrestin on the plasma membrane.

3.2 RESULTS

3.2.1 Construct validation

For single-molecule experiments, βArr2 and the β_2AR were labelled with two distinct organic fluorophores via insertion of Halo and SNAP tags, respectively. SNAP-β_2AR [267] and βArr2-Halo constructs were validated for functionality by both TIRF imaging and cell-based BRET assays. By TIRF, the cellular expression, βArr2 plasma membrane recruitment, dye pair testing, photobleaching rates, dye saturation labelling and non-specific binding were investigated.

Functional characterisation of the Halo-tagged βArr2 construct was first demonstrated by NanoBRET measurements, monitoring association of βArr2 with the plasma membrane (measured by K-ras), β_2AR and CCPs after stimulation of β_2AR in HEK293 cells with the high-affinity β_2AR agonist, Isoprenaline (**Figure 3.1**). After stimulation, βArr2 maintains a steady, increased interaction with the membrane and CCPs over 60 minutes, with receptor interactions increasing and then decaying to an elevated plateau after initial stimulation. This is likely due to receptor internalisation and reduced interactions with arrestin being observed over the time window. Arrestin recruitment to the plasma membrane after receptor stimulation was also confirmed by TIRF imaging (**Figure 3.2**), with a clear increase in fluorescent spots observed on the plasma membrane after Isoprenaline interrogation. Additionally, β_2AR internalisation was increased with the βArr2-Halo construct, as seen by a decrease in K-ras-Venus association after stimulation with increasing concentrations of βArr2 (**Figure 3.2**). Together, these results suggest that our βArr2-Halo construct is functionally able to bind to the membrane, CCPs, receptors, recruits after receptor stimulation and is able to induce receptor internalisation.

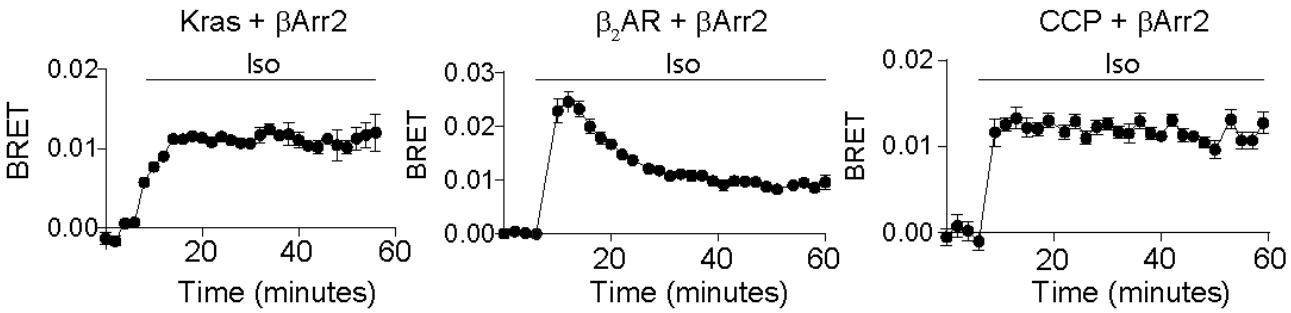

Figure 3.1 Functional characterisation of the Halo-tagged βArr2 construct by NanoBRET. Shown are the results of real-time measurements monitoring BRET between NanoLuc fused to K-ras (plasma membrane recruitment; left), β_2AR (receptor binding; middle) or clathrin light chain (CCP recruitment; right) and βArr2-Halo labelled with Halo-R110. Cells were stimulated with isoprenaline (10 μM). Iso, isoprenaline. Data are mean ± s.e.m, n=4 independent experiments

SNAP-β_2AR was labelled with a non-membrane penetrant dye, which increases the TIRF S:N ratio by reducing intracellular fluorescence. Thus, only receptors present only on the plasma membrane are observed. βArr2-Halo is expressed in the cytoplasm, so a cell-penetrant dye was required to label these molecules. As such, Halo was used to tag βArr2, due to the availability of bright, photostable dyes available for Halo which can cross the membrane [343]. βArr2 was labelled with Halo-Janelia-549 (JF549) and Halo-Janelia-646, but JF549 was found to exhibit better photophysical properties including a reduced blinking and photobleaching. After testing dyes for SNAP-tagged receptors, it was found that and SNAP-Surface549 had the best properties, however due to the requirement for J549 labelling of arrestins, SNAP-AlexaFluor 647 (AF647) was used to enable two-colour imaging, at the expense of photostability. This was corrected with a non-invasive, non-cytotoxic hypoxia setup, used to increase fluorophore lifetime (described in section 2.3.1). Fluorescence decay curves were generated from SMM experiments and average fluorescence half-lives of JF549 ($\tau\sim$ 52 s) and AF647 ($\tau\sim$ 17 s) were estimated (**Figure 3.3**).

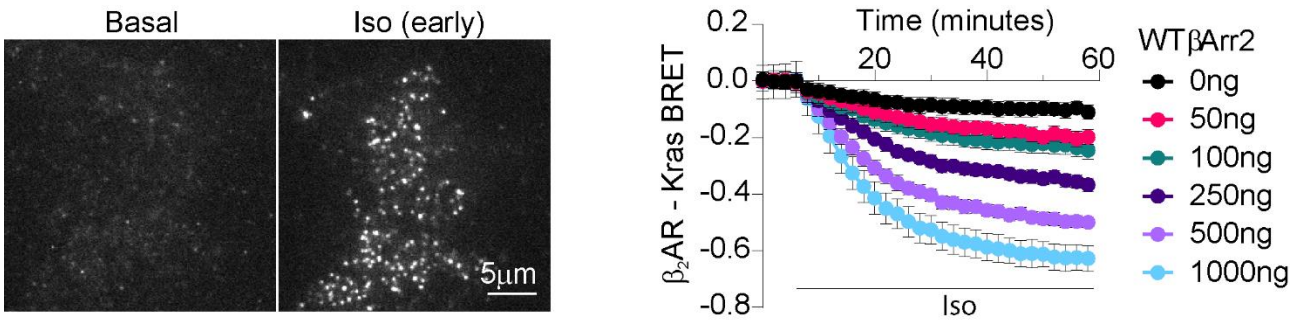

Figure 3.2 βArr2 plasma membrane recruitment and GPCR internalisation. (Left) Representative single-molecule experiment showing rapid plasma membrane translocation of individual βArr2-Halo molecules upon after 2-minute stimulation with isoprenaline (10 µM) in CHO-K1 cells. (Right) Real-time measurements monitoring BRET in CRISPR HEK293 cells lacking endogenous βArr1/2, between Nanoluc fused to β_2AR and K-ras fused to Venus and in the presence of increasing concentrations of βArr2. Iso, isoprenaline. Data are mean ± s.e.m, n=4 independent experiments

Saturation labelling of JF549 and AF647 was achieved in cells expressing β_2AR carrying either an intracellular Halo tag or extracellular SNAP tag in the presence of increasing concentrations of dye (**Figure 3.3**). Saturating concentrations of 1μm JF549 and AF647 were used in SMM experiments, which was also incident with very low levels of non-specific binding (<1%) (**Figure 3.3**).

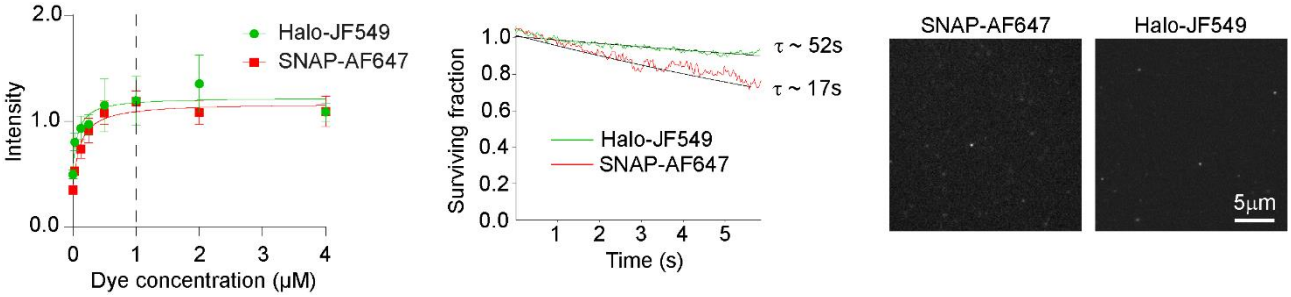

Figure 3.3 Fluorescent imaging controls. (Left) Photobleaching rates. Shown are the photobleaching curves for Halo-JF549 and SNAP-AF647 obtained from single-molecule experiments. (Middle) Labelling efficiency. Shown are fluorescence intensity values in cells expressing β_2AR carrying either an intracellular Halo tag or an extracellular SNAP tag, incubated with increasing concentrations of Halo-JF549 or SNAP-AF647, respectively. Saturating concentrations of both dyes (1 μM) were subsequently used for single-molecule microscopy experiments. (Right) Non-specific labelling. Mock-transfected CHO-K1 cells were labelled with either SNAP-AF647 or Halo-JF549 and imaged by single-molecule microscopy. e, Photobleaching rates. Shown are the photobleaching curves for Halo-JF549 and SNAP-AF647 obtained from single-molecule experiments.

3.2.2 Single-molecule visualisation of βArr2 and β_2AR molecules

SNAP-β_2AR and βArr2-Halo were transiently expressed at low physiological densities in live CHO-K1 cells (plasma membrane densities of 0.62 ± 0.14 and 0.43 ± 0.20 molecules/μm^2 under basal conditions, respectively) and simultaneously imaged by fast multi-colour TIRF microscopy with single particle tracking. Additionally, clathrin-coated pits (CCPs) were visualised by co-transfection of GFP-labelled clathrin light chain (**Figure 3.4**). Data were

acquired both under basal conditions and after early (2-7min) and late (8-15 min) stimulation with the full β-adrenergic agonist isoprenaline (Iso). Under both basal and stimulated conditions, βArr2 molecules were observed to stochastically translocate from the cytoplasm to the plasma membrane. This resulted in their sudden appearance in the TIRF field-of-view, where they then diffused on the plasma membrane before disappearing (**Figure 3.4**).

β_2AR and βArr2 could both be observed laterally diffusing on the plasma membrane, binding to CCPs, most often independent of each other. In fact, βArr2 molecules were mostly observed arriving on the plasma membrane and diffusing without an accompanying receptor – similar to results obtained by Eichel et al. [315]. Of note, the > 95% of βArr2 molecules appeared at sites on the plasma membrane that were not occupied by β_2ARs (**Figure 3.5**). Although accumulation of βArr2 molecules on the plasma membrane after isoproterenol stimulation was observed, similar to BRET results, the rate of new βArr2 molecules appearing on the plasma membrane was remarkably similar between basal and stimulated conditions (**Figure 3.5**). Interestingly, the agonist-induced accumulation of βArr2 molecules was found to be largely due to an increase in their lifetime at the plasma membrane, which had at least one fast ($\tau_{fast} \sim 0.58$ s) and one slow ($\tau_{slow} \sim 4.54$ s) component. In particular, isoproterenol caused a ~8-fold increase in the molecules belonging to the slow component (**Figure 3.5**).

This suggests that agonist activation of receptors increases the amount of βArr2 on the plasma membrane by facilitating more productive interactions that lead to arrestin capture. This makes sense, given that receptor and arrestin concentrations near the plasma membrane are unlikely to change in concentration on the milliseconds scale of signalling. Since the average lifetime of βArr2 on the plasma membrane (0.98 ± 1.36 s) was much shorter than the

fluorophore lifetime (τ~ 52 s), their disappearance was mostly due to dissociation from the plasma membrane rather than photobleaching.

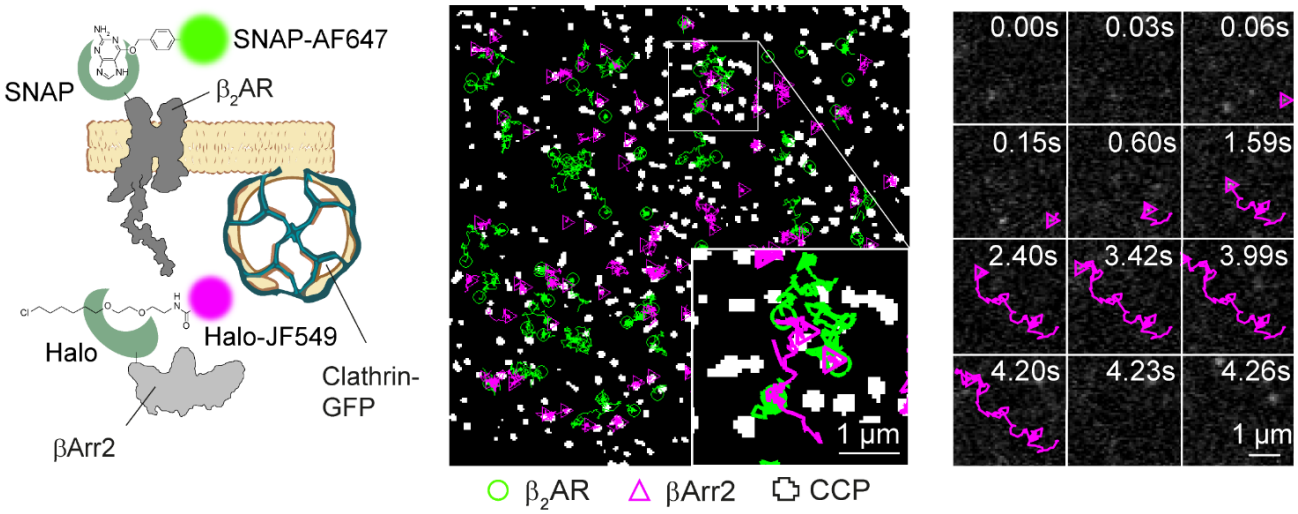

Figure 3.4 Single-molecule imaging of β2AR receptors and βArr2. (Left) Labelling strategy. β_2AR was labelled with SNAP-AF647 via a SNAP-tag fused to its N-terminus. βArr2 was labelled with Halo-JF549 via a Halo-tag fused to its C-terminus. (Middle) Selected frame from a tracked single-molecule image sequence from 3-colour experiments, with trajectories overlaid. Inset, expanded view of the white box. (Right). Representative trajectory of a βArr2 molecule appearing on the plasma membrane and transiently diffusing without an accompanying receptor.

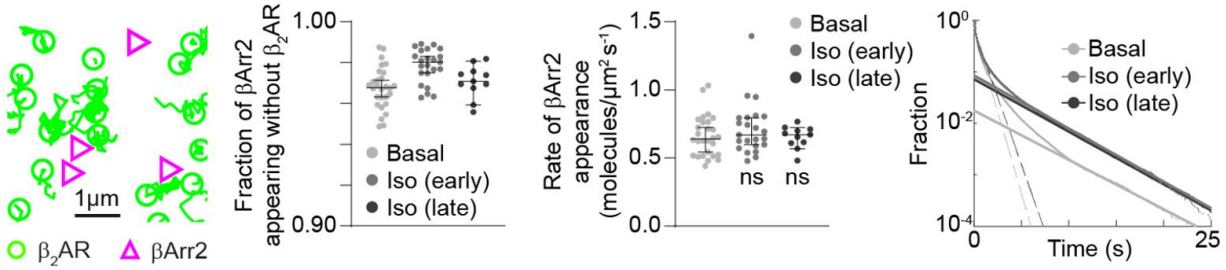

Figure 3.5 βArr2 arrive on the membrane without an accompanying receptor. Sites of βArr2 appearance on the plasma membrane. (Left) representative single-molecule trajectories showing the appearance of βArr2 molecules (magenta) at sites unoccupied by receptors (green) and quantification of the proportion of arrestin molecules appearing at unoccupied sites. Rates of βArr2 appearance on the plasma membrane and Lifetimes of βArr2 molecules at the plasma membrane. Shown are the two main components estimated by exponential fitting (right).

To gain insights into the diffusion properties of β_2AR and βArr2 molecules on the plasma membrane trajectories were initially evaluated by computing their time-averaged mean square displacement (TA-MSD) (**Figure 3.6**). This generates a single diffusion coefficient and anomalous diffusion coefficient for each trajectory (see section 2.4.2). Prior to agonist stimulation, β_2AR were mostly mobile on the plasma membrane (78.3 ± 4.2% mobile trajectories), with a smaller immobile fraction observed. Additionally, most mobile molecules were diffusing freely ($\alpha \sim 1$) (**Figure 3.7**). After stimulating with isoprenaline (10μM), an ~31% increase in the immobile fraction was observed. Interestingly, changes in βArr2 diffusion as detected by TA-MSD were less apparent compared to β_2AR after stimulation. A distinct mobile and immobile fraction were found basally and with isoprenaline stimulation for βArr2 (**Figure 3.7**). As described, heterogeneous diffusing populations were found for both molecules β_2AR and βArr2, the equilibrium of which changed after stimulation. Additionally, molecules were seen to transition between periods of free and trapped diffusion on the membrane, which called into question the use of a single diffusion coefficient for their analysis.

TA-MSD traditionally suffers from two major issues. First, a single diffusion coefficient is assigned to a trajectory, which averages over multiple diffusive states and obscures information about them. Secondly, confined/trapped trajectories cannot be well-approximated using anomalous diffusion scaling, as there is negligible change in displacement. As such, it is difficult to interpret whether the decrease in diffusion coefficient is due to an average slowing down of all trajectories or indeed an increase in the fraction of immobile trajectories. To further understand the role of molecular confinement/trapping in β_2AR and βArr2 trajectories, a new approach was used to analyses these phases separately [333].

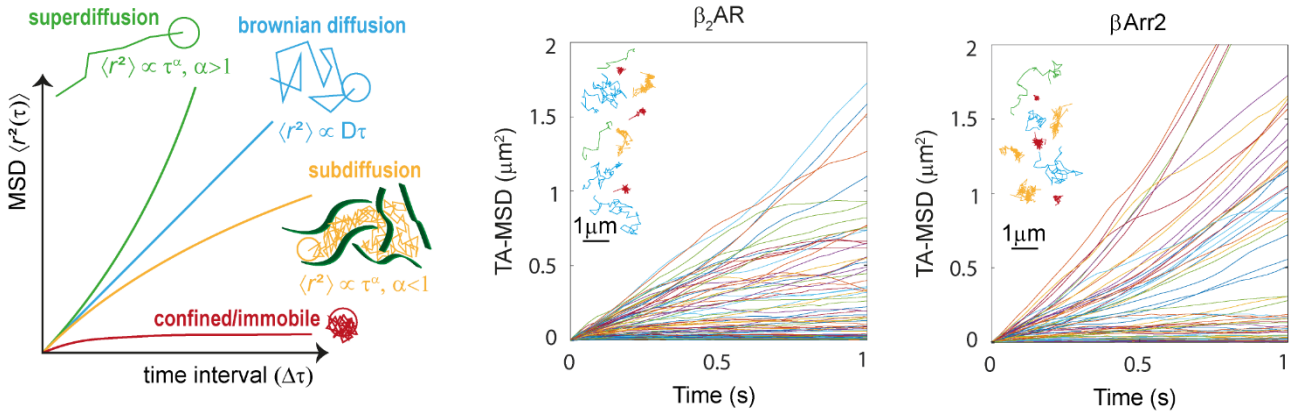

Figure 3.6 Time-averaged mean square displacement (TA-MSD) analysis. (Left) mean square displacement as a function of time, with different diffusive behaviours outlined. (Right) Representative TA-MSD curves of SNAP-β2AR and βArr2-Halo trajectories.

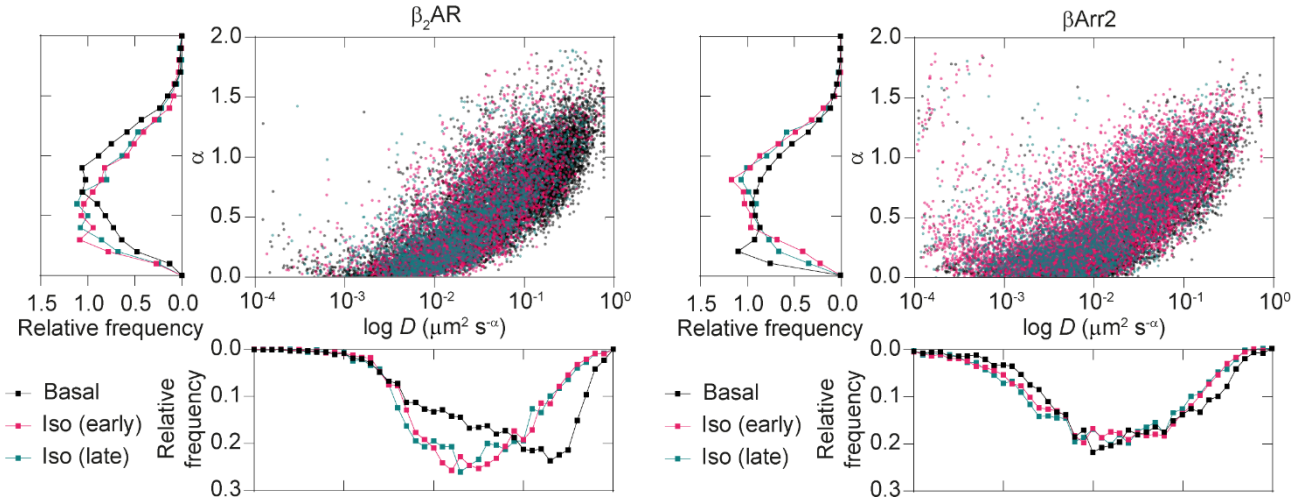

Figure 3.7 Distributions of β2AR and βArr2 diffusion from TA-MSD analysis. Scatter plots and distributions of diffusion coefficient (D) and anomalous diffusion exponent (α) values estimated for β2AR and βArr2 trajectories before (basal) and after isoprenaline (10μM) stimulation. Iso, isoprenaline. Early, 2-7 min. Late, 8-15 min. n = 28, 23 and 11 cells for basal, Iso (early) and Iso (late), respectively.

3.2.3 Spatial confinement analysis identifies increases in molecular trapping of βArr2 and β2AR on CCPs after stimulation

To study altering phases of confinement and free diffusion in β2AR and βArr2, the distances between each pair of coordinates over the trajectory were computed, measuring against a defined length-scale. If the distance between points in the group is smaller than the length-scale for a given amount of time, the molecule is considered confined (see section 2.4.4). Transitions between free and confined diffusion for β2AR and βArr2 were separated in trajectories using this model (**Figure 3.8**), where molecules can be seen to alternate phases of free diffusion and spatial confinement. These diffusive states were concatenated with β2AR and βArr2 localisation on CCPs, producing a series of states based on diffusion and localisation.

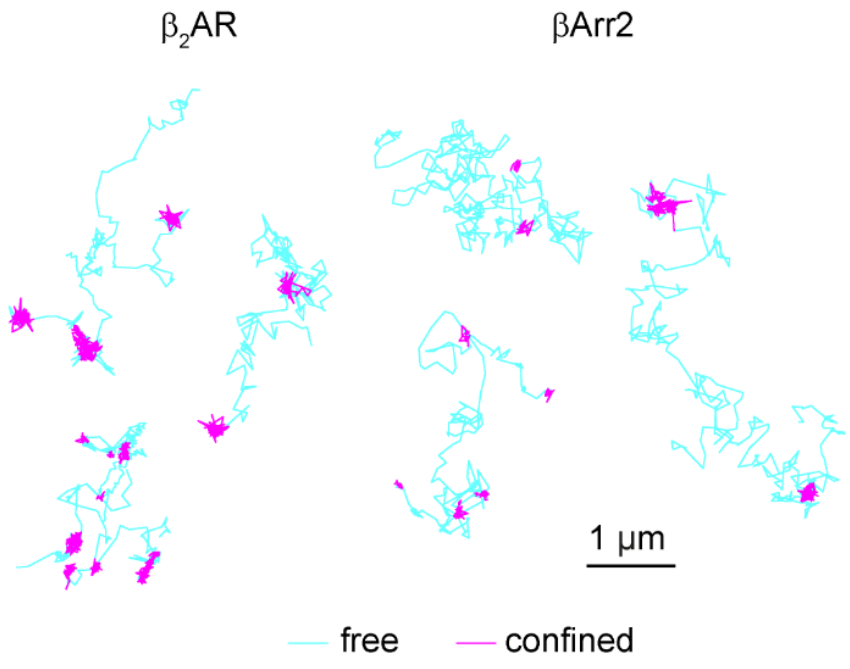

Figure 3.8 Spatial confinement analysis. Application of the spatial confinement analysis in section 2.3.4 on real β2AR and βArr2 trajectories. Shown are representative trajectories alternating phases of free diffusion and spatial confinement diffusing on the plasma membrane.

Under basal conditions, βArr2 molecules spent 52.3 ± 10.7% of their time freely diffusing, 22.6 ± 6.2% confined outside CCPs and 14.0 ± 8.3% trapped in CCPs (**Figure 3.9**). By comparison, the corresponding values for β_2AR were 70.5 ± 8.2%, 18.5 ± 6.0% and 2.9 ± 1.9% (**Figure 3.9**). These results are similar to those obtained with TA-MSD, but provide the ability to localise segments of the trajectory in space and time, providing more detailed insight into the mechanisms of diffusion on the plasma membrane. Isoprenaline stimulation caused ~4-fold and ~2-fold increases in the frequency of β_2AR and βArr2 molecules trapped in CCPs and a modest increase (~1.4-fold) in that of β_2ARs confined outside CCPs (**Figure 3.9**). Interestingly, the durations of individual diffusion states were similar among all conditions, except for those of βArr2 trapped inside CCPs, which increased after agonist stimulation (**Figure 3.10**). This suggests that it is a shift in the frequency of molecules occupying states of free or confined diffusion after stimulation, not an increase in the time spent within those states.

Overall, there results unexpectedly revealed that βArr2 is in equilibrium between a cytosolic and a membrane-bound fraction, with βArr2 molecules spontaneously translocating to the plasma membrane under basal conditions and exploring space on the lipid bilayer via lateral diffusion.

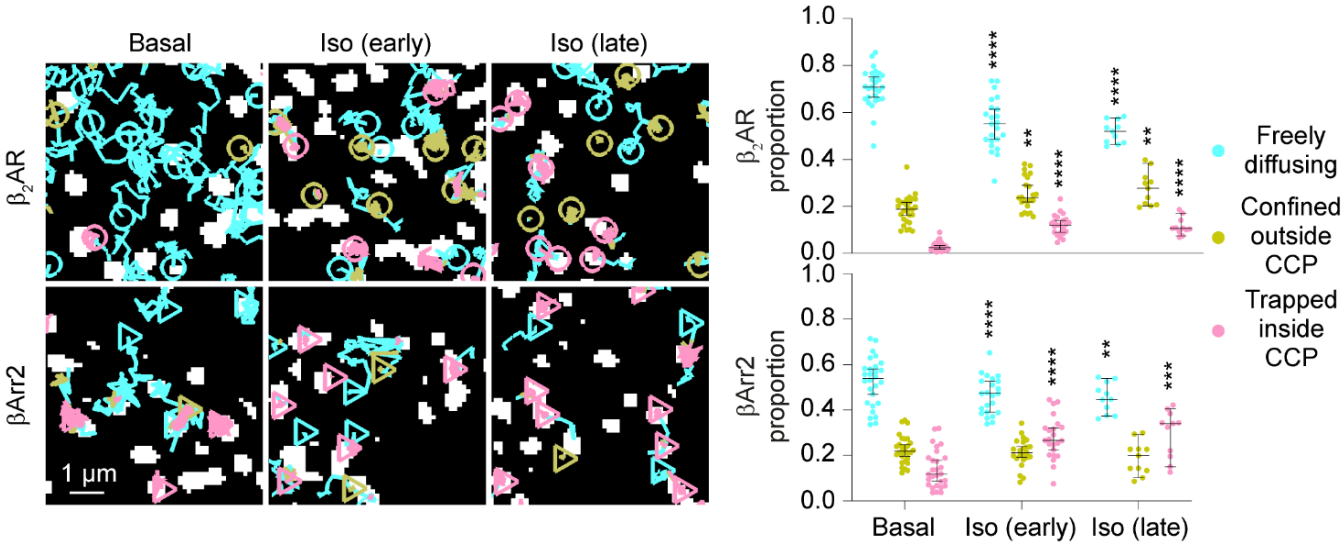

Figure 3.9 Isoprenaline-induced changes in diffusion localisation of β2AR and βArr2. Diffusivity states of β2AR (top) and βArr2 (bottom) molecules. Left, representative trajectories in cells stimulated with isoprenaline (10 μM; late) over CCP binary masks. Trajectory segments were assigned to three diffusivity states based on the results of a spatial confinement analysis and their colocalisation with CCPs. Right, corresponding distributions. Iso, isoprenaline. Early, 2-7 min. Late, 8-15 min. Data are median ± 95% confidence interval. n = 28, 23 and 11 cells for basal, Iso (early) and Iso (late), respectively. Differences are statistically significant by Kruskal Wallis test. *P < 0.05, **P < 0.01, ***P < 0.001, ****P < 0.0001 versus basal by t-test with Bonferroni correction. ns, statistically not significant. Images are representative of a minimum of 4 independent experiments.

3.2.4 Agonist stimulation leads to an increased frequency of β2AR-βArr2 interactions that are highly dynamic and occur via lateral diffusion

β2AR and βArr2 were found to have increased molecular trapping on CCPs after agonist-induced receptor activation. The question of how long β2ARs and βArr2 molecules were interacting with each other was then posed, and whether they interacted together on CCPs. This information is presently unknown, but has generally been assumed to be sufficient for receptor–β-arrestin complexes to reach CCPs without dissociating [101,107,108].

Remarkably, most single-molecule colocalisations were transient and often involved laterally diffusing β_2ARs and βArr2 molecules (**Figure 3.11**), a new finding in the field – but one predicted through some structural studies [140]. To estimate the frequency and duration of the underlying interactions, a previously developed method based on deconvolution of apparent colocalisation times with those of random colocalisations was applied [253]. Random colocalisations times were estimated by imaging βArr2 with the unrelated integral membrane protein CD86, which does not interact with GPCRs or βArr2. It was estimated that β_2AR–βArr2 interactions occurred with an association rate (k_{on}) of 0.062 μm^2 $molecule^{-1}$ s^{-1} (95% confidence interval: 0.071–0.056) and lasted on average ~0.7 s (dissociation rate/k_{off} = 1.34 s^{-1}; 95% confidence interval: 1.37–1.31) in the absence of agonist (**Figure 3.11**). Isoprenaline stimulation caused ~1.4 and ~1.8-fold increases in k_{on} at early and late time points, respectively, whilst causing no significant changes in k_{off} (**Figure 3.11**). These results suggested that agonist-stimulation mainly controls β_2ARs–βArr2 interactions by increasing the rate of formation of productive receptor–arrestin complexes, rather than increasing their duration, similar to previous observations for receptor–G protein interactions [253].

The plasma membrane localisation of β_2AR–βArr2 interactions was then investigated, in addition to whether they involved confined or freely diffusing molecules. Under basal conditions, colocalisation between β_2AR and βArr2 mainly involved free molecules (38%) or molecules confined outside CCPs (43%) (**Figure 3.12**). The latter interactions could be at least partially explained by co-trapping of β_2ARs and βArr2 in small nanodomains delimited by the actin cytoskeleton (**Figure 3.13**). This might suggest the formation of structural nanodomains that are not segmented by CCPs for GPCR-arrestin interactions. Additionally, they might be sites for the scaffolding of proteins for the formation of CCPs. It is tempting to speculate, given that

previous work has shown that the actin cytoskeleton also compartmentalises GPCR-G protein signalling, that some of these sites may contain GPCR megaplexes of GPCR, G protein and β-arrestin. As expected, isoprenaline stimulation increased (~2.4-fold) the proportion of single-molecule colocalisation events between trapped molecules in CCPs (**Figure 3.12**). Although CCPs only make up a small fraction of the plasma membrane (~8%), they are the primary site for receptor-arrestin interactions after stimulation, highlighting their importance in signalling.

These results revealed that β_2AR–βArr2 interactions are highly transient, lasting much shorter than generally assumed, and mainly involve laterally diffusing β-arrestin and receptor molecules.

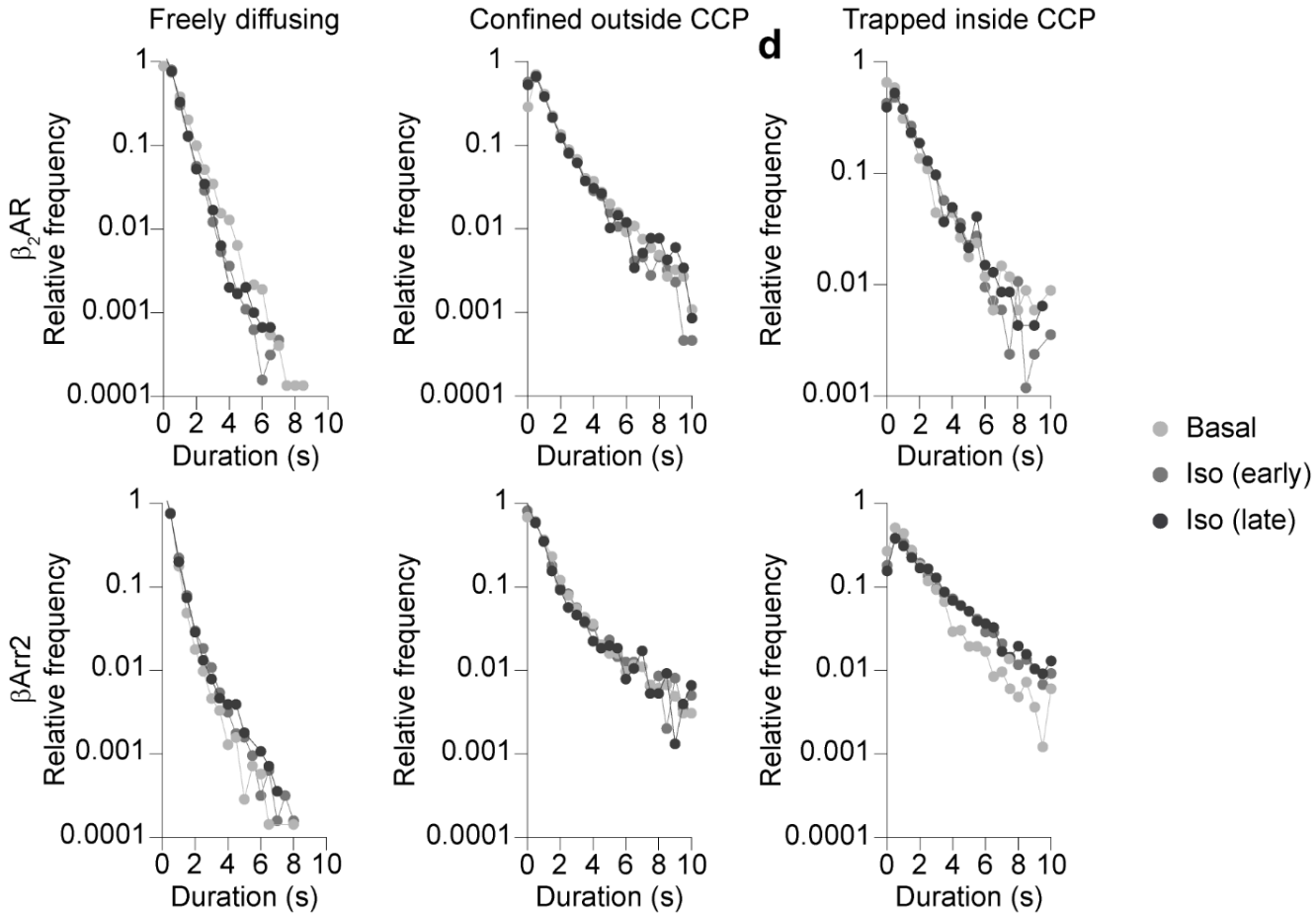

Figure 3.10 Sub-trajectory diffusion duration changes after agonist stimulation. Distributions of the durations of β_2AR (top) and βArr2 (bottom) trajectory segments characterised by free diffusion, confinement outside CCPs, and confinement (i.e., trapping) inside CCPs. Shown are the results before (basal) and after stimulation with isoprenaline (10 μM). Iso, isoprenaline. Early, 2-7 min. Late, 8-15 min. n = 28, 23 and 11 cells for basal, Iso (early) and Iso (late), respectively.

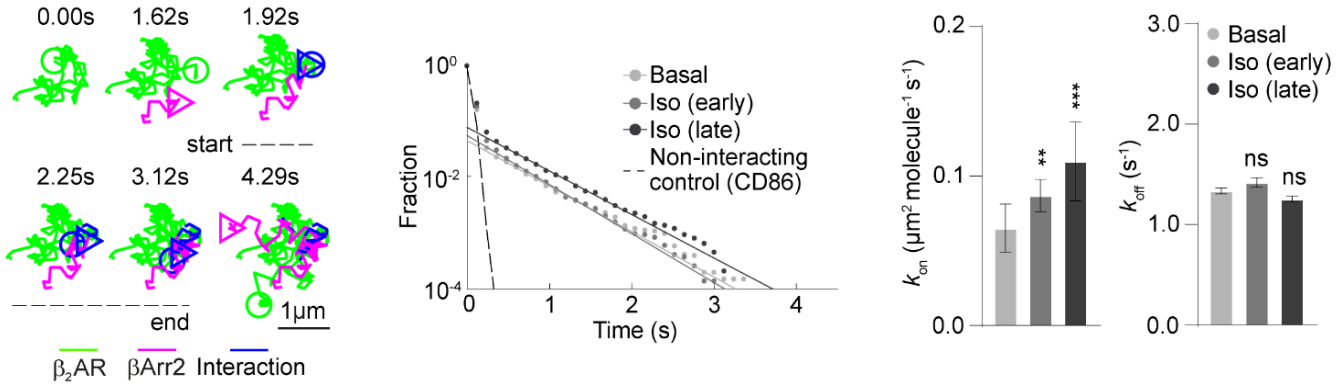

Figure 3.11 β_2AR-βArr2 interaction analysis. (Left) transient (~1.2 s) single-molecule colocalisation between a β_2AR and a βArr2 molecule diffusing on the plasma membrane.

(Middle) Relaxation curves of β_2AR–βArr2 interactions, based on deconvolution of apparent colocalisation times. CD86 was used as a non-interacting control. Estimated k_{on} and k_{off} of β_2AR–βArr2 interactions. Iso, isoprenaline. Early, 2-7 min. Late, 8-15 min. Data are median ± 95% confidence interval. n = 28, 23 and 11 cells for basal, Iso (early) and Iso (late), respectively. Differences in k_{on} are statistically significant by Kruskal Wallis test. *P < 0.05, **P < 0.01, ***P < 0.001, ****P < 0.0001 versus basal by t-test with Bonferroni correction. Differences in k_{off} values versus basal were assessed by two-tailed unpaired t-test with Bonferroni correction.

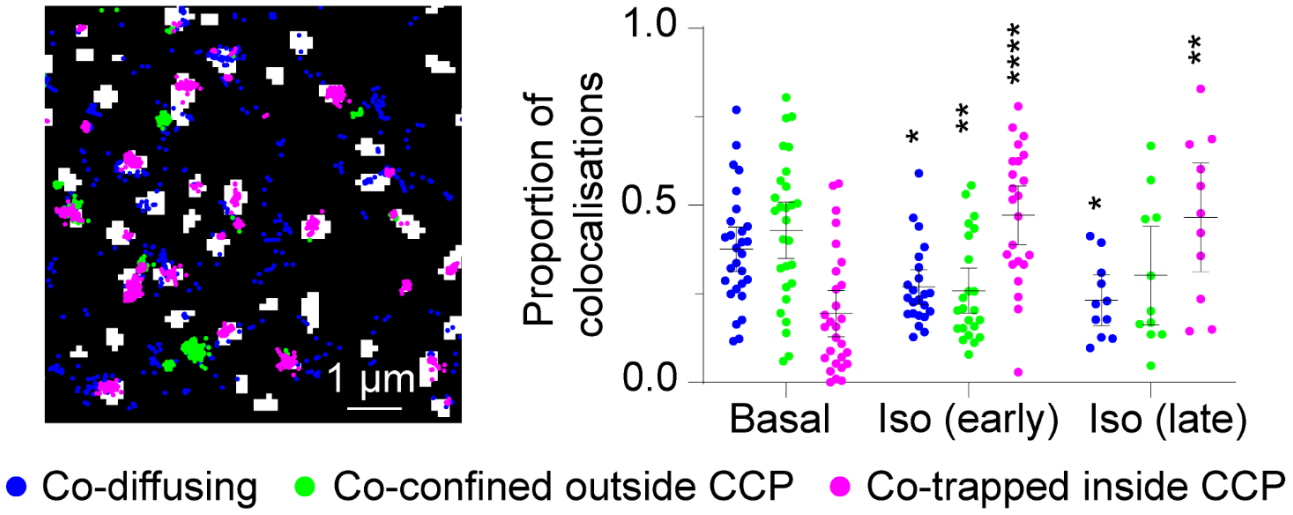

Figure 3.12 **Spatial distribution of β_2AR-βArr2 interactions.** (Left) representative spatial map in a cell stimulated with Iso (late) and (Right) overall distributions of β_2AR–βArr2 colocalisation events, colour-coded based on the diffusivity states of the involved molecules. Iso, isoprenaline. Early, 2-7 min. Late, 8-15 min. Data are median ± 95% confidence interval. n = 28, 23 and 11 cells for basal, Iso (early) and Iso (late), respectively. Differences are statistically significant by Kruskal Wallis test. *P < 0.05, **P < 0.01, ***P < 0.001, ****P < 0.0001 versus basal by t-test with Bonferroni correction. ns, statistically not significant. Image is representative of a minimum of 4 independent experiments.

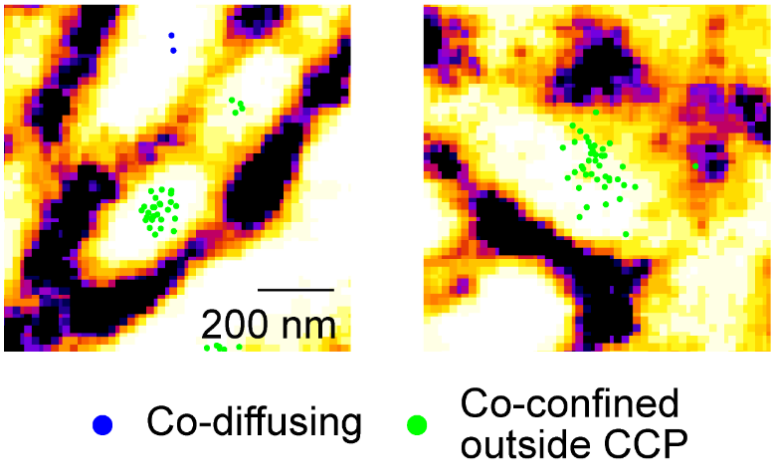

Figure 3.13 Spatial distribution of β_2AR-βArr2 interactions on Actin. β_2AR–βArr2 single-molecule colocalisations over super-resolved (SRRF) image of actin filaments after 2 minutes

isoprenaline stimulation. Images are representative of a minimum of 3 independent experiments.

3.2.5 β_2AR and βArr2 most often arrive independently at CCPs

To investigate the sequence of events involved in β_2AR-arrestin interactions, βArr2 and β_2AR molecules at each frame a state out of a set of 6 unique states (A1-6 and R1-6, respectively), which considered their motion (free/confined), mutual colocalisation (present/absent) and trapping at CCPs (present/absent) (**Figure 3.14**). A dummy state (A0/R0) was added to represent non-visible molecules prior/after their appearance/disappearance from the plasma membrane. This information was used to build Markov chains describing the relative occupancy of the states and their transitions. These probabilistic models assume the Markov property, which states that probability distribution of future states depend only on the current state (**Figure 3.14**). With this, possible transitions can be determined between the defined states as a transition rate. These models were built by Yann Lanoiselée within our lab, for which I was an end-user – inputting microscopy data into the scripts.

Under basal conditions, most receptors were frequently exchanging between a freely diffusing state (R1) and a state corresponding to confinement outside CCPs (R3), with smaller fractions of receptors trapped in CCPs alone (R5). Only minor fractions of β_2ARs were co-diffusing with βArr2 molecules (R2), co-confined outside CCPs (R4) or co-trapped in CCPs (R6). βArr2 showed a similar pattern albeit with a relatively higher proportion of molecules trapped in CCPs (A5). Isoprenaline stimulation increased the proportion of both molecules trapped alone in CCPs, although the effect was more pronounced for β_2AR than for βArr2 (4 and 1.5-fold, respectively) (**Figure 3.15**).

Of note, the transition rates from the states corresponding to β_2AR and βArr2 co-diffusion (R2, A2) to those corresponding to co-trapping in CCPs (R6, A6) were almost non-existent, suggesting that receptors and arrestins do not arrive at CCPs together, as the classical model

would suggest. The main transition leading to β_2AR and βArr2 co- trapping in CCPs (R6, A6) was from the states corresponding to either molecule already trapped alone in CCPs (R5, A5) and a diffusing molecule arriving (**Figure 3.15**).

The sequence of states that precedes and follows single-molecule β_2AR-βArr2 colocalisations was then considered, by summarising the relative frequencies that led to an observed state of interest. The analysis revealed that the majority of βArr2 molecules (~84%) were laterally diffusing alone on the plasma membrane (A1) prior to colocalising with β_2AR (**Figure 3.16**). Similarly, most (~86%) βArr2 molecules continued to diffuse on the plasma membrane (A1) after dissociating from colocalisations with receptors.

Consistently, the state corresponding to βArr2 co-trapped with β_2AR in CCPs (A6) was preceded mostly by βArr2 diffusing on the plasma membrane alone (A1) or βArr2 confined outside CCPs (**Figure 3.16**); which might suggest two separate modalities of βArr2 engagement with CCPs, the former by lateral diffusion and the latter as sites of new CCP formation. This hypothesis is supported by the finding that there is an increase in the transitional probability of both confined (A3) → trapped inside CCP (A5) and co-confined (A4) → co-trapped inside CCP (A6) (**Figure 3.15**), suggesting the synthesis of CCPs at the sites of arrestin and receptor confinement on the membrane.

Importantly, β_2AR and βArr2 were rarely observed reaching CCPs together (3% prior to stimulation, 3.4% after stimulation). A small fraction (~8%) of βArr2 also recruited to CCPs from the absent state, suggesting direct recruitment to CCPs from the cytoplasm. Additionally, there is a recidivism in the interactions preceding and succeeding βArr2 and β_2AR co-diffusion and co-trapping inside CCPs, with most molecules interacting transiently (**Figure 3.16**). βArr2

molecules continue diffusing on the plasma membrane after transient interactions with receptors until they reach and become trapped in CCPs alone (**Figure 3.17**). Remarkably, βArr2 molecules which visited multiple CCPs via lateral diffusion were observed (**Figure 3.17**), supporting previous studies which suggest that βArr2 binding to CCPs can be reversible [119].

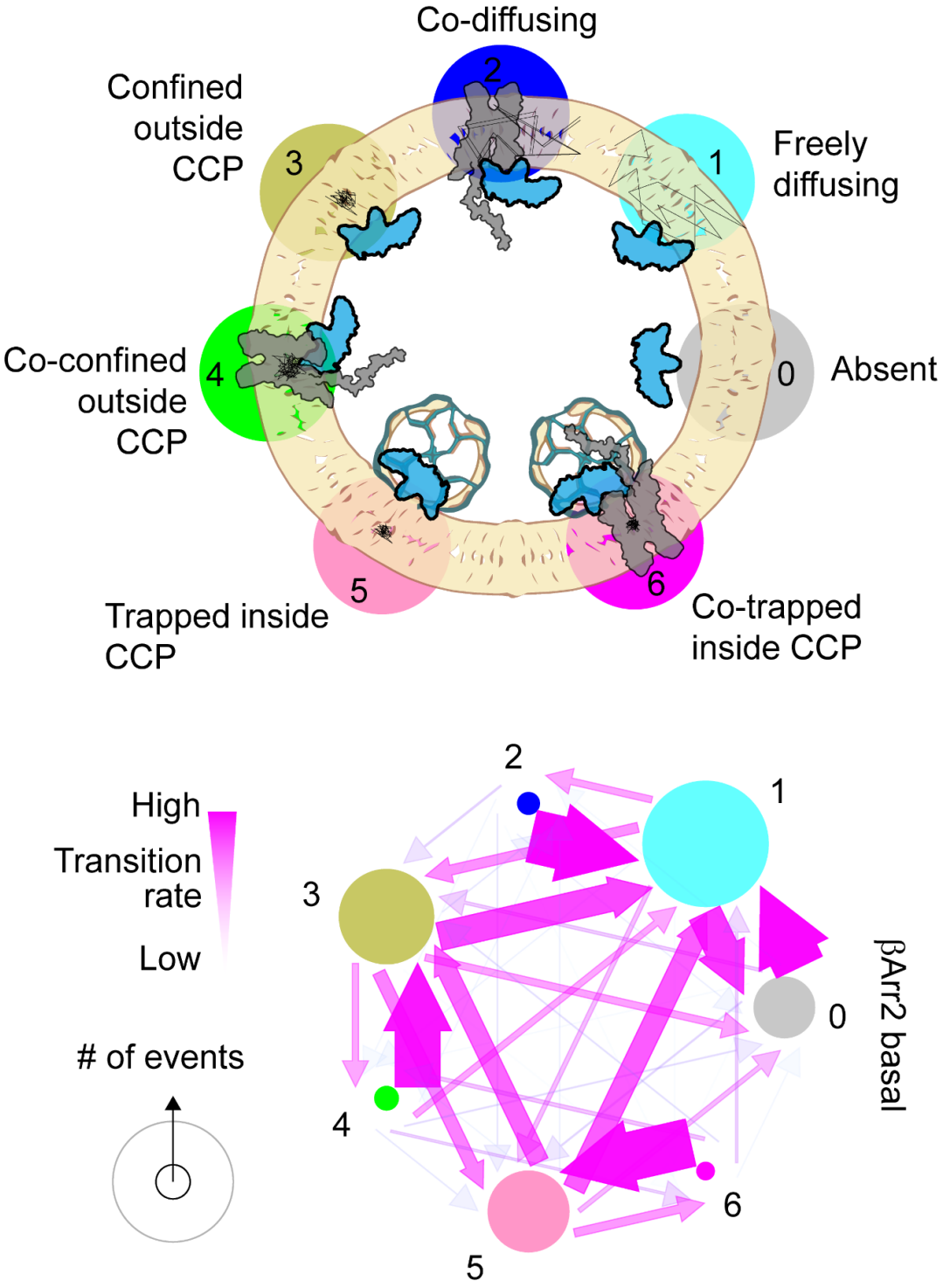

Figure 3.14 Markov Chain analysis schematic. For each frame, β_2AR and βArr2 molecules were assigned to a unique state based on their mutual interactions and diffusion properties (Top). Markov chains showing relative state occupancies (# of events, circle size) and forward transition probabilities (arrow size/opacity) for β_2AR and βArr2 under basal conditions. n = 51147 transitions for βArr2 basal.

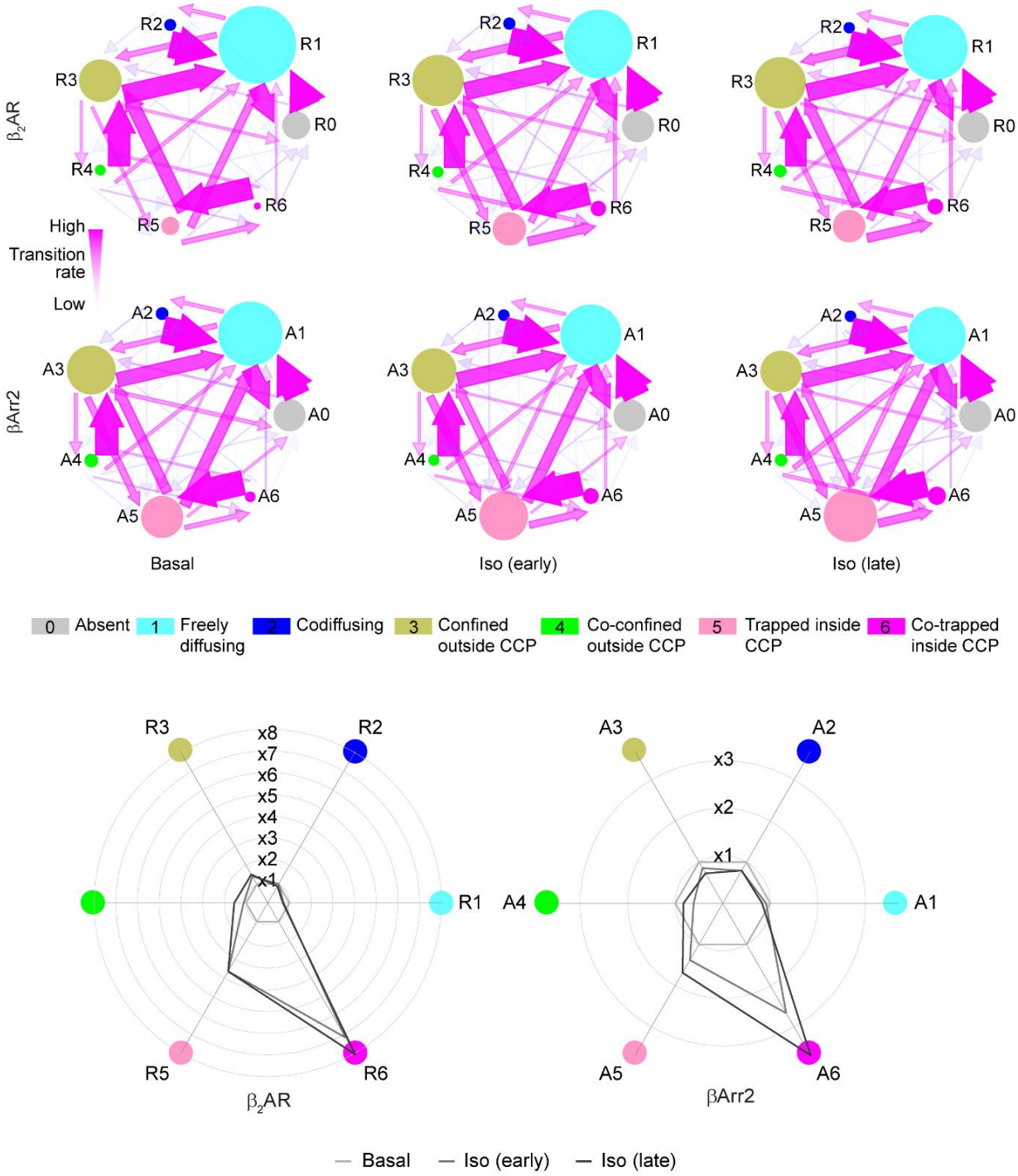

Figure 3.15 **Sequence of events in β2AR–βArr2 interactions on the plasma membrane.** (Top) Markov chains showing the relative state occupancies and forward transition probabilities for β2AR and βArr2 under basal and Iso (early) and Iso (late) conditions. (Bottom) Radar plots showing the changes in state occupancies induced by isoprenaline (10 μM) stimulation. Radar plots are normalised to the corresponding basal levels. Iso, isoprenaline. Early, 2-7 min. Late, 8-15 min. n = 88851, 52658, 27741, 51147, 58254, 22769 transitions for β2AR basal, β2AR Iso (early), β2AR Iso (late), βArr2 basal, βArr2 Iso (early), βArr2 Iso (late), respectively.

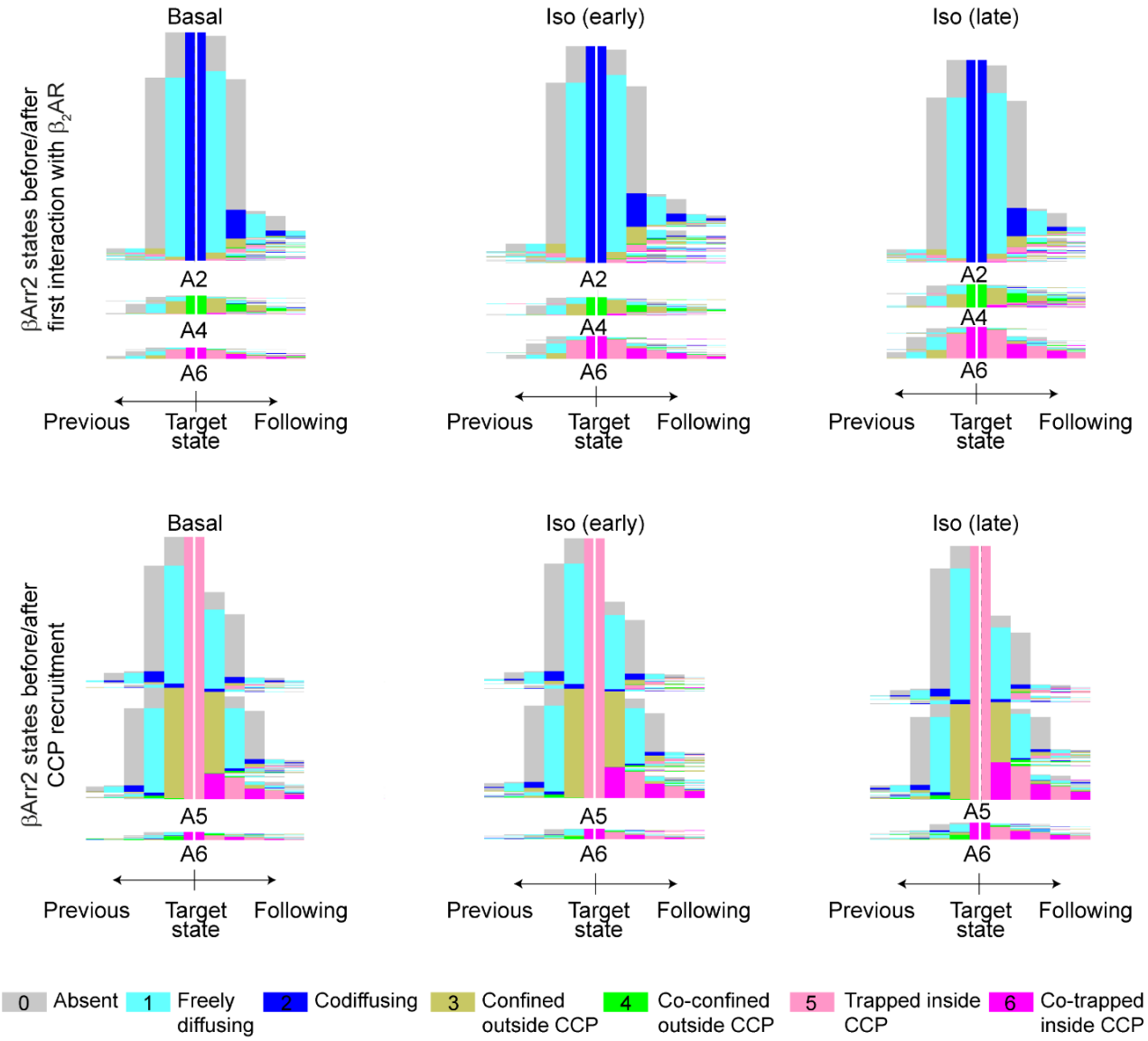

Figure 3.16 History of events in βarr2-β2AR interactions and CCP recruitment. (Top) History plots summarising the relative frequencies of all observed sequences of βArr2 states preceding and following the three states (A2, A4, A6) corresponding to β2AR–βArr2 interactions. (Bottom) History plots summarising the βArr2 states preceding and following the two states (A5, A6) corresponding to βArr2 trapped inside a CCP. Data before and after each target state are sorted independently to facilitate visualisation. Iso, isoprenaline. Early, 2-7 min. Late, 8-15 min n = 88851, 52658, 27741, 51147, 58254, 22769 transitions for β2AR basal, β2AR Iso (early), β2AR Iso (late), βArr2 basal, βArr2 Iso (early), βArr2 Iso (late), respectively.

.

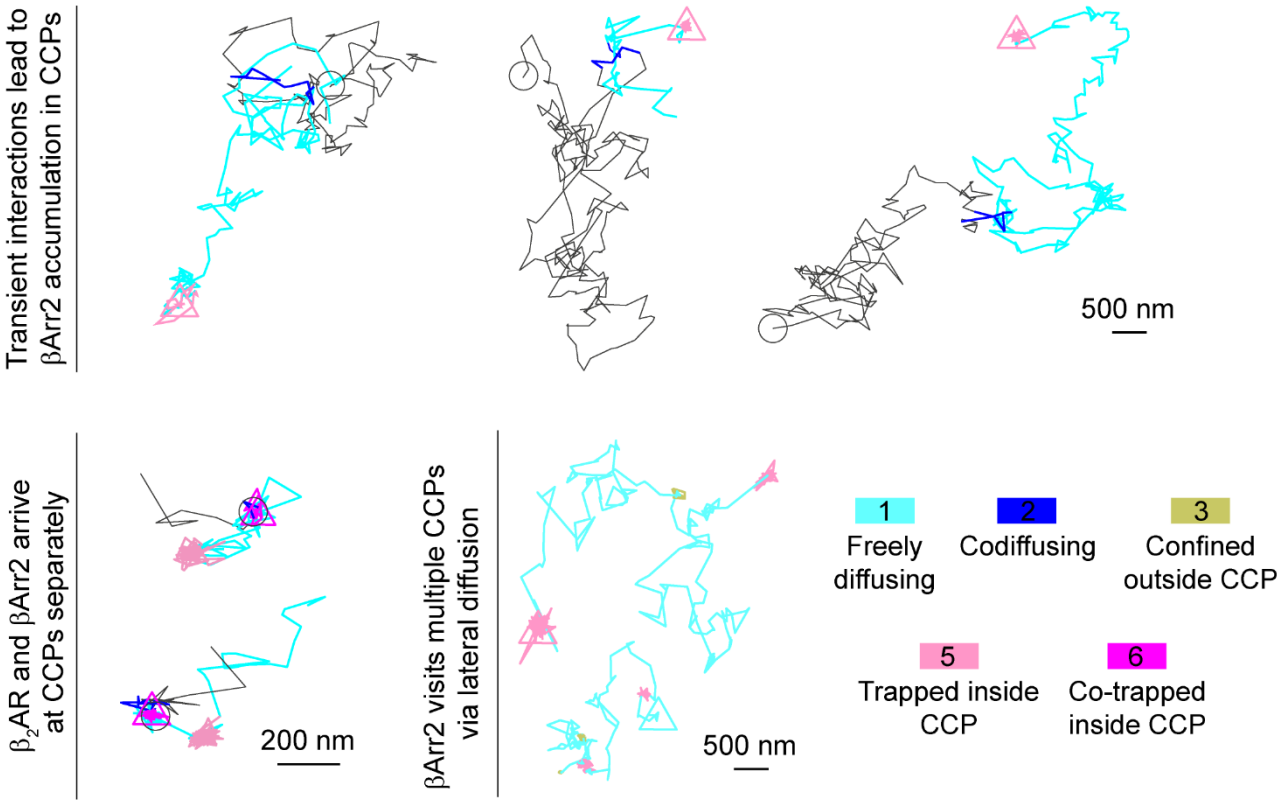

Figure 3.17 Trajectory examples. (Top) Examples of βArr2 molecules undergoing transient interactions with a β_2AR to then reach a CCP without an accompanying receptor. The βArr2 trajectory is colour-coded according to the corresponding βArr2 states. The β_2AR trajectory is shown in grey. (Bottom left) Examples of βArr2 molecules visiting multiple CCPs and a β_2AR arriving to a βArr2-occupied CCP by lateral diffusion. (Bottom right) Examples of βArr2 molecules visiting multiple CCPs via lateral diffusion without interacting with a receptor.

3.3 CONCLUSIONS

These results unexpectedly indicated that βArr2 largely behaves as a membrane protein, interacting with receptors and reaching CCPs prevalently via lateral diffusion and that the vast majority of βArr2 molecules reach CCPs alone and not via co-diffusion with an interacting receptor, as generally assumed.

4 The GPCR C-tail mediates βArr2 activation and lipids stabilise active-like βArr2 on the plasma membrane

4.1 PREFACE

Classical studies comparing different GPCRs and chimeric receptors identified two main classes of GPCRs based on their interactions with β-arrestins and trafficking properties [107,108]. Class A GPCRs, such as the β_2ARs, bind β-arrestins relatively weakly and appear to dissociate from β-arrestins during internalisation. In contrast, Class B GPCRs have been proposed to bind β-arrestins more strongly and co-internalise with receptors in endosomes, where they are seen colocalising for extended periods of time [107]. Typical examples of Class B GPCRs are the vasopressin V2 receptor or the β_2V_2 chimera [140], which carries the C-tail of the vasopressin V2 receptor fused to the β_2AR core. It is still contested whether it is interactions directly with the receptor C-tail that govern activation of β-arrestins or whether interactions with the GPCR core or other structural elements do so.

It is however known that arrestin exhibits complex inter-domain rotations after activation, in addition to conformational shifts that expose residues important in GPCR activation, such as the finger loop region (FLR) [27]. Even more recently, cryo-EM studies from Nobel-prize winning labs have found interactions with phospholipids at the GPCR binding interface in addition to stabilising interactions of the arrestin C-edge with the plasma membrane [120]. Here, those interactions were investigated to determine which components are important for mediating β-arrestin recruitment, diffusion, receptor interactions and downstream signalling.

4.2 RESULTS

4.2.1 C-tail affinity for β-arrestin drives trafficking to CCPs

To investigate the contribution of the strength of receptor C-tail –β-arrestin interactions on signalling, two additional receptor constructs were introduced: β_1AR and a chimeric β_2AR carrying the C-tail of the vasopressin V_2 receptor (β_2V_2). These receptors are widely used as models of weak and strong affinity for β-arrestin, respectively (**Figure 4.1**) [142,246] . β_1AR is thought to have only weak interactions with βArr2 and as such, does not internalise much at CCPs [246]. This mechanism has been linked to worsening of heart failure due to chronic signalling after excess catecholamine release [169,181]. Conversely, the C-tail of the β_2V_2 becomes highly phosphorylated and confers strong binding with arrestins [45].

It has previously been shown that β_2V_2-arrestin complexes represents a dynamic mixture of tail (partially engaged) and core (fully engaged) conformations [140]. Additionally, these studies have suggested that β_2V_2 C-tail interactions with arrestin mediate internalisation and arrestin signalling [344], but how these processes occur on a molecular basis in the cell is yet to be clarified.

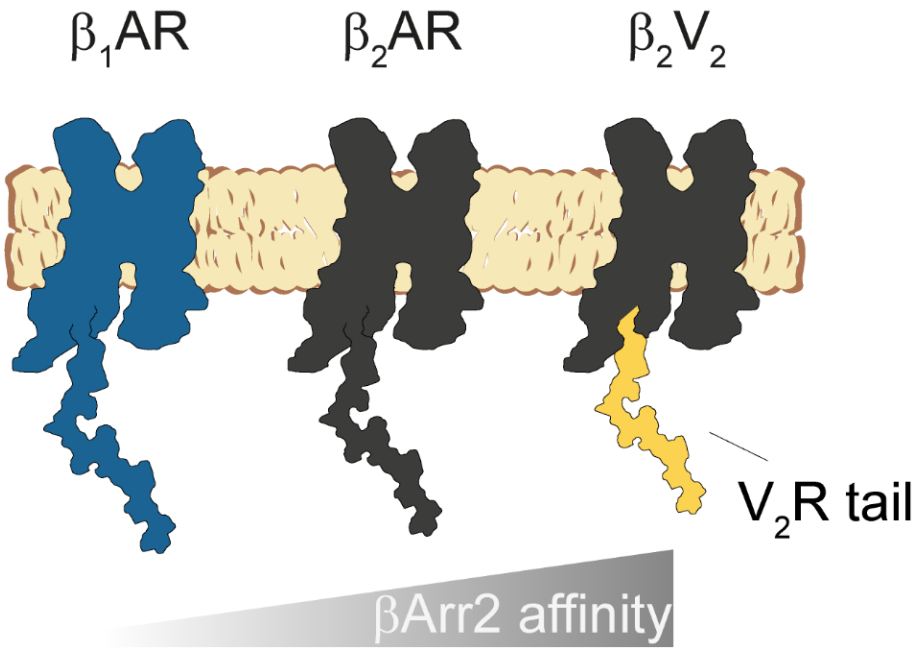

Figure 4.1 A panel of β-adrenergic receptors with varying βArr2 affinity. Schematic of the three investigated receptors (β_1AR, β_2AR and β_2V_2), with increasing affinity between arrestin and the receptor C-tail.

β_1AR and β_2V_2 were interrogated via NanoBRET assays, to quantify their interactions with the plasma membrane via K-ras, CCPs and βArr2. As expected, all receptors recruited βArr2 to the plasma membrane upon isoprenaline stimulation (**Figure 4.2**). The strength of βArr2 recruitment to the plasma membrane followed the expected order of β_2V_2>β_2AR>β_1AR, as previously discussed. Differential kinetics were observed for GPCR-βArr2 interactions as verified by BRET. β_2V_2 saw a consistent increase in receptor-βArr2 interactions over the hour-long BRET window. Class B receptors, such as the V_2R, are known to internalise frequently and internalise in vesicles with β-arrestin, which might explain the sustained interactions observed over the BRET cycle. β_1AR saw the smallest increase in agonist-induced receptor-arrestin interactions by BRET, as expected (**Figure 4.2**).

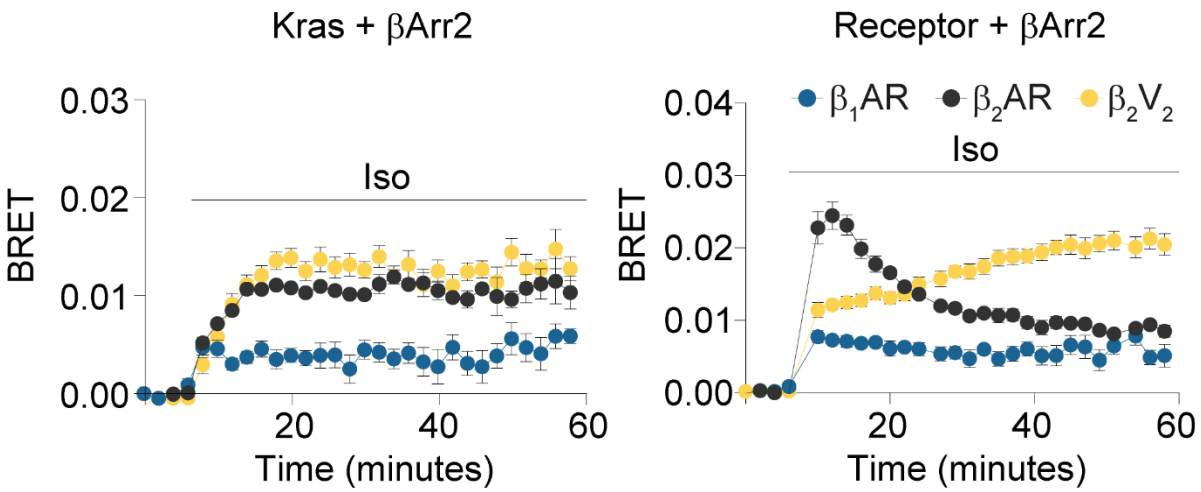

Figure 4.2. BRET assays of β-adrenergic receptor panel. Kinetics of βArr2 recruitment to either receptor or the plasma membrane upon isoprenaline (10 μM) stimulation. Shown are the results of real-time measurements monitoring BRET between NanoLuc fused to the plasma membrane marker Kras (left) or the receptor C-termini (right) and βArr2-Halo labelled with Halo-R110. K-ras P experiments were performed in the presence of unlabelled receptor (β_1AR or β_2AR or β_2V_2). Iso, isoprenaline. Data are mean ± s.e.m, n=4 independent experiments.

By single-molecule imaging, β_1AR were mostly mobile (83.5 ± 4.2%) prior to isoprenaline stimulation, as measured by TA-MSD, and saw only a negligible change in diffusion characteristics of the free portion after stimulation (**Figure 4.3**). For β_2V_2, a large increase in the immobile fraction was observed after stimulation (21.3% → 61.2% immobile trajectories) (**Figure 4.3**). βArr2 free diffusion was similar amongst the tested receptors (**Figure 4.3**). By analysing colocalisation with CCPs, a strong accumulation of β_2V_2 and, to a lesser extent, β_2AR molecules in CCPs after isoprenaline stimulation, with only a minor increase for β_1AR was revealed (**Figure 4.4**). This follows the rank order of βArr2 affinity for the receptor C-tail (β_2V_2→β_2AR→β_1AR). Similar proportions of βArr2 were observed trapped inside CCPs under basal conditions for β_1AR, β_2AR and β_2V_2. This effect was not as pronounced as receptor CCP trapping, suggesting that receptor and arrestin CCP accumulation might not be stoichiometric.

Interestingly, receptors trapped outside CCPs followed the same rank order, with β_2V_2 seeing the highest reduction in freely diffusing molecules after stimulation to account for these increases in molecular trapping (**Figure 4.4**). This observation was not seen for βArr2 with the tested receptors and suggests the formation of receptor nanodomains after stimulation that are independent of CCPs.

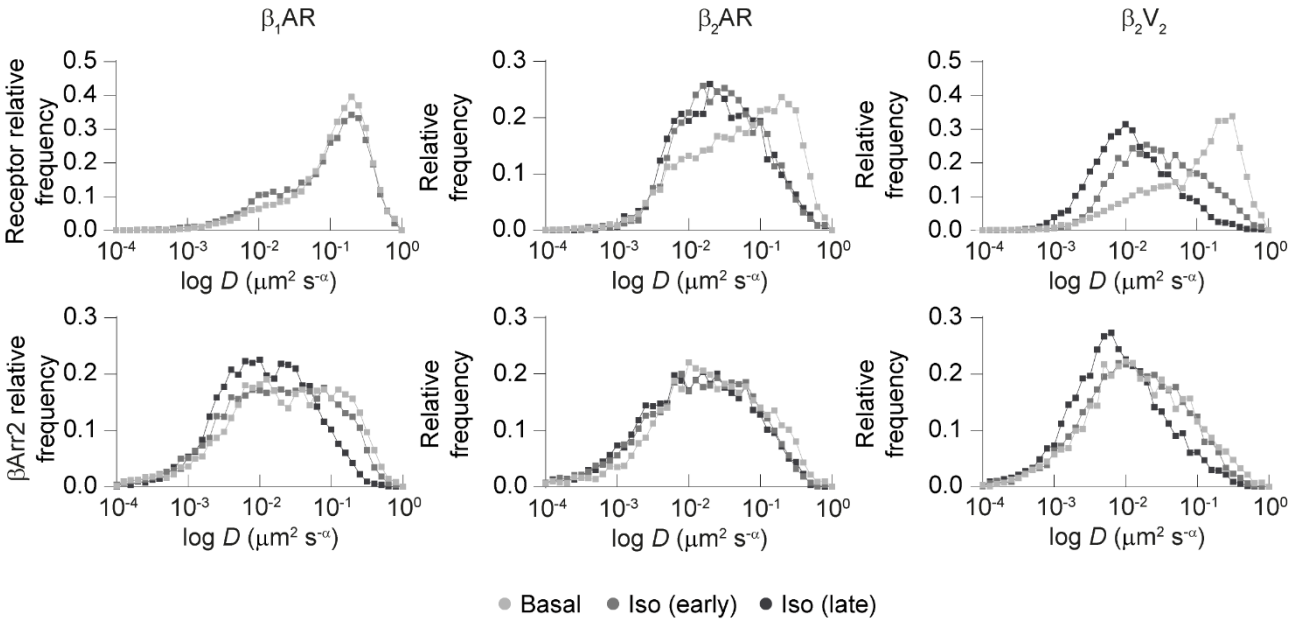

Figure 4.3 TA-MSD analysis of β-adrenergic receptor panel. Shown are results obtained in cells expressing βArr2-Halo and either SNAP-β_1AR, β_2AR, or β_2V_2 before (basal) and after isoprenaline (10 μM) stimulation. β_2AR is included for comparison. Distributions of diffusion coefficient (*D*) values estimated for receptor (top) and βArr2 (bottom) molecules based on TA-MSD analysis of entire trajectories. Iso, isoprenaline. Early, 2-7 min. Late, 8-15 min. n = 31, 21, 16, 28, 23, 11, 24, 16, 11 cells for β_1AR basal, β_1AR Iso (early), β_1AR Iso (late), β_2AR basal, β_2AR Iso (early), β_2AR Iso (late), β_2V_2 basal, β_2V_2 Iso (early), β_2V_2 Iso (late), respectively.

The kinetics of βArr2 interactions with the three receptors were then compared, estimated via deconvolution analysis (**Figure 4.5**). Basal interactions between β_1AR and βArr2 were undistinguishable from those observed with the control CD86, consistent with the notion that unstimulated β_1AR has a very low affinity for βArr2 [345]. In contrast, the detected basal β_2V_2–βArr2 interactions (k_{on} 0.028 μm² molecule^{-1} s^{-1}; 95% confidence interval: 0.031–0.025) were

comparable to the case of β_2AR-βArr2.). Isoprenaline stimulation increased k_{on} for all three receptors (β_1AR ND; β_2AR ~1.8-fold; β_2V_2R ~12-fold; **Figure 4.5**), to an extent that agreed with their affinity for βArr2. This is consistent with our understanding of increasing receptor C-tail affinity propagating interactions with arrestin [27,246,342,344].

Smaller differences were observed among k_{off} values, with β_1AR seeing the largest trend for increasing after stimulation. Indeed, an estimated average interaction time of around ~1s was found for all conditions, with the exception of β_1AR after early stimulation (~2.9 s). These results showed that the interaction of three representative GPCRs with βArr2 is mainly controlled by their association rate (k_{on}) and that receptor–β-arrestin interactions are short-lived even in the case of the strongly interacting (Class B) β_2V_2 receptor. Additionally, these results support the receptor C-tail mediating the increase in interaction frequency for β-AR-βArr2 interactions.

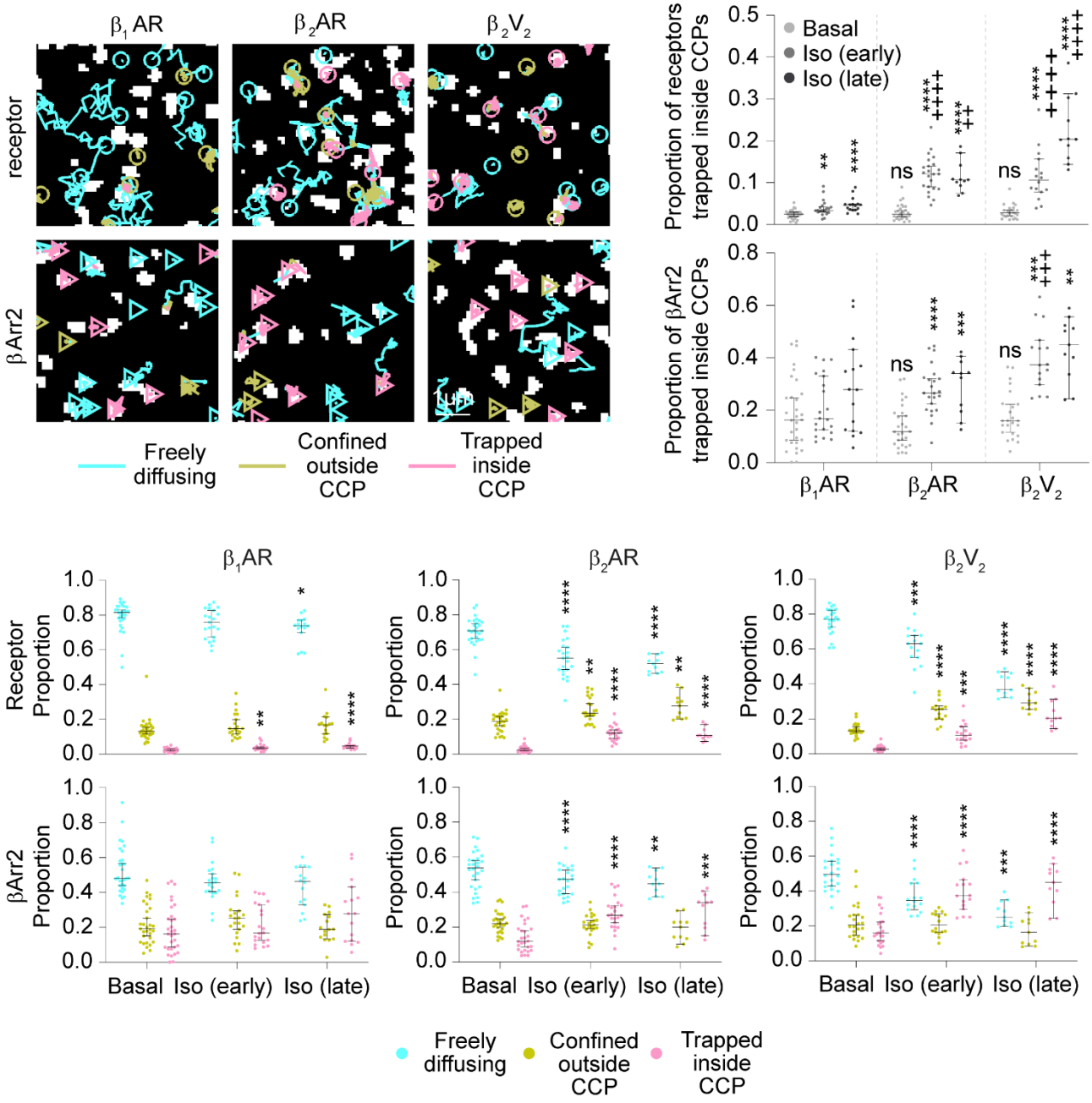

Figure 4.4 Diffusivity states of β-adrenergic receptor panel and βArr2 molecules. Trajectory segments were assigned to three diffusivity states. (Top) representative trajectories of individual receptor and βArr2 molecules in cells stimulated with isoprenaline (10 µM; late), with corresponding proportions of molecules trapped inside CCPs shown to the right. (Bottom) All lateral mobility distributions of receptor and βArr2 molecules. Data are median ± 95% CI. Iso, isoprenaline. Early, 2-7 min. Late, 8-15 min. n = 31, 21, 16, 28, 23, 11, 24, 16, 11 cells for β1AR basal, β1AR Iso (early), β1AR Iso (late), β2AR basal, β2AR Iso (early), β2AR Iso (late), β2V2 basal, β2V2 Iso (early), β2V2 Iso (late), respectively. Results are statistically significant by Kruskal Wallis test. *P < 0.05, **P < 0.01, ***P < 0.001, ****P < 0.0001 versus basal by t-test with Bonferroni correction. Data for β2AR are the same as those shown in Figure 3.9.

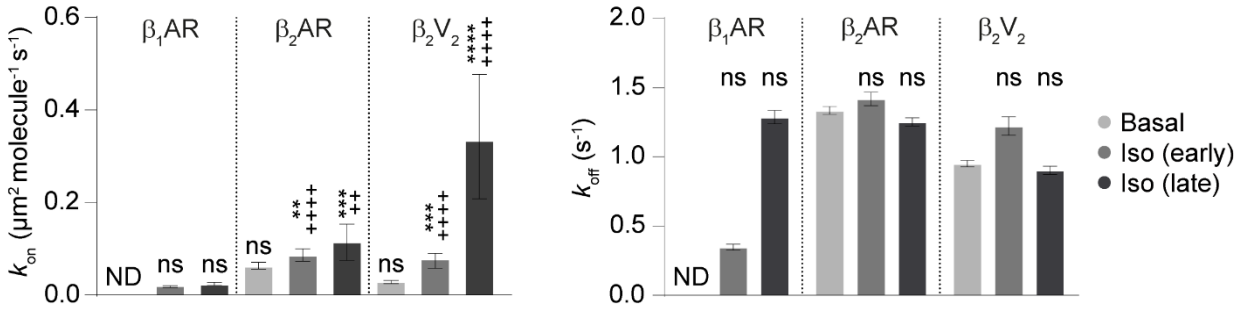

Figure 4.5 β-adrenergic receptor panel - βArr2 interactions. Estimated (Left) k_{on} and (Right) k_{off} values for β_1AR, β_2AR and β_2V_2–βArr2 interactions. Iso, isoprenaline. Early, 2-7 min. Late, 8-15 min. Data are median ± 95% CI and 31, 21, 16, 28, 23, 11, 24, 16, 11 cells for β_1AR basal, β_1AR Iso (early), β_1AR Iso (late), β_2AR basal, β_2AR Iso (early), β_2AR Iso (late), β_2V_2 basal, β_2V_2 Iso (early), β_2V_2 Iso (late), respectively. Differences in koff values versus basal were assessed by two-tailed unpaired t-test with Bonferroni correction. k_{on} differences are statistically significant by a Kruskal Wallis test, **P < 0.01, ***P < 0.001, ****P < 0.0001 versus corresponding basal condition, and ++P < 0.01, +++P < 0.001, ++++P < 0.0001 versus corresponding β_1AR condition by t-test with Bonferroni correction. ns, statistically not significant.

β_1AR is not known to traffic to CCPs as significantly as β_2AR or β_2V_2 after stimulation, but in the literature, β_1ARs are known to promote β-arrestin-dependent ERK signalling, by activating β-arrestin trafficking to CCPs without the receptor [106]. As for β_2AR, basal colocalisations between β_1AR or β_2V_2R and βArr2 molecules mainly involved (free/confined) molecules outside CCPs, with variable degrees of trapping in CCPs observed after isoprenaline stimulation, dependent on the receptor (higher for β_2V_2 and lower for β_1AR) (**Figure 4.6**).

On analysing the Markov chains for β_1AR and β_2V_2R, the same transitions were observed as described for β_2AR in section 3.2.5 (**Figure 4.7**), and were remarkably similar to each other. Similar results, albeit with some quantitative differences, were observed for both receptors. Remarkably, even in the case of the strongly interacting β_2V_2 receptor after isoproterenol stimulation, the vast majority of βArr2 molecules (83 %) reached CCPs alone (**Figure 4.7**). These results unexpectedly indicated that, after transient interaction for Class B receptors,

receptor and β-arrestin molecules mostly reach CCPs separately via lateral diffusion and not via co-diffusion as long-lived complexes.

β_1AR, β_2AR and β_2V_2 had similar transition probabilities between states but β_2V_2 had a higher proportion of trapping events on CCPs of both receptor alone and receptor co-trapped with arrestins (6-fold and 17-fold increases over basal β_2V_2) (**Figure 4.8**). β-adrenergic receptors became trapped alone in CCPs (R5) after stimulation according to their βArr2 affinity (**Figure 4.8**). This is interesting, given that βArr2 was trapped alone in CCPs (A5) similarly for all receptors (**Figure 4.8**), suggesting that βArr2 and receptors may form signalling nanodomains in CCPs independent of each other. Additionally, an 8-fold increase in co-trapping events outside of CCPs was observed for only β_2V_2 with βArr2 after stimulation (**Figure 4.8**). β_1AR had lower transition probabilities for events that led to receptor confinement/trapping and smaller proportions of trapping events of receptors trapped in CCPs (**Figure 4.7**). Overall, these results show that β-adrenergic receptors exhibit similar mechanisms of action with β-arrestin. We hypothesise that increasing β-arrestin affinity is governed through the C-tail interaction, leading to more productive interactions with receptors on the membrane based on their affinity for the given receptors.

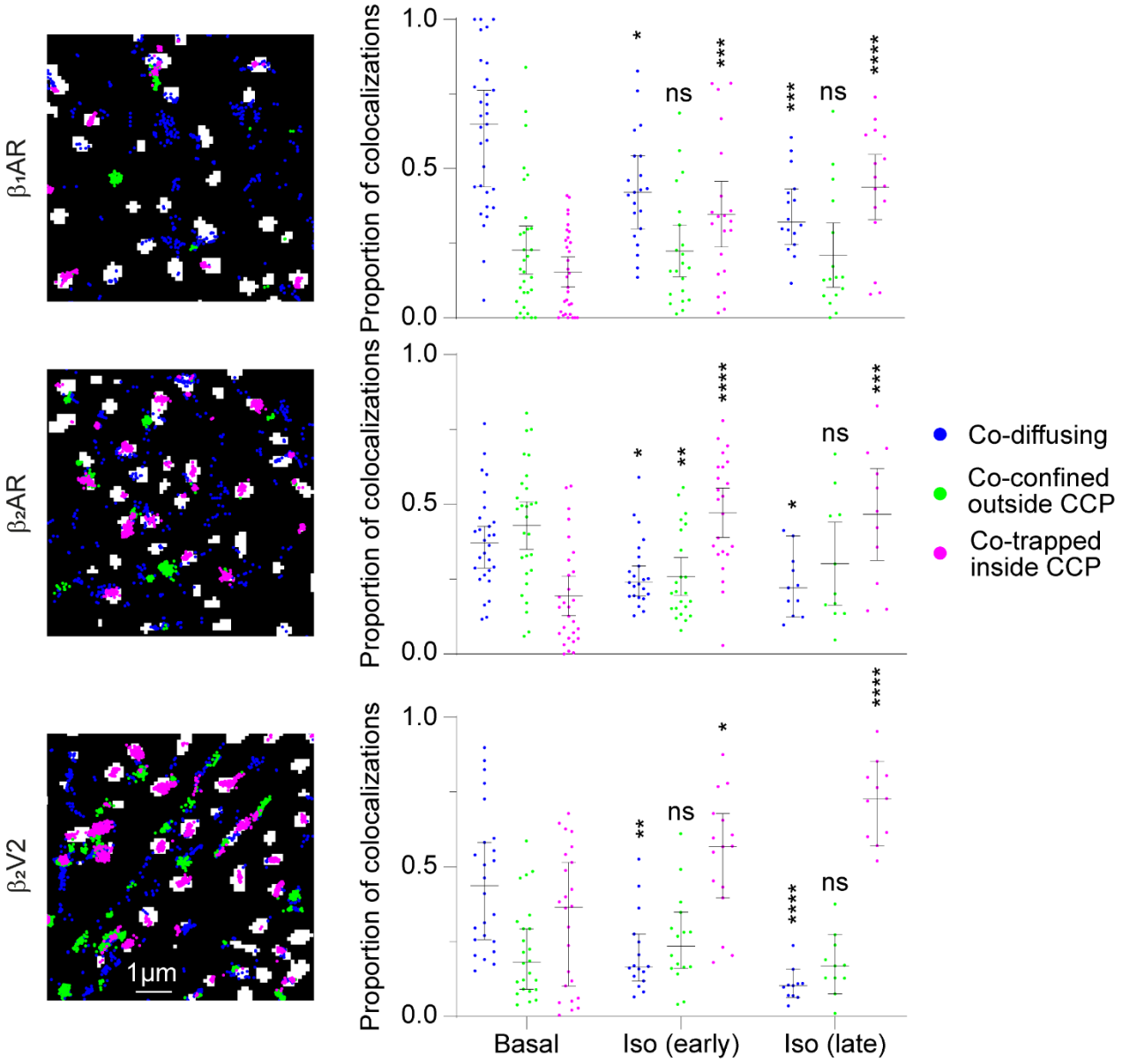

Figure 4.6 Spatial analysis of receptor–βArr2 single-molecule colocalisation events. Shown are the results obtained in cells expressing βArr2-Halo and either SNAP-β_1AR, β_2AR, or β_2V_2 before (basal) and after isoprenaline (10 µM) stimulation. β_2AR is included for comparison. Iso, isoprenaline. Early, 2-7 min. Late, 8-15 min. Data are median ± 95% CI. Results are statistically significant by Kruskal Wallis test. *P < 0.05, **P < 0.01, ***P < 0.001, ****P < 0.0001 versus basal by t-test with Bonferroni correction. n = 31, 21, 16, 28, 23, 11, 24, 16, 11 cells for β_1AR basal, β_1AR Iso (early), β_1AR Iso (late), β_2AR basal, β_2AR Iso (early), β_2AR Iso (late), β_2V_2 basal, β_2V_2 Iso (early), β_2V_2 Iso (late), respectively. Images are representative of a minimum of 3 independent experiments.

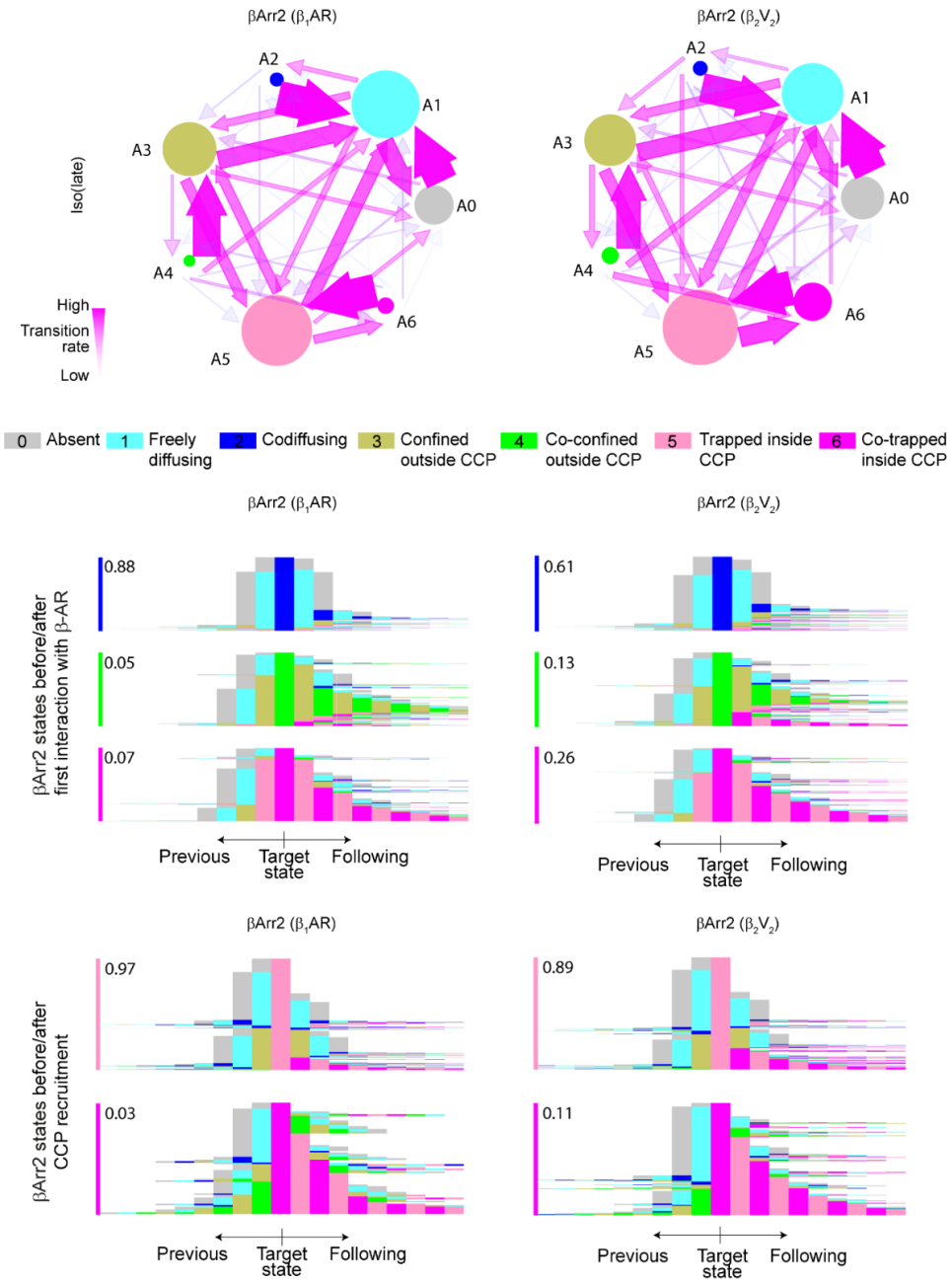

Figure 4.7 Markov Chain analysis of β-adrenergic receptors with varying βArr2 affinity. (Top) Markov chains showing the relative state occupancies and forward transition probabilities for βArr2 when co-transfected with CCP and either β_1AR (left) or β_2V_2 (right) under Iso (late) conditions. Iso, isoprenaline. (Middle) History plots summarising the relative frequencies of all observed sequences of βArr2 states preceding and following the three states (A2, A4, A6) corresponding to β-AR–βArr2 interactions (β_1AR [left], β_2V_2 [right])]. (Bottom) History plots summarising the βArr2 states preceding and following the two states (A5, A6) corresponding to βArr2 trapped inside a CCP.

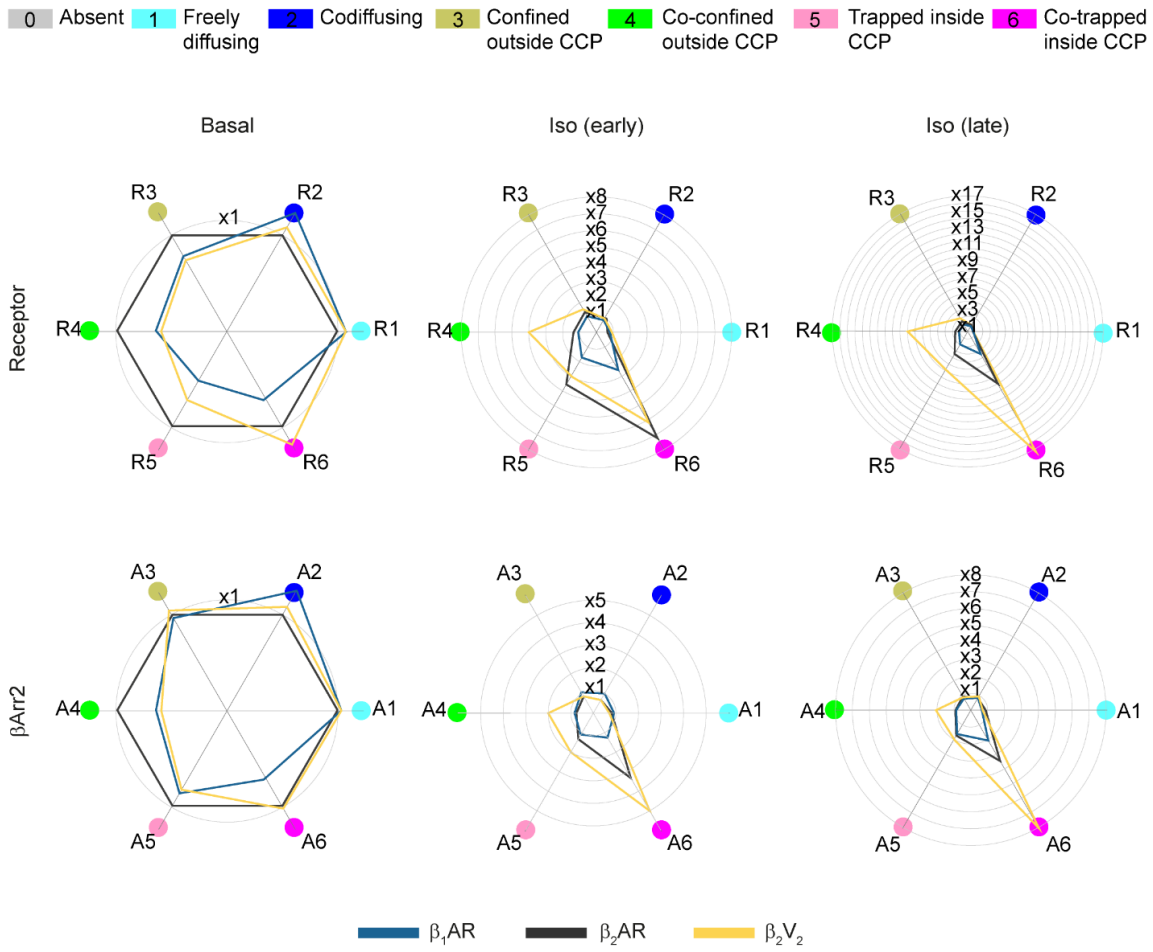

Figure 4.8 Change in state occupancy of β-adrenergic receptors and βArr2 after isoprenaline stimulation. Corresponding radar plots from Markov chain analysis, obtained from single-molecule experiments showing the changes in state occupancies induced by isoprenaline (10 μM) stimulation of β_1AR (blue), β_2AR (black) and β_2V_2 (yellow). (Top) receptor radar plots and (Bottom) corresponding βArr2 radar plots. **.** Iso, isoprenaline. Early, 2-7 min. Late, 8-15 min. WT βArr2 is included for comparison. n = 31, 21, 16, 28, 23, 11, 24, 16, 11 cells for β_1AR basal, β_1AR Iso (early), β_1AR Iso (late), β_2AR basal, β_2AR Iso (early), β_2AR Iso (late), β_2V_2 basal, β_2V_2 Iso (early), β_2V_2 Iso (late), respectively.

4.2.2 The receptor C-tail, but not receptor core, is indispensable for β-adrenergic receptor interactions with βArr2

By using a family of β-adrenergic receptors with differing C-tail affinities for βArr2, the observed differences in plasma membrane recruitment, CCP recruitment of receptor/βArr2,

interactions of receptor/βArr2 and diffusion dynamics are positively correlated with affinity for βArr2, supposedly through the C-tail. Although these 3 receptors differ mostly in the C-tail and their purported affinity for βArr2 is mediated by it, this does not preclude other interaction modalities as being important.

β-arrestin has been proposed to interact with receptors via two main distinct poses; the first of which involving interactions between its N-domain polar core and the receptor phosphorylated C-tail and the second one between the arrestin finger-loop region (FLR) and the receptor core [27,140,246]. To dissect the contribution of either modality, β_2AR constructs carrying a deletion in either the third intracellular loop (ΔICL3), which interferes with the core interaction, or C-tail (ΔC-tail), which prevents the C-tail interaction, were studied (**Figure 4.9**). Whereas the ΔC-tail truncation disrupts phosphorylation-mediated interaction with β-arrestin, the ΔICL3 deletion has been demonstrated to disrupt β-arrestin core interaction using comprehensive bimane fluorescence spectroscopy analyses [346,347].

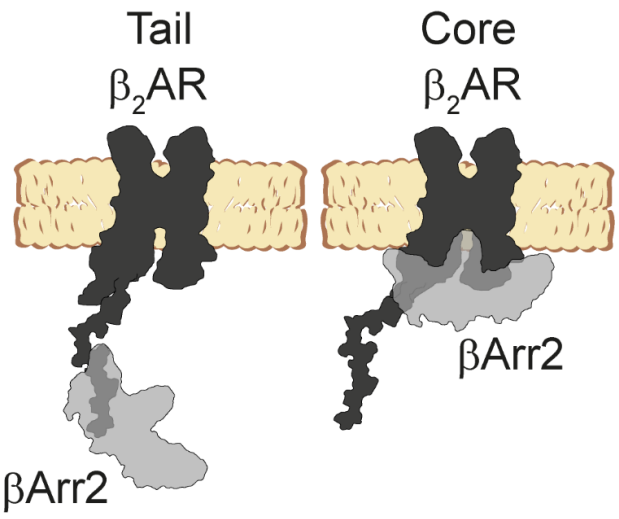

Figure 4.9 Tail and core conformations. Schematic of C-tail and core receptor-arrestin interactions, as identified by the lab of Arun Shukla [140].

Firstly, the ΔICL3 mutant was still capable of agonist-dependent βArr2 interactions, βArr2 plasma membrane recruitment and βArr2 translocation to CCPs (**Figure 4.10**), as shown by BRET and consistent with previous results [346]. In contrast, the ΔC-tail mutant failed to promote agonist-dependent β_2AR–βArr2-interactions, βArr2 translocation to the plasma membrane and βArr2 accumulation in CCPs via BRET (**Figure 4.10**). By single-molecule imaging, ΔICL3-β_2AR and corresponding βArr2 were found to exhibit diffusion similar to WT receptors and increases in trapping at CCPs were observed after stimulation for both receptor and arrestin (**Figure 4.11**). For ΔC-tail-β_2AR experiments, receptors and arrestins had significantly reduced accumulation in CCPs after stimulation, highlighting their role in mediating CCP accumulation of arrestin (**Figure 4.11**).

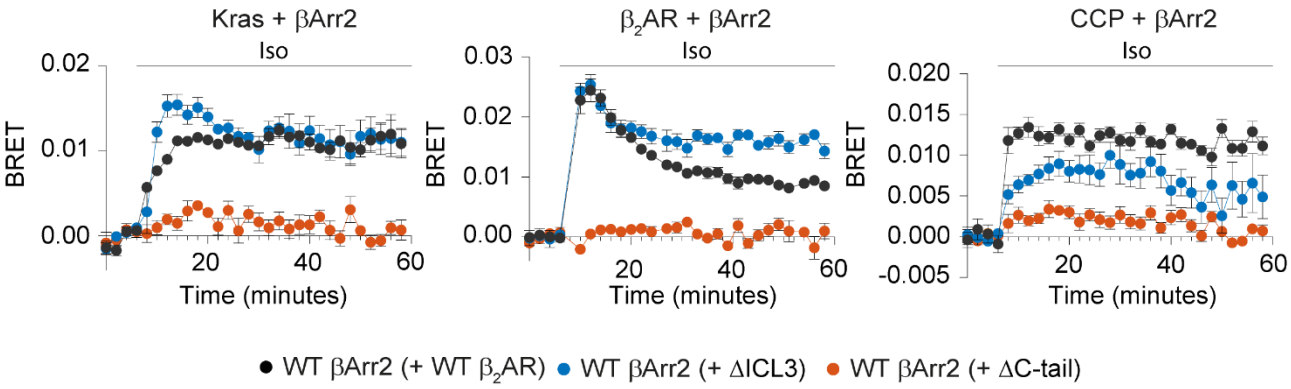

Figure 4.10 β_2AR mutant-induced βArr2 kinetics by BRET. Kinetics of βArr2 to the plasma membrane (left), receptor (middle), or CCPs (right) in HEK293 cells stimulated with isoprenaline (10 μM). Shown are the results of real-time measurements monitoring BRET between NanoLuc fused to the plasma membrane marker K-ras (left) or the receptor N-terminus (middle) or clathrin light chain and βArr2-Halo labelled with Halo-R110. K-ras and CCP experiments were performed in the presence of unlabelled receptor (WT or ΔICL3 or ΔC-tail). Iso, isoprenaline. Data are mean ± s.e.m, n=3 independent experiments

Estimated interaction times with βArr2 for the ΔICL3-β_2AR were comparable with WT β_2AR at all stimulation time-points (**Figure 4.12**), further supporting the finding that the core interaction is dispensable for βArr2-receptor interactions. Prior to stimulation, the ΔC-tail-

β_2AR did not interact with βArr2, beyond random colocalisations, when compared to the CD86 non-interacting control (**Figure 4.12**). Similarly, after stimulation of ΔC-tail-β_2AR, no increases in interactions were observed beyond random colocalisations, highlighting the importance of interactions with the receptor C-tail in the activation of receptors and arrestin. ΔICL3-β_2AR – βArr2 interactions occurred preferentially on CCPs after stimulation, similar to WT β_2AR (**Figure 4.13**). Comparatively, ΔC-tail-β_2AR and βArr2 mainly colocalised via lateral diffusion on the plasma membrane (**Figure 4.13**), likely as a result of increased βArr2 recruitment to the membrane and increased transient colocalisations.

Radar plots from Markov chain analysis further support these findings; interestingly highlighting that βArr2 can become trapped alone in CCPs regardless of the receptor employed, given that is has a C-tail (**Figure 4.14**). This suggests that transient, dynamic interactions with the receptor are sufficient to enable some trapping of arrestin in CCPs through transient interactions. These results indicate that βArr2 engagement with the receptor C-tail but not its core is required for agonist-induced accumulation of both receptors and arrestins in CCPs.

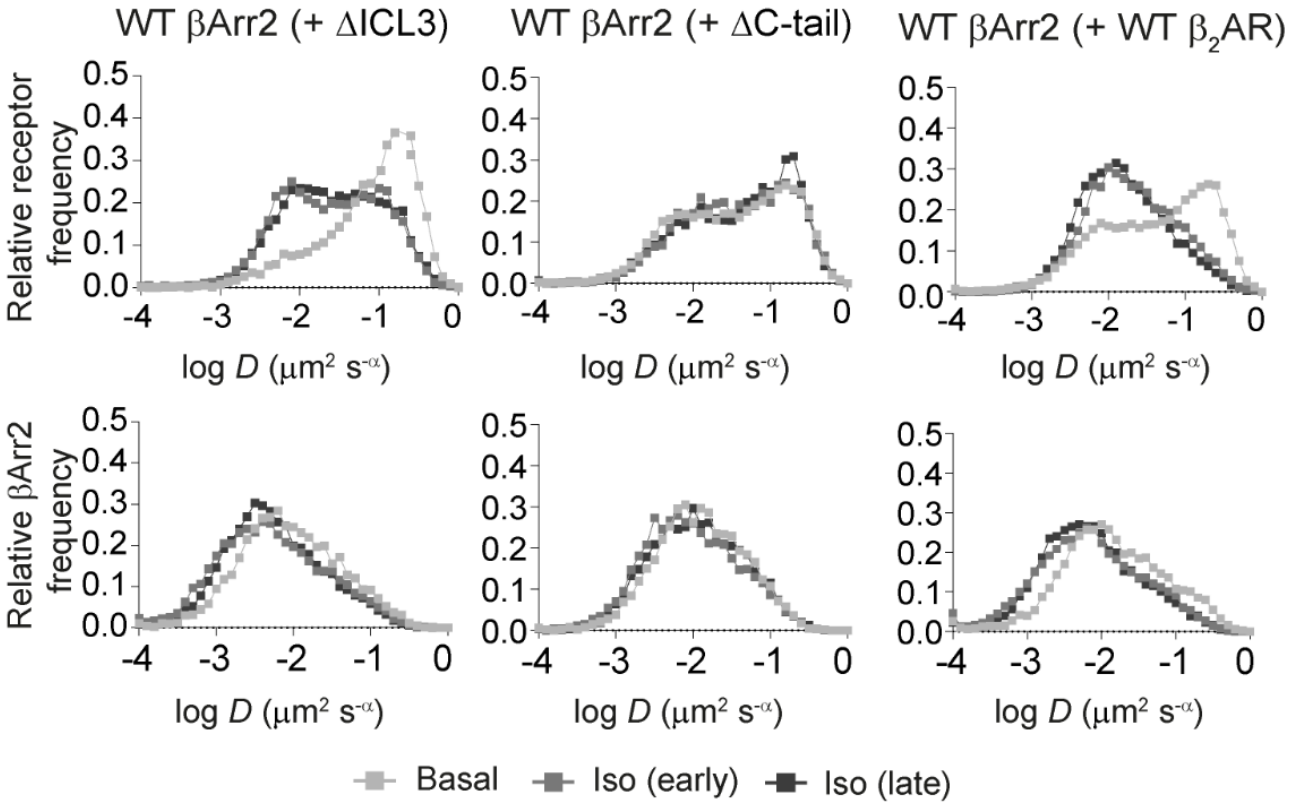
WT βArr2 (+ ΔICL3)
WT βArr2 (+ ΔC-tail)
WT βArr2 (+ WT β2AR)
Relative receptor frequency
Relative βArr2 frequency
log D (μm² s⁻ᵅ)
Basal
Iso (early)
Iso (late)

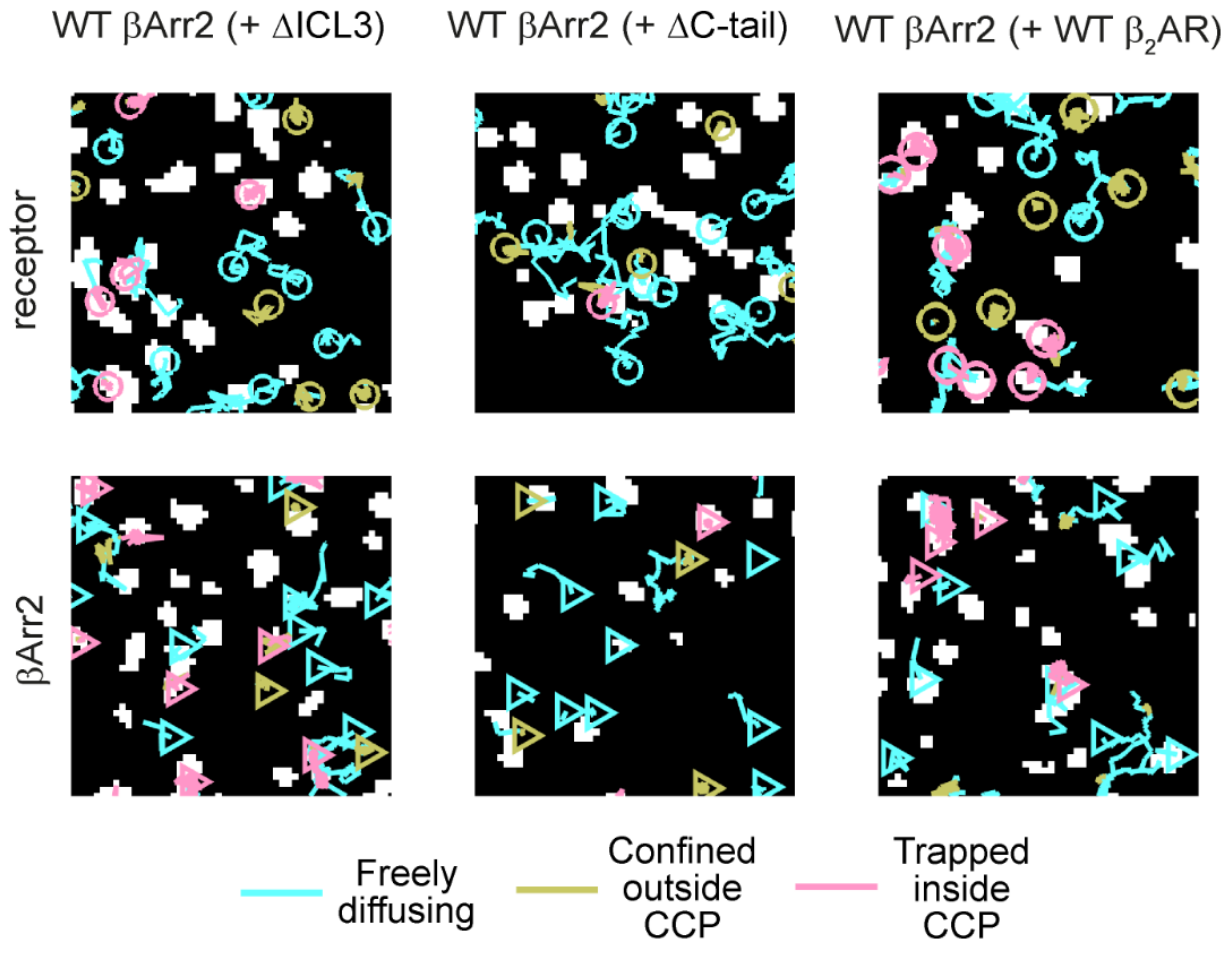
WT βArr2 (+ ΔICL3)
WT βArr2 (+ ΔC-tail)
WT βArr2 (+ WT β2AR)
receptor
βArr2
Freely diffusing
Confined outside CCP
Trapped inside CCP

Figure 4.11 Diffusion of β2AR mutants. All experiments include CHO-K1 cells transfected with WT βArr2 and CCP-GFP and either ΔICL3 β2AR (left), ΔC-tail β2AR (middle) or WT β2AR (right). (Top) TA-MSD analysis of the β2AR and corresponding βArr2. (Bottom) βArr2 diffusivity states on and off CCPs. Shown are representative trajectories after stimulation with isoprenaline (10 μM) for 8-15 min (late). Cells expressing WT β2AR and βArr2 are included for comparison. Iso, isoprenaline. Early, 2-7 min. Late, 8-15 min. Data are median ± 95% CI. Iso, isoprenaline. Early, 2-7 min. Late, 8-15 min. n = 28, 23, 11, 23, 15, 14, 25, 17, 16 cells for WT basal, WT Iso (early), WT Iso (late), ΔICL3 basal, ΔICL3 Iso (early), ΔICL3 Iso (late), ΔC-tail basal, ΔC-tail Iso (early) and ΔC-tail Iso (late), respectively.

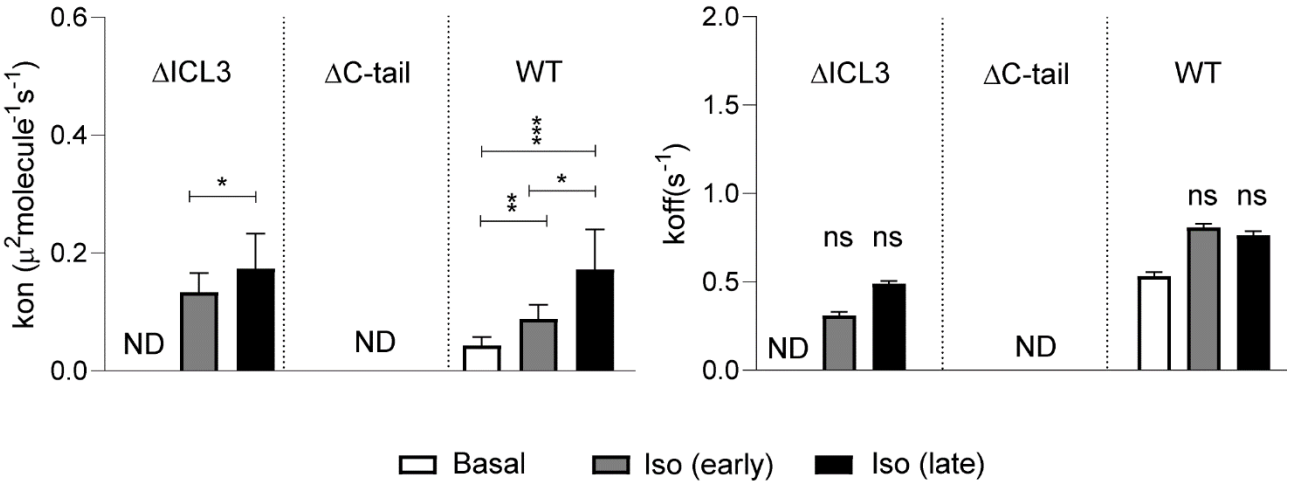

Figure 4.12 β2AR mutant – βArr2 interactions by deconvolution analysis. Estimated (Left) k_{on} and (Right) k_{off} values for WT β2AR or β2AR ΔICL3 or β2AR ΔC-tail interactions with βArr2. Iso, isoprenaline. Early, 2-7 min. Late, 8-15 min. Data are median ± 95% CI and 31, 21, 16, 28, 23, 11, 24, 16, 11 cells for β1AR basal, β1AR Iso (early), β1AR Iso (late), β2AR basal, β2AR Iso (early), β2AR Iso (late), β2V2 basal, β2V2 Iso (early), β2V2 Iso (late), respectively. Differences in koff values versus basal were assessed by two-tailed unpaired t-test with Bonferroni correction. k_{on} differences are statistically significant by a Kruskal Wallis test, **P < 0.01, ***P < 0.001, ****P < 0.0001 versus corresponding basal condition by t-test with Bonferroni correction. ns, statistically not significant.

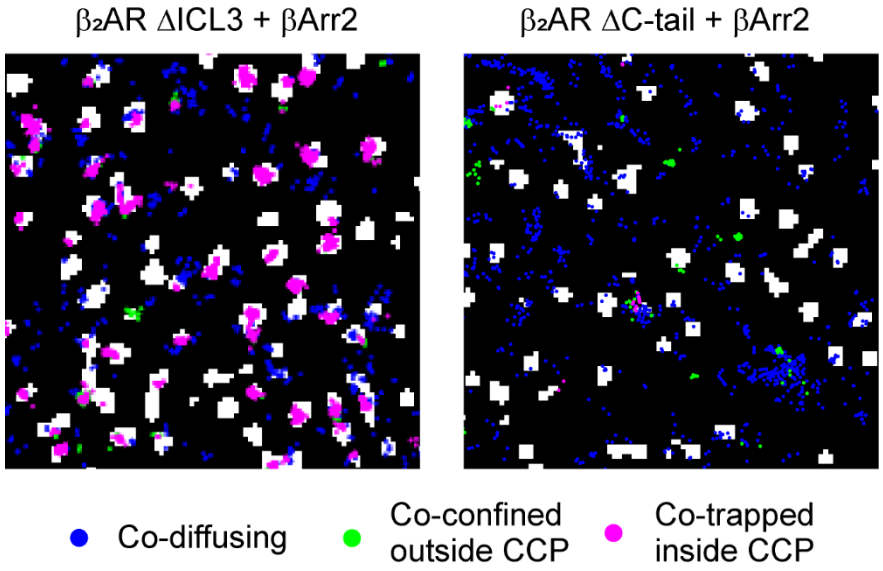

Figure 4.13 Spatial distribution of β2AR mutant – βArr2 colocalisations after isoprenaline stimulation. Shown are representative examples of cells expressing βArr2, CCP and either β2AR-ΔICL3 or β2AR-ΔC-tail after isoprenaline (10 μM) stimulation (8-15min).

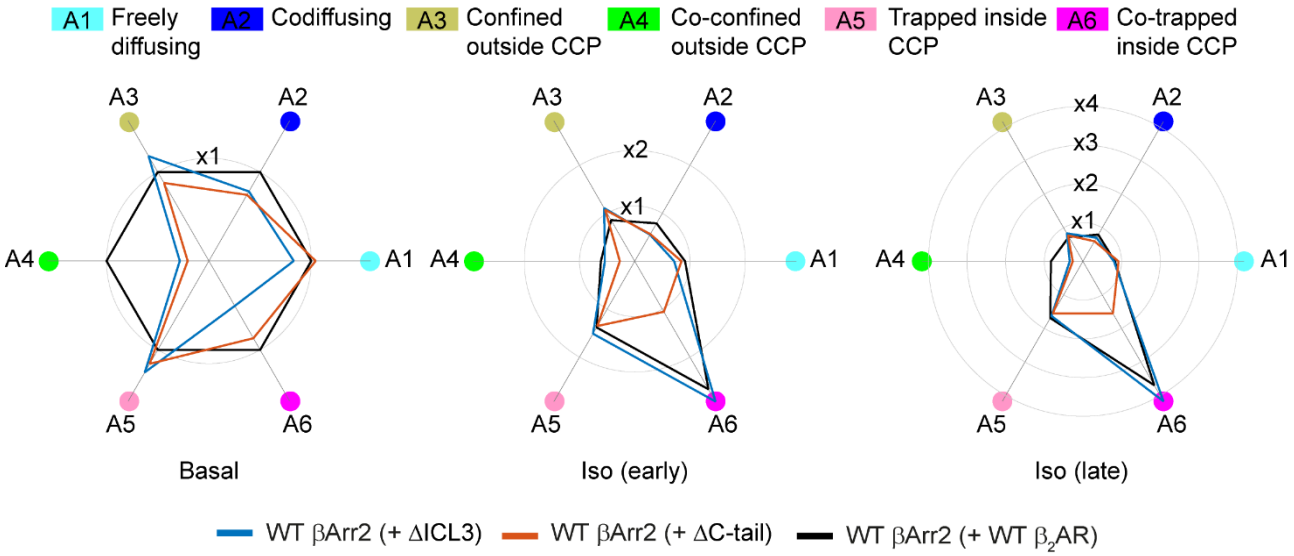

Figure 4.14 Change in state occupancy of β-adrenergic receptor mutants and βArr2 after isoprenaline stimulation. Corresponding βArr2 radar plots from Markov chain analysis, obtained from single-molecule experiments showing the changes in state occupancies induced by isoprenaline (10 μM) stimulation of β2AR-ΔICL3 (blue), WT β2AR (black) and β2AR-ΔC-tail (orange). Iso, isoprenaline. Early, 2-7 min. Late, 8-15 min. WT βArr2 is included for comparison. n = 31, 21, 16, 28, 23, 11, 24, 16, 11 cells for β1AR basal, β1AR Iso (early), β1AR Iso (late), β2AR basal, β2AR Iso (early), β2AR Iso (late), β2V2 basal, β2V2 Iso (early), β2V2 Iso (late), respectively.

4.2.3 Interactions with the plasma membrane are required for the lateral diffusion of βArr2, receptor interactions and accumulation in CCPs

β-arrestin is classically thought of as a cytosolic protein, which binds directly to GPCRs and travels as a complex to CCPs. Results obtained by single-molecule microscopy [315], including those described here, instead find that β-arrestin acts more as a membrane protein, diffusing on the plasma membrane without an accompanying receptor. This raises the question: if β-arrestin is not bound to GPCRs when laterally diffusing on the plasma membrane, what does it bind to? Only recently have interactions with the cell membrane been elucidated for β-arrestin, with high-resolution structures being published via cryo-EM in lipid nanodiscs by Nobel prize winning labs [17,21,25,109].

In particular, select β-arrestin residues have been found to bind at the interface of phosphatidyl-inositol 4,5-bisphosphate (PIP2) and GPCRs, including NTSR1 and β-adrenergic receptors [120]. This has been supported by biophysical studies of visual arrestin [123]. Further to this, many residues have been reported along the C-edge of β-arrestin that insert into the membrane [119,120,123]. These structures do not however provide the dynamics of arrestin interacting with the membrane in live cells, where the arrival, diffusion and interactions can be observed in real time. We hypothesised that βArr2 molecules that diffused alone on the plasma membrane and βArr2 molecules seen translocating to the plasma membrane without a receptor might be directly bound to the lipid bilayer.

To first test this hypothesis, TIRF experiments were performed in which βArr2 expression was varied with cells sequentially bleached to a working single-molecule density. Here, the freely diffusing and trapped molecules on the membrane were extrapolated from fluorescence measurements to predict original densities. Given that GPCRs are expressed at relatively low

densities in cells [348] and lipids form a mostly unsaturable source of interaction sites, we postulated that freely diffusing arrestins would increase linearly with arrestin expression. Conversely, trapped arrestins have been found to bind to sites such as CCPs, which are limited on the plasma membrane. Thus, we postulated that trapped molecules would saturate at high cellular densities of βArr2.

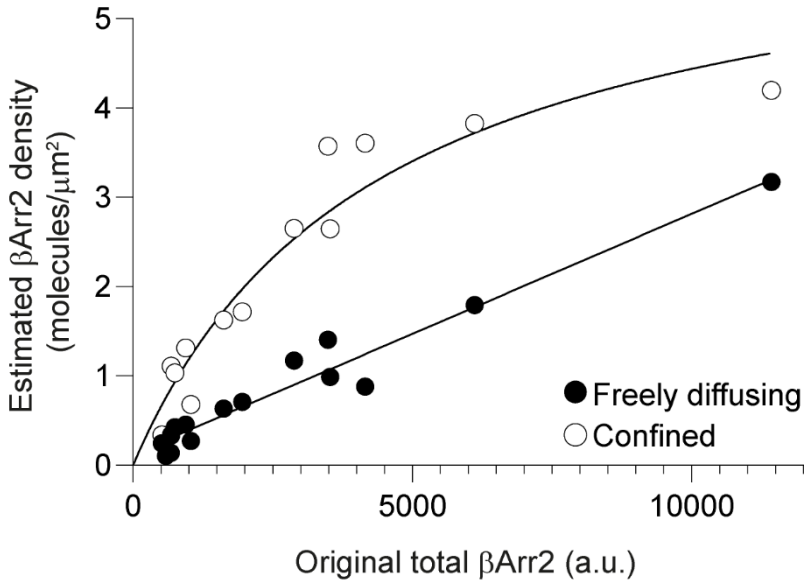

Figure 4.15 Freely diffusing βArr2 bind to a non-saturable site on the membrane. Densities of freely diffusing βArr2 molecules on the plasma membrane of cells in which βArr2 expression was varied ~ 25-fold. n = 15 cells over 3 independent experiments.

Results showed no saturation proportional increase of freely diffusing βArr2 molecules on the plasma membrane as a function of tested densities (~25-fold expression disparity) (**Figure 4.15**), consistent with their binding to high abundance sites such as membrane lipids rather than low-abundance receptors. In contrast, saturation was observed for trapped βArr2 molecules as the concentration increased (**Figure 4.15**). Additionally, the average duration of βArr2 lateral diffusion was longer than the estimated duration of receptor-arrestin interactions (even in the case of the strong β_2V_2), suggesting that they were likely due to an interaction with the lipid bilayer itself rather than with unlabelled GPCRs present on the plasma membrane.

To further test our hypothesis, a panel of βArr2 mutants carrying substitutions of key basic amino acids that mediate binding to plasma membrane sites. First, a mutant was used which disrupts binding to CCPs through interactions with both clathrin light chain and AP2. (ΔCCP/AP2 mutant). Next, a phosphatidylinositol 4,5-bisphosphate (PIP2) binding site known to interface with binding with GPCRs was mutated (ΔPIP2 binding, **Figure 4.16**) and finally, residues on the C-edge which are thought to mediate binding to the plasma membrane were mutated based on the available structures (ΔELA [extended lipid anchoring], R189Q/F191E/L192S/M193G/T226S/K227E/T228S/ K230Q/K231E/K233Q/R237E/ K251Q/K325Q/K327Q/V329S/V330D/R332E (**Figure 4.16**). The introduction of multiple mutations was required due to extensive contacts of βArr2 with the lipid bilayer.

Mutations for the ΔELA mutant were selected based on a recent structure derived of βArr1 embedded in lipid nanodiscs [349]. Mostly, positively charged residues (that can interact with negatively charged lipid head groups) and hydrophobic residues (interacting with lipophilic lipid tails) were mutated into negatively charged Asp/Glu amino acids. Additionally, Asn/Ser residues were used to prevent the build-up of negative charge in arrestin.

Mutating the PIP2 binding site alone (ΔPIP2 mutant) interfered with agonist-dependent βArr2 translocation to β_2AR as well as to the plasma membrane, but had less effect on its accumulation at CCPs, as shown by BRET (**Figure 4.17**). Interestingly, the kinetics of ΔPIP2 binding to CCPs was slower than WT arrestin, reaching a maximum response after 4-6 reads (~8-10 mins). Clathrin/AP2 binding-deficient βArr2 mutants (ΔCCP/AP2) were able to translocate to the plasma membrane after isoprenaline stimulation and interact with receptors but could not translocate to CCPs (**Figure 4.17**). Interestingly, more β_2AR-βArr2 association was observed for the ΔCCP/AP2 mutant than WT βArr2 by BRET. In contrast to the other mutants, the ΔELA

mutant was not only largely defective in agonist-dependent translocation and CCP accumulation (**Figure 4.17**), but also in its ability to diffuse on the plasma membrane (**Figure 4.18**).

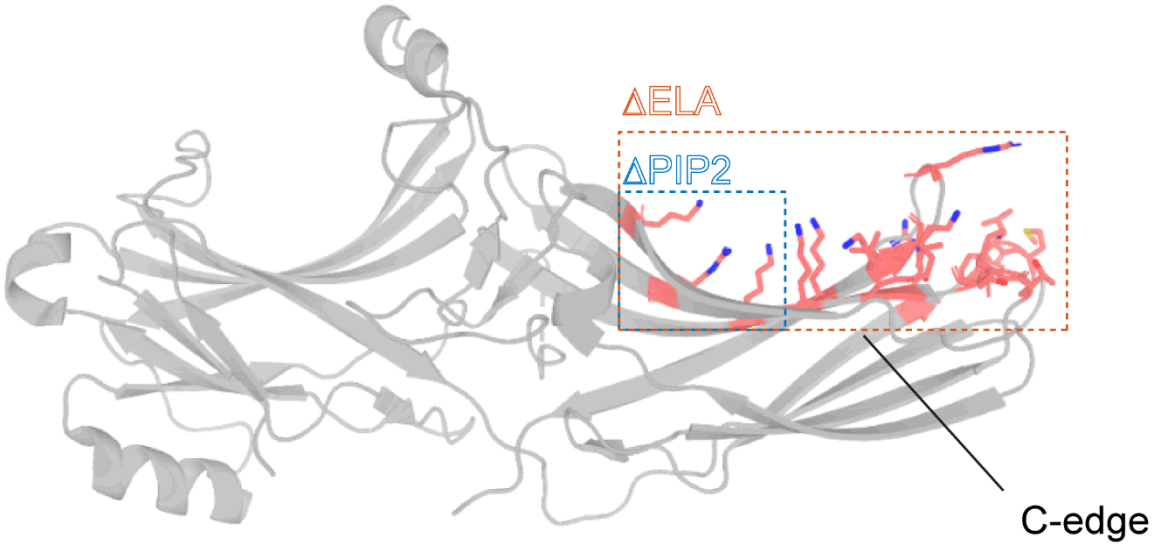

Figure 4.16 Schematic of βArr2 mutations to disrupt binding to membrane lipids. ΔPIP2 (K233Q/R237Q/K251Q; blue box) and ΔELA (R189Q/F191E/L192S/M193G/T226S/K227E /T228S/K230Q/K231E/K233Q/R237E/K251Q/K325Q/K327Q/V329S/V330D/R332E; orange box) modelled on the structure of βArr2 (rcsb:5TV1).

These results were supported by single-molecule microscopy experiments. ΔCCP/AP2 βArr2 was still able to translocate to the membrane and had high diffusivity even after isoprenaline stimulation of receptors (**Figure 4.18**), not becoming trapped at CCPs. This ruled out the possibility that laterally diffusing βArr2 molecules might be bound to the plasma membrane via clathrin or AP2.

ΔPIP2 βArr2 was recruited somewhat to the plasma membrane and had similar diffusivity to WT βArr2 and was able to trap at CCPs. Conversely, the ΔELA mutant saw no increase in agonist-dependent translocation to the plasma membrane, and those arrestins which did arrive had reduced lateral diffusion (**Figure 4.18**). By measuring the frequency of trajectories that

explore a given area in their lifetime, the given space explored by the various mutants was compared (**Figure 4.18**). The ΔELA mutant saw a significant decrease in exploration of space, with the ΔCCP/AP2 mutant tending to explore more space than WT βArr2. As such, for the ΔELA mutant, the few arrestins which did translocate to the plasma membrane bound only transiently and had significantly reduced lateral diffusion compared to WT arrestin.

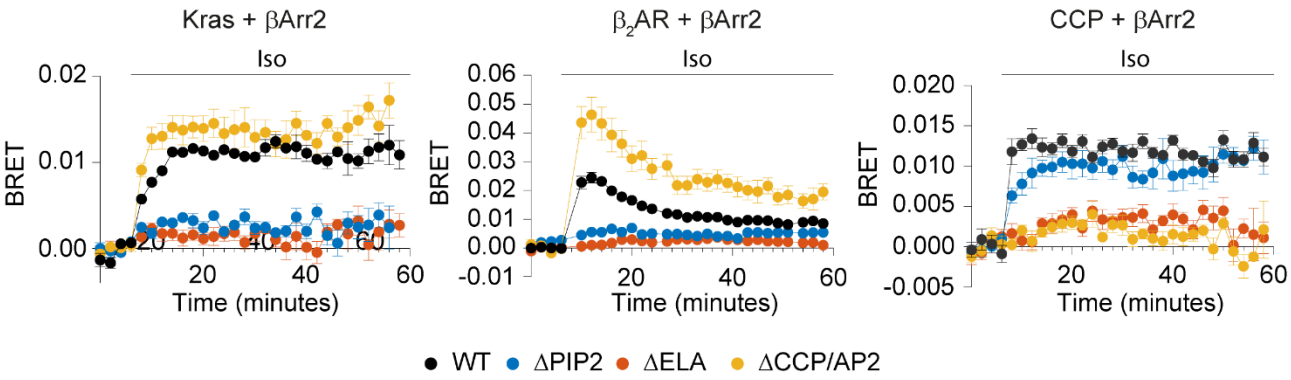

Figure 4.17 β2AR mutant-induced βArr2 kinetics by BRET. Kinetics of βArr2 to the plasma membrane (left), receptor (middle), or CCPs (right) in HEK293 cells stimulated with isoprenaline (10 μM). Shown are the results of real-time measurements monitoring BRET between NanoLuc fused to the plasma membrane marker K-ras (left) or the receptor N-terminus (middle) or clathrin light chain and βArr2-Halo labelled with Halo-R110. K-ras and CCP experiments were performed in the presence of unlabelled receptor (WT β2AR). Iso, isoprenaline. Data are mean ± s.e.m, n=3 independent experiments.

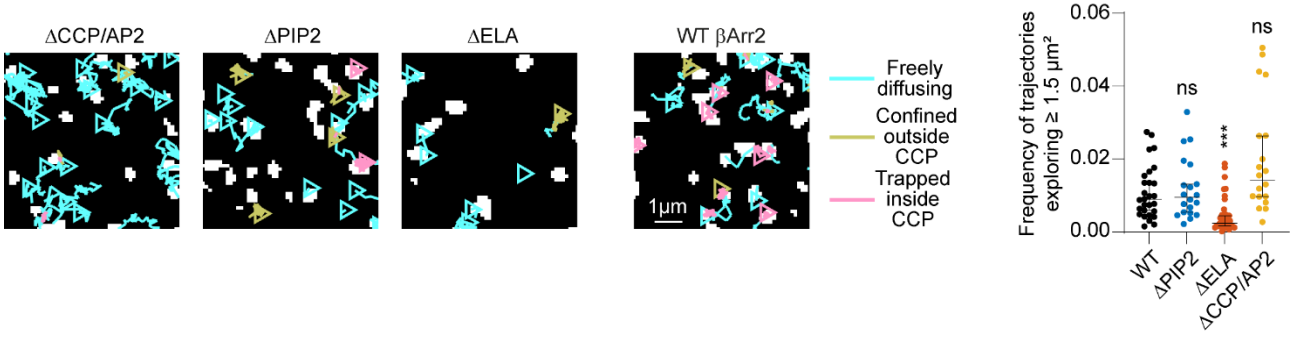

Figure 4.18 Space exploration by βArr2 with mutations in CCP and membrane lipid binding. (Left) Diffusivity states of the ΔCCP/AP2, ΔPIP2 and ΔELA βArr2 mutants. Shown are representative trajectories in cells stimulated with isoprenaline (10 μM; late). (Right) Propensity of mutant βArr2 to explore the plasma membrane. Shown are the relative frequencies of molecules exploring > 1.5 μm² in unstimulated cells. Images are representative of a minimum of 4 independent experiments.

Interaction analysis of the three βArr2 mutants confirmed a decrease in interactions between the ΔPIP2 and ΔELA βarr2 with β_2AR (**Figure 4.19**). In contrast, the ΔCCP/AP2 saw an increase in associations with receptors compared to WT (**Figure 4.19**). This follows results observed in BRET assays, where higher interactions were observed between ΔCCP/AP2 βArr2 and Nluc-β_2AR. BRET assays generate ensemble measurements and do not discriminate between long interactions and increased, transient colocalisations – which might account for the increased colocalisations observed in both experiments. Our interpretation is that because ΔCCP/AP2 βArr2 is able to recruit to the membrane but not internalise via CCPs, its density on the membrane increases after stimulation, thus resulting in increased transient interactions with receptors on the membrane.

Given that arrestins were still able to traffic and co-trap in CCPs with ΔPIP2 arrestin (**Figure 4.20**), even with reduced receptor interactions, PIP2 might constitute only a tertiary component of arrestin-receptor interactions, that acts to increases the likelihood of productive interactions, consistent with a role of PIP2 in facilitating receptor-arrestin interactions. Interestingly, the recruitment of ΔPIP2 arrestin to CCPs was slower than WT arrestin, with a maximum response observed only in Iso(late), which fits remarkably with data found in BRET experiments.

For the ΔELA mutant, which was found to have significantly reduced lateral diffusion and plasma membrane recruitment; receptor interactions were reduced (**Figure 4.19**) and the ability for arrestin to translocate to CCPs was effectively eliminated (**Figure 4.20**). This further supports the model that transient interactions of diffusing proteins on the plasma membrane lead to the CCP accumulation and signalling of β-arrestin, and shows that the C-edge of arrestin is required to interact with lipids on the plasma membrane to maintain this lateral diffusion.

Overall, these results support a model in which βArr2 binds directly to the plasma membrane with a major contribution of hydrophobic residues in the C-edge, whereas the previously identified PIP2 binding site appears dispensable for membrane anchoring.

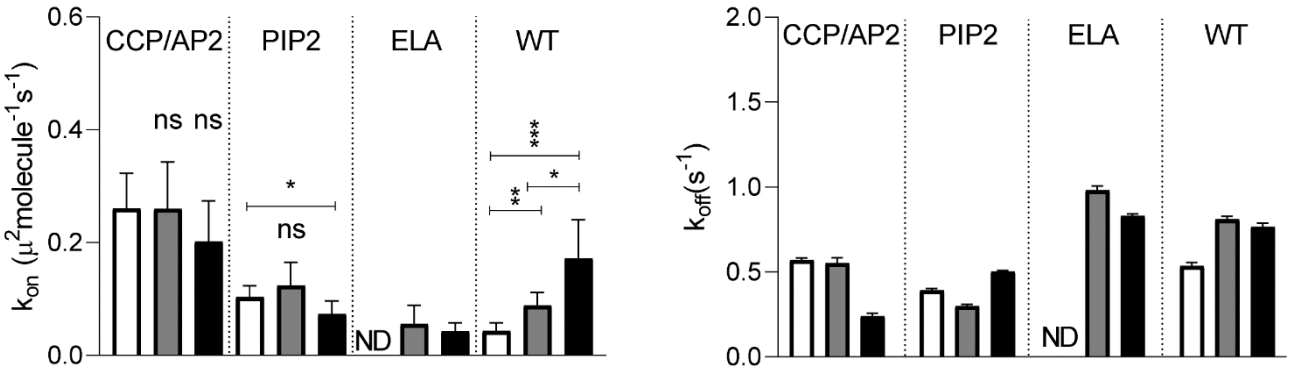

Figure 4.19 βArr2 mutant – β2AR interactions by deconvolution analysis. Estimated (Left) k_{on} and (Right) k_{off} values for WT β2AR or β2AR ΔICL3 or β2AR ΔC-tail interactions with βArr2. Iso, isoprenaline. Early, 2-7 min. Late, 8-15 min. Data are median ± 95% CI and 28, 23, 11, 20, 13, 16, 21, 10, 15, 35, 9 and 15 cells for wild-type (WT) basal, WT Iso (early), WT Iso (late), ΔCCP/AP2 basal, ΔCCP/AP2 Iso (early), ΔCCP/AP2 Iso (late), ΔPIP2 basal, ΔPIP2 Iso (early), ΔPIP2 Iso (late), ΔELA basal, ΔELA Iso (early) and ΔELA Iso (late), respectively Differences in koff values versus basal were assessed by two-tailed unpaired t-test with Bonferroni correction. k_{on} differences are statistically significant by a Kruskal Wallis test, **P < 0.01, ***P < 0.001 versus corresponding basal condition by t-test with Bonferroni correction. ns, statistically not significant.

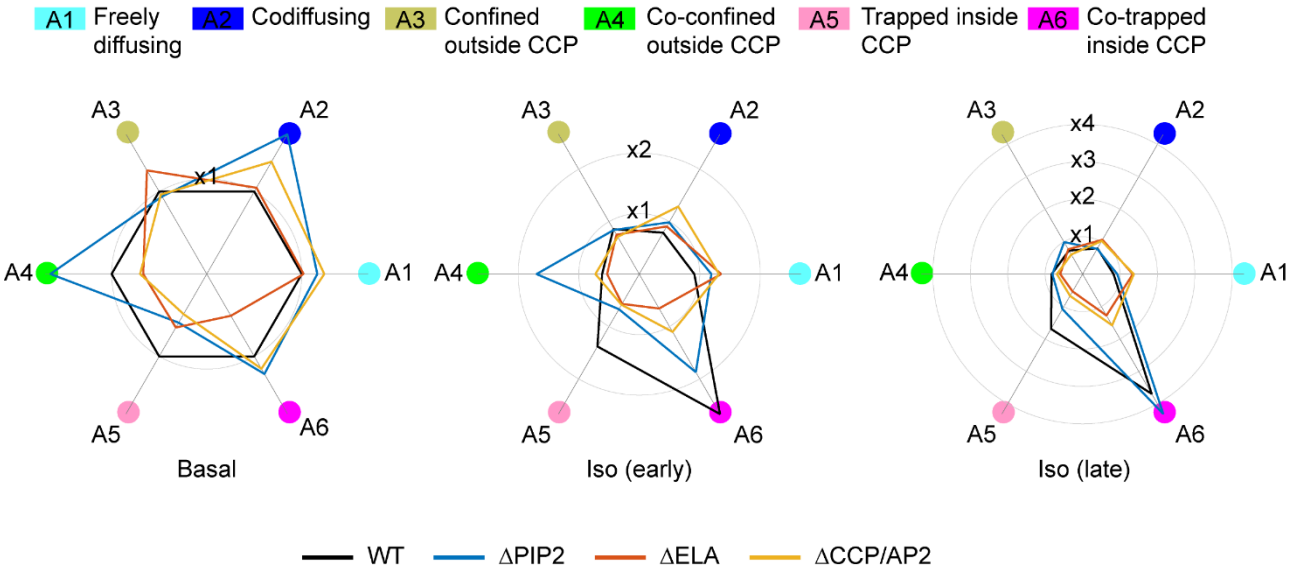

Figure 4.20 Radar plots from Markov Chain analysis of βArr2 plasma membrane mutants. Corresponding βArr2 radar plots from Markov chain analysis, obtained from single-molecule experiments showing the changes in state occupancies induced by isoprenaline (10 μM) stimulation of β_2AR in the presence of βArr2 mutants and CCP. Iso, isoprenaline. Early, 2-7 min. Late, 8-15 min. WT βArr2 is included for comparison. n = 51147, 58254, 22769, 43242, 37370, 40079, 38095, 20436, 30530, 76129, 18683, and 27349 transitions for wild-type (WT) basal, WT Iso (early), WT Iso (late), ΔCCP/AP2 basal, ΔCCP/AP2 Iso (early), ΔCCP/AP2 Iso (late), ΔPIP2 basal, ΔPIP2 Iso (early), ΔPIP2 Iso (late), ΔELA basal, ΔELA Iso (early) and ΔELA Iso (late), respectively

4.2.4 Molecular Dynamics reveal that βArr2 spontaneously inserts into the lipid bilayer via the C-edge and unexpectedly, the arrestin FLR

In support of recent structural data on receptor–β-arrestin complexes in lipid nanodiscs [120], which show only a static image of the proposed mechanism, results obtained here show directly that βArr2 molecules diffuse alone on the plasma membrane, directly bound to the lipid bilayer. To verify this dynamicity in a structural setting with simulated molecules, molecular dynamics (MD) simulations were performed by the laboratory of Jana Selent, with βArr2 in close proximity to the plasma membrane. This work was part of a new collaboration between our labs, where our findings and mutational data was used to by the Selent lab to generate simulations of β-arrestin in the plasma membrane.

Here, spontaneous penetration of the βArr2 C-edge into the lipid bilayer was observed (**Figure 4.21**). Interestingly, this occurs only in 10% of simulations (4/40), which supports our model of lipid interactions on the C-edge of βArr2 generating an equilibrium of arrestin in the cytoplasm and on the plasma membrane, even in a pre-receptor-activated state. Fascinatingly, MD simulations also found that C-edge membrane penetration could, rarely, be followed by membrane penetration of the βArr2 finger loop (**Figure 4.21**), a key β-arrestin region involved in interaction with the receptor core and associated with arrestin activation [27].

Based on extended MD simulations with annotation of amino acids, the major lipid anchoring sites in found in simulations were on the C-edge (L192, M193, R332, G333), as well as two potential additional sites in in the finger loop (V71, L72) and C-loop (F245, S246) (**Figure 4.22**), the latter of which has previously been suggested as a membrane anchor [123].

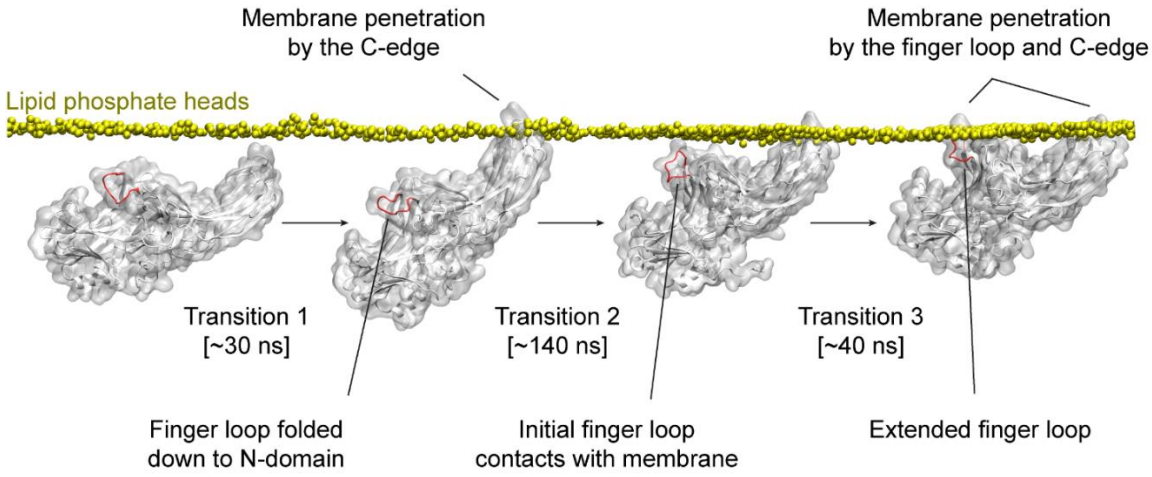

Simulated transition	Replicates	Starting conformation	No of times observed
Membrane penetration by C-edge (Transition 1)	x 50 [50 ns]	Arrestin not contacting membrane	4 / 40
Membrane penetration by fingerloop (Transition 2 to 3)	x 4 [200 ns]	Arrestin anchored by C-edge	1 / 4

Figure 4.21 Molecular Dynamics (MD) simulations of spontaneous βArr2 interactions with the plasma membrane. (Top) transition 1→ transition two is a representative Molecular dynamics (MD) simulation showing spontaneous insertion of the βArr2 C-edge into the lipid bilayer, visualised from 40 x 60ns production runs. Transition 2→transition 3 is representative of 4 x 200ns simulations of C-edge anchored βArr2, where a second interaction involving the finger loop region (FLR) was found in ¼ simulations. (Bottom) Table showing MD simulation results.

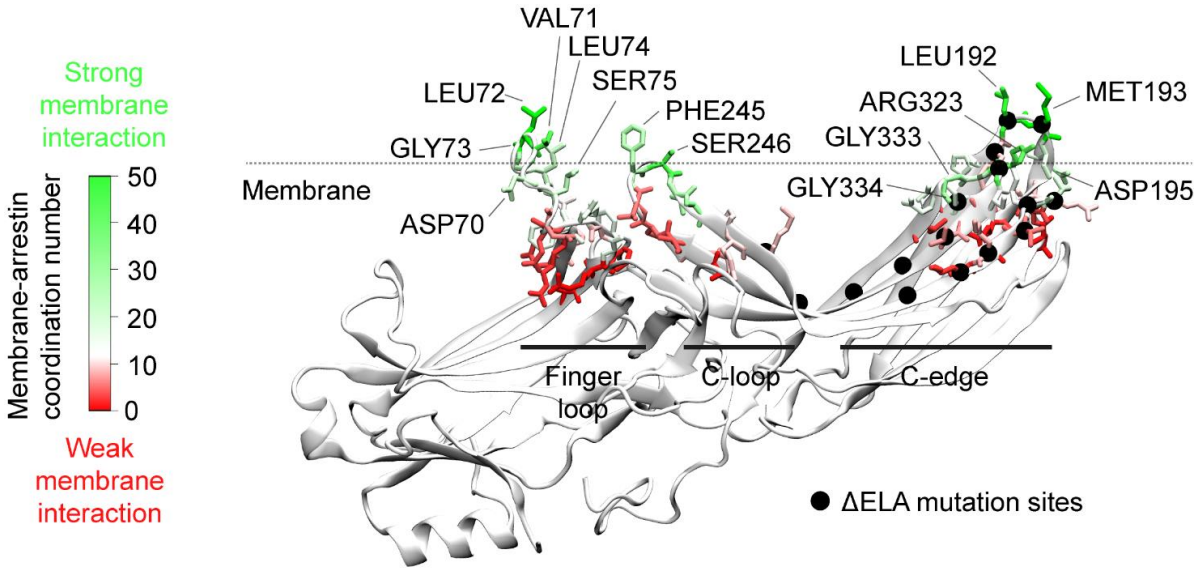

Figure 4.22 Extended MD simulations with amino acid annotation. Results of extended MD simulations (3 μs accumulated time) of membrane-bound βArr2. Plotted are the lipid coordination numbers for each βArr2 residue, revealing a major interaction site in the C-edge and two additional potential sites in the C-loop and finger loop. βArr2 lipid anchoring mutant residues (ΔELA mutant) are shown as a comparison. Residues are plotted if they interacted with the membrane for more than 33% of the frames in the simulation.

These simulations suggest that the membrane might prime βArr2 in an active-like conformation, where it is more likely to form productive interactions with receptors. To explore the conformational space of the fully membrane-anchored βArr2 (i.e. finger loop, C-loop and C-edge), the inter-domain rotation angle between the N- and C-domain was measured, which is a metric typically used to determine the activation state of β-arrestin (inactive-like < 15º, active-like > 15º) [342].

Interestingly, it was found that interaction of βArr2 with the lipid bilayer is associated with a shift of the inactive-like βArr2 equilibrium towards active-like conformations with rotation angles > 15º (**Figure 4.23**). When simulating βArr2 anchored in the plasma membrane with an inactive and active finger-loop region, which mimics a pre- and post- receptor activated βArr2, it was found that arrestins with an active-like FLR bound more stably to the plasma membrane.

We hypothesised a model, where interaction with the membrane primes βArr2 for interactions with receptors by placing them in close proximity in active-like conformations. Arrestins which interact with receptors are more likely to adopt conformations with an active FLR and thus maintain their localisation on the plasma membrane for downstream signalling.

Altogether, these findings provided strong evidence that βArr2 can spontaneously insert into the lipid bilayer and remain associated with it for time sufficient to explore the plasma membrane via lateral diffusion.

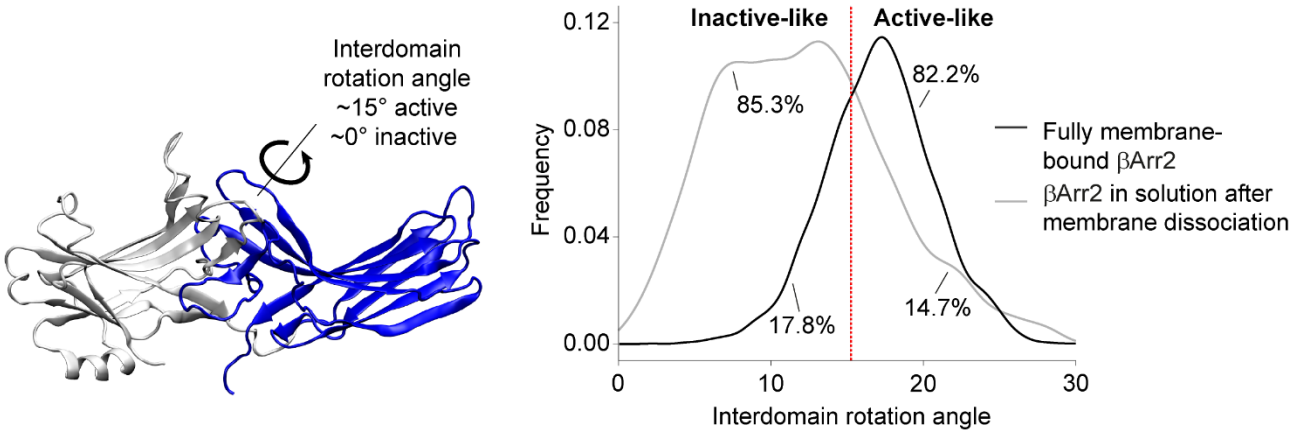

Figure 4.23 Membrane-bound βArr2 are in active-like conformations. Results of MD simulations comparing βArr2 conformations in solution and bound to the lipid bilayer. The inter-domain rotation angle between the N- and C-domains is used as a measure of βArr2 activation (>15^{o} inter-domain angle is considered active-like).

4.2.5 The βArr2 finger loop region (FLR) is required for productive β-arrestin activity on the plasma membrane

MD simulations revealed a previously unrecognised potential interaction of the finger loop with the plasma membrane and suggested that this interaction can stabilise the finger loop in an active-like state. To determine the effect of the arrestin FLR on βArr2 activity in cells, a βArr2

mutant carrying a deletion in the finger loop (ΔFLR), was introduced into the single-molecule microscopy imaging workflow. Mechanistically, the arrestin FLR is thought to form a polar core and locks into a closed conformation prior to meeting a receptor [349]. After interaction with the receptor C-tail (tail interaction), whose proximal residues displace the polar interactions, the FLR is thought to adopt an open conformation and interact with the receptor core (core interaction) (**Figure 4.24**). The polar motifs in the FLR are thought to mediate different interactions with the receptor tail, dependent on the phosphorylation pattern [27,346,349]. This can activate arrestin with differing efficiencies and allow adoption of different conformations [350].

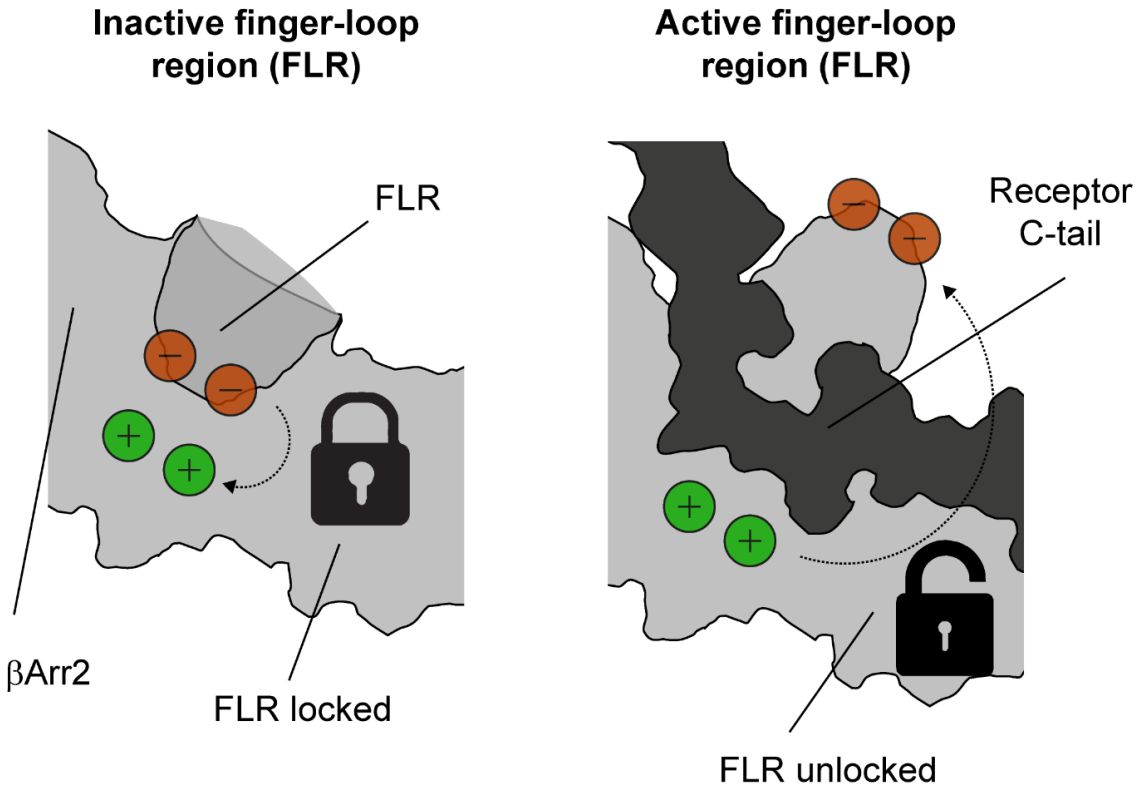

Figure 4.24 Schematic of finger-loop region (FLR) activation by GPCRs. Adapted from *Sente et al.* [350], this schematic shows the currently understood mechanism of the FLR lock. (Left) Prior to receptor engagement, negative charges of the FLR interact to form a polar core in β-arrestin. (Right) When β-arrestin comes into contact with a phosphorylated GPCR C-tail, the polar core is disrupted which causes a rotation between the N- and C- domains of β-arrestin and opens the FLR, unlocking more interaction sites for other proteins.

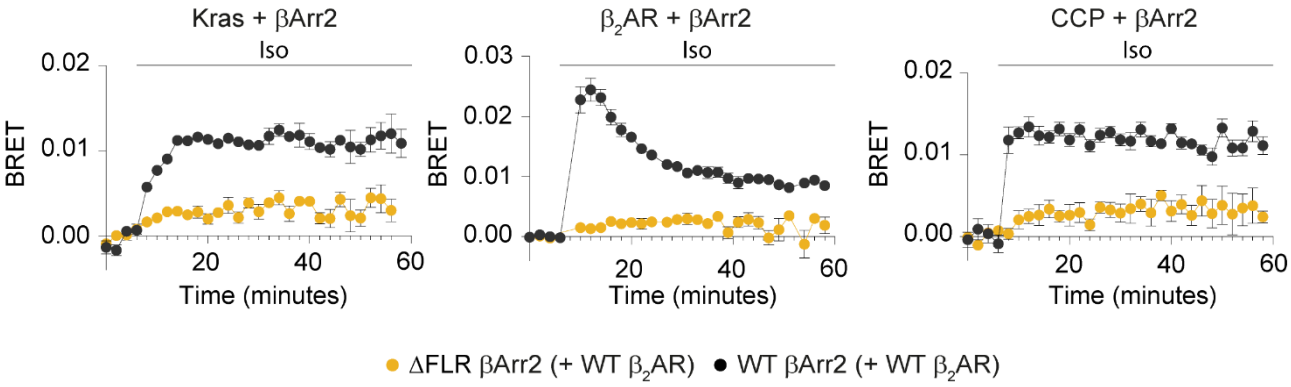

Figure 4.25 Finger-loop region (FLR) βArr2 mutant kinetics by BRET. Kinetics of βArr2 to the plasma membrane (left), receptor (middle), or CCPs (right) in HEK293 cells stimulated with isoprenaline (10 μM). Shown are the results of real-time measurements monitoring BRET between NanoLuc fused to the plasma membrane marker K-ras (left) or the receptor N-terminus (middle) or clathrin light chain and ΔFLR-βArr2-Halo labelled with Halo-R110. K-ras and CCP experiments were performed in the presence of unlabelled receptor (WT β_2AR). Iso, isoprenaline. Data are mean ± s.e.m, n=3 independent experiments.

Firstly, the arrestin ΔFLR mutant failed to translocate to the plasma membrane, β_2AR and accumulate in CCPs upon agonist stimulation, as measured by BRET (**Figure 4.25**). In single-molecule experiments, the ΔFLR arrestins were found to have similar diffusion properties on the plasma membrane as WT βArr2 but did not accumulate in CCPs after agonist-induced receptor stimulation (**Figure 4.26**). This fits with the hypothesis that FLR membrane association is involved in βArr2 activation and trafficking, but not necessarily required for lateral diffusion.

Additionally, the ΔFLR arrestin did not co-accumulate in CCPs with receptors and perhaps most importantly, did not trap alone in CCPs (**Figure 4.27**). Given that previous results found that βArr2 could trap alone in CCPs similarly regardless of the receptor employed, this suggests that active-like β-arrestin FLR is required for receptor-independent CCP accumulation. This supports the model view of the FLR mediating receptor-independent β-arrestin signalling, observed by Eichel et al. [315].

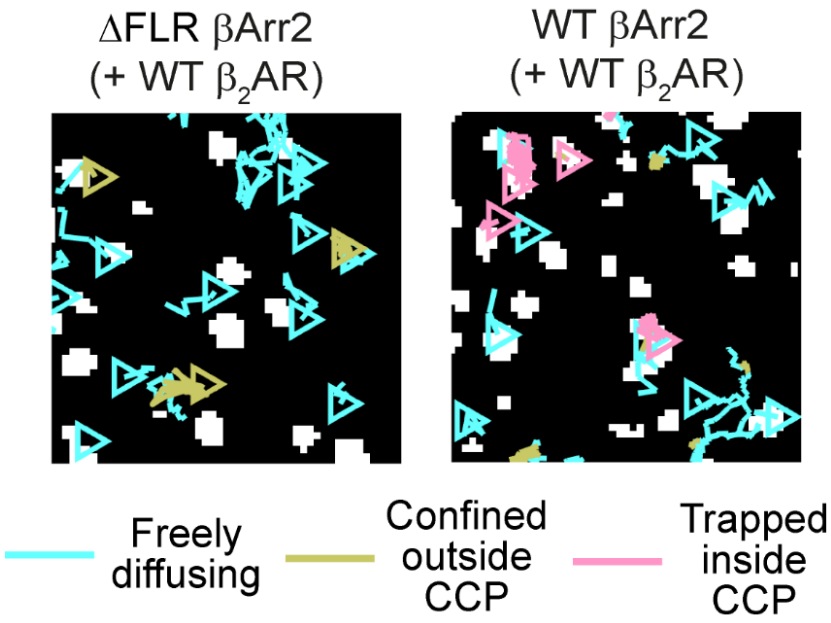

Figure 4.26 ΔFLR βArr2 lack of trapping at CCPs. Diffusivity of the ΔFLR βArr2 mutant compared to WT. Shown are representative trajectories in cells stimulated with isoprenaline (10 μM; late). Images are representative of a minimum of 4 independent experiments.

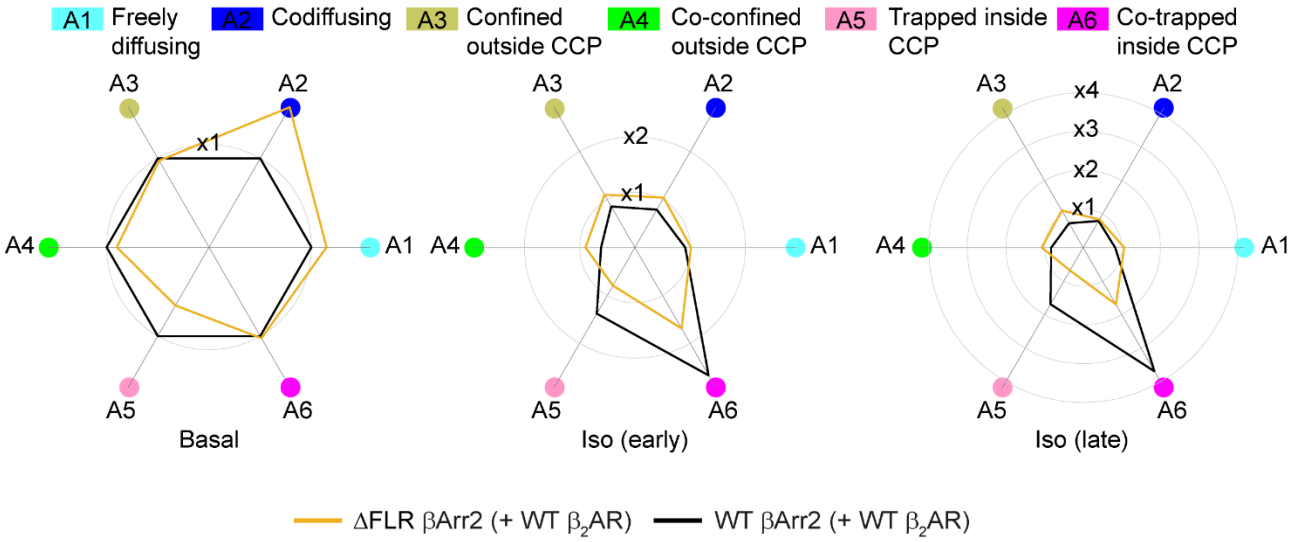

Figure 4.27 Radar plots from Markov Chain analysis of ΔFLR βArr2. Corresponding βArr2 radar plots from Markov chain analysis, obtained from single-molecule experiments showing the changes in state occupancies induced by isoprenaline (10 μM) stimulation of β2AR in the presence of ΔFLR βArr2 and CCP. Iso, isoprenaline. 51,147, 58,254, 22,769, 57,627, 64,695, and 46,518 transitions for WT basal, WT Iso (early), WT Iso (late), ΔFLR basal, ΔFLR Iso (early) and ΔFLR Iso (late), respectively.

All of these results are in striking contrast to the ΔICL3 β_2AR mutant, which was dispensable for arrestin CCP accumulation and arrestin-GPCR interactions, in agreement with previous studies [346,351]. Conversely, the receptor C-tail was found to be indispensable for signalling. In combination with the findings for the ΔFLR arrestin mutant, this suggests that perhaps the initial depolarisation of the FLR from the closed conformation (tail interaction) is more important in activating arrestin than interacting directly with the receptor core (core interaction). Moreover, these results suggest that an intact finger loop is required for βArr2 activation and accumulation in CCPs.

4.2.6 Laterally diffusing βArr2 are active on the plasma membrane

MD simulations revealed a previously unrecognised potential interaction of the finger loop with the plasma membrane and suggested that this interaction can promote or stabilise the finger loop in an active-like state. Using the ΔFLR βArr2 mutant in single-molecule experiments, it was found that βArr2 could still diffuse on the plasma membrane without the FLR, but had significantly reduced interactions with CCPs and receptors, suggesting that these arrestins are less active. To test the hypothesis of whether the βArr2 which diffuse on the plasma membrane are in active-like conformations, an intrabody based on a single-chain variable fragment (ScFv30) that selectively recognises active βArr1/2 conformations was used [140] (**Figure 4.28**).

BRET experiments were performed in HEK293 CRISPR/Cas-9 cells with βArr1 and βArr2 knocked out, which allows visualisation of plasma membrane recruitment of the ScFv30 in cells containing no β-arrestin. This is because there is no endogenous arrestin present in the cells and arrestin transfection can be controlled exogenously. Cells with re-expressed βArr2

confirmed the ability of ScFv30 to recognize active βArr2, as shown by its plasma membrane translocation following isoprenaline stimulation, only in cells which contained transfected βArr2 (**Figure 4.29**). TIRF imaging of ScFv30-labelled β-arrestin in the CRISPR KO cells exemplified the arrestin knockout phenotype, given that ScFv30-Halo was only recruited to the plasma membrane after isoprenaline stimulation when exogenous WT βArr2 was introduced into the cells (**Figure 4.30**). In the case of cells without WT βArr2, the density of spots was similar to that observed outside of cells on the background, and this did not change after stimulation with the agonist isoprenaline.

Remarkably, single-molecule imaging revealed striking similarities between the behaviour of βArr2 and ScFv30 in CHO CRISPR βArr1/2 KO cells, including the occurrence of laterally diffusing ScFv30 molecules on the plasma membrane with characteristics superimposable to those of βArr2 (**Figure 4.31**). ScFv30 labelled arrestins were capable of reaching and becoming trapped at CCPs without an accompany receptor, and increases in trapping were observed after stimulation of β_2AR (**Figure 4.32**). These effects were not seen in cells without exogenous βArr2 expression, validating the use of ScFv30 to label arrestin.. Altogether, these results strongly support a model in which βArr2 remains bound to the plasma membrane in an active-like conformation after having transiently interacted with a receptor, allowing βArr2 to reach CCPs alone.

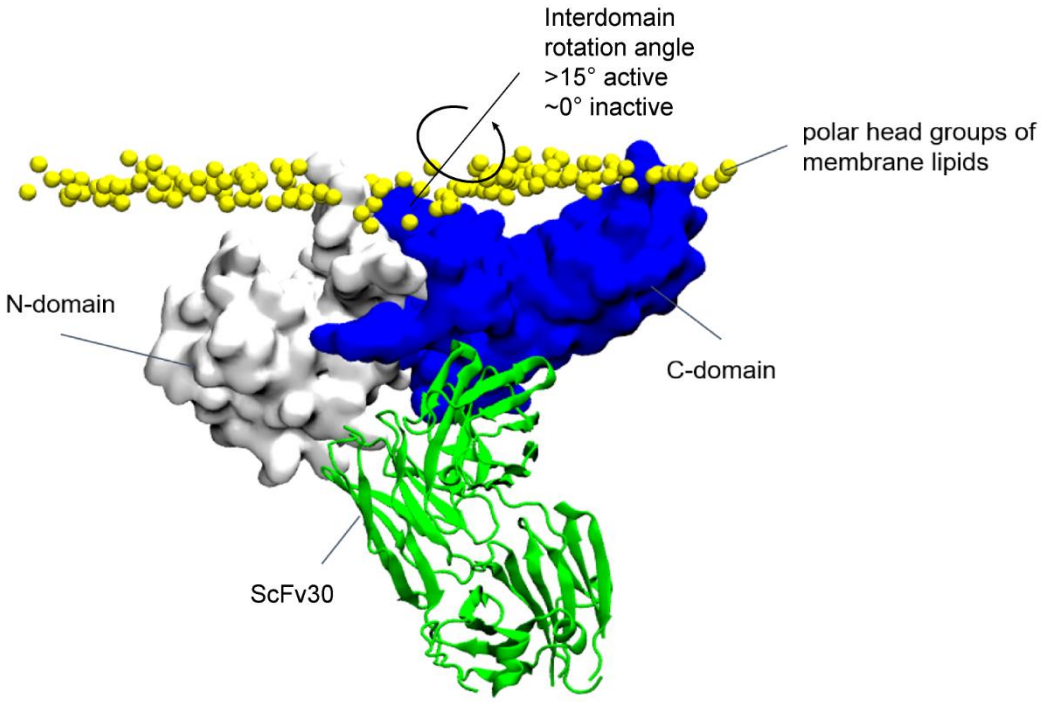

Figure 4.28 Schematic of ScFv30 binding to active β-arrestin. Recognition of active membrane-bound βArr2 by ScFv30. The structural model was obtained by aligning the membrane-bound βArr2 conformation obtained in MD simulations to the crystal structure of the βArr1–Fab30 complex (PDB 4JQI).

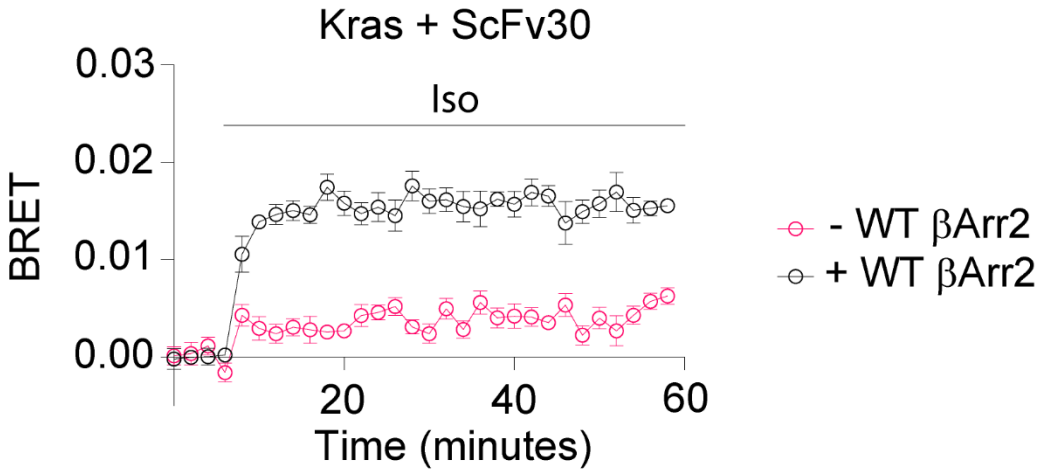

Figure 4.29 ScFv30 recruitment to the plasma membrane in β-arrestin KO cells. Kinetics of ScFv30 recruitment to the plasma membrane in βArr1/2 CRISPR-Cas9 knockout HEK cells with/without βArr2 re-expression upon isoprenaline (10 μM) stimulation. Measured is recruitment of ScFv30-Halo labelled with Halo-R110 to Kras-NanoLuc labelled with furimazine, either with or without WT βArr2 present. Data are mean ± s.e.m. and n = 3 biological replicates

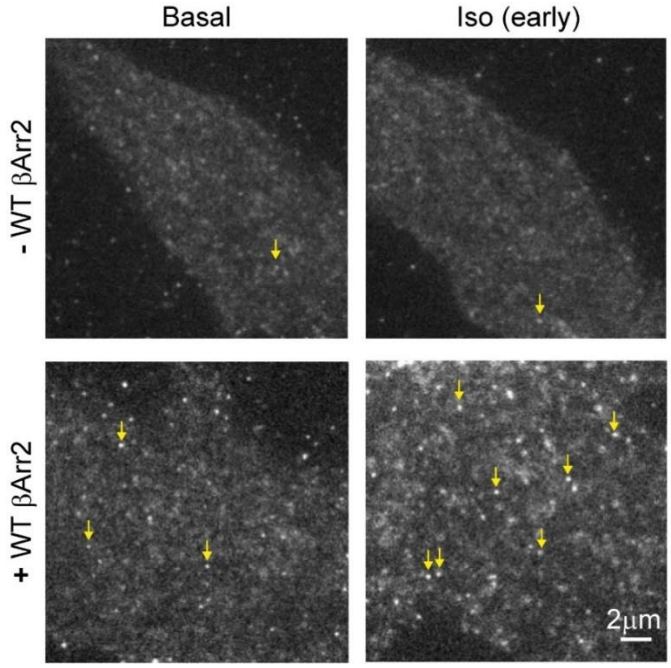

Figure 4.30 TIRF imaging of βArr1/2 CRIPSR CHO knockout cells. Representative single-molecule TIRF images of ScFv30-Halo, which selectively labels active βArr2, in cells expressing β_2AR and either with or without WT-βArr2. Images are representative of 3 independent experiments and example diffraction-limited spots are labelled with yellow arrows in cells before and after stimulation with isoprenaline (10μm).

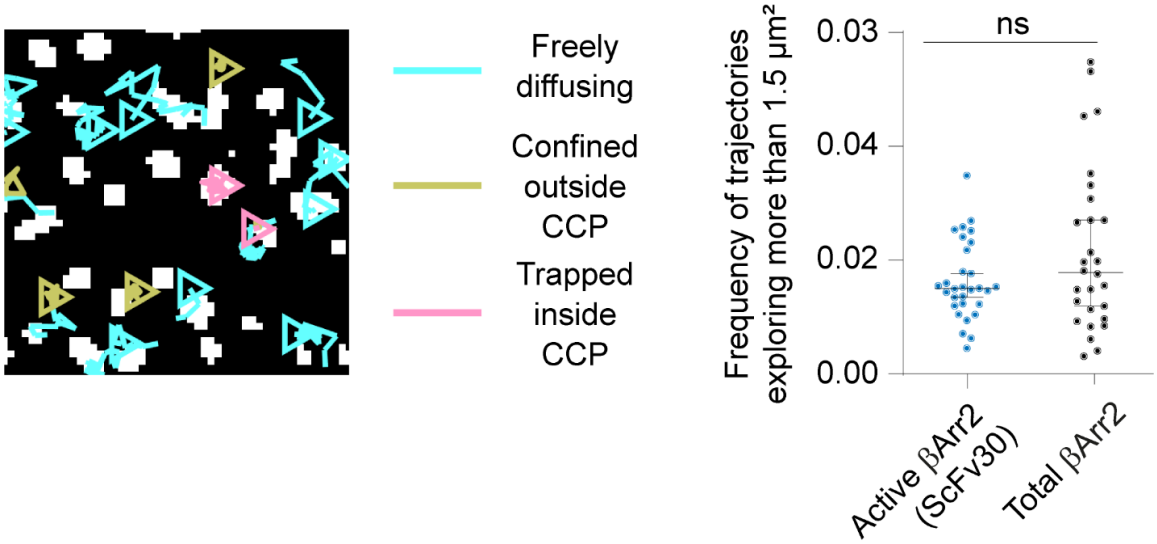

Figure 4.31 Diffusion of ScFv30 on the plasma membrane. (Left) Diffusivity states of active β-arrestin on the plasma membrane as revealed by single-molecule visualisation with ScFv30. Shown are representative trajectories in cells stimulated with isoproterenol (10 μM) for 8-15 min (late). (Right) Propensity of active β-arrestin detected by ScFv30 to explore the plasma membrane. Total βArr2 from labelling of βArr2-Halo is shown for comparison. Shown are the relative frequencies of molecules exploring ≥ 1.5 μm^2 in unstimulated cells

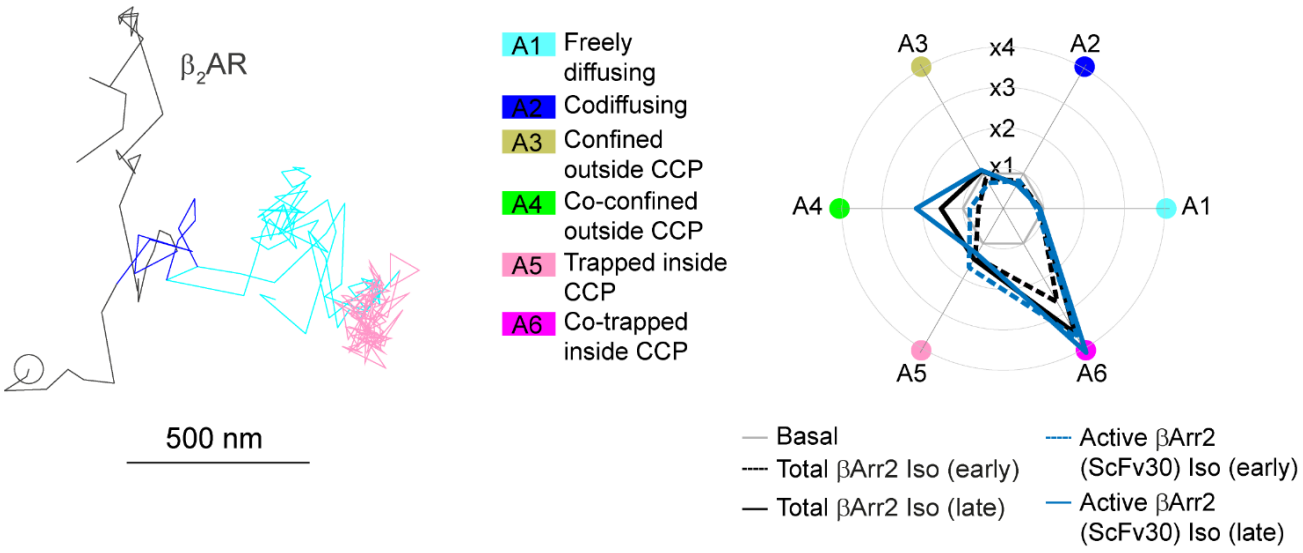

Figure 4.32 Laterally diffusing βArr2 are active on the plasma membrane. (Left) Example of an active β-arrestin molecule, visualised with ScFv30, undergoing a transient interaction with a β2AR molecule to then diffuse away alone and reach a CCP without the receptor. (Right) Radar plot obtained from single-molecule experiments comparing the behaviour of ScFv30 recognising active β-arrestin and total βArr2. n=4 independent experiments and 64,757, 65,227, and 99,428 transitions for ScFv30 basal, ScFv30 Iso (early), and ScFv30 Iso (late), respectively. Experiments were performed in β-arrestin CRISPR KO CHO-K1 cells.

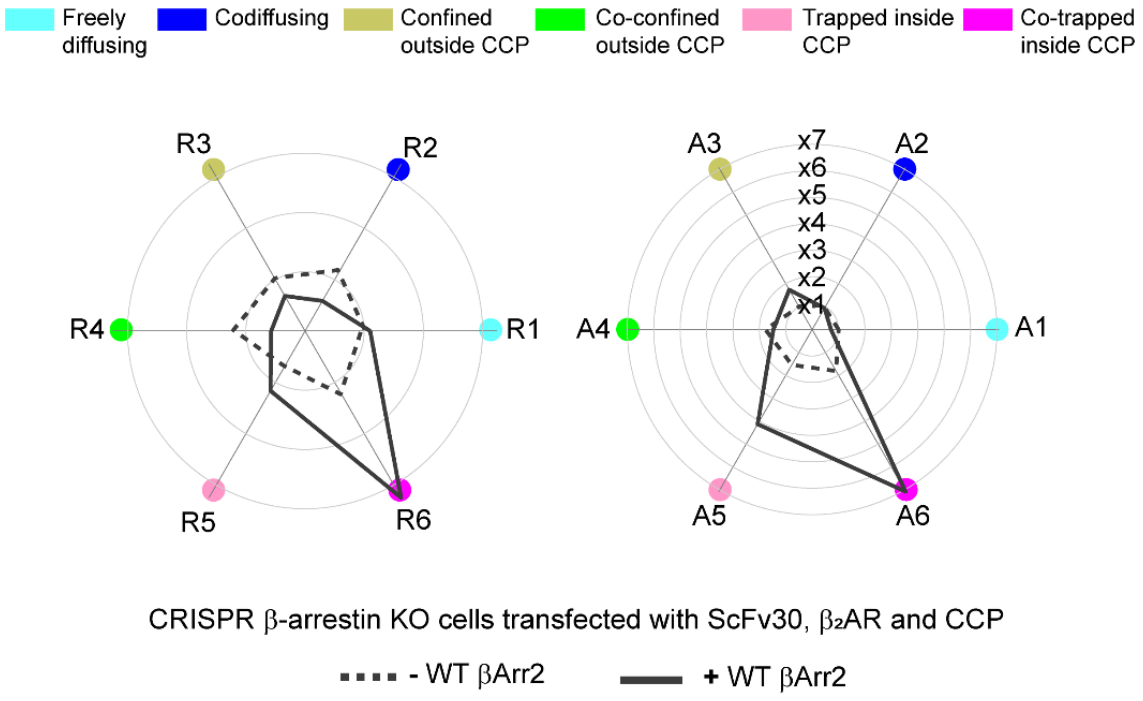

Figure 4.33 Confirmation of ScFv30 labelling of βArr2 in CRISPR cells. Radar plot obtained from single-molecule experiments comparing the behaviour of ScFv30 recognising active-like β-arrestin and total βArr2.

4.3 CONCLUSIONS

According to the current model, which is largely based on ensemble measurements, β-arrestin is assumed to translocate to an active receptor upon agonist stimulation, remaining bound to the receptor until they reach a CCP together. In contrast, single-molecule results presented here provide direct strong evidence that βArr2 mainly behaves as a membrane protein that finds its target receptor via lateral diffusion and remains bound to the plasma membrane after having transiently interacted with the receptor ($\tau \sim 1$ s) (**Figure 4.34**). This is in support of recent findings by Eichel et al. and adds value to recent structural studies [119,315,349], which suggest lipid interactions are vital in mediating arrestin-GPCR interactions.

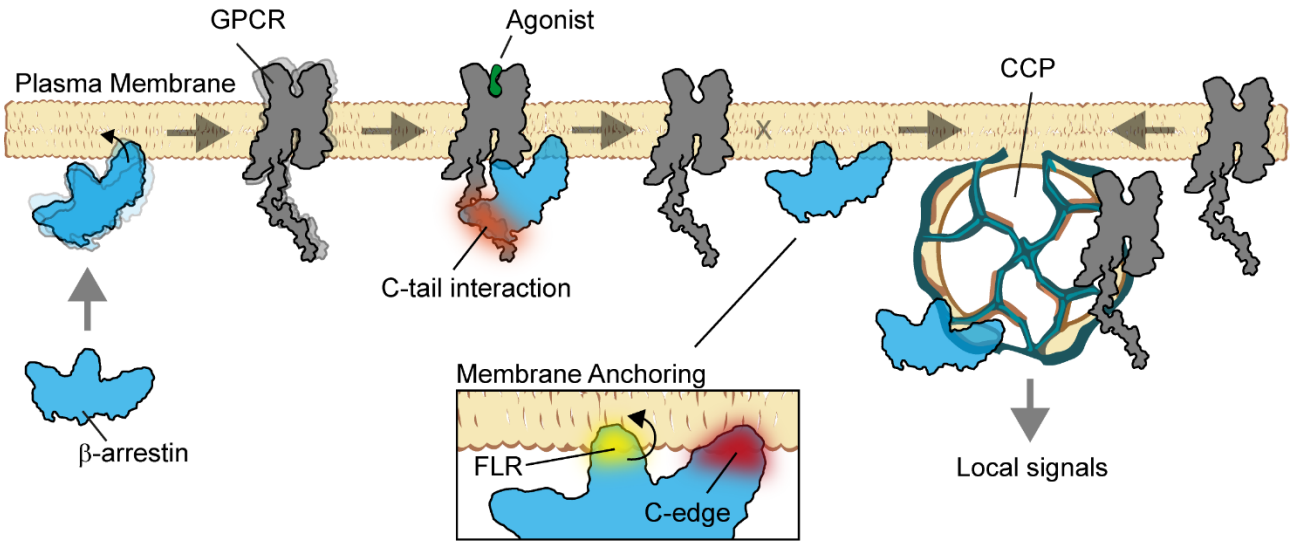

Figure 4.34 Proposed model of GPCR–β-arrestin interactions on the plasma membrane. β-arrestin in the cytoplasm more frequently adopt inactive conformations and can spontaneously bind to the plasma membrane via the insertion of the C-edge into the lipid bilayer. Interactions with the GPCR C-tail triggers β-arrestin activation on the membrane, including β-arrestin interdomain rotation and extension of the finger loop region (FLR). Upon dissociation from the receptor, the interaction of the extended finger loop with the lipid bilayer stabilises β-arrestin in a membrane-bound active-like conformation, allowing it to reach CCPs via lateral diffusion without an accompanying receptor. The FLR activation is required for

efficient binding to CCPs and active conformations likely enables binding to other, previously unqualified effector proteins as interaction partners for β-arrestin.

Stimulation with a β-adrenergic agonist revealed an increase in trapping of GPCRs and β-arrestin at clathrin-coated pits (CCPs), which was due to an equilibrium shift in the global proportion of molecules transitioning through states of trapping as opposed to increased lifetimes of the trapping events themselves. Using a panel of β-adrenergic receptors with varying affinities for β-arrestin through the receptor C-tail and β_2AR with mutated tail and core sites, the dependence of trapping at CCPs and arrestin-GPCR interactions was found to require interaction of βArr2 with the C-tail. The similarity of the ICL3 β_2AR mutant with respects to our multi-colour single-particle tracking experiments suggest that the ICL3 may instead be involved in desensitisation to G-proteins, for which further work would be required to confirm. Additionally, direct estimates of the frequency and duration of receptor-arrestin interactions were elucidated, finding that most are short-lived (~1s), with the addition of agonist controlling the rate of productive interactions. This is similar to previous studies with G proteins [253], and might present a general mechanism for how GPCRs interact with effector proteins on the plasma membrane.

Using probabilistic statistical models, the sequence of events most likely to occur from βArr2 arrival on the plasma membrane to their departure were delineated. These datasets are extremely rich, with each frame for each trajectory containing their diffusional states, their interactions and localisation on the membrane. It was found that arrestins arrived on the plasma membrane mostly at sites without a receptor present, and that they could transiently engaged multiple receptors or CCPs, fluctuating between multiple diffusive states. Given more time, studies on the current dataset could be generated to investigate homo-interactions and stoichiometry of β-arrestin in response to agonist stimulation or even study the nanoscale

arrangement of arrestin around the CCP. The latter is particularly interesting, given that a recent single-molecule study suggested that β-arrestin can adopt docking poses either around CCPs to stabilise their generation or accumulate inside CCPs for signalling [119,124].

A panel of β-arrestin mutants were generated to determine the important structural components which facilitate interactions of arrestin with plasma membrane lipids and CCPs. It was found that binding to the plasma membrane could only be saturated for those molecules trapped in CCPs, suggesting that the freely diffusing molecules were binding to an unsaturable source, such as lipids. Disrupting binding to the membrane lipid PIP2 reduced recruitment of arrestin to the plasma membrane and receptors, however we found that these molecules were still able to diffuse and trap at CCPs, just with a reduced total number. Only when multiple residues across the C-edge of arrestin were mutated was an almost abrogated lateral diffusion demonstrated, which included reduced interactions with the receptor and binding to CCPs as a result. These data show that maintenance of arrestin interactions with lipids is required for arrestin binding to the membrane, interactions with receptors and lastly trapping in CCPs.

Using a mutant which was unable to interact with clathrin and the associated adaptor protein AP2, βArr2 was unable to become trapped at CCPs. Even with continued receptor interactions for this mutant, a lack of ability to bind directly to clathrin components meant that β-arrestin continued diffusing laterally on the membrane. This suggests that arrestin is able to hook on to CCPs, and that increases in CCP trapping after stimulation are due to conformational changes which make arrestin more likely to bind to CCPs and become trapped there.

Through molecular dynamics, we found that arrestin can self-associate with the plasma membrane through both the C-edge and additionally via the arrestin FLR, a surprising find since this is commonly associated with arrestin activation and signalling. Mutating out the arrestin

FLR, which is known to bind to the receptor core and has been suggested to mediate arrestin activation, reduced recruitment to CCPs and receptors after agonist stimulation, confirming its role in arrestin activation. Moreover, results with a nanobody (ScFv30) that selectively recognises active β-arrestin combined with MD simulations suggest that the observed transient interactions with a GPCR are capable of catalysing βArr2 into active-like conformations, which are stabilised by lipid interactions. This membrane-anchored active-like βArr2 state is sufficiently long lived to allow βArr2 to diffuse to CCPs alone, where we anticipate it could mediate G protein-independent signalling without the need for an accompanying receptor.

The model derived here has been driven by cell-based assays, microscopy, mathematical modelling and molecular dynamics simulations; all of which consolidate a new understanding of β-arrestin on the plasma membrane, which is driven by dynamic interactions with GPCRs and structural elements, through lateral diffusion of β-arrestin.

4.4 Supplementary Table

Trajectories analysed for interaction analysis and Markov chains *(1-200 frame trajectory segments)*		
β_1AR-βArr2	**Receptor channel**	**Arrestin channel**
Basal	79406	47484
Early	49852	31705
Late	42659	26649
β_2AR-βArr2		
Basal	58864	44012
Early	34053	39186
Late	17941	16349
β_2V_2-βArr2		
Basal	54963	36171
Early	28552	23997
Late	18404	17812
β_2AR-βArr2 ΔCCPAP2		
Basal	40429	34657

Early	17956	23926
Late	30875	32808
β_2AR-βArr2 ΔPIP2		
Basal	51521	35562
Early	16761	18197
Late	33285	27166
β_2AR-βArr2 ΔLAM		
Basal	106226	66717
Early	19743	17786
Late	33917	28006
β_2AR ΔICL3-βArr2		
Basal	57490	36820
Early	26645	26017
Late	31769	25794
β_2AR ΔC-tail-βArr2		
Basal	68158	50372
Early	33248	34407
Late	36025	30538
β_2AR-βArr2 ΔFLR		
Basal	58353	46666
Early	32463	41115
Late	29876	36450
β_2AR-ScFV30		
Basal	85732	61873
Early	48531	50876
Late	81892	82198

5 Towards imaging endogenous β-adrenergic receptors in cardiac myocytes with single-molecule microscopy

5.1 PREFACE

Existing drugs have been developed under the assumption that GPCRs are simple binary switches, which limits current therapeutic capabilities to turning them on/off with agonists/antagonists. This is often insufficient to produce the desired biological effects. For instance, β-adrenergic receptor agonists improve contractility in heart failure, but prolonged usage induces fibrosis, myocyte apoptosis and arrhythmias – increasing mortality [352]. New pharmacological entities are in development consistently for these receptors, but there is an urgent need to develop innovative strategies that target GPCRs beyond their traditional pharmaceutical profile.

New findings challenge the binary GPCR model [119,253,315,353], including work presented in this thesis with regards to β-arrestin signalling. It has been suggested that GPCRs assume different conformations linked to specific biological effects, which can be stabilised by different ligands – known as 'biased signalling'. These effects are thought to occur via selective activation of G proteins or β-arrestins and are dependent spatial localisation, temporal activation, signalling molecule expression and many other factors. GPCR signalling has been shown to occur at intracellular sites and not just on the plasma membrane [354], which might be exploited pharmacologically and with therapeutic benefits [65,267].

The complexity of drug binding to receptors in the context of a dynamic, living cell are poorly understood, especially when concatenated with evolving understandings of signalling localisation, structural nanodomains and signalling bias. In order to answer these fundamental questions, it will be crucial to thoroughly understand all key interactions involving GPCRs,

adaptor proteins, the cytoskeleton and membrane lipids in the cells they naturally occupy. Alterations in the organisation of β-adrenergic receptors has been implicated in diseases like heart failure, where signalling of endogenous hormones becomes defunct [150,215,225,355]. To understand how these modulate GPCR signalling requires study in the cardiac myocytes themselves but exceeds basic understandings of activation/inhibition. The frequency, duration and precise location of these interactions are presently unknown, mostly due to technical limitations in directly visualising the components.

5.1.1 Alternate approaches to imaging GPCRs

β-AR signalling has so far, in this thesis, been studied in CHO cells, which are an immortal cell line that do not express endogenous β-ARs, but are ideal morphologically for single-molecule imaging. These are relatively simple cells and are unlikely to exhibit the same level of complexity to that of the primary cells where β-adrenergic receptors exhibit their effects in nature. As such, investigation of these receptors in primary cells, such as cardiac myocytes, provides a unique model to study the spatiotemporal organisation of GPCR signalling, providing the opportunity to study it under normal and pathological conditions [170].

In this study, we used self-labelling enzymes with small, organic fluorophores to study GPCRs and their related signalling proteins by single-molecule microscopy. These provide many benefits when considered over fluorescent proteins (FPs), such as GFP and YFP, such as increased brightness, better photostability, experimental flexibility from multiple dye choices and the ability to label only plasma membrane proteins if required, due to cell-impermeable dyes. There are also some associated caveats, with the requirement for covalent labelling of

dyes introducing an increased background noise, labelling efficiency considerations and the presence of dark proteins (unlabelled proteins in the pool of total protein).

Other labelling methods exist, such as quantum dots (QD), which are colloidal semiconductor nanomaterials whose atomic core size is proportional to their emission. They are some of the brightest molecules available for fluorescent imaging, have the narrowest absorption spectra and least photobleaching. They are however associated with extreme blinking at high laser powers, which severely hampers SPT experiments due to an inability to connect trajectory segments. All of the above-described methods can be used to label a protein-of-interest (POI), but there also remains the possibility to indirectly label a POI by labelling another molecule it is known to interact with, such as a ligand.

5.1.2 Fluorescent ligands for GPCRs

The development of fluorescent ligands for GPCRs - which are composed of a pharmacophore (often a high-affinity agonist or antagonist) bound to a fluorophore by a linker (**Figure 5.1**) - has enabled the development of a new family of fluorescent moieties, which have furthered understanding of GPCR signalling without having to tag the receptors directly. This has advantages for being able to study receptors in their native environments and allows the visualisation of unmodified receptors. Conjugation of fluorophores to pharmacophores often has dramatic changes on the pharmacology due to the added steric bulk, and these molecules should be considered as novel pharmacological tools [356]. Some of these alterations in properties include a change in receptor selectivity, loss of affinity compared to the native compound or increased affinity for non-GPCR targets, such as the plasma membrane [323,356].

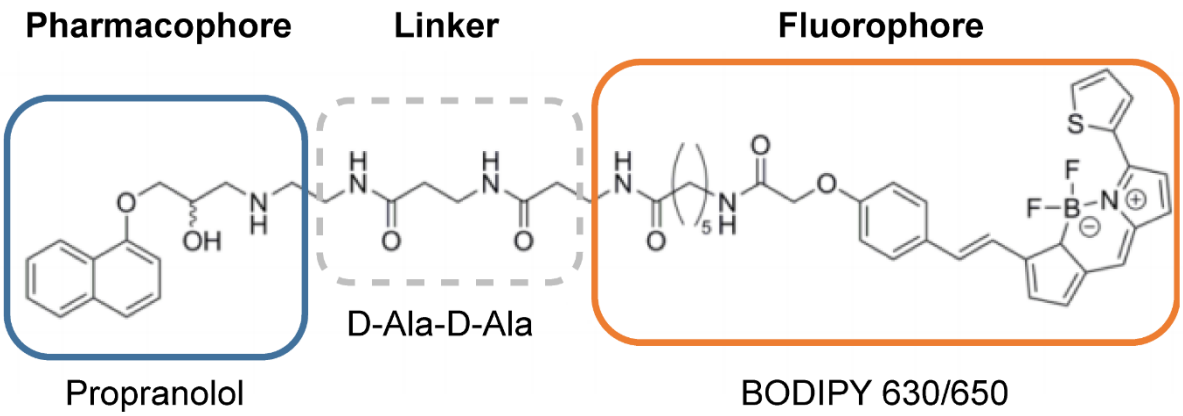

Figure 5.1 Fluorescent ligand schematic. Shown here is Propranolol-BODIPY-630/650 (D-Ala-D-Ala), figure adapted from Baker et al [323]. A pharmacophore (Propranolol) is conjugated to a fluorescent moiety (BODIPY 630/650) by a covalent linker dipeptidase (D-Ala-D-Ala).

A variety of fluorophore labels have been conjugated to fluorescent ligands, but the best are selected for their photophysical properties, geometry and lack of ligand binding interference. Fluorescent ligands have been used extensively in high-throughput screening of GPCRs, confocal microscopy and flow cytometry [357-359], but their uses in single molecule methods are only recently being examined [360]. To lessen the impact on pharmacophore efficacy at receptors, small fluorescent labels are used in addition to a linker, which prevents detrimental effects of the fluorophore on pharmacophore-receptor interactions [359] (**Figure 5.1**). Using a non-covalent labelling system also means that ligands can be washed off if required, which provides the opportunity to test specificity and label a sample multiple times. Without the requirement of genetically modified receptors, fluorescent ligands can be used to study endogenous proteins in immortal cell lines, primary cells and are even being used *in vivo* to study drug trafficking through an entire organism [265].

Considerations in selection of a fluorophore for fluorescent ligand synthesis include the emission and excitation wavelengths, quantum yield and photobleaching susceptibility. The

most commonly used fluorophores used for GPCR fluorescent ligands are boron-dipyrromethene (BODIPY), Rhodamines (e.g. SiR), Cyanines (e.g. Cy3) and Alexa Fluors (e.g. Alexa Fluor 647) [361,362]. BODIPY dyes see most use, given the dye availability over a diverse range of wavelengths, increased brightness and openly published synthetic pathways [363-365] – making them easy to replicate.

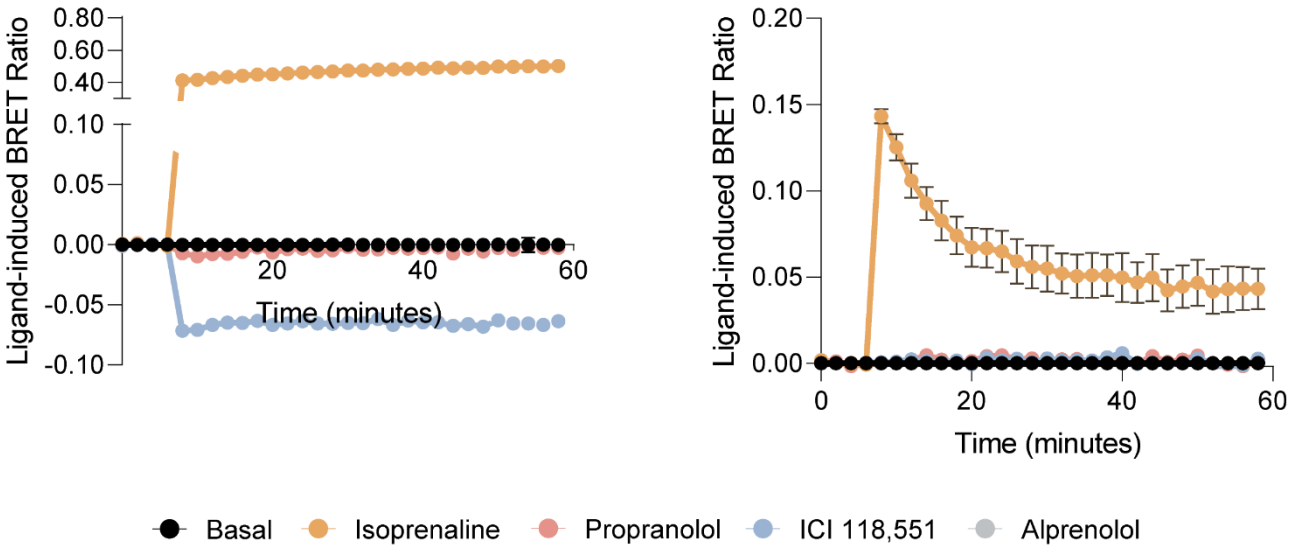

Figure 5.2 Pharmacology at β2-adrenergic receptors by G protein binding. Shown are the results of real-time measurements monitoring BRET between NanoLuc fused to β2AR and Gαs-Venus (left) or βArr2-Venus. Cells were interrogated with 10μM isoprenaline, ICI 118,551, propranolol or Alprenolol after 4 basal reads. Data are mean ± s.e.m, n=2 independent experiments

5.1.3 Fluorescent ligands for β-adrenergic receptors

Few fluorescent ligands have been successfully generated for β-ARs [323], but they have been used extensively for decades to map receptor localisation and clustering in physiologically relevant cells [366,367]. These initial ligands were later found to be non-selective, non-specific and their binding to autofluorescent granules was similar to that of GPCRs [368,369]. More recent studies have employed well-characterised BODIPY ligands and have enabled the visualisation of

binding to α_1-adrenergic receptors in murine tissue slices, which enables the determination of receptor density and might be important in biomarker determination of GPCRs for diseases like prostate cancer, where α_1AR is up-regulated [370].

Baker et al. developed a panel of fluorescent β-AR antagonists conjugated to BODIPY 630/650, which have a high affinity for β_2AR and moderate affinities for β_1AR [323]. Fluorescent propranolol derivatives were found to be an antagonist of β_2AR with nanomolar affinity and was used to selectively label adrenergic receptors in CHO cells, which was confirmed by blocking binding with preincubation of molar excess of ICI 118,551, a β_2-selective ligand [323]. Propranolol is a canonical β-adrenergic antagonist, one of the first discovered and most well-characterised. More recently, β-adrenergic receptors were studied *in vivo* by Alcobia et al. [371], with the use of an updated Propranolol-BODIPY 630/650, conjugated with a D-Ala-D-Ala linker. Here, fluorescent propranolol binding and stably transfected NanoLuc-tagged β_2AR were used to monitor GPCR-ligand binding after xenografting cancer tissue into a mouse [371].

Propranolol has been shown as an effective treatment for breast cancer metastasis *in vitro*, and researchers found that the brightness of NanoLuc luminescence enabled visualisation of BRET between intravenous furimazine (NanoLuc substrate) and fluorescent Propranolol-BODIPY 630/650 at sites of the stably transfected xenograft. This response was shown to be specific by intravenous injection of a high-affinity β_2-selective antagonist, which decreased the BRET signal at the xenograft [371].

ICI 118,551 has a higher affinity at β_2AR (K_d ~1nM), compared to β_1AR and β_3AR (K_d ~ 120nM and ~300nM respectively), an over 100-fold familial selectivity [372,373]. ICI 118,551 has been shown to display inverse agonist activity at β_2-adrenergic receptors *in vitro* [374] (**Figure 5.2**). In

the failing heart, ICI 118,551 has been shown to have direct negative inotropic effects [375], suggesting that it does not act as a neutral antagonist. Inverse agonism by ICI 118,551 explained by ICI 118,551 having a higher affinity for an alternative conformation of active receptors, which is more likely to bind inhibitory G proteins. ICI 118,551 has indeed been found to be pertussis-toxin sensitive, suggesting that it recruits Gαi to receptors [375,376].

A fluorescent ligand for ICI 118,551 was recently developed after identification of a suitable fluorophore attachment point in the crystal structure of human β_2AR bound to ICI 118,551 [377]. In this study, a panel of fluorescent ligands were developed with varying linkers and fluorophore conjugates, all showing specific binding to β_2AR with nanomolar efficacy. By generating saturable binding curves in HEK293 cells transfected with Nluc-tagged β-adrenergic receptors and labelled with fluorescent ICI 118,551, the compounds were highly selective at β_2AR ($K_d \sim 50$nM), with only compound 9a displaying specific binding to β_1AR, but with an order of magnitude less affinity ($K_d \sim 250$nM) [377].

5.1.4 Unsolved problems for β-adrenergic signalling in Cardiac Myocytes

A major question that remains with regards to β-adrenergic receptor signalling is how specificity is maintained in cases where biochemical pathways converge. It is commonly known that β_1AR and β_2AR are known to be expressed in cardiac myocytes. Though both of these receptors couple Gαs proteins and induce the accumulation of cAMP to stimulate contractility, chronic stimulation of both receptors leads to differing downstream effects on cardiac pathophysiology [150,170,184,200,215,355]. In particular, β_1AR is known to stimulate PKA and stimulate cardiac hypertrophy and myocyte apoptosis through gene transcription [79].

Spatial compartmentalisation of β_2AR, but not β_1AR, has been shown to be restricted in the T-tubules and caveolae of cardiac myocytes – with β_1AR expressed ubiquitously across the cell crest [317]. This compartmentalisation has revealed that cAMP generation by β_2AR occurs only in the T-tubules in healthy tissue [378]. This organisation is disrupted in heart failure, leading to the loss of local cAMP signals and a loss of signalling tone and efficiency. This loss of local cAMP at T-tubules, which remain close to muscle nodes where contractility is required, is reminiscent of synapses which have lost their ability to signal at active zones.

It is still unclear whether it is the localisation of adrenergic receptors, GRKs, adenylyl cyclases, cAMP or degradation that maintains such specific targeting of adrenergic signalling in cardiac myocytes. Although previous studies suggest that GPCR signalling is confined in a spatiotemporal fashion [379], direct observation of endogenous receptors compartmentalised in physiological relevant cells remains sparse. This has been a result of a lack of visualisation tools with sufficient brightness and resolving capability of seeing typically low-expressed endogenous receptors in difficult to image cells. Expression levels as low as <1 receptor per μm^2 mean that the signal to noise in resolving power against background can be very low [380,381]. Use of confocal and widefield microscopy is still very limited in capability for endogenous receptor imaging, but TIRF imaging has allowed some progress in viewing endogenously labelled receptors with fluorescent ligands – which often use very bright dyes with high quantum yields [382].

5.1.5 Aim of this study

Although β-adrenergic fluorescent ligands have found use in confocal microscopy, plate-based assays and *in vivo* imaging, their use in single-molecule microscopy has been limited. There is a

precedent for the use of fluorescent ligands to characterise stoichiometry, lateral diffusion and receptor localisation on the single-molecule scale [302]. This requires characterisation of unlabelled ligands prior to fluorescent ligand study in addition to comparison between direct and indirect labelled receptors

Figure 5.3).

In this study, the lateral diffusion of β-adrenergic receptors in response to a panel of β-adrenergic ligands was assessed, including antagonists, inverse agonists and agonists (**Figure 5.4**). In Chapters 3 and 4 of this thesis and concomitant with previous understandings, immobilisation of receptors on CCPs is synonymous with β-arrestin activity. After validation of unlabelled ligands with SNAP-tagged β-adrenergic receptors in CHO cells, fluorescent ligands were employed to image WT β-adrenergic receptors and were compared against SNAP-tagged receptor models. An imaging assay that utilised live adult, rat cardiac myocytes was then developed to perform single particle tracking on endogenous β-adrenergic receptors in these cells for the first time, comparing the lateral diffusion to that in immortal cell lines.

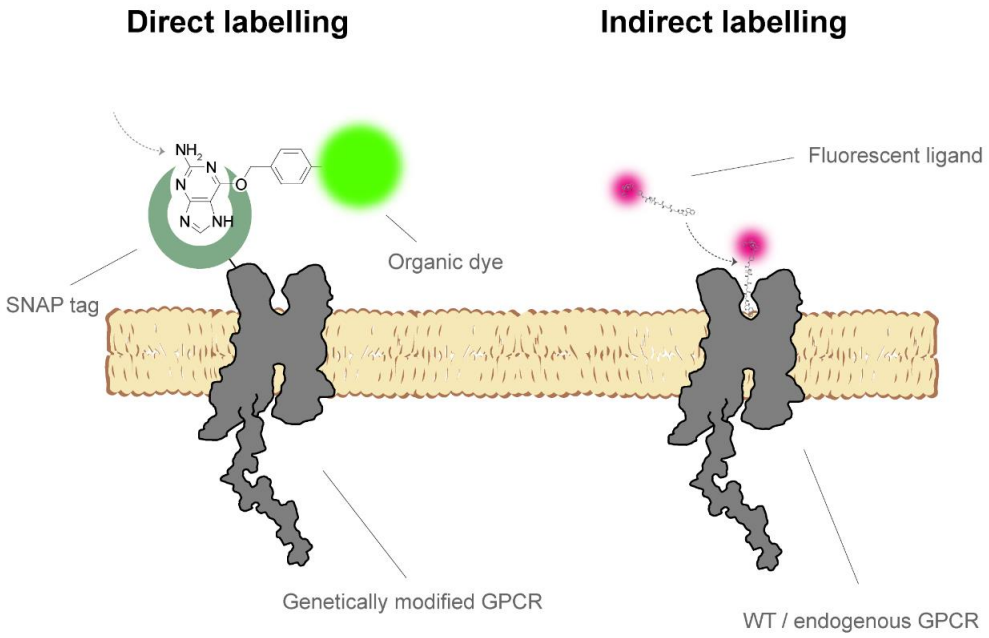

Figure 5.3 Direct and Indirect labelling of GPCRs for single-molecule imaging. GPCRs can be genetically modified, by covalent linkage of tags that bind organic dyes, as are used in Chapters 3 and 4 of this thesis. This precludes the visualisation of wild-type and endogenous GPCRs, so chemically modified ligands, which fluorescence, can instead be used to visualise these receptors.

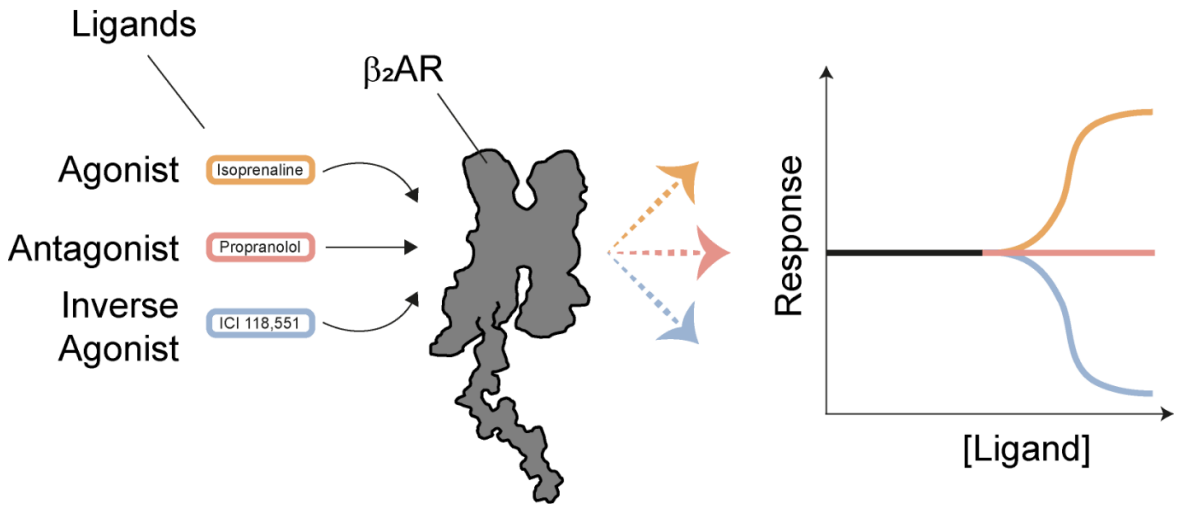

Figure 5.4 Simple schematic of ligand pharmacology. Actions of agonists, antagonists and inverse agonists on β-adrenergic receptor pharmacology. Simply put, agonists increase a particular response, neutral antagonists have no direct effect on pharmacology but compete for the active binding sites, and inverse agonists decrease a particular response.

5.2 RESULTS

5.2.1 Diffusion of SNAP-β_2AR in response to a β-adrenergic ligand panel

β_2AR was previously labelled with SNAP and imaged via single-molecule microscopy (see section 3.2.2), where it was found that the full agonist, isoprenaline, increased the molecular trapping of β_2AR at CCPs, by a β-arrestin-driven mechanism. The effects of an adrenergic ligand panel were tested on SNAP-tagged receptors, so the effects of fluorescent ligands could be compared when labelling WT receptors.

SNAP-β_2AR was transiently transfected at low physiological densities in CHO-K1 cells and was imaged by fast TIRF microscopy and analysed by single particle tracking in response to a range of ligands (**Figure 5.5**). Observed changes after Isoprenaline (agonist) stimulation includes immobilisation of receptors on the membrane, which can be interpreted in the TA-MSD graph as a decrease in the average diffusion speed. This is accompanied by a shift in the average anomalous diffusion exponent (α) from ~1, which indicates Brownian motion, towards sub-diffusion processes (α<0.75), which explore space less effectively (**Figure 5.5**).

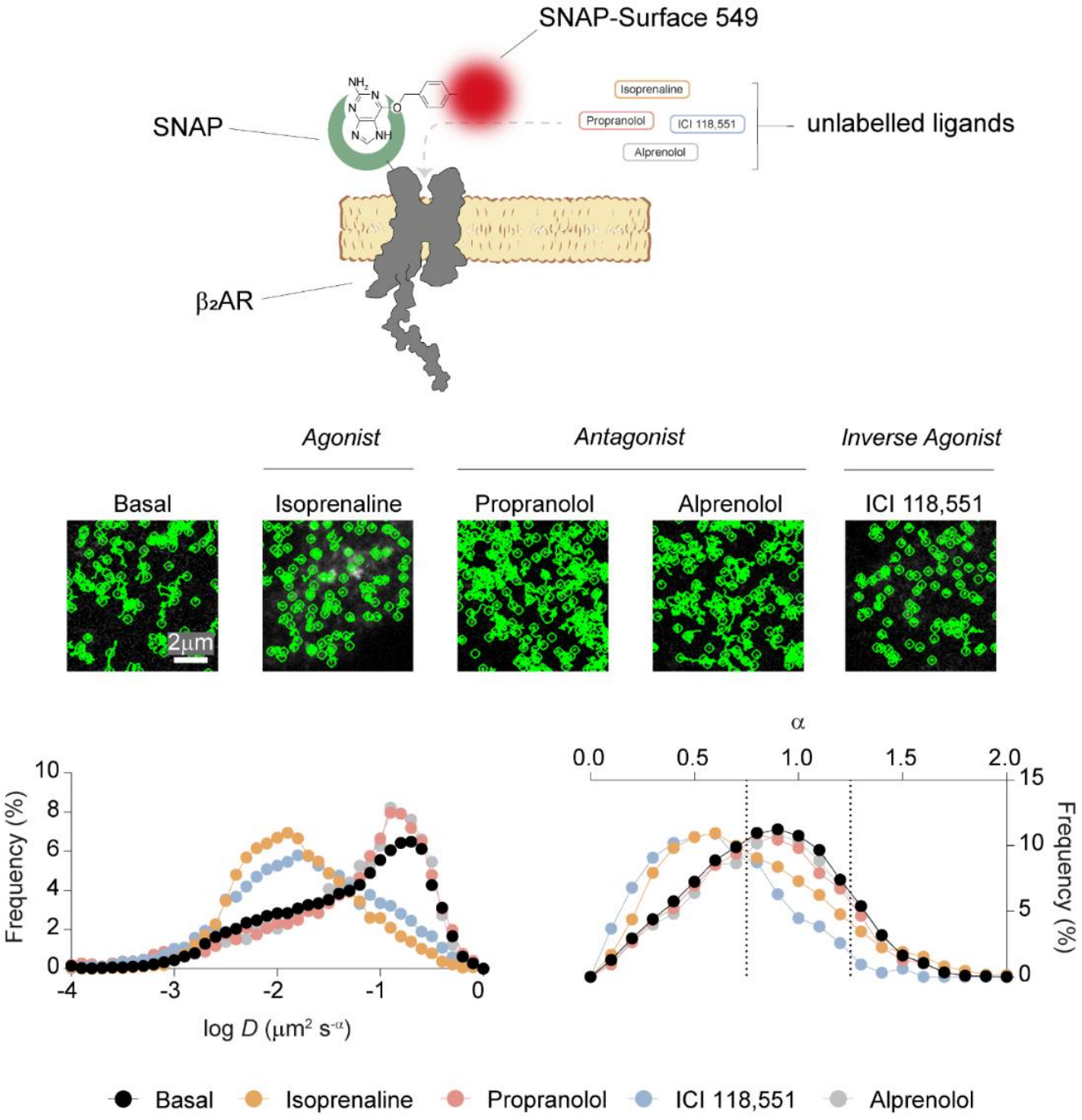

Figure 5.5 TIRF imaging of a β-adrenergic ligand panel (Top) Labelling strategy where SNAP-β_2AR was labelled with SNAP-Surface549 via a SNAP-tag fused to its N-terminus and interrogated with 10μM unlabelled ligands. (Middle) Selected frames from tracked single-molecule image sequences, with trajectories overlaid. (Bottom) diffusion coefficient (D) and anomalous diffusion exponent (α) values for β_2AR during basal and stimulation with a variety of ligands, including Isoprenaline (agonist), Propranolol and Alprenolol (antagonist) and ICI 118,551 (inverse agonist). n = 22, 19 and 21, 20 and 22 cells for Basal, Isoprenaline, Propranolol, ICI 118,551 and Alprenolol respectively. Images are representative of a minimum of 4 independent experiments.

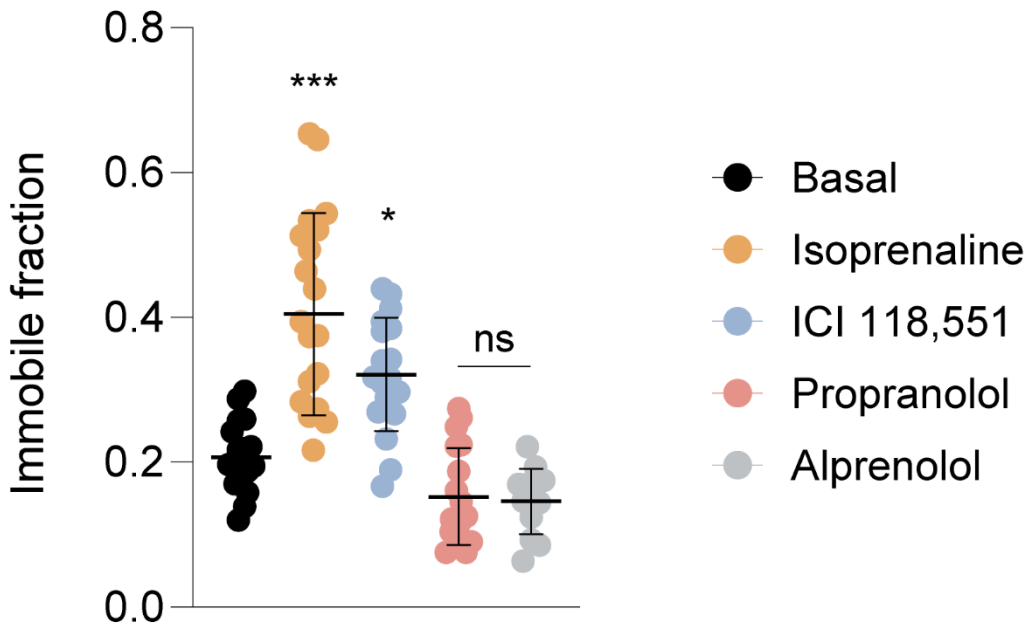

Figure 5.6 Immobility of β-adrenergic receptors with a diverse ligand panel. Fraction of immobile SNAP-β_2AR molecules per frame after interrogation with a diverse ligand panel. Movies were collected during 4-10 minutes after ligand addition. n = 22, 19 and 21, 20 and 22 cells for Basal, Isoprenaline, Propranolol, ICI 118,551 and Alprenolol respectively. Differences are statistically significant by Kruskal Wallis test. *P < 0.05, **P < 0.01, ***P < 0.001, ****P < 0.0001 versus basal by t-test with Bonferroni correction. ns, statistically not significant. Images are representative of a minimum of 4 independent experiments.

After interrogation with the well-known β_2AR antagonists: Propranolol and Alprenolol (**Figure 5.2**), receptors remained largely mobile on the plasma membrane (**Figure 5.5**). Receptors imaged after antagonist treatment trended towards being more diffusive than basal receptors, with less immobile molecules per frame (**Figure 5.6**). Combined with the knowledge that isoprenaline (full-agonist) leads to an increase in receptor immobility (**Figure 5.6**), this might suggest that antagonists stabilise receptors in inactive-like conformations, which are less likely to become immobilised and form signalling nanodomains. The inverse agonist, ICI 118,551, which is known to stabilise receptor conformations that reduce G protein signalling [377], led to an increase in immobility similar to stimulation with the full-agonist isoprenaline (**Figure 5.5**,

Figure 5.6). In Chapters 3 and 4, β-adrenergic receptor immobility was found to be as a result of β-arrestin signalling. Further multi-colour single-molecule study of ICI 118,551 could provide interesting insights, to see if ICI 118,551 indeed leads to an increase of β_2AR and β-arrestin interactions.

These data show the differential effects of ligands which bind β_2AR on receptor diffusion, highlighting the increase in immobility observed by agonists which was previously shown to be as a result of nanodomain organisation after receptor stimulation [253]. Further, these data show a distinct lack of change observed in receptor mobility on antagonist binding. This fits with the classical model of GPCR signalling, where antagonists bind the receptor without inducing any endemic effect on their activation. Lastly, these data suggest that an inverse agonist, which has reduced binding to G proteins, mediates similar diffusive effects on observed β_2ARs. This suggests that immobilisation of receptors is not fully dependent on G proteins.

5.2.2 Optimisation of β-adrenergic receptor labelling with fluorescent ligands in CHO cells

Results described above provide a framework whereby receptor diffusion is dependent on the bound ligand. Neutral antagonists were found to have no effect on the lateral diffusion of β-adrenergic receptors, whereas agonists and inverse agonists were found to cause an increase in immobility on the membrane. To characterise the effect of fluorescent analogues of these ligands on receptor diffusion, previously validated β-adrenergic fluorescent ligands were tested. This can inform us on endogenous receptor localisation, expression levels, ligand specificity and ligand-binding kinetics in physiologically relevant cells [265]. For single-molecule imaging, this provides the opportunity to label wild-type or endogenous receptors with

fluorescent ligand analogues which have innate fluorescence, specificity and also exert pharmacological effects.

Fluorescent ligands from the Cell Signalling laboratories in Nottingham were used to label wild-type β-adrenergic receptors in CHO cells. In particular, fluorescent analogues of both Propranolol and ICI 118,551 labelled with BODIPY 630/650 were used (Prop-BY630 & ICI-BY630 respectively). Here, the effects of unlabelled ligands on SNAP-tagged receptors could be compared with fluorescent ligands used to label WT-receptors. Both ICI 118,551-BODIPY 630/650 and ICI 118,551-BODIPY FL from Goulding et al. were tested for work in this thesis [377], however the latter (ICI 118,551-BODIPY FL) was found to exhibit significant spectral bleed-through and had a much lower brightness. As such, ICI 118,551-BODIPY 630/650 was used for further experiments.

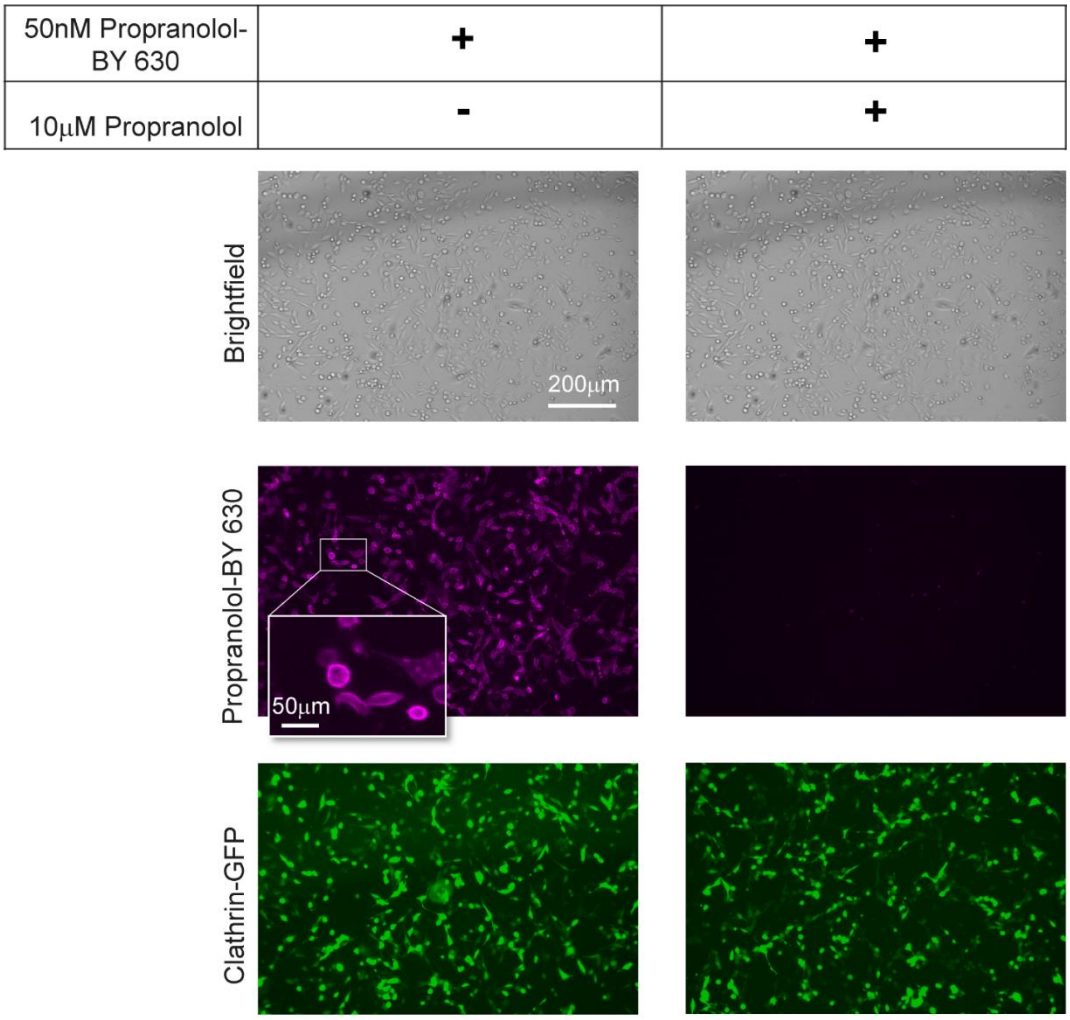

Figure 5.7. Specific binding of fluorescent Propranolol-BODIPY 630/650 to WT β2-adrenergic receptors. Example images from a blocking experiment, determining specific binding of a fluorescent GPCR ligand. 50nM Prop-BY630 was incubated with CHO cells (see top Brightfield panels) expressing WT-β_2AR for 5 minutes and imaged on an EVOS FL widefield imaging system. The fluorescent labelling of WT-β_2AR can be observed on the plasma membrane (inset picture) and is specific by co-incubation with a molar excess of non-fluorescent propranolol. Cells were co-transfected with Clathrin-GFP. Images are representative of 3 independent experiments.

Prop-BY630 has previously been validated for specific binding to β-adrenergic receptors through bioluminescence imaging and pharmacological assays and has a comparable K_d to non-fluorescent propranolol (binding affinity of ~50nM) [371]. Additionally, Prop-BY630 was found to have a residency time of around 40 minutes in the receptor binding cleft, making it ideal for

imaging applications [371]. This was confirmed by widefield imaging of WT-β_2AR transfected CHO cells with Prop-BY630 (**Figure 5.7**). Coincubation of a molar excess of non-fluorescent propranolol eliminated fluorescent signal, and plasma membrane expression of β_2AR could be observed in cells labelled with fluorescent ligand alone (**Figure 5.7**). ICI-BY630 was similarly tested and identical results were obtained (data not shown). To determine the concentration of fluorescent ligands that saturated receptor binding in cells, increasing concentrations of Prop-BY630 and ICI-BY630 were incubated in cells and cellular fluorescence was compared vs background fluorescence using epifluorescence imaging on the custom-built TIRF (**Figure 5.8**). Saturating concentrations of ~56nM and ~49nM were found for Prop-BY630 and ICI-BY630 respectively, which correlates well with concentrations used to saturate labelling in previous studies [371,377].

TIRF imaging revealed some issues with the use of fluorescent ligands for single molecule imaging using the current workflow (30min dye incubation using 50nM Prop-BY630, followed by 3 x 5-minute washes). It was found that increasing concentrations and time incubation of fluorescent ligand led to a high fluorescent background, as expected. Labelling for 5 minutes provided a much-reduced background, within the acceptable range for single-molecule imaging, and required no subsequent washes (**Figure 5.9**). Dyes were found to saturate receptor labelling at similar concentrations when labelling for 5 minutes. Interestingly, fluorescent ligands were not significantly detected below the TIRF field-of-view, which is a known property of BODIPY dyes that have an increased quantum yield when bound to proteins in a lipid environment [383].

Prop-BY630 and ICI-BY630 labelled WT β_2ARs were then optimised for their ability to label WT β-adrenergic receptors in live CHO cells. A labelling density that saturated receptor labelling

was determined, which could be used to label without an increase of fluorescent background. TIRF image sequences were obtained of cells labelled with Prop-BY630 and ICI-BY630 and the same cells were subsequently incubated with a molar excess of unlabelled propranolol (**Figure 5.9**). It was found that fluorescent ligands displaced gradually over a period of 30 minutes, with non-fluorescent propranolol slowly replacing the bound-fluorescent ligand, both confirming their long residency time and confirming specificity on the single-molecule level. Lastly, ICI-BY630 was found to be specific for the labelling of b2AR, as expected (**Figure 5.10)**

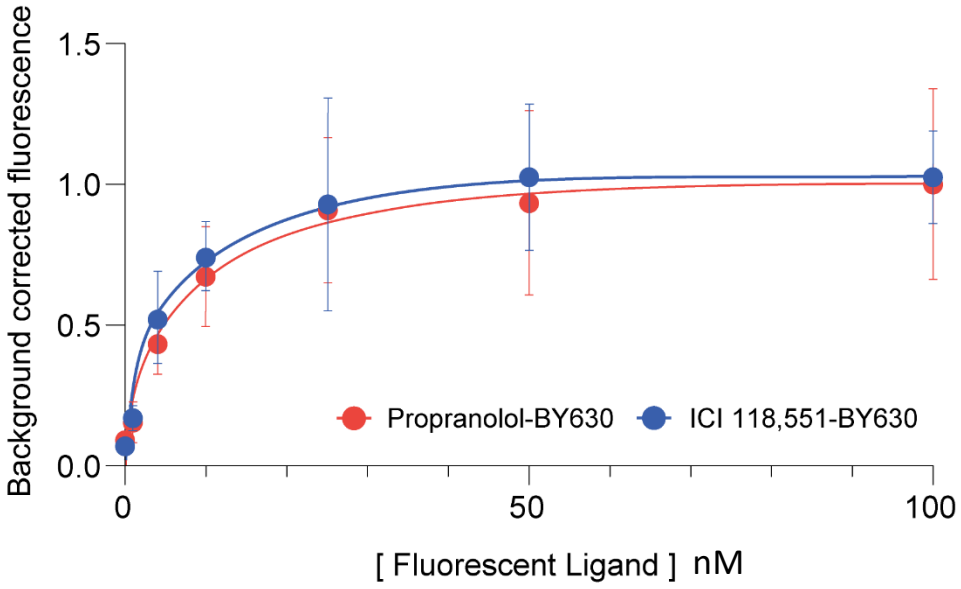

Figure 5.8 Fluorescent ligand binding to β-adrenergic receptors. Saturation labelling of transfected WT β_2-adrenergic receptors in CHO cells with Propranolol-BY630 (red) & ICI 118,551-BY630 (blue). Receptors were labelled for 5 minutes prior to imaging. Data are shown as mean ± SD of 25 and 28 cell replicates for Prop-BY630 and ICI-BY630, respectively. n=3 independent experiments

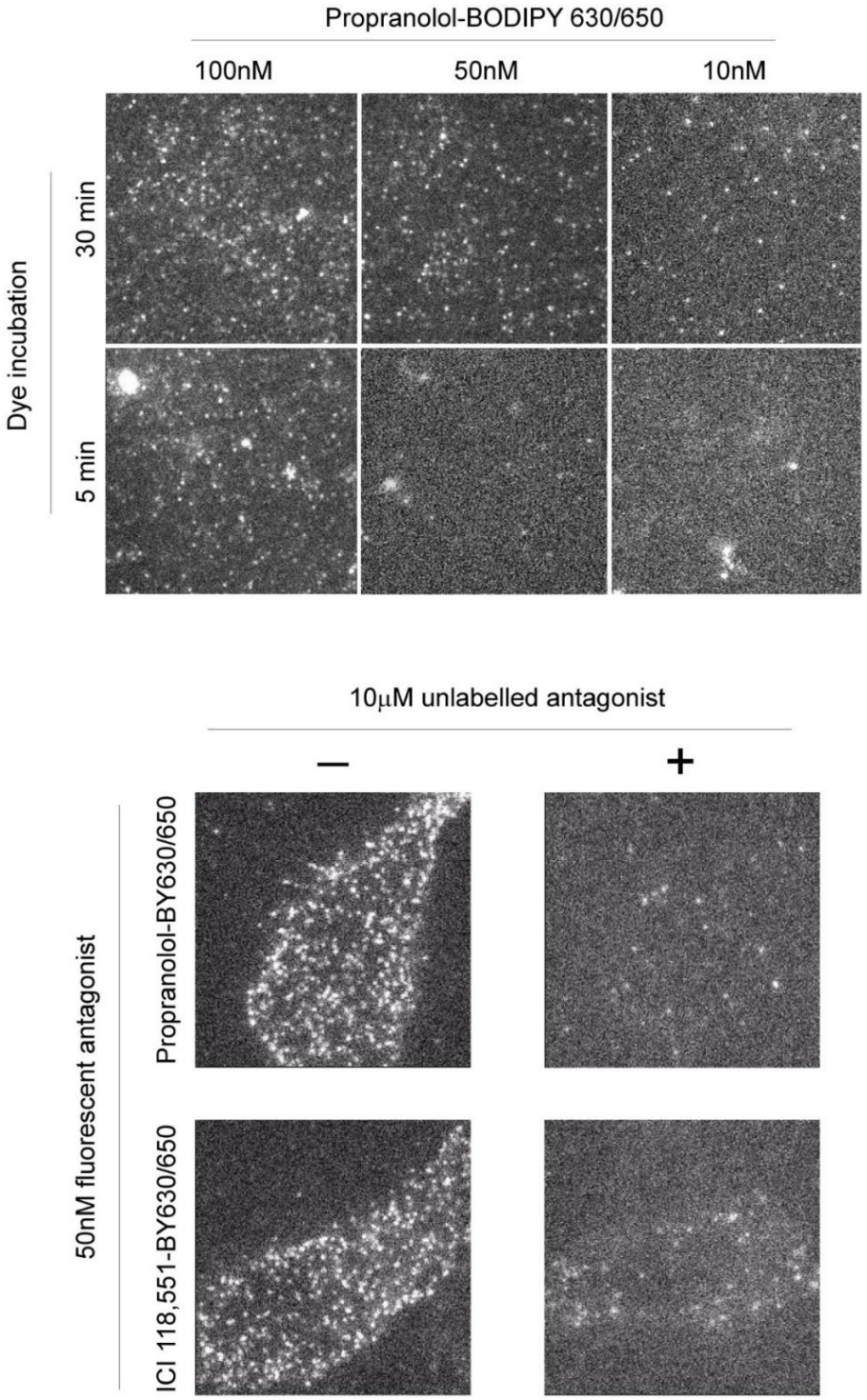

Figure 5.9 TIRF imaging of fluorescent ligands. (Top) Comparison of dye incubation and concentration on the fluorescent background of glass coverslips. 50nM dye and 5-minute labelling were chosen for ongoing experiments. (Bottom) Specific binding of Prop-BY630 and ICI-BY630 to transfected WT β_2-adrenergic receptors in CHO cells. Coincubation of 10μM non fluorescent Propranolol reduced specific binding for both ligands. n=3 independent experiments

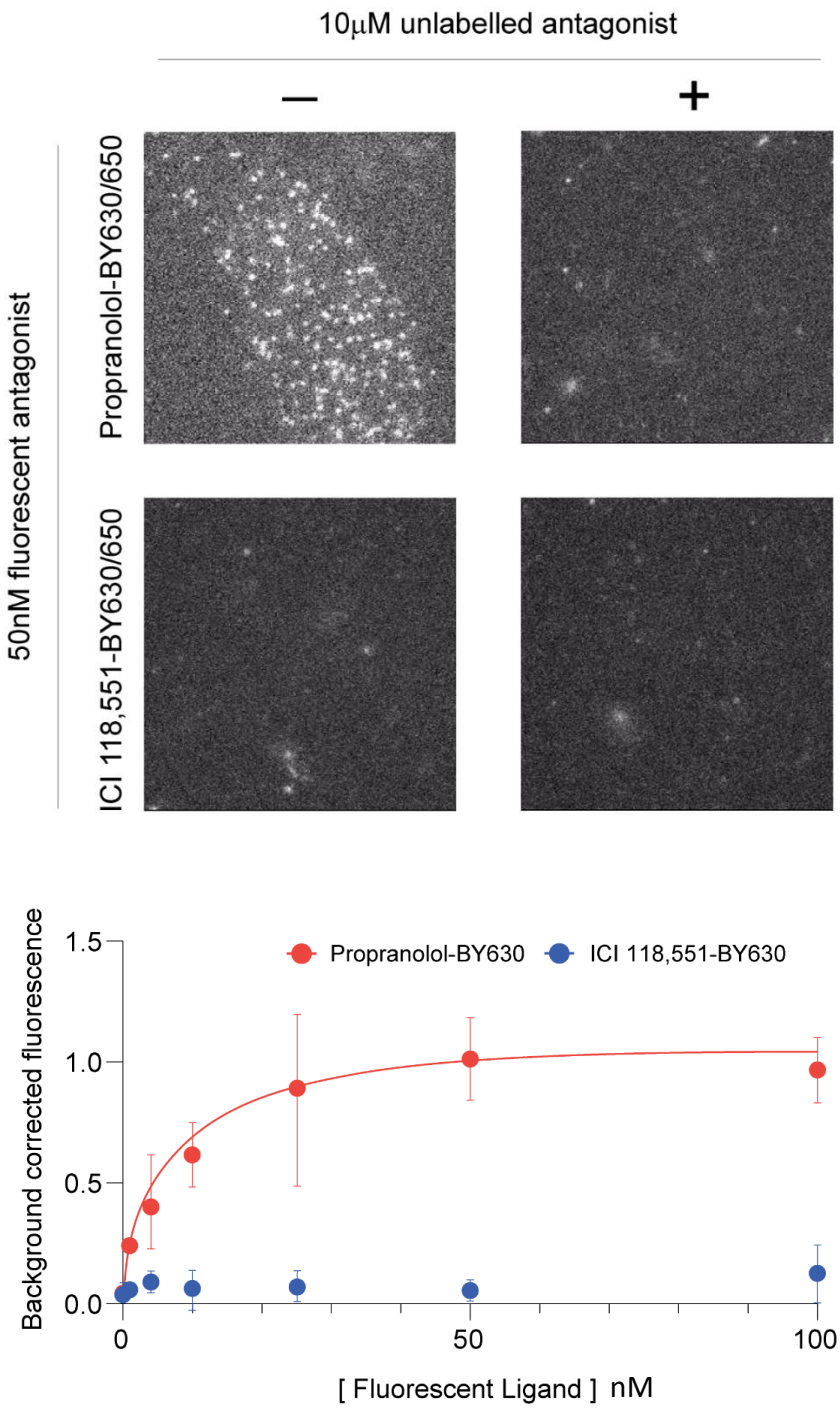

Figure 5.10 Confirmation that ICI 118,551-BY630 is β_2AR-specific. (Top) TIRF imaging WT-β_1AR with Prop-BY630 & ICI-BY630 in CHO cells transfected with WT-β_1AR, with specific binding observed for Prop-BY630 but not ICI-BY630 – demonstrating the latter ligands' specificity for β_2AR (see Figure 5.9). Specificity was determined in the presence of a molar excess (10μM) unlabelled Propranolol. (Bottom) Saturation labelling of transfected WT β_1AR with Propranolol-BY630 (red) & ICI 118,551-BY630 (blue). Receptors were labelled for 5 minutes prior to imaging. Data are shown as mean ± SD of 19 and 20 cell replicates for Prop-BY630 and ICI-BY630, respectively. n=3 independent experiments.

5.2.3 Single-molecule imaging of WT β_2-adrenergic receptors in CHO cells

After optimising labelling conditions, single-molecule imaging of WT β-adrenergic receptors was conducted in CHO cells, targeting receptors with fluorescent ligands as labels. Fluorescent ligands were found to exhibit much better photophysical properties compared to SNAP-tag ligands that were previously used to label SNAP-tagged receptors. Indeed, receptors could be imaged with negligible changes in overall fluorescence over the imaging window (~33 seconds).

Prop-BY630 labelled WT β_2AR were highly diffusive when bound to the ligand (87.7 ± 4.2% mobile) (**Figure 5.11**). This is identical to results obtained for SNAP-tagged receptors that were imaged with native Propranolol. Previously, ligands which activate β-arrestin pathways were found to increase β-adrenergic receptor immobility (**Figure 5.5**), with neutral antagonists having little effect on diffusion. Given that Prop-BY630 was found to immobilise receptors similarly to native Propranolol it likely acts also as a neutral antagonist. This is expected, and in line with previous pharmacological findings for Prop-BY630 [323]. ICI-BY630 labelled WT β_2AR had a lower fraction of diffusing molecules (70.2 ± 3.1% mobile) (**Figure 5.11**). These results obtained for fluorescent ligand labelling of WT β_2AR are also like those results obtained for non-fluorescent ICI-118,551 labelling of SNAP-β_2AR (**Figure 5.12**).

This confirms the use of fluorescent ligands as a proxy for direct receptor labelling, which adds the capability to label endogenous receptors. It was also confirmed that ICI-BY630 can be used to specifically target β_2AR, whereas Prop-BY630 would label both β_1AR and β_2AR in endogenous receptor populations. Lastly, these results show that fluorescent ligands induce similar changes in diffusion of receptors to their non-fluorescent counterparts.

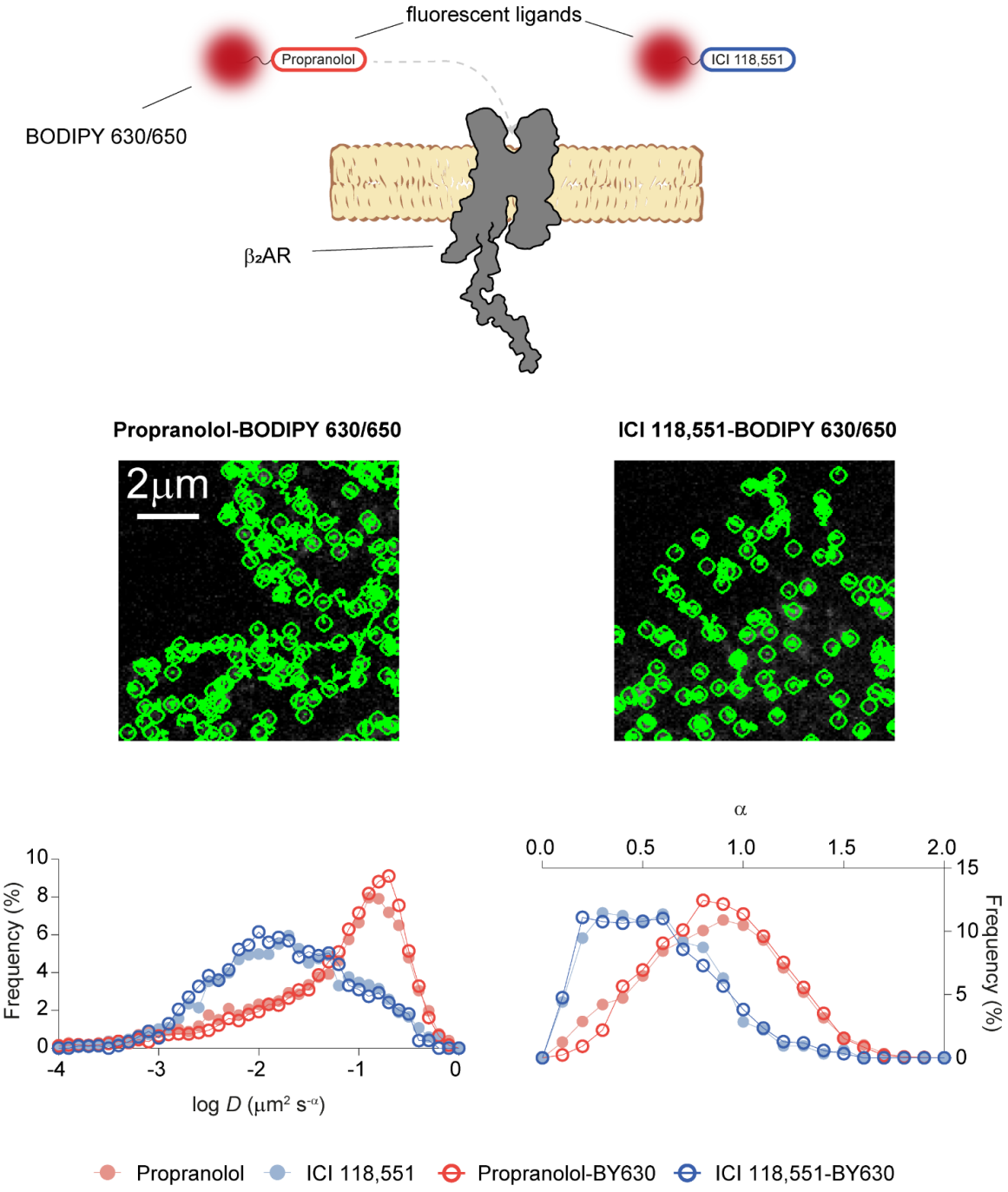

Figure 5.11 Single-molecule imaging of WT β2AR. (Top) Labelling strategy where transfected WT β2AR was labelled with 50nM Prop-BY630 or ICI-BY630 for study of their diffusion. (Middle) Selected frames from a tracked single-molecule image sequence, with trajectories overlaid. (Bottom) diffusion coefficient (D) and anomalous diffusion exponent (α) values for β2AR labelled with fluorescent ligands. Propranolol and ICI 118,551 (coloured circles) are data of SNAP-tagged receptors from Figure 5.5 for comparison. n = 19, 21, 23 and 22 cells for Propranolol, ICI 118,551, Propranolol-BY630 and ICI 118,551-BY630, respectively. Images are representative of a minimum of 4 independent experiments.

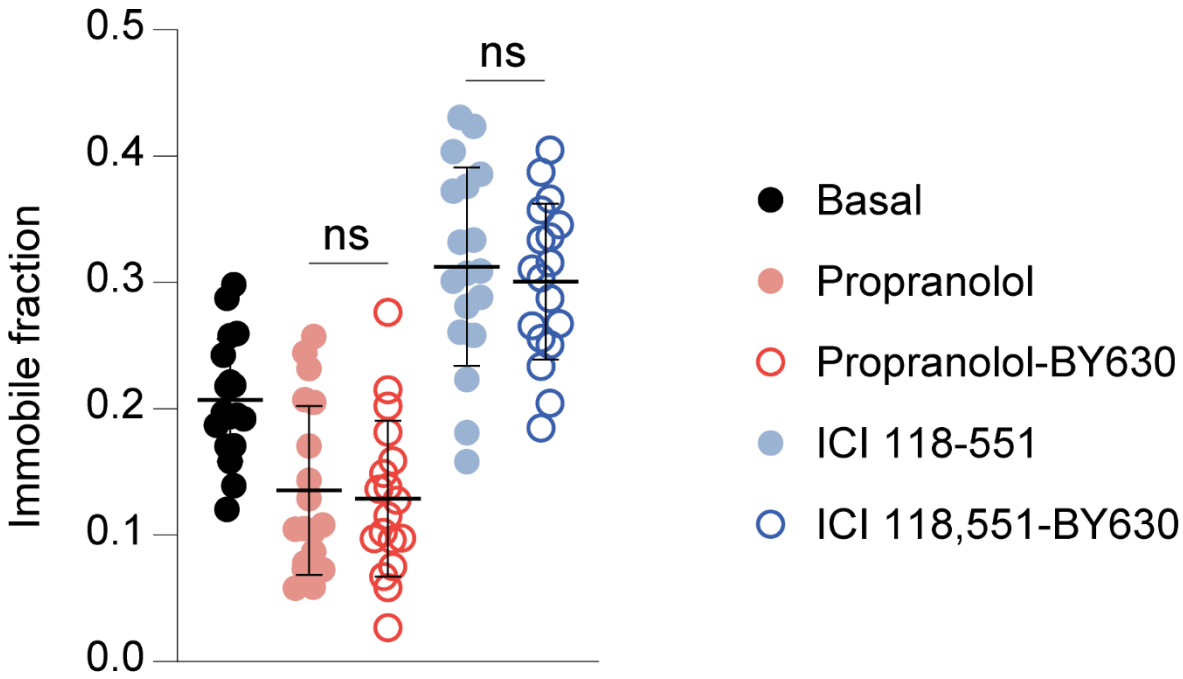

Figure 5.12 Comparison of β2AR immobility for unlabelled and fluorescent ligands. Fraction of immobile β2AR molecules per frame after interrogation with ligands. Movies were collected during 4-10 minutes after ligand addition. Propranolol and ICI 118,551 (coloured circles) are data of SNAP-tagged receptors from Figure 5.5 for comparison. n = 19, 21, 23 and 22 cells for Propranolol, ICI 118,551, Propranolol-BY630 and ICI 118,551-BY630, respectively. Images are representative of a minimum of 4 independent experiments. Differences are statistically significant by Kruskal Wallis test. *P < 0.05, **P < 0.01, ***P < 0.001, ****P < 0.0001 versus basal by t-test with Bonferroni correction. ns, statistically not significant. Images are representative of a minimum of 4 independent experiments.

5.2.4 Isolation of Adult Mouse Cardiac Myocytes for single-molecule imaging of endogenous β-adrenergic receptors

After labelling transfected WT β-adrenergic receptors with fluorescent ligands in CHO cells, imaging of endogenous receptors in physiologically relevant cells was sought out. This provides the opportunity to study the diffusion of endogenous receptors in complex cell membranes, where they exert their biological actions. In cardiac myocytes, it remains unclear on how the localisation of β-adrenergic receptor signalling results in chronic heart failure. Our

understanding of adrenergic heart failure has increased in recent years, due to advances in the ability to isolate viable cardiac myocytes and imaging methodologies [329]. The finding that β_2AR loses nanodomain organisation on the t-tubules of cardiac myocytes in heart failure, which leads to a loss of tone in cAMP and lack of action potential generation [150], has been particularly important. Additionally, the localisation of signalling molecules such as PDEs, arrestins and enzymes has been shown as altered in heart failure, though we still understand very little about where these effectors interact, for how long and how changes in their signalling leads to the development of the pathophysiology for heart failure. Single particle tracking in cardiac myocytes provides the opportunity to visualise receptors and signalling molecules diffusing and interacting in real-time, visualising changes in localisation and interactions in both healthy and diseased tissue.

The study of adult cardiac myocytes, which have a fully developed morphology (characterised by their size and presence of T-tubules), has been constrained by the complexity of these cells. Isolation of cardiac myocytes traditionally requires retrograde aortic perfusion using a specialised Langendorff apparatus, which is technically challenging, requires extensive training and requires surgery on live mice. Ackers-Johnson et al. recently developed a methodology which allows robust isolation of adult mouse cardiac myocytes using minimal laboratory equipment and requiring posthumous isolation and enzymatic digestion of the myocardium [329]. As part of a collaboration with the group of Davor Pavlovic at the University of Birmingham, isolated adult mouse cardiac myocytes were used for single molecule imaging experiments (**Figure 5.13**).

A Langendorff-based perfusion system is replaced with a simple needle and forceps clamp. After excision of the heart from the cadaver, a routine of dissociation buffers are slowly injected

into the left ventricle and clamping of the aorta allows deep perfusion of the myocardium through the coronary tract. Hearts are submerged into EDTA buffer to also inhibit contraction and coagulation, whilst also dissociating the ECM from the cardiac myocytes. After gentle disruption of the digested tissue, a stop buffer was added, and cells are passed through a strainer and multiple rounds of gravity-settling into myocyte and non-myocyte fractions (**Figure 5.13**). This method should yield an average of ~1 million myocytes per left ventricle with >80% viability – which is similar to Langendorff-based procedures. The cardiac myocytes are viable when rod-shaped and are considered calcium-tolerant when they are not contracting. Only non-beating myocytes were captured for single-molecule imaging purposes. First, beating cells indicates a lack of calcium tolerance in the buffer, which exerts cellular stress and leads to apoptosis. Indeed, cells which were found to beat could be observed dying over a period of minutes. Secondly, and perhaps more obviously, beating cells move – which makes studying entire trajectories over an imaging window highly unlikely.

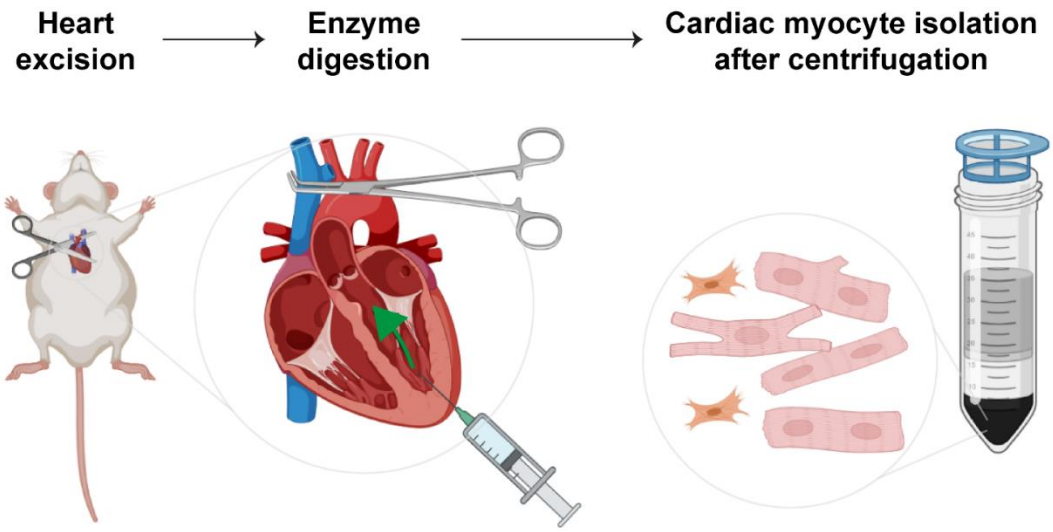

Figure 5.13 Schematic of Cardiac Myocyte isolation. Isolation of cardiac myocytes, via a Langendorff-free system. This system has many advantages as it requires only simple equipment and no advanced training. After excision of the heart, enzymatic buffers are perfused to digest the tissue, before a gravimetric settling, where the myocytes are collected from the pellet.

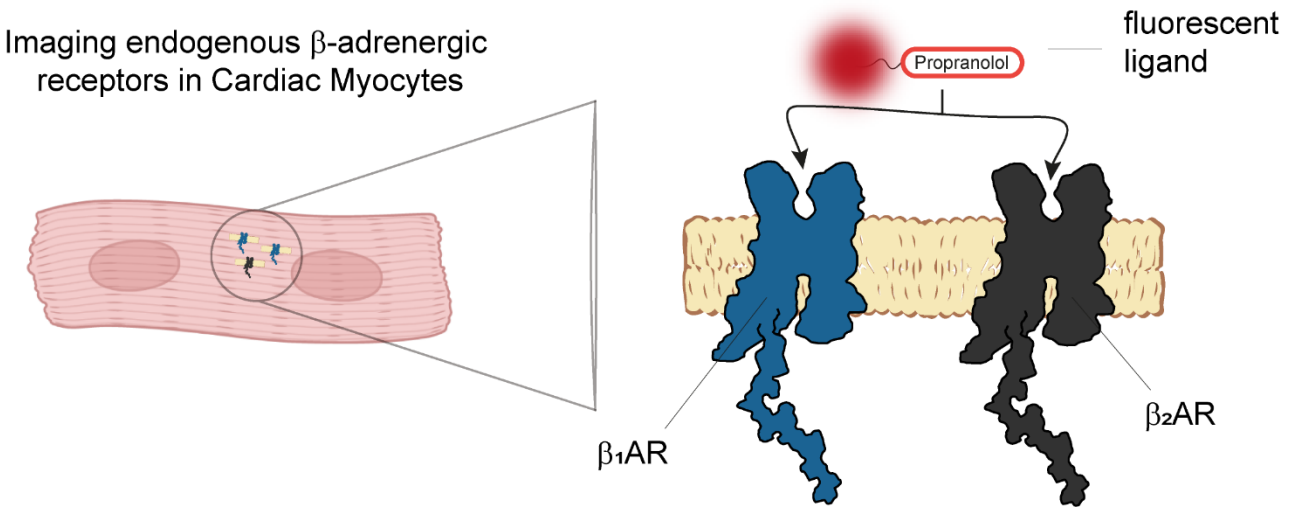

Figure 5.14 Labelling of β-adrenergic receptors in cardiac myocytes. Use of Prop-BY630 to non-selectively label both β_1AR and β_2AR endogenously in cardiac myocytes.

Initial experimental issues arose in the procurement of mice due to the COVID-19 pandemic, which significantly restricted access to the animal house. It was found that cardiac myocytes could be isolated, but their continued culture was not possible due to significant decreases in viability. Through this, only limited experimental data on the diffusion of β-adrenergic receptors was garnered, as myocytes needed to be imaged on the day of isolation. Additionally, cardiac myocytes were found to have low adherence to glass coverslips coated that were coated with Poly-D-Lysine, even after incubation with myocytes at 37°C for 1 hour. Incubations of glass coverslips with 10mg/ml laminin supplemented were found to significantly increase myocyte adherence and was thus used to adhere cells prior to imaging experiments.

5.2.5 Single-molecule imaging of endogenous β-adrenergic receptors in adult mouse cardiac myocytes

After cardiac myocyte isolation, cells were first treated with saturating concentrations of fluorescent propranolol (50nM Prop-BY630). Given that Prop-BY630 is a non-specific β-adrenergic antagonist with similar affinities for both β_1AR and β_2AR, receptor populations observed in cardiac myocytes cannot be distinguished. This provides an opportunity to see a global representation of β-adrenergic receptor diffusion in these cells (**Figure 5.14**), but without the use of receptor-specific ligands, conclusions between receptors are confounded. Viable cardiac myocytes display heterogeneous morphologies, as can be observed in the brightfield image of **Figure 5.15**, though they can easily be distinguished from dead and non-myocyte cells due to their large size, rod-shaped appearance, and visibility of tubular structures. Cells were labelled with Prop-BY630, indicating the expected presence of β-adrenergic receptors in adult mouse cardiac myocytes (**Figure 5.15**). Prop-BY630 was found to specifically label β-adrenergic receptors in cardiac myocytes, given that incubation of cells with a molar excess of non-fluorescent propranolol resulted in a loss of fluorescence (**Figure 5.15**), like results obtained in CHO cells. Fluorescence from Prop-BY630 labelling was lower in cardiac myocytes than transfected CHO cells, suggesting a lower receptor expression, as expected.

Single-molecule imaging of adult mouse cardiac myocytes, labelled with saturating concentrations of Prop-BY630, required extensive optimisation. These cells are often >100μm in length and can be tens of micrometres in depth, with a cell membrane that forms ribbons and a topologically inhomogeneous surface for imaging. In particular, TIRF visualises the plasma membrane adjacent to the coverslip so cardiac myocytes present a suboptimal imaging

medium. To combat this, coverslips were coated with laminin, which increases cellular adherence – increasing the likelihood of finding suitable cells for imaging.

Additionally, the perfect focus system (PFS), which auto-calibrates an optimal z position on the TIRF microscope, was disabled. This stopped the microscope adjusting mid-acquisition to different imaging planes, given that receptors were present at multiple z altitudes and diffused in the z-plane. Lastly, the imaging plane was adjusted to form highly inclined and laminated optical sheet (HILO imaging) (**Figure 5.16**). This increases image intensity at the cost of SNR, whilst still maintaining a reduced background noise when compared to epifluorescence. By inclining the light beam into a thin optical sheet, the evanescent TIRF wave more deeply penetrates the sample, which increases the brightness of spots and enables visualisation of receptor diffusion on a thicker z axis.

Brightfield

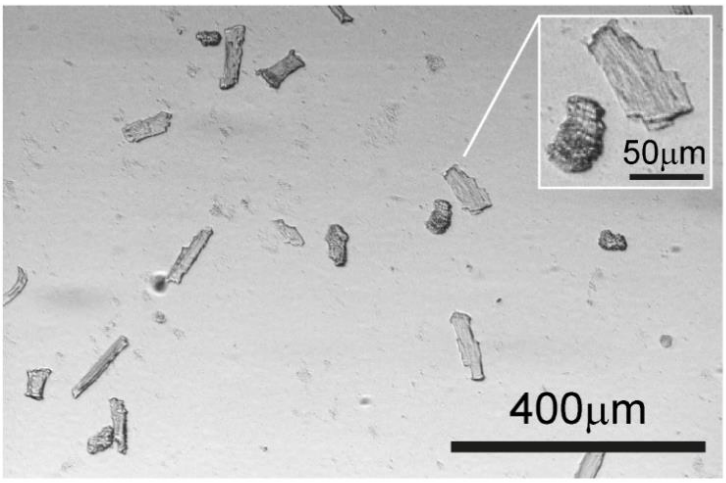

+ 50nM Propranolol BY630

+ 50nM Propranolol BY630
+ 10mM Propranolol

Figure 5.15 Widefield imaging of Prop-BY630 labelled adult mouse cardiac myocytes. Example images from a blocking experiment, determining binding of 50nM Prop-BY630 was incubated in adult mouse cardiac myocytes for 5 minutes and imaged on an EVOS FL widefield imaging system. (Top) Brightfield image of cardiac myocytes, with inset showing a dead and alive cardiac myocyte – which can be differentiated by circularisation, apoptotic granules, and lack of rod-shaped appearance in the dead cell. The fluorescent labelling of endogenous β-adrenergic receptors can be observed on the plasma membrane and is specific by co-incubation with a molar excess of non-fluorescent propranolol. Images are representative of 3 independent experiments.

After optimisation, β-adrenergic receptors were imaged as diffraction-limited spots, diffusing on the plasma membrane of adult mouse cardiac myocytes. Prop-BY630 was found to extensively label receptors across the membrane of myocytes, with the striated myofibrils clearly seen. β-adrenergic receptors on the basolateral membrane of cardiac myocytes were successfully tracked, using our single particle tracking methodologies (**Figure 5.17**). Like results obtained in CHO cells, receptors were found to diffuse on the plasma membrane of cardiac myocytes when labelled with Prop-BY630 – with both diffusive and immobile trajectories observed (**Figure 5.17**). These results show diffusion of endogenous β-adrenergic receptors in isolated mouse cardiac myocytes, which had been beating as a part of an adult myocardium less than an hour before imaging.

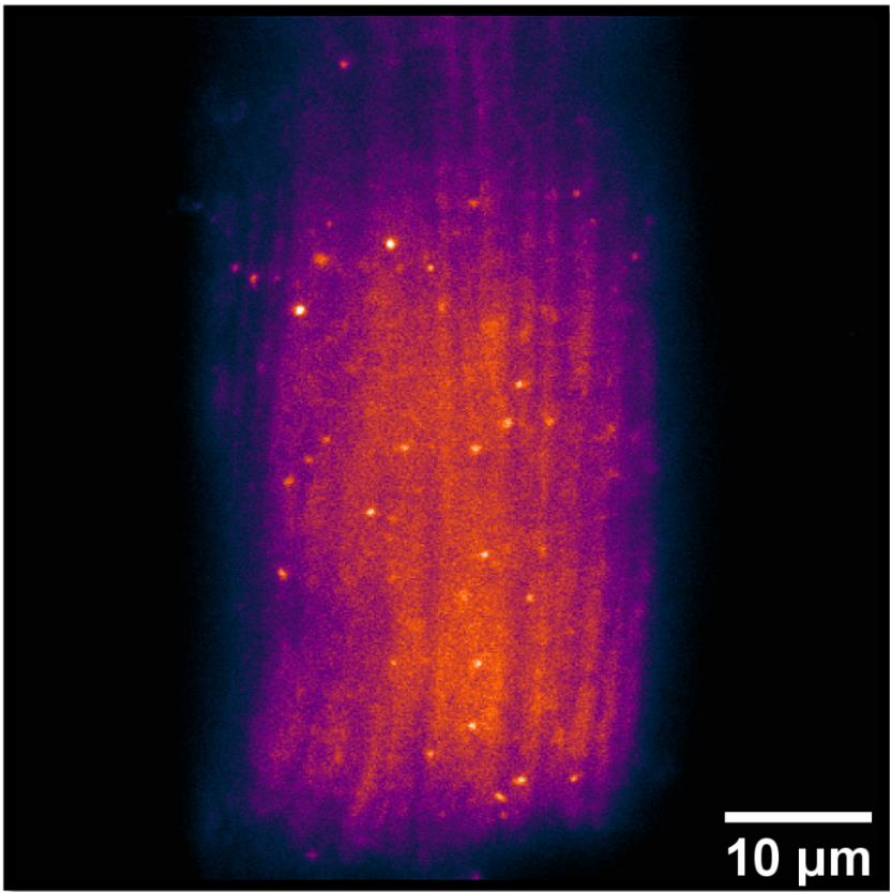

Figure 5.16 HILO imaging of individual endogenous β-adrenergic receptors. Representative frame from single-molecule HILO images where endogenous receptors were labelled with 50nM Prop-BY630. In HILO, a highly inclined and laminated optical sheet of light is used to penetrate a further field of view than TIRF imaging, used previously.

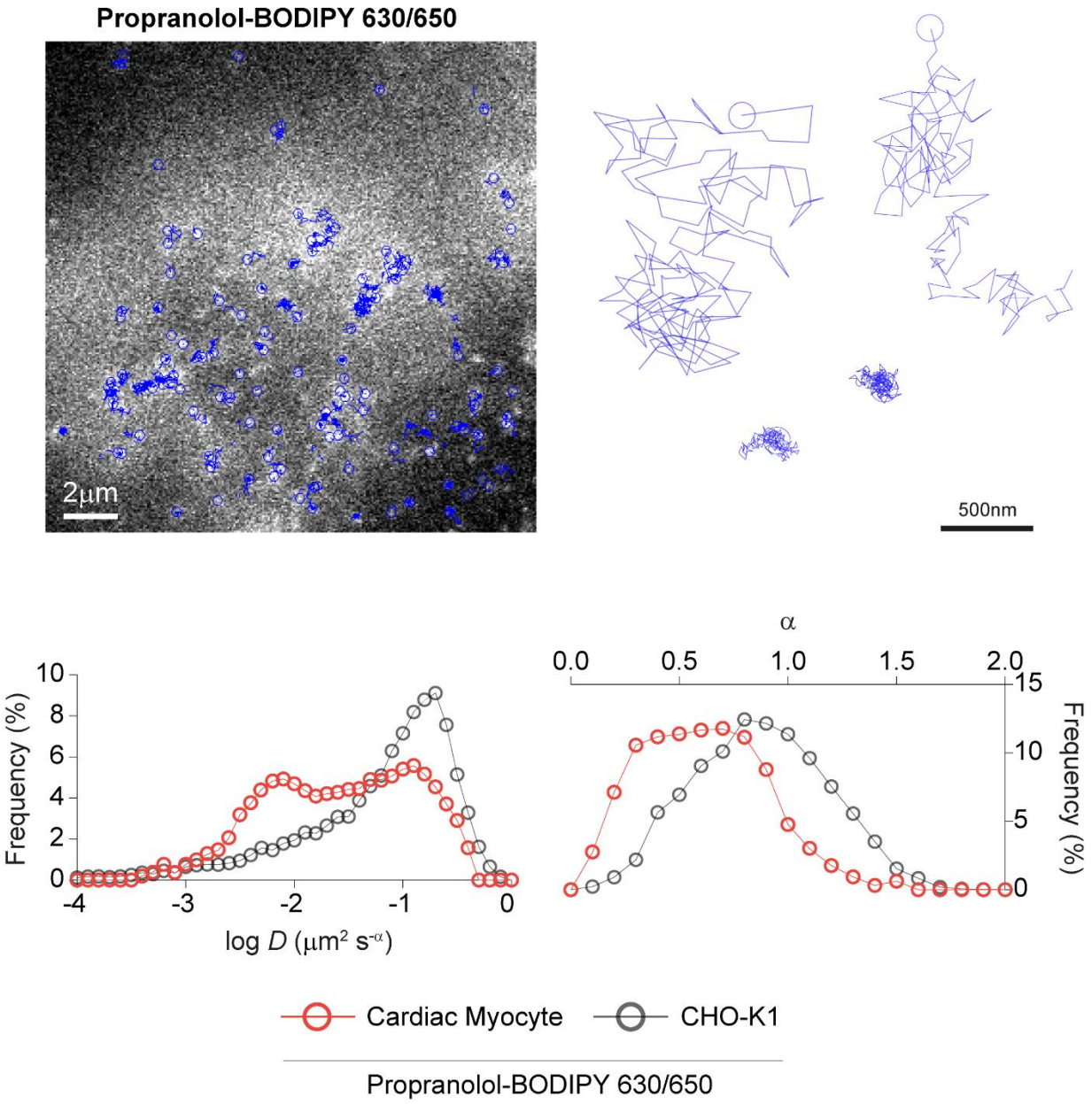

Figure 5.17 Single-molecule imaging of endogenous β-adrenergic receptors in mouse cardiac myocytes. (Top Left) Selected frame from a tracked single-molecule image sequence from experiments where isolated adult mouse cardiac myocytes were labelled with 50nM Prop-BY630, with trajectories overlaid. (Top Right) Representative trajectories from the movie, with endogenous receptors can be seen to be both highly diffusive and trapped on the membrane. (Bottom) Comparison of diffusion for Prop-BY630-labelled receptors in cardiac myocytes and previously accrued CHO cells. Diffusion coefficient (D) and anomalous diffusion exponent (α) values are shown. n = 19 and 23 cells for Prop-BY630 labelling in cardiac myocytes and CHO cells, respectively. Images are representative of 4 independent experiments.

Trajectory positions from cardiac myocytes were quantitatively analysed to study their diffusion over time to generate their time-averaged mean squared displacement (TA-MSD), as in Chapters 3 and 4. Interestingly, when comparing diffusion of receptors labelled with Prop-BY630 in cardiac myocytes vs CHO cells, cardiac myocyte labelled receptors were found to have a reduced diffusion coefficient and had shifted diffusion towards molecules exhibiting anomalous diffusion. Given that results were obtained with the same fluorescent ligand in both cardiac myocytes and CHO cells, it might suggest that cardiac myocytes have more specialised structures which impede receptor diffusion naturally. This is supported by the increase in sub-diffusive molecules (α<0.75) observed in cardiac myocytes, which indicates diffusion that is constrained in space (**Figure 5.17**).

The average diffusion coefficient of receptors diffusing in cardiac myocytes labelled with Prop-BY630 was 0.0132 $\mu m^2 s^{-1}$, similar to results obtained by Valentine & Haggie in cardiac H9c2 cells for β-adrenergic receptors [316]. In turn, average diffusion coefficients obtained in CHO cells for Prop-BY630 were found to be ten times larger on average (average D = 0.156 $\mu m^2 s^{-1}$), a difference between primary and immortal cells also noted previously [316]. Interestingly, diffusion coefficient curves exhibit a biphasic behaviour, which might indicate a diffusing and an immobile fraction of molecules, as can be observed in the trajectories of **Figure 5.17**. Prop-BY630 has no specificity between β-adrenergic receptors, so the observed diffusion is most likely a mixture of both β_1AR and β_2AR; which precludes the ability to comment on each receptors' diffusion separately. Combined with the difference observed between cardiac myocytes and CHO cells, this highlights the need for specific fluorescent ligands.

ICI-BY630 was previously shown to selectively label β_2AR [377] (**Figure 5.18**). Identical to experiments with Prop-By630, receptors were successfully labelled in cardiac myocytes with

ICI-BY630, where they were found to diffuse on the plasma membrane. Compared to Prop-BY630, where receptors were diffusive in CHO cells and had a somewhat decreased diffusion coefficient in cardiac myocytes; ICI-BY630 was found to have similar diffusive properties in both CHO and cardiac myocytes (**Figure 5.19**). Importantly, these results unexpectedly showed that Prop-BY630 and ICI-BY630 labelled receptors diffused similarly in cardiac myocytes when they were observed as different in CHO cells.

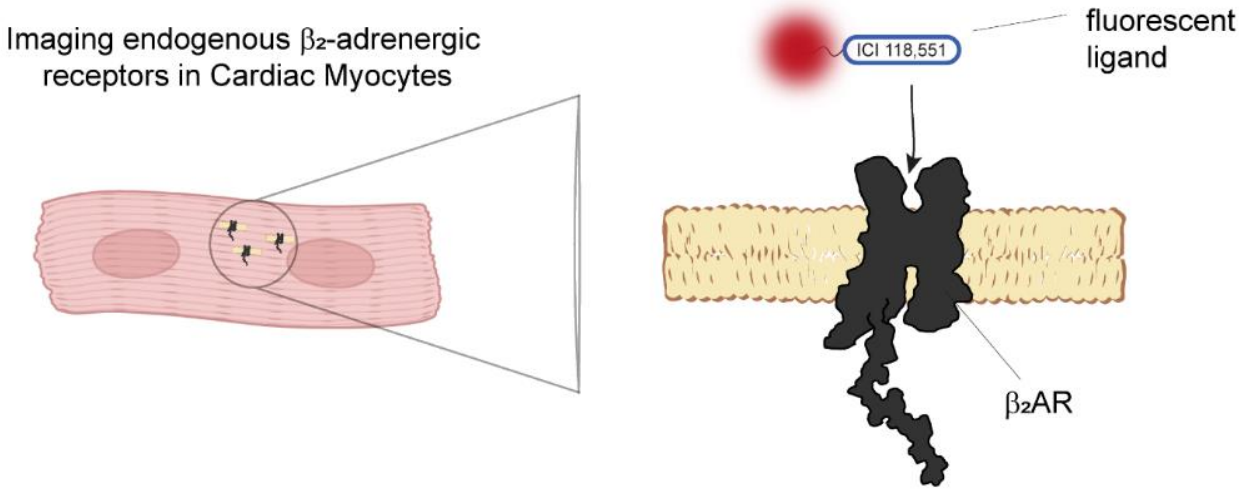

Figure 5.18. Labelling of β_2-adrenergic receptors in cardiac myocytes. Use of ICI-BY630 to selectively label β_2AR endogenously in cardiac myocytes.

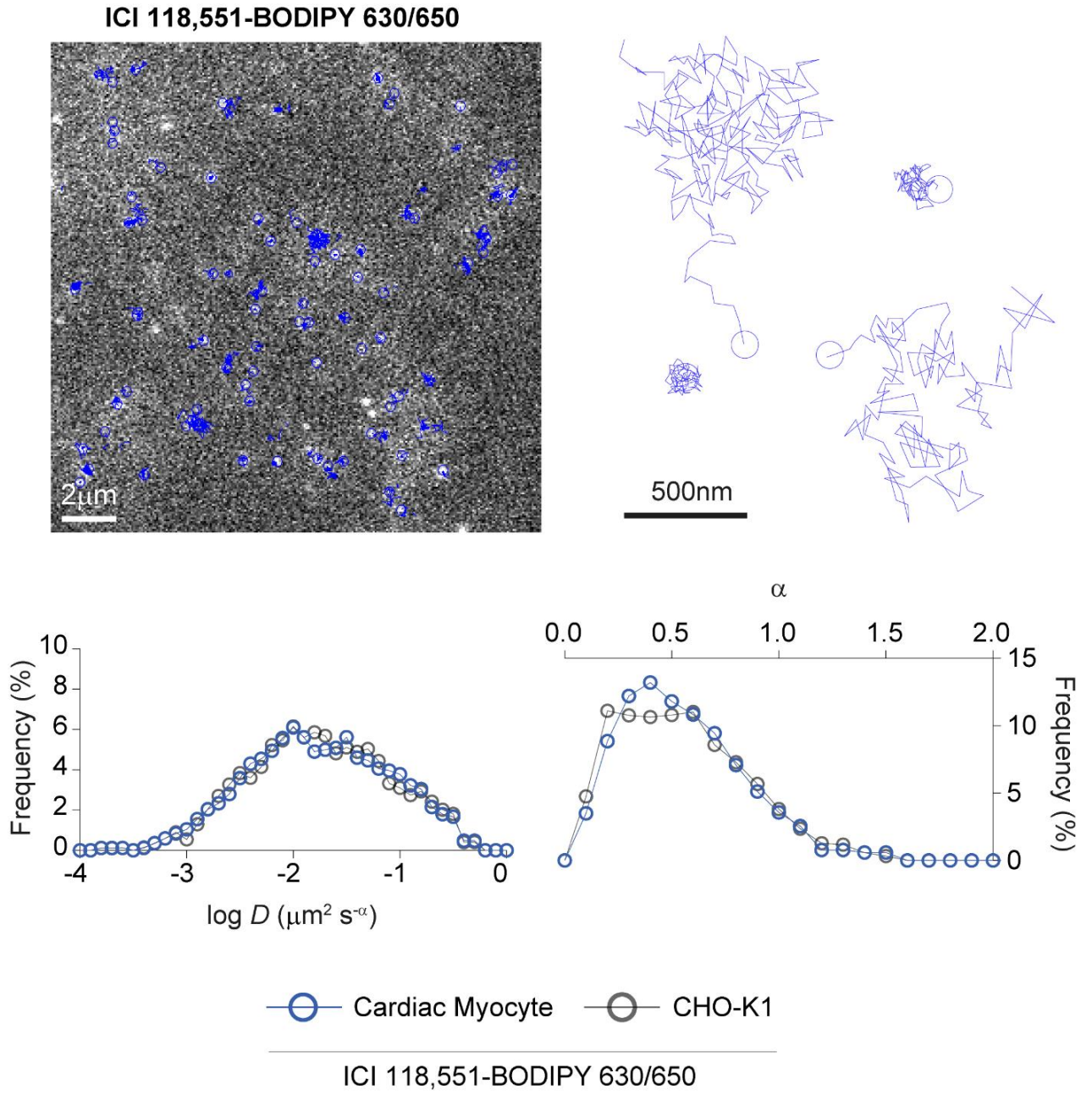

Figure 5.19 Single-molecule imaging of endogenous β_2-adrenergic receptors in mouse cardiac myocytes. (Top Left) Selected frame from a tracked single-molecule image sequence from experiments where isolated adult mouse cardiac myocytes were labelled with 50nM ICI-BY630, with trajectories overlaid. (Top Right) Representative trajectories from the movie, with endogenous receptors can be seen to be both highly diffusive and trapped on the membrane. (Bottom) Comparison of diffusion for ICI-BY630-labelled receptors in cardiac myocytes and previously accrued CHO cells. Diffusion coefficient (D) and anomalous diffusion exponent (α) values are shown. n = 20 and 22 cells for ICI-BY630 labelling in cardiac myocytes and CHO cells, respectively. Images are representative of 4 independent experiments.

5.3 CONCLUSIONS

The advancement of optical imaging technologies, labelling strategies and development of algorithms to track single molecules means that GPCRs in primary cells can now be studied with unprecedented spatiotemporal resolution. In this study, an assay was optimised to study the diffusion of endogenous β-adrenergic receptors in adult mouse cardiac myocytes. This was done with the intention of imaging endogenous GPCRs in physiologically relevant cells, which requires multiple obstacles to overcome – compared to studying SNAP-tagged receptors in immortal cell lines.

Previous studies have explored receptor localisation in myocytes with super-resolution, by viral transduction of genetically modified receptors into cells [170]. These studies have highlighted the importance of localised cAMP signals produced by β_2AR in the t-tubules of cardiac myocytes, in addition to broader cAMP signals generated by β_1AR across the myocyte membrane. Loss of these signals has been shown to lead to cardiac degeneration and chronic heart failure [150,215]. Other studies have studied receptor diffusion in cardiac myocyte-like cells, such as H9c2 – which act as a non-primary cell proxy without the specialised morphological features of cardiac myocytes [316]. In particular, these works have highlighted the importance of the actin cytoskeleton in confining receptor diffusion in nanodomains on the plasma membrane of these cells, finding that cAMP signalling was aberrant when receptor confinement via actin was disrupted with latrunculin treatment.

More recent studies have used FCS combined with confocal imaging to study the ensemble diffusion of β-ARs labelled with fluorescent ligands [317], as a means to study endogenous receptor diffusion. This study again finds that β_2AR is expressed in the t-tubular network, linked by cytoskeletal scaffolds which are crucial in maintaining signalling. Aforementioned studies

do not visualise individual receptors in real-time in primary cells, either favouring a cell line with SPT or cardiac myocytes with FCS. This is in part due to the complex imaging medium that cardiac myocytes present, which adds a difficulty in imaging sparse, endogenous receptors with sufficient brightness so that they may be tracked.

Here, fluorescent ligands were used first in CHO cells to confirm their use as a proxy to SNAP-tagged receptors – finding that receptor diffusion was identical regardless of the labelling strategy. Similar to previous studies with other GPCRs [253], it was found that ligand choice affected diffusion of receptors – with antagonists having no effect on receptor diffusion and agonists leading to an increase in immobility of receptors. Additionally, it was found that an inverse agonist, ICI 118,551, was found to increase receptor immobility, like agonists. For the first time, adrenergic receptors were directed imaged in cardiac myocytes from adult mice to image the endogenous β-adrenergic receptor populations, where it was found that regardless of the ligand employed – receptors exhibited a higher degree of immobility. Though this data is confounding for purposes of this study, it is interesting to consider that the spatial localisation of receptors in these specialised cells likely goes beyond simple pharmacology. This is in line with other findings from Chapters 3 and 4 and supports a complex microenvironment which would require further study to elucidate the mechanisms of.

These findings highlight the importance of different cellular models for understanding GPCR signalling. In CHO cells, we are able to see the different effects that ligands have on the individual diffusion of receptors, due to causing differing interactions with downstream signalling proteins and leading to organisation in signalling nanodomains. In cardiac myocytes, it seems likely that these specialised cells' receptors are already organised in highly efficient nanodomains through genetic regulation of the cytoskeleton and adaptor proteins, so the

effects of individual ligands on receptor diffusion are not seen. Instead, these cells form the physiologically relevant cellular model, which have the potential to become aberrant under disease conditions such as cardiac heart failure. It may be, that after further study, receptors can be found as unorganised and reliant on ligand-mediated changes on nanodomain organisation in cardiac myocytes, which is likely to be too ineffective to maintain physiological cardiac signalling.

6 DISCUSSION

6.1 OVERVIEW OF FINDINGS

In this thesis, single-molecule analysis was used to follow membrane binding and plasma membrane diffusion of β-adrenergic receptors and β-arrestin2 (βArr2), with Halo- and SNAP-tags, respectively. It was found that βArr2 binds the membrane independently of GPCR interactions and much like a membrane protein, and that membrane binding of βArr2 involves its C-edge and finger loop – the latter of which is typically thought to only mediate arrestin activation. These findings build on previous work by Lally et al. [123], who identified contacts of the β-arrestin C-edge with the plasma membrane, but not the finger loop. Further study by Eichel et al. [315] provided intriguing evidence for persistent arrestin activity on the plasma membrane, independent of GPCRs, but also raised many questions. Mainly, there is a lack of direct visualisation of GPCR-independent β-arrestin, diffusing alone on the plasma membrane. Additionally, these studies provided no evidence of changes in β-arrestin diffusivity, by use of mutants or otherwise, which meant that no further insights could be gleamed on what key interactions mediate arrestins lifetime on the membrane.

Although this study builds on these (and previous) papers, the mechanism proposed here is distinct and conceptually profoundly different in a multitude of ways. First, it is shown here that βArr2 spontaneously inserts into the plasma membrane under basal conditions, without needing to bind to a receptor for lateral diffusion. In contrast, Lally et al. only observed βArr1 membrane interactions in the context of the arrestin-receptor complex, proposing that the membrane helps stabilise the high affinity state of the complex [123]. Additionally, it is directly shown in this study, that the newly revealed basal lipid βArr2 binding is required for βArr2-receptor interactions, with these interactions occurring via lateral diffusion. This suggests that

βArr2 *de facto* behaves like a membrane protein, which is conceptually different from the widely accepted model. According to the classical model, arrestin does not interact with the plasma membrane under basal conditions and instead directly translocating from the cytoplasm to active receptors.

Although previous models are based on studying these events through various methods, this body of work is a direct observation of single β-arrestin molecules in living cells, tracking them during their entire lifetime on the membrane. This was not possible previously and this unique spatial and temporal resolution is the reason why we were able to determine that arrestin gets recruited to receptors via lateral diffusion and not necessarily from the cytoplasm.

Using βArr2 mutants, it was found that PIP2 interactions were dispensable for βArr2 association with the membrane, but were crucial in mediating specific binding to clathrin-coated pits (CCPs) and GPCRs. All mutations used in this project (except for the ΔELA) have been used and validated extensively (Clathrin-AP2: [101,102] PIP2: [103] FLR: [27,106,315]). It was not assumed that all βArr2 mutants would bind normally to receptors. Indeed, the main hypothesis was that binding to receptors and the plasma membrane would be cooperative. Therefore, it was expected that interfering with membrane binding would also affect receptor interactions. This is also consistent with work by the Kobilka group [124], that further supports the importance of PIP2 binding for the formation of receptor-βArr complexes.

As there are around 800 GPCRs, it would be unfeasible to test them all. However, three model GPCRs that encompass a range of interaction strengths with βArr2 have been included. In particular, the β_2AR was most heavily investigated, which is by far most widely used prototypical GPCR. Overall, the consensus in the literature is that for most receptors, the interaction with the C-tail is the prevailing interaction for βArr activation [27,246,344,346]. This data

is consistent with that consensus. The main finding here is that βArr2 pre-association is key for receptor-βArr interactions and that those are, at least for the three tested model GPCRs, much more transient than previously assumed.

Based on the finding that βArr2 was not recruited to the mutant β_2AR with a C-tail deletion, which impedes GRK-mediated phosphorylation, it was concluded that GPCR phosphorylation is necessary for βArr2 binding to the receptor on the plasma membrane. Experiments deleting the receptor ICL3 showed that this region was dispensable. Though this finding seems true for β_2AR, it doesn't mean it is generalisable for other GPCRs. However, though there might be differences in the contribution of C-tail vs core among receptors, there is a prevailing consensus in the literature that in most cases the C-tail mechanism is essential in GPCR phosphorylation. There are conflicting reports in the literature regarding the effects of β2-adrenergic receptor ICL3 deletion on the interaction of β-arrestins with the β_2-adrenergic receptor transmembrane core. β-Arrestin1 has been shown to productively interact with the transmembrane core of β_2-adrenergic receptor ΔICL3 when the receptor was artificially phosphorylated, suggesting that ICL3 might principally influence receptor phosphorylation by GRKs [120].

Although this data is consistent with that consensus, the aim was not to investigate the subtle balance between C-tail and receptor core. Further tests than the already tested three model GPCRs, of 1-2 additional key GPCRs from different sub-families, would strengthen these findings and offers the opportunity for further study of different sub-families. In conclusion, the proposed mechanism here involves canonical βArr2 activation by the receptor C-tail as well as βArr2-membrane interactions mediated by hydrophobic amino acids in the C-edge. Conversely, Eichel et al. propose a rather different mechanism, triggered by non-canonical β-arrestin activation by the receptor core and without participation of the C-edge [315].

Here, a previously unknown and exciting role of the arrestin finger loop was discovered, in providing a "memory" after βArr2 activation, which is distinct from its role in binding to the receptor core. Specifically, it was shown that after βArr2 activation by the receptor C-tail, the finger loop in active βArr2 (via a nanobody recognising active arrestin) interacts with the lipid bilayer to stabilise βArr2 in an active-like conformation that remains bound to the membrane after receptor dissociation (something we now directly visualise at single-molecule level with a conformation-sensitive intrabody). This is an entirely new role for the finger loop and is likely to be important for future understandings of β-arrestin activity. This is because it provides a molecular mechanism to explain how arrestin can remain in an active conformation after transient receptor interactions, something that was not explained by previous studies.

Using a deconvolution of GPCR-arrestin interaction times, in addition to molecular dynamics simulations, we concluded that βArr2 interaction with GPCRs was transient, and that most βArr2 molecules arrive at CCPs by themselves, not in complex with bound GPCRs. Based on this, a sequence of events accompanying βArr2 signalling were deduced. The aim was to investigate the events that occur until β-arrestin reached CCPs or receptors. Indeed, arrestin could clearly be seen getting trapped and accumulating in CCPs, which is likely a consequence of cooperative interactions of βArr2 with AP2, clathrin, PIP2 and GPCRs, which also reached CCPs independently. Once accumulated in CCPs, it is easy to imagine how arrestin would efficiently move to endosomes, clustered together with receptors. It is highly plausible that additional mechanisms might be stabilising βArr-receptor complexes in CCPs and/or endosomes, which could provide a further body of work.

In conclusion, these findings were only made possible by the innovative single-molecule approach applied in living cells, which for the first time enabled the direct visualisation of

individual βArr2 molecules for their entire lifetime on the plasma membrane (from their translocation from the cytoplasm to trapping in CCPs). Importantly, this allowed direct dissection of the precise sequence of events involved in β-arrestin activation.

6.2 CRITIQUE OF THE SINGLE-MOLECULE STUDY

Despite extensive work by several world-leading groups, there are still major gaps in the current model of GPCR-β-arrestin interactions. This is not because there is anything wrong with previous measurements. This is because several fundamental aspects of the model cannot be investigated with ensemble measurements and rather require single-molecule approaches. Importantly, the central hypothesis that receptors and β-arrestin would form stable complexes on the plasma membrane of intact cells and diffuse together to CCPs pervades our understanding of GPCR interactions with signalling molecules. Additionally, this hypothesis is based on very indirect observations. There is, with current published knowledge, no direct measurement in the literature of the duration of such complexes at the plasma membrane of living cells.

In this study of GPCR-β-arrestin interactions, the fact that very transient interactions are seen does not contradict in any way previous results of ensemble measurements, as those only looked at changes in the equilibrium between β-arrestin in the cytoplasm or plasma membrane, and not at the underlying dynamics. Without contradicting previous results, these findings are of high importance because they reveal a much more dynamic picture than previously thought, and a key contribution of membrane pre-association, which simply could not be seen with previous approaches. Findings such as these show the power of single-molecule approaches, given that they can be used to directly visualise the proteins diffusing, though they are not

without fault. Careful consideration is needed in experiment design, imaging parameters and downstream computational analyses – so as not to misinterpret the observed results.

The interpretation of single-molecule data has been shown as often reliant on the expression levels of tested molecules [232,384]. It was therefore important to select cells which had similar epifluorescent background fluorescence when performing single-molecule experiments. This was particularly important when studying the β-arrestin mutants, where it was found that significantly less molecules were recruited to the plasma membrane. If cells were used which had varying levels of expression, this data may have been confounded. The disadvantage of this, of course, is that selecting cells of similar expression levels makes it difficult to identify imposed changes of mutants on cellular expression. It may be that excessive mutation of receptors or arrestins leads to aberrant expression of the proteins.

However, most of the downstream analyses used compared basal vs stimulated populations amongst receptor-mutant combinations. This included the confinement, interaction, and Markov chain analyses, which means that even if basal changes were present in protein expression or membrane activity, changes could still be detected, and aberrances could be accounted for when interrogated with ligands. This is particularly important for the for the results obtained for the ΔELA mutant, where no plasma membrane recruitment was observed, even after agonist stimulation. It should be noted that the ΔELA βArr2 is a harsh mutation of the arrestin C-edge, with 17 mutations of hydrophobic and polar residues aiming to perturb arrestin from the plasma membrane. Further experiments beyond epifluorescent confirmation of cellular expression, such as protein folding and in-depth structural analysis, would be required for this mutant to increase confident that the impaired recruitment and plasma membrane diffusion is specific and not a broader disruption.

Much of this study required quantification of the transitions between diffusing and confined states, with a major finding being that agonist increases the time trapped and co-trapped in CCPs for both receptor and arrestin. Additionally, through Markov chain analysis, it was found that co-diffusing molecules rarely transition to being co-trapped in CCPs, as the classical model predicts, instead arriving separately through some catalytic interaction. The accelerated transition between CCP trapping reflects the fact that receptors and βArr2 mainly reach CCPs separately. Receptors reaching CCPs where βArr2 is already present and vice-versa were commonly observed – suggesting that these sites are still as important in receptor and arrestin clustering, just via a route different than previously thought. Given that receptor labelling was ~90%, it can be confidently assumed that most arrestin molecules did reach CCPs alone.

Given the huge amount of highly quantitative data generated, careful consideration was needed when displaying data. For radar plots of Markov chain data, these only partially tell the story, given that they provide only information on state occupancy, but not transition frequency. The Markov chains themselves provide information on the changes in transition rates, but it is hard to clearly decipher which transitions are changing after ligand addition, since the mechanism driving the biology seems to be occurring in the same manner. Indeed, for all tested receptors, a near-identical pathway was observed in transition rates between Markov chain states, but with differences observed greatly in the number of the number of those states occurring, either before or after stimulation. For the history plots, where the states pre- and exceeding a state of interest, were concatenated – it was found that arrestin co-trapping in CCPs with receptors was often preceded by co-confined complexes outside CCPs which was mostly preceded by arrestin and receptor diffusing separately on the plasma membrane. Given that Markov chains do not

have a 'memory' of the prior states, but instead determine transitional probabilities for a given state, this data was only accessible on plotting a history of molecular interactions.

This is difficult to interpret and would require further study, but seems to suggest that CCP biogenesis may occur around GPCR-arrestin nanodomains on the plasma membrane. This is likely, since CCPs are intimately associated with cytoskeletal structures, which provide barriers to membrane protein diffusion and, as our group have previously shown, can contribute to accumulation of GPCRs and their partners in small nanodomains facilitating their interactions [253]. 4-colour imaging of receptors, arrestins, CCPs and actin could provide evidence for or against this hypothesis. Additionally, study of the signalling molecules crucial in the cascades mediating arrestin signalling would be beneficial to support this hypothesis, such as a single-molecule analysis of ERK, AP2 or other downstream effectors' diffusion and localisation – concomitant with GPCR and arrestin imaging.

It is interesting that previous studies have shown that a constitutively active arrestin mutant leads to constitutive accumulation in CCPs [315]. Moreover, a catalytic arrestin activation by β_1AR, which does not significantly accumulate in CCPs after stimulation has previously been shown to lead to arrestin accumulation in CCPs, inducing ERK1/2 activation independently of the activating receptor [315]. These results set a precedent for GPCR activation of arrestin to provide 'action at a distance', where transient interactions provide a memory for arrestin to signal elsewhere on the membrane. Here, it was found that the plasma membrane, albeit with low efficiency, drives arrestin into active-like conformations. This transition is catalysed by interaction with active, phosphorylated receptors – as shown by a lack of interactions with C-tail deficient receptors.

Previous studies have also shown that after dissociating from agonist-activated GPCRs, β-arrestins continue to interact with the plasma membrane, remain in an active conformation, and enter clathrin-coated structures without the receptor [324]. This study however adds to this by presenting a high-resolution description of the order of events, showing that the receptor also enters CCPs alone, rather than in complex with β-arrestins.

Single-molecule imaging of ERK and arrestin on the plasma membrane would be interesting, as GPCR-independent arrestin-ERK interactions would confirm the signalling capacity of these arrestin on the plasma membrane. This could be used to confirm whether the occupancy of CCPs by arrestin alone have any signalling differences from arrestins co-trapped with receptors; in the accumulation of ERK or other signalling molecules. The β-blocker, carvedilol, has been suggested as a β-arrestin biased ligand which is non-selective among adrenergic receptors [190,347].

Carvedilol has been shown to activate ERK whilst driving inverse agonism of Gαs-mediated cAMP signalling [385,386]. Additionally, carvedilol-stimulated adrenergic receptors have been associated with transactivation of the epidermal growth factor receptor (EGFR) by inducing ERK activation [56,126]. The mechanisms responsible for carvedilol's efficacy in the clinic, which has been shown as superior to that of other β-blockers [190,386], are not yet understood. Single-molecule imaging of Carvedilol with receptors and arrestins or G proteins would be fascinating, as it could help understand these findings, by observing the induction of nanoscale signalling patterns on GPCRs.

6.3 FUTURE DEVELOPMENT OF SINGLE-MOLECULE STUDIES

In Chapters 3 & 4 of this thesis, immortal cell lines were used to generate single-molecule datasets. This has the advantage of using cells which: replicate quickly, are tolerant of transduction with plasmid DNA, are clones of each other for means of reproducibility and form a well-tested cellular model in the scientific community for repetition of work. The disadvantages of using immortal cell lines are that they have chromosomal abnormalities that permit them to grow indefinitely. To call these cells 'human' still, is debatable. This raises questions as to whether they form a realistic representation of how cells in our bodies might react to external stimuli.

For single-molecule imaging, this raises the important question of whether emerging spatiotemporal landscapes found in our experiments are even seen in nature. With the hope of understanding GPCR signalling more thoroughly, so that their pathogenesis can be studied to find new modes of drug targeting in disease, this question needs to be answered. For example, is the nanoscale organisation of β-adrenergic receptors in CCPs with β-arrestin observed in cardiac myocytes, and do aberrations in this organisation impact disease pathology?

The foundations of answering this question were addressed in Chapter 5 of this thesis, which formed a large body of optimisation work to begin imaging primary cardiac myocytes with single-molecule precision. Endogenous cardiac myocyte receptors needed to be imaged, which required an alternate mode of receptor labelling. This was achieved using fluorescent ligands, which form the only method of endogenous receptor labelling that is unlikely to affect their natural diffusional behaviour whilst maintaining native pharmacology. Fluorescent antibodies to GPCRs do exist, though their efficacy is sometimes questionable. Their size can also preclude the binding of pharmacophores and make GPCRs significantly heavier, given that antibodies

outsize GPCRs in hundreds of kilodaltons. Targeting receptors with nanobodies provides an alternate approach, but these are thought to stabilise receptors in specific conformations, which precludes the study of inactive receptors. Utilising fluorescent ligands enables the investigation of the mechanism of drug action and modulation of GPCR signalling whilst also providing a strategy to label endogenous receptors. Fluorescent ligands also enable the direct visualisation of ligand-bound receptors, which provides the opportunity to directly attest to ligand-mediated control of the timing, duration, and location of receptor interactions.

After optimisation of labelling concentrations, wash times and confirming specificity, fluorescent ligands were used in this study to label adrenergic receptors in both immortal cells and cardiac myocytes. It was found that receptors were more immobile in cardiac myocytes hen compared to immortal cell lines. Propranolol (neutral antagonist) labelled receptors exhibited high levels of immobility in cardiac myocytes, with the inverse agonist ICI 118,551 displaying similar levels of immobility. In CHO cells, these two could be distinguished easily in terms of their effect on receptor diffusion. Co-staining myocytes with markers for t-tubules and cytoskeletal components would be an important next step, in determining the localisation of the already immobile receptors on the myocyte surface.

It would be interesting to test a fluorescent agonist in cardiac myocytes, to observe if further immobilisation and clustering is observed, or whether the cells are pre-primed in their nanodomain organisation on the membrane and intracellular changes are instead taking effect, with signalling proteins. Adenoviral vectors have seen some success in transduction of adult cardiac myocytes, so fluorescently tagged signalling proteins such as arrestins could be visualised, but overall, these cells are stress-insensitive and other models are likely more effective to study.

Further experiments using neonatal rat cardiac myocytes (NRCM), which are more amenable to transfection and have less specialised structures than adult cells, might be useful in studying receptor diffusion with signalling proteins. Fluorescent ligands could still be used to label endogenous receptors, with fluorescent G proteins or arrestins being transfected in, to study protein-protein interactions and diffusion. Additionally, disease models of cardiac myocytes could be tested with fluorescent agonists and antagonists, where chronic catecholamine stimulation has altered GPCR organisation and signalling capacity. In particular, NRCM hypertrophy is a well-established model and could be used to study the nanoscopic organisation of adrenergic receptors using β_1- and β_2- specific fluorescent antagonists. Studying normal and hypertrophic cardiac myocytes by single-molecule imaging could confirm or deny the still contentious topic, of whether β_2- specificity on t-tubules is lost in cardiac myocytes undergoing cardiac failure. A difficulty in studying these primary cell models is in the inter-cell variation present. These cells form a heterogenous population and large numbers of cells and experiments would be required to generate robust data, which requires the use of many animals.

Another approach to image receptor organisation in physiologically relevant cells, without the use of animal models, would be to use human induced pluripotent stem cells (iPSCs), which can be differentiated into cardiac myocyte lineages through specific growth with transcription factors from biopsies [387,388]. This would also have the advantage of manipulating the pluripotent cells with genetic mutations in proteins responsible for contributing to organisational defects in β-adrenergic cardiomyopathies, such as the myosin heavy chain (β/MYH7) or cardiac actin (ACTC1) [389]. Combining these cellular models under a single-molecule imaging framework,

would, for the first time provide a dynamic characterisation of the nanoscale organisation of β-adrenergic signalling in primary cardiac myocytes.

It is important to combine the single-molecule imaging with phenotypic, biochemical and structural studies to confirm their validity. Ensemble BRET measurement and pharmacological assays of G protein and β-arrestin activation/recruitment, cAMP production and ERK activation ensure that expected signalling outcomes are observed for the proteins, ligands and cells used [33,251,354]. These data can be correlated with measurements of downstream phenotypic effects that occur with the onset of heart failure, such as alterations in proliferation, apoptosis and cellular morphology. This would include evaluation of whether different ligands, such as carvedilol, induce specific patterns of ERK phosphorylation that have been linked to cardiac myocyte survival.

The use of emerging pharmacological tools described earlier, such as nanobodies, can be used to stabilise receptors and signalling proteins in specific conformations. These single-chain antigen binding proteins are based on fragments of camelid heavy-chain antibodies, can be made synthetically to bind a protein of interest and concurrently be used as an imaging sensor. A nanobody was used by Ghosh et al., which was found to stabilise β-arrestin in conformations which precluded CCP interactions and inhibited GPCR endocytosis, without affecting ERK activation [346,390]. This is interesting and fits with our model of β-arrestin, where dynamic activation of arrestin on the plasma membrane results in different nanodomains which can lead to GPCR internalisation or signalling.

Use of these nanobodies is of extreme interest for single-molecule studies, as they provide a novel framework for fine-tuning GPCR signalling by specifically inhibiting subsections of the signalling pathway. Other nanobodies that have been characterised by Arun Shukla's lab can

sterically interfere with G protein binding (Nb6B9: [347]) or can selectively stabilise receptor-G protein complexes (Nb37: [63]). It should be noted that in our hands, ScFv30, a nanobody which recognises active β-arrestin by binding to receptor-arrestin complexes, also binds to β-arrestin independent of receptors on the plasma membrane. This shows that these nanobodies have capabilities beyond their structural use as stabilisers/inhibitors of complex formation. Other nanobodies could be developed, such as those which could block the receptor C-tail interaction with arrestin, which was found in this study to be crucial in downstream accumulation in CCPs. This would enable recapitulation of the results obtained in this study with WT receptors that have been selectively inhibited in a specific interaction.

Another interesting experiment would be the use of Pepducins, which are cell-penetrating palmitoylated peptides derived from GPCR intracellular loops that are thought to bias GPCR signalling towards G protein or arrestin pathways [391]. These structures anchor the intracellular leaflet of the plasma membrane and target GPCR/signalling protein complexes via allosteric interactions. ICL3-9 transfection has been shown to bias endogenous β_2AR signalling towards G protein phenotypes [391], whilst ICL1-9 has been shown to selectively lead to activation of β-arrestin and promote cardiac myocyte contraction through arrestin pathways [183]. It would be interesting to determine whether these Pepducins lead to a shift in the equilibrium of GPCR-arrestin interaction duration and location in our single-molecule microscopy assay, and whether they are capable of biasing the formation of protein complexes in live cells on the nanoscale. Use of fluorescent Pepducins could also clarify their mechanism of action, as it is currently controversial on whether Pepducins directly bind to GPCRs or work fully allosterically, instead shifting the intracellular signalling protein landscape towards G protein or arrestin activation.

Together, the use of these pharmacological tools with primary cell models will allow the control of spatiotemporal features of GPCR signalling, to produce specific pharmacological effects and observe the diffusional and organisational changes they lead to. These outcomes can be observed in real-time and with high spatial precision, and could be used to help further develop and test conceptually new GPCR modulators that could ultimately be transferred to the clinic. These further studies are beyond the scope of this thesis, but will provide a deep mechanistic understanding that will be crucial to design new drugs that have the potential for improved efficacy and less side effects, capable of modulating GPCR signalling in ways not possible with the currently available FDA-approved drugs.

6.4 CONCLUSIONS

The introduction of single-molecule microscopy and other advanced optical methods are helping answer crucial and yet unresolved questions regarding the fundamental mechanisms that drive GPCR signalling in living cells. Current models reveal a complex scenario, in which receptors and signalling partners interact dynamically on the plasma membrane, with a similarly complex nanodomain organisation. This enables the generation of signals which are highly organised in space and time. Single-molecule microscopy of native proteins in live cells is in its infancy, but will likely have major contributions to understanding the mechanisms that drive pathological conditions, where the organised nature of the membrane is disrupted. Given that current models design drugs mostly on the premise of GPCRs acting as on/off switches, with agonist and antagonist potential – new models could instead generate novel drugs based on targeting GPCR activity in space and time.

Current approaches yield poor success rates with high economic burdens, largely due to the late-stage failure of clinical drugs in human studies. There is a need for a more rational drug development, which is based on completed models of signalling. This could enable the activation or inhibition of receptors in specific subcellular nanodomains or reversing nanoscale organisational changes imposed in diseases such as heart failure. The overall aim would be the design of new pharmacological approaches, which instead look towards targeting the complex activity of GPCRs and signalling proteins, through their diffusion and organisation on the membrane.

These methodologies will become more impactful as technical improvements are made, such as in the sensitivity of cameras/detectors, fluorophores with better photophysics and automation of large imaging datasets. Single-molecule microscopy generates large datasets, which are computationally heavy and time consuming. The generation of new modelling methods, based on deep learning approaches or artificial intelligence, will enable a faster extraction of quantitative information to help understand the biology. The days of single-molecule microscopy understandings of GPCR pharmacology are upon us, and we are looking forward to helping uncover the results, one molecule at a time [2].

7 REFERENCES

1 Theakston, E., Walker, C., O'Sullivan, M. & Rajagopal, V. Stochastic modelling of cardiac cell structure. *Annu Int Conf IEEE Eng Med Biol Soc* **2010**, 3257-3260, doi:10.1109/IEMBS.2010.5627229 (2010).

2 Calebiro, D. & Grimes, J. G Protein-Coupled Receptor Pharmacology at the Single-Molecule Level. *Annual review of pharmacology and toxicology* **60**, 73-87, doi:10.1146/annurev-pharmtox-010919-023348 (2020).

3 Pierce, K. L., Premont, R. T. & Lefkowitz, R. J. Seven-transmembrane receptors. *Nat Rev Mol Cell Biol* **3**, 639-650, doi:10.1038/nrm908 (2002).

4 Hauser, A. S., Attwood, M. M., Rask-Andersen, M., Schiöth, H. B. & Gloriam, D. E. Trends in GPCR drug discovery: new agents, targets and indications. *Nature Reviews Drug Discovery* **16**, 829, doi:10.1038/nrd.2017.178 (2017).

5 Sutherland, E. W. & Rall, T. W. Fractionation and characterization of a cyclic adenine ribonucleotide formed by tissue particles. *J Biol Chem* **232**, 1077-1091 (1958).

6 Weis, W. I. & Kobilka, B. K. The Molecular Basis of G Protein-Coupled Receptor Activation. *Annual review of biochemistry* **87**, 897-919, doi:10.1146/annurev-biochem-060614-033910 (2018).

7 Benovic, J. L. *et al.* Functional desensitization of the isolated beta-adrenergic receptor by the beta-adrenergic receptor kinase: potential role of an analog of the retinal protein arrestin (48-kDa protein). *Proc Natl Acad Sci U S A* **84**, 8879-8882 (1987).

8 Pitcher, J. A. *et al.* Role of beta gamma subunits of G proteins in targeting the beta-adrenergic receptor kinase to membrane-bound receptors. *Science* **257**, 1264-1267, doi:10.1126/science.1325672 (1992).

9 Shenoy, S. K. & Lefkowitz, R. J. beta-Arrestin-mediated receptor trafficking and signal transduction. *Trends Pharmacol Sci* **32**, 521-533, doi:10.1016/j.tips.2011.05.002 (2011).

10 Smith, J. S. & Rajagopal, S. The beta-Arrestins: Multifunctional Regulators of G Protein-coupled Receptors. *J Biol Chem* **291**, 8969-8977, doi:10.1074/jbc.R115.713313 (2016).

11 Peterson, Y. K. & Luttrell, L. M. The Diverse Roles of Arrestin Scaffolds in G Protein-Coupled Receptor Signaling. *Pharmacol Rev* **69**, 256-297, doi:10.1124/pr.116.013367 (2017).

12 Palczewski, K. *et al.* Crystal structure of rhodopsin: A G protein-coupled receptor. *Science* **289**, 739-745, doi:10.1126/science.289.5480.739 (2000).

13 Cherezov, V. *et al.* High-resolution crystal structure of an engineered human beta2-adrenergic G protein-coupled receptor. *Science* **318**, 1258-1265, doi:10.1126/science.1150577 (2007).

14 Rasmussen, S. G. *et al.* Crystal structure of the human beta2 adrenergic G-protein-coupled receptor. *Nature* **450**, 383-387, doi:10.1038/nature06325 (2007).

15 Yang, D. *et al.* G protein-coupled receptors: structure- and function-based drug discovery. *Signal Transduct Target Ther* **6**, 7, doi:10.1038/s41392-020-00435-w (2021).

16 Zhang, Y. *et al.* Cryo-EM structure of the activated GLP-1 receptor in complex with a G protein. *Nature* **546**, 248-253, doi:10.1038/nature22394 (2017).

17 Safdari, H. A., Pandey, S., Shukla, A. K. & Dutta, S. Illuminating GPCR Signaling by Cryo-EM. *Trends Cell Biol* **28**, 591-+, doi:10.1016/j.tcb.2018.06.002 (2018).

18 Kang, Y. *et al.* Cryo-EM structure of human rhodopsin bound to an inhibitory G protein.

Nature **558**, 553-558, doi:10.1038/s41586-018-0215-y (2018).

19 Lebon, G. *et al.* Agonist-bound adenosine A2A receptor structures reveal common features of GPCR activation. *Nature* **474**, 521-525, doi:10.1038/nature10136 (2011).

20 Rosenbaum, D. M. *et al.* Structure and function of an irreversible agonist-beta(2) adrenoceptor complex. *Nature* **469**, 236-240, doi:10.1038/nature09665 (2011).

21 Liang, Y. L. *et al.* Phase-plate cryo-EM structure of a class B GPCR-G-protein complex. *Nature* **546**, 118-123, doi:10.1038/nature22327 (2017).

22 Cao, C. *et al.* Structural basis for signal recognition and transduction by platelet-activating-factor receptor. *Nat Struct Mol Biol* **25**, 488-495, doi:10.1038/s41594-018-0068-y (2018).

23 Garcia-Nafria, J., Nehme, R., Edwards, P. C. & Tate, C. G. Cryo-EM structure of the serotonin 5-HT1B receptor coupled to heterotrimeric Go. *Nature* **558**, 620-623, doi:10.1038/s41586-018-0241-9 (2018).

24 Koehl, A. *et al.* Structure of the μ-opioid receptor–Gi protein complex. *Nature* **558**, 547-552, doi:10.1038/s41586-018-0219-7 (2018).

25 Liang, Y. L. *et al.* Cryo-EM structure of the active, Gs-protein complexed, human CGRP receptor. *Nature* **561**, 492-497, doi:10.1038/s41586-018-0535-y (2018).

26 Kang, Y. *et al.* Crystal structure of rhodopsin bound to arrestin by femtosecond X-ray laser. *Nature* **523**, 561-567, doi:10.1038/nature14656 (2015).

27 Cahill, T. J., 3rd *et al.* Distinct conformations of GPCR-beta-arrestin complexes mediate desensitization, signaling, and endocytosis. *Proc Natl Acad Sci U S A* **114**, 2562-2567, doi:10.1073/pnas.1701529114 (2017).

28 Manglik, A. & Kobilka, B. The role of protein dynamics in GPCR function: insights from the beta2AR and rhodopsin. *Curr Opin Cell Biol* **27**, 136-143, doi:10.1016/j.ceb.2014.01.008 (2014).

29 Manglik, A. *et al.* Structural Insights into the Dynamic Process of beta2-Adrenergic Receptor Signaling. *Cell* **161**, 1101-1111, doi:10.1016/j.cell.2015.04.043 (2015).

30 Latorraca, N. R., Venkatakrishnan, A. J. & Dror, R. O. GPCR Dynamics: Structures in Motion. *Chem Rev* **117**, 139-155, doi:10.1021/acs.chemrev.6b00177 (2017).

31 de Mendoza, A., Sebe-Pedros, A. & Ruiz-Trillo, I. The evolution of the GPCR signaling system in eukaryotes: modularity, conservation, and the transition to metazoan multicellularity. *Genome Biol Evol* **6**, 606-619, doi:10.1093/gbe/evu038 (2014).

32 Calebiro, D. & Maiellaro, I. cAMP signaling microdomains and their observation by optical methods. *Frontiers in cellular neuroscience* **8**, 350, doi:10.3389/fncel.2014.00350 (2014).

33 Maiellaro, I., Lohse, M. J., Kittel, R. J. & Calebiro, D. cAMP Signals in Drosophila Motor Neurons Are Confined to Single Synaptic Boutons. *Cell Rep* **17**, 1238-1246, doi:10.1016/j.celrep.2016.09.090 (2016).

34 Smith, J. S., Lefkowitz, R. J. & Rajagopal, S. Biased signalling: from simple switches to allosteric microprocessors. *Nature reviews. Drug discovery* **17**, 243-260, doi:10.1038/nrd.2017.229 (2018).

35 Wootten, D., Christopoulos, A., Marti-Solano, M., Babu, M. M. & Sexton, P. M. Mechanisms of signalling and biased agonism in G protein-coupled receptors. *Nat Rev Mol Cell Biol* **19**, 638-653, doi:10.1038/s41580-018-0049-3 (2018).

36 Kim, T. H. *et al.* The role of ligands on the equilibria between functional states of a G protein-coupled receptor. *J Am Chem Soc* **135**, 9465-9474, doi:10.1021/ja404305k (2013).

37 Basith, S. *et al.* Exploring G Protein-Coupled Receptors (GPCRs) Ligand Space via Cheminformatics Approaches: Impact on Rational Drug Design. *Front Pharmacol* **9**,

doi:ARTN 12810.3389/fphar.2018.00128 (2018).

38 Wingler, L. M. *et al.* Angiotensin Analogs with Divergent Bias Stabilize Distinct Receptor Conformations. *Cell* **176**, 468-478.e411, doi:10.1016/j.cell.2018.12.005 (2019).

39 Fredriksson, R., Lagerstrom, M. C., Lundin, L. G. & Schioth, H. B. The G-protein-coupled receptors in the human genome form five main families. Phylogenetic analysis, paralogon groups, and fingerprints. *Mol Pharmacol* **63**, 1256-1272, doi:10.1124/mol.63.6.1256 (2003).

40 Lander, E. S. *et al.* Initial sequencing and analysis of the human genome. *Nature* **409**, 860-921, doi:10.1038/35057062 (2001).

41 Venter, J. C. *et al.* The sequence of the human genome. *Science* **291**, 1304-1351, doi:10.1126/science.1058040 (2001).

42 Senoo, H., Sesaki, H. & Iijima, M. A GPCR Handles Bacterial Sensing in Chemotaxis and Phagocytosis. *Dev Cell* **36**, 354-356, doi:10.1016/j.devcel.2016.02.006 (2016).

43 Jaakola, V. P. *et al.* The 2.6 angstrom crystal structure of a human A2A adenosine receptor bound to an antagonist. *Science* **322**, 1211-1217, doi:10.1126/science.1164772 (2008).

44 Ichiyama, S. *et al.* The structure of the third intracellular loop of the muscarinic acetylcholine receptor M2 subtype. *FEBS Lett* **580**, 23-26, doi:10.1016/j.febslet.2005.11.042 (2006).

45 Shukla, A. K. *et al.* Structure of active beta-arrestin-1 bound to a G-protein-coupled receptor phosphopeptide. *Nature* **497**, 137-141, doi:10.1038/nature12120 (2013).

46 Ross, E. M. & Wilkie, T. M. GTPase-activating proteins for heterotrimeric G proteins: regulators of G protein signaling (RGS) and RGS-like proteins. *J Annual review of biochemistry* **69**, 795-827 (2000).

47 Wess, J. G-protein-coupled receptors: molecular mechanisms involved in receptor activation and selectivity of G-protein recognition. *FASEB J* **11**, 346-354 (1997).

48 Milligan, G. & Bouvier, M. Methods to monitor the quaternary structure of G protein-coupled receptors. *FEBS J* **272**, 2914-2925, doi:EJB4731 10.1111/j.1742-4658.2005.04731.x (2005).

49 Ross, E. M. & Gilman, A. G. Resolution of some components of adenylate cyclase necessary for catalytic activity. *J Biol Chem* **252**, 6966-6969 (1977).

50 Gilman, A. G. G proteins: transducers of receptor-generated signals. *Annual review of biochemistry* **56**, 615-649, doi:10.1146/annurev.bi.56.070187.003151 (1987).

51 Brust, T. F., Conley, J. M. & Watts, V. J. Gα(i/o)-coupled receptor-mediated sensitization of adenylyl cyclase: 40 years later. *Eur J Pharmacol* **763**, 223-232, doi:10.1016/j.ejphar.2015.05.014 (2015).

52 Syrovatkina, V., Alegre, K. O., Dey, R. & Huang, X. Y. Regulation, Signaling, and Physiological Functions of G-Proteins. *J Mol Biol* **428**, 3850-3868, doi:10.1016/j.jmb.2016.08.002 (2016).

53 Logothetis, D. E., Kurachi, Y., Galper, J., Neer, E. J. & Clapham, D. E. J. N. The βγ subunits of GTP-binding proteins activate the muscarinic K+ channel in heart. **325**, 321 (1987).

54 Haga, K. & Haga, T. Activation by G protein beta gamma subunits of agonist- or light-dependent phosphorylation of muscarinic acetylcholine receptors and rhodopsin. *J Biol Chem* **267**, 2222-2227 (1992).

55 Koch, W. J., Inglese, J., Stone, W. C. & Lefkowitz, R. J. The binding site for the beta gamma subunits of heterotrimeric G proteins on the beta-adrenergic receptor kinase. *J Biol Chem* **268**, 8256-8260 (1993).

56 Luttrell, L. M., Della Rocca, G. J., van Biesen, T., Luttrell, D. K. & Lefkowitz, R. J. Gbetagamma subunits mediate Src-dependent phosphorylation of the epidermal growth factor

receptor. A scaffold for G protein-coupled receptor-mediated Ras activation. *J Biol Chem* **272**, 4637-4644, doi:10.1074/jbc.272.7.4637 (1997).

57 Ikeda, S. Modulation of Ca2+ channels by G-protein beta gamma subunits. *Nature* **380**, 258-262 (1996).

58 Ikeda, S. R. Voltage-dependent modulation of N-type calcium channels by G-protein β γsubunits. *Nature* **380**, 255 (1996).

59 De Waard, M. *et al.* Direct binding of G-protein betagamma complex to voltage-dependent calcium channels. *Nature* **385**, 446-450, doi:10.1038/385446a0 (1997).

60 Camps, M. *et al.* Stimulation of phospholipase C by guanine-nucleotide-binding protein beta gamma subunits. *European journal of biochemistry* **206**, 821-831, doi:10.1111/j.1432-1033.1992.tb16990.x (1992).

61 De Lean, A., Stadel, J. M. & Lefkowitz, R. J. A ternary complex model explains the agonist-specific binding properties of the adenylate cyclase-coupled beta-adrenergic receptor. *J Biol Chem* **255**, 7108-7117 (1980).

62 Samama, P., Cotecchia, S., Costa, T. & Lefkowitz, R. J. A mutation-induced activated state of the beta 2-adrenergic receptor. Extending the ternary complex model. *J Biol Chem* **268**, 4625-4636 (1993).

63 Rasmussen, S. G. *et al.* Structure of a nanobody-stabilized active state of the beta(2) adrenoceptor. *Nature* **469**, 175-180, doi:10.1038/nature09648 (2011).

64 Rasmussen, S. G. *et al.* Crystal structure of the beta2 adrenergic receptor-Gs protein complex. *Nature* **477**, 549-555, doi:10.1038/nature10361 (2011).

65 Lohse, M. J., Maiellaro, I. & Calebiro, D. Kinetics and mechanism of G protein-coupled receptor activation. *Curr Opin Cell Biol* **27**, 87-93, doi:10.1016/j.ceb.2013.11.009 (2014).

66 Malik, R. U. *et al.* Detection of G protein-selective G protein-coupled receptor (GPCR) conformations in live cells. *J Biol Chem* **288**, 17167-17178, doi:10.1074/jbc.M113.464065 (2013).

67 Carlsson, A., Rasmussen, E. B. & Krist Jansen, P. The urinary excretion of adrenaline and noradrenaline by schizophrenic patients during reserpine treatment. *Journal of neurochemistry* **4**, 318-320, doi:10.1111/j.1471-4159.1959.tb13211.x (1959).

68 Carlsson, A. Detection and assay of dopamine. *Pharmacol Rev* **11**, 300-304 (1959).

69 Hsieh, A. C., Carlson, L. D. & Gray, G. Role of the sympathetic nervous system in the control of chemical regulation of heat production. *Am J Physiol* **190**, 247-251, doi:10.1152/ajplegacy.1957.190.2.247 (1957).

70 Lefkowitz, R. J., Caron, M. G. & Stiles, G. L. Mechanisms of membrane-receptor regulation. Biochemical, physiological, and clinical insights derived from studies of the adrenergic receptors. *N Engl J Med* **310**, 1570-1579, doi:10.1056/NEJM198406143102406 (1984).

71 Stiles, G. L., Caron, M. G. & Lefkowitz, R. J. Beta-adrenergic receptors: biochemical mechanisms of physiological regulation. *Physiol Rev* **64**, 661-743, doi:10.1152/physrev.1984.64.2.661 (1984).

72 Strosberg, A. D. Structure, function, and regulation of adrenergic receptors. *Protein Sci* **2**, 1198-1209, doi:10.1002/pro.5560020802 (1993).

73 Salazar, N. C., Chen, J. & Rockman, H. A. Cardiac GPCRs: GPCR signaling in healthy and failing hearts. *Biochim Biophys Acta* **1768**, 1006-1018, doi:10.1016/j.bbamem.2007.02.010 (2007).

74 Daaka, Y. *et al.* Essential role for G protein-coupled receptor endocytosis in the activation of mitogen-activated protein kinase. *J Biol Chem* **273**, 685-688 (1998).

75 Myagmar, B. E. *et al.* Adrenergic Receptors in Individual Ventricular Myocytes: The Beta-1 and Alpha-1B Are in All Cells, the Alpha-1A Is in a Subpopulation, and the Beta-2 and Beta-3 Are Mostly Absent. *Circ Res* **120**, 1103-1115, doi:10.1161/CIRCRESAHA.117.310520 (2017).

76 Rockman, H. A. *et al.* Control of myocardial contractile function by the level of beta-adrenergic receptor kinase 1 in gene-targeted mice. *J Biol Chem* **273**, 18180-18184, doi:10.1074/jbc.273.29.18180 (1998).

77 Rockman, H. A. *et al.* Expression of a beta-adrenergic receptor kinase 1 inhibitor prevents the development of myocardial failure in gene-targeted mice. *Proc Natl Acad Sci U S A* **95**, 7000-7005, doi:10.1073/pnas.95.12.7000 (1998).

78 Chesley, A. *et al.* The beta(2)-adrenergic receptor delivers an antiapoptotic signal to cardiac myocytes through G(i)-dependent coupling to phosphatidylinositol 3'-kinase. *Circ Res* **87**, 1172-1179, doi:10.1161/01.res.87.12.1172 (2000).

79 Communal, C., Singh, K., Sawyer, D. B. & Colucci, W. S. Opposing effects of beta(1)- and beta(2)-adrenergic receptors on cardiac myocyte apoptosis : role of a pertussis toxin-sensitive G protein. *Circulation* **100**, 2210-2212, doi:10.1161/01.cir.100.22.2210 (1999).

80 Hayato, R. *et al.* β3-Adrenergic activation of sequential Ca2+ release from mitochondria and the endoplasmic reticulum and the subsequent Ca2+ entry in rodent brown adipocytes. **49**, 400-414 (2011).

81 Spaethling, J. M. *et al.* Single-cell transcriptomics and functional target validation of brown adipocytes show their complex roles in metabolic homeostasis. *FASEB J* **30**, 81-92, doi:10.1096/fj.15-273797 (2016).

82 Braun, K., Oeckl, J., Westermeier, J., Li, Y. & Klingenspor, M. Non-adrenergic control of lipolysis and thermogenesis in adipose tissues. *J Exp Biol* **221**, doi:10.1242/jeb.165381 (2018).

83 Pfister, C. *et al.* Retinal S antigen identified as the 48K protein regulating light-dependent phosphodiesterase in rods. *Science* **228**, 891-893 (1985).

84 Wilden, U., Hall, S. W. & Kuhn, H. Phosphodiesterase activation by photoexcited rhodopsin is quenched when rhodopsin is phosphorylated and binds the intrinsic 48-kDa protein of rod outer segments. *Proc Natl Acad Sci U S A* **83**, 1174-1178 (1986).

85 Gurevich, E. V. & Gurevich, V. V. Arrestins: ubiquitous regulators of cellular signaling pathways. *Genome Biol* **7**, 236, doi:10.1186/gb-2006-7-9-236 (2006).

86 Kohout, T. A., Lin, F. S., Perry, S. J., Conner, D. A. & Lefkowitz, R. J. beta-Arrestin 1 and 2 differentially regulate heptahelical receptor signaling and trafficking. *Proc Natl Acad Sci U S A* **98**, 1601-1606, doi:10.1073/pnas.041608198 (2001).

87 Conner, D. A. *et al.* beta-Arrestin1 knockout mice appear normal but demonstrate altered cardiac responses to beta-adrenergic stimulation. *Circ Res* **81**, 1021-1026 (1997).

88 Bohn, L. M. *et al.* Enhanced morphine analgesia in mice lacking beta-arrestin 2. *Science* **286**, 2495-2498 (1999).

89 Xiao, K. *et al.* Functional specialization of beta-arrestin interactions revealed by proteomic analysis. *Proc Natl Acad Sci U S A* **104**, 12011-12016, doi:10.1073/pnas.0704849104 (2007).

90 Ferrandon, S. *et al.* Sustained cyclic AMP production by parathyroid hormone receptor endocytosis. *Nat Chem Biol* **5**, 734-742, doi:10.1038/nchembio.206 (2009).

91 Pitcher, J. A. *et al.* Feedback inhibition of G protein-coupled receptor kinase 2 (GRK2) activity by extracellular signal-regulated kinases. *J Biol Chem* **274**, 34531-34534 (1999).

92 Premont, R. T. *et al.* The GRK4 subfamily of G protein-coupled receptor kinases. Alternative splicing, gene organization, and sequence

conservation. *J Biol Chem* **274**, 29381-29389 (1999).

93 Penela, P., Ribas, C. & Mayor, F., Jr. Mechanisms of regulation of the expression and function of G protein-coupled receptor kinases. *Cell Signal* **15**, 973-981 (2003).

94 Lorenz, W. *et al.* The receptor kinase family: primary structure of rhodopsin kinase reveals similarities to the beta-adrenergic receptor kinase. *Proc Natl Acad Sci U S A* **88**, 8715-8719, doi:10.1073/pnas.88.19.8715 (1991).

95 Pitcher, J. A., Freedman, N. J. & Lefkowitz, R. J. G protein-coupled receptor kinases. *Annual review of biochemistry* **67**, 653-692, doi:10.1146/annurev.biochem.67.1.653 (1998).

96 Ferguson, S. S., Barak, L. S., Zhang, J. & Caron, M. G. G-protein-coupled receptor regulation: role of G-protein-coupled receptor kinases and arrestins. *Canadian journal of physiology and pharmacology* **74**, 1095-1110, doi:10.1139/cjpp-74-10-1095 (1996).

97 Yang, Z. *et al.* Phosphorylation of G Protein-Coupled Receptors: From the Barcode Hypothesis to the Flute Model. *Mol Pharmacol* **92**, 201-210, doi:10.1124/mol.116.107839 (2017).

98 Diviani, D. *et al.* Effect of different G protein-coupled receptor kinases on phosphorylation and desensitization of the alpha1B-adrenergic receptor. *J Biol Chem* **271**, 5049-5058, doi:10.1074/jbc.271.9.5049 (1996).

99 Goodman, O. B., Jr. *et al.* Beta-arrestin acts as a clathrin adaptor in endocytosis of the beta2-adrenergic receptor. *Nature* **383**, 447-450, doi:10.1038/383447a0 (1996).

100 Krupnick, J. G., Goodman, O. B., Jr., Keen, J. H. & Benovic, J. L. Arrestin/clathrin interaction. Localization of the clathrin binding domain of nonvisual arrestins to the carboxy terminus. *J Biol Chem* **272**, 15011-15016 (1997).

101 Laporte, S. A. *et al.* The beta2-adrenergic receptor/betaarrestin complex recruits the clathrin adaptor AP-2 during endocytosis. *Proc Natl Acad Sci U S A* **96**, 3712-3717, doi:10.1073/pnas.96.7.3712 (1999).

102 Laporte, S. A., Oakley, R. H., Holt, J. A., Barak, L. S. & Caron, M. G. The interaction of beta-arrestin with the AP-2 adaptor is required for the clustering of beta 2-adrenergic receptor into clathrin-coated pits. *J Biol Chem* **275**, 23120-23126, doi:10.1074/jbc.M002581200 (2000).

103 Gaidarov, I., Krupnick, J. G., Falck, J. R., Benovic, J. L. & Keen, J. H. Arrestin function in G protein-coupled receptor endocytosis requires phosphoinositide binding. *Embo j* **18**, 871-881, doi:10.1093/emboj/18.4.871 (1999).

104 Kang, D. S., Tian, X. & Benovic, J. L. Role of beta-arrestins and arrestin domain-containing proteins in G protein-coupled receptor trafficking. *Curr Opin Cell Biol* **27**, 63-71, doi:10.1016/j.ceb.2013.11.005 (2014).

105 Kang, Y. *et al.* A structural snapshot of the rhodopsin-arrestin complex. *FEBS J* **283**, 816-821, doi:10.1111/febs.13561 (2016).

106 Eichel, K., Jullie, D. & von Zastrow, M. beta-Arrestin drives MAP kinase signalling from clathrin-coated structures after GPCR dissociation. *Nat Cell Biol* **18**, 303-310, doi:10.1038/ncb3307 (2016).

107 Oakley, R. H., Laporte, S. A., Holt, J. A., Barak, L. S. & Caron, M. G. Association of beta-arrestin with G protein-coupled receptors during clathrin-mediated endocytosis dictates the profile of receptor resensitization. *J Biol Chem* **274**, 32248-32257, doi:10.1074/jbc.274.45.32248 (1999).

108 Oakley, R. H., Laporte, S. A., Holt, J. A., Caron, M. G. & Barak, L. S. Differential affinities of visual arrestin, beta arrestin1, and beta arrestin2 for G protein-coupled receptors delineate two major classes of receptors. *J Biol Chem* **275**, 17201-17210, doi:10.1074/jbc.M910348199 (2000).

109 Morris, K. L. *et al.* Cryo-EM of multiple cage architectures reveals a universal mode of clathrin self-assembly. *Nat Struct Mol Biol* **26**, 890-898, doi:10.1038/s41594-019-0292-0 (2019).

110 Beautrait, A. *et al.* A new inhibitor of the beta-arrestin/AP2 endocytic complex reveals interplay between GPCR internalization and signalling. *Nat Commun* **8**, 15054, doi:10.1038/ncomms15054 (2017).

111 Jean-Charles, P. Y., Kaur, S. & Shenoy, S. K. G Protein-Coupled Receptor Signaling Through beta-Arrestin-Dependent Mechanisms. *J Cardiovasc Pharmacol* **70**, 142-158, doi:10.1097/FJC.0000000000000482 (2017).

112 Yarar, D., Waterman-Storer, C. M. & Schmid, S. L. A dynamic actin cytoskeleton functions at multiple stages of clathrin-mediated endocytosis. *Mol Biol Cell* **16**, 964-975, doi:10.1091/mbc.e04-09-0774 (2005).

113 Loerke, D. *et al.* Cargo and dynamin regulate clathrin-coated pit maturation. *PLoS Biol* **7**, e57, doi:10.1371/journal.pbio.1000057 (2009).

114 Kaksonen, M., Toret, C. P. & Drubin, D. G. A modular design for the clathrin- and actin-mediated endocytosis machinery. *Cell* **123**, 305-320, doi:10.1016/j.cell.2005.09.024 (2005).

115 Lefkowitz, R. J., Rajagopal, K. & Whalen, E. J. New roles for beta-arrestins in cell signaling: not just for seven-transmembrane receptors. *Molecular cell* **24**, 643-652, doi:10.1016/j.molcel.2006.11.007 (2006).

116 Mayer, D. *et al.* Distinct G protein-coupled receptor phosphorylation motifs modulate arrestin affinity and activation and global conformation. *Nat Commun* **10**, 1261, doi:10.1038/s41467-019-09204-y (2019).

117 Shenoy, S. K. & Lefkowitz, R. J. Multifaceted roles of beta-arrestins in the regulation of seven-membrane-spanning receptor trafficking and signalling. *Biochem J* **375**, 503-515, doi:10.1042/BJ20031076 (2003).

118 Shenoy, S. K. *et al.* Ubiquitination of beta-arrestin links seven-transmembrane receptor endocytosis and ERK activation. *J Biol Chem* **282**, 29549-29562, doi:10.1074/jbc.M700852200 (2007).

119 Jung, S. R. *et al.* beta-arrestin-dependent PI(4,5)P2 synthesis boosts GPCR endocytosis. *Proc Natl Acad Sci U S A* **118**, doi:10.1073/pnas.2011023118 (2021).

120 Staus, D. P. *et al.* Structure of the M2 muscarinic receptor-beta-arrestin complex in a lipid nanodisc. *Nature* **579**, 297-302, doi:10.1038/s41586-020-1954-0 (2020).

121 Smith, J. S. *et al.* Noncanonical scaffolding of Galphai and beta-arrestin by G protein-coupled receptors. *Science* **371**, doi:10.1126/science.aay1833 (2021).

122 Huang, W. *et al.* Structure of the neurotensin receptor 1 in complex with beta-arrestin 1. *Nature* **579**, 303-308, doi:10.1038/s41586-020-1953-1 (2020).

123 Lally, C. C., Bauer, B., Selent, J. & Sommer, M. E. C-edge loops of arrestin function as a membrane anchor. *Nat Commun* **8**, 14258, doi:10.1038/ncomms14258 (2017).

124 Janetzko, J., Von Zastrow, M. & Kobilka, B. Membrane phosphoinositides stabilize GPCR-arrestin complexes and offer temporal control of complex assembly and dynamics. *FASEB J* (2022).

125 Della Rocca, G. J., Maudsley, S., Daaka, Y., Lefkowitz, R. J. & Luttrell, L. M. Pleiotropic coupling of G protein-coupled receptors to the mitogen-activated protein kinase cascade. Role of focal adhesions and receptor tyrosine kinases. *J Biol Chem* **274**, 13978-13984 (1999).

126 Luttrell, L. M. *et al.* Beta-arrestin-dependent formation of beta2 adrenergic receptor-Src protein kinase complexes. *Science* **283**, 655-661, doi:10.1126/science.283.5402.655 (1999).

127 Luttrell, L. M. *et al.* Activation and targeting of extracellular signal-regulated kinases by beta-arrestin scaffolds. *Proc Natl Acad Sci U S A* **98**, 2449-2454, doi:10.1073/pnas.041604898 (2001).

128 Tohgo, A., Pierce, K. L., Choy, E. W., Lefkowitz, R. J. & Luttrell, L. M. beta-Arrestin scaffolding of the ERK cascade enhances cytosolic ERK activity but

inhibits ERK-mediated transcription following angiotensin AT1a receptor stimulation. *J Biol Chem* **277**, 9429-9436, doi:10.1074/jbc.M106457200 (2002).

129 Wei, H. *et al.* Independent beta-arrestin 2 and G protein-mediated pathways for angiotensin II activation of extracellular signal-regulated kinases 1 and 2. *Proc Natl Acad Sci U S A* **100**, 10782-10787, doi:10.1073/pnas.1834556100 (2003).

130 DeFea, K. A. *et al.* beta-arrestin-dependent endocytosis of proteinase-activated receptor 2 is required for intracellular targeting of activated ERK1/2. *J Cell Biol* **148**, 1267-1281, doi:10.1083/jcb.148.6.1267 (2000).

131 Tohgo, A. *et al.* The stability of the G protein-coupled receptor-beta-arrestin interaction determines the mechanism and functional consequence of ERK activation. *J Biol Chem* **278**, 6258-6267, doi:10.1074/jbc.M212231200 (2003).

132 O'Hayre, M. *et al.* Genetic evidence that β-arrestins are dispensable for the initiation of β(2)-adrenergic receptor signaling to ERK. *Sci Signal* **10**, doi:10.1126/scisignal.aal3395 (2017).

133 Grundmann, M. *et al.* Lack of beta-arrestin signaling in the absence of active G proteins. *Nat Commun* **9**, 341, doi:10.1038/s41467-017-02661-3 (2018).

134 Goel, R., Phillips-Mason, P. J., Raben, D. M. & Baldassare, J. J. alpha-Thrombin induces rapid and sustained Akt phosphorylation by beta-arrestin1-dependent and -independent mechanisms, and only the sustained Akt phosphorylation is essential for G1 phase progression. *J Biol Chem* **277**, 18640-18648, doi:10.1074/jbc.M108995200 (2002).

135 Povsic, T. J., Kohout, T. A. & Lefkowitz, R. J. Beta-arrestin1 mediates insulin-like growth factor 1 (IGF-1) activation of phosphatidylinositol 3-kinase (PI3K) and anti-apoptosis. *J Biol Chem* **278**, 51334-51339, doi:10.1074/jbc.M309968200 (2003).

136 Li, H. *et al.* Chronic stress promotes lymphocyte reduction through TLR2 mediated PI3K signaling in a beta-arrestin 2 dependent manner. *J Neuroimmunol* **233**, 73-79, doi:10.1016/j.jneuroim.2010.11.015 (2011).

137 Scott, M. G. *et al.* Differential nucleocytoplasmic shuttling of beta-arrestins. Characterization of a leucine-rich nuclear export signal in beta-arrestin2. *J Biol Chem* **277**, 37693-37701, doi:10.1074/jbc.M207552200 (2002).

138 DeWire, S. M., Ahn, S., Lefkowitz, R. J. & Shenoy, S. K. Beta-arrestins and cell signaling. *Annu Rev Physiol* **69**, 483-510, doi:10.1146/annurev.ph.69.013107.100021 (2007).

139 Gurevich, V. V., Hanson, S. M., Song, X., Vishnivetskiy, S. A. & Gurevich, E. V. The functional cycle of visual arrestins in photoreceptor cells. *Prog Retin Eye Res* **30**, 405-430, doi:10.1016/j.preteyeres.2011.07.002 (2011).

140 Shukla, A. K. *et al.* Visualization of arrestin recruitment by a G-protein-coupled receptor. *Nature* **512**, 218-222, doi:10.1038/nature13430 (2014).

141 Latorraca, N. R. *et al.* Molecular mechanism of GPCR-mediated arrestin activation. *Nature* **557**, 452-456, doi:10.1038/s41586-018-0077-3 (2018).

142 Puthenveedu, M. A. & von Zastrow, M. Cargo regulates clathrin-coated pit dynamics. *Cell* **127**, 113-124, doi:10.1016/j.cell.2006.08.035 (2006).

143 Ying, Z. *et al.* Lipoic acid effects on established atherosclerosis. *Life Sci* **86**, 95-102, doi:10.1016/j.lfs.2009.11.009 (2010).

144 Richards, M. A. *et al.* Transverse tubules are a common feature in large mammalian atrial myocytes including human. *Am J Physiol Heart Circ Physiol* **301**, H1996-2005, doi:10.1152/ajpheart.00284.2011 (2011).

145 Sedarat, F., Xu, L., Moore, E. D. & Tibbits, G. F. Colocalization of dihydropyridine and ryanodine receptors in neonate rabbit heart using confocal microscopy. *Am J Physiol Heart Circ Physiol* **279**, H202-209, doi:10.1152/ajpheart.2000.279.1.H202 (2000).

146 Pinali, C., Bennett, H., Davenport, J. B., Trafford, A. W. & Kitmitto, A. Three-dimensional reconstruction of cardiac sarcoplasmic reticulum reveals a continuous network linking transverse-tubules: this organization is perturbed in heart failure. *Circ Res* **113**, 1219-1230, doi:10.1161/CIRCRESAHA.113.301348 (2013).

147 Jayasinghe, S. U. *et al.* Hypothalamo-pituitary adrenal axis and sympatho-adrenal medullary system responses to psychological stress were not attenuated in women with elevated physical fitness levels. *Endocrine* **51**, 369-379, doi:10.1007/s12020-015-0687-6 (2016).

148 Jayasinghe, V. R., Flores-Barrera, E., West, A. R. & Tseng, K. Y. Frequency-Dependent Corticostriatal Disinhibition Resulting from Chronic Dopamine Depletion: Role of Local Striatal cGMP and GABA-AR Signaling. *Cereb Cortex* **27**, 625-634, doi:10.1093/cercor/bhv241 (2017).

149 Sheard, T. M. D. *et al.* Three-Dimensional and Chemical Mapping of Intracellular Signaling Nanodomains in Health and Disease with Enhanced Expansion Microscopy. *ACS Nano* **13**, 2143-2157, doi:10.1021/acsnano.8b08742 (2019).

150 de Lucia, C., Eguchi, A. & Koch, W. J. New Insights in Cardiac beta-Adrenergic Signaling During Heart Failure and Aging. *Front Pharmacol* **9**, 904, doi:10.3389/fphar.2018.00904 (2018).

151 Rapundalo, S. T., Lathrop, D. A., Harrison, S. A., Beavo, J. A. & Schwartz, A. Cyclic AMP-dependent and cyclic AMP-independent actions of a novel cardiotonic agent, OPC-8212. *Naunyn Schmiedebergs Arch Pharmacol* **338**, 692-698, doi:10.1007/BF00165636 (1988).

152 Fabiato, A. & Fabiato, F. Effects of magnesium on contractile activation of skinned cardiac cells. *J Physiol* **249**, 497-517, doi:10.1113/jphysiol.1975.sp011027 (1975).

153 Fabiato, A. & Fabiato, F. Dependence of calcium release, tension generation and restoring forces on sarcomere length in skinned cardiac cells. *Eur J Cardiol* **4 Suppl**, 13-27 (1976).

154 MacLennan, D. H. & Kranias, E. G. Phospholamban: a crucial regulator of cardiac contractility. *Nat Rev Mol Cell Biol* **4**, 566-577, doi:10.1038/nrm1151 (2003).

155 MacLennan, D. H., Asahi, M. & Tupling, A. R. The regulation of SERCA-type pumps by phospholamban and sarcolipin. *Ann N Y Acad Sci* **986**, 472-480, doi:10.1111/j.1749-6632.2003.tb07231.x (2003).

156 Kuschel, M. *et al.* G(i) protein-mediated functional compartmentalization of cardiac beta(2)-adrenergic signaling. *J Biol Chem* **274**, 22048-22052, doi:10.1074/jbc.274.31.22048 (1999).

157 Kuschel, M. *et al.* beta2-adrenergic cAMP signaling is uncoupled from phosphorylation of cytoplasmic proteins in canine heart. *Circulation* **99**, 2458-2465, doi:10.1161/01.cir.99.18.2458 (1999).

158 Macdougall, D. A. *et al.* Caveolae compartmentalise beta2-adrenoceptor signals by curtailing cAMP production and maintaining phosphatase activity in the sarcoplasmic reticulum of the adult ventricular myocyte. *J Mol Cell Cardiol* **52**, 388-400, doi:10.1016/j.yjmcc.2011.06.014 (2012).

159 Wright, P. T. *et al.* Caveolin-3 regulates compartmentation of cardiomyocyte beta2-adrenergic receptor-mediated cAMP signaling. *J Mol Cell Cardiol* **67**, 38-48 (2014).

160 Agarwal, G. *et al.* Cardiovascular dysfunction and catecholamine cardiomyopathy in pheochromocytoma patients and their reversal following surgical cure: results of a prospective

case-control study. *Surgery* **150**, 1202-1211, doi:10.1016/j.surg.2011.09.001 (2011).

161 Agarwal, S. R. *et al.* Effects of cholesterol depletion on compartmentalized cAMP responses in adult cardiac myocytes. *J Mol Cell Cardiol* **50**, 500-509, doi:10.1016/j.yjmcc.2010.11.015 (2011).

162 Wypijewski, K. J. *et al.* Identification of caveolar resident proteins in ventricular myocytes using a quantitative proteomic approach: dynamic changes in caveolar composition following adrenoceptor activation. *Mol Cell Proteomics* **14**, 596-608, doi:10.1074/mcp.M114.038570 (2015).

163 Yao, Y. *et al.* The differential protein and lipid compositions of noncaveolar lipid microdomains and caveolae. *Cell Res* **19**, 497-506, doi:10.1038/cr.2009.27 (2009).

164 Kozera, L., White, E. & Calaghan, S. Caveolae act as membrane reserves which limit mechanosensitive I(Cl,swell) channel activation during swelling in the rat ventricular myocyte. *PLoS One* **4**, e8312, doi:10.1371/journal.pone.0008312 (2009).

165 Siddiqui, M. R. *et al.* Caveolin-1-eNOS signaling promotes p190RhoGAP-A nitration and endothelial permeability. *J Cell Biol* **193**, 841-850, doi:10.1083/jcb.201012129 (2011).

166 Hill, M. M. *et al.* PTRF-Cavin, a conserved cytoplasmic protein required for caveola formation and function. *Cell* **132**, 113-124, doi:10.1016/j.cell.2007.11.042 (2008).

167 Hill, M. M. *et al.* Co-regulation of cell polarization and migration by caveolar proteins PTRF/Cavin-1 and caveolin-1. *PLoS One* **7**, e43041, doi:10.1371/journal.pone.0043041 (2012).

168 Xiao, R. P., Cheng, H., Zhou, Y. Y., Kuschel, M. & Lakatta, E. G. Recent advances in cardiac beta(2)-adrenergic signal transduction. *Circ Res* **85**, 1092-1100, doi:10.1161/01.res.85.11.1092 (1999).

169 Xiao, R. P. Beta-adrenergic signaling in the heart: dual coupling of the beta2-adrenergic receptor to G(s) and G(i) proteins. *Sci STKE* **2001**, re15, doi:10.1126/stke.2001.104.re15 (2001).

170 Nikolaev, V. O. *et al.* Beta2-adrenergic receptor redistribution in heart failure changes cAMP compartmentation. *Science* **327**, 1653-1657, doi:science.1185988 10.1126/science.1185988 (2010).

171 Rybin, V. O., Xu, X., Lisanti, M. P. & Steinberg, S. F. Differential targeting of beta -adrenergic receptor subtypes and adenylyl cyclase to cardiomyocyte caveolae. A mechanism to functionally regulate the cAMP signaling pathway. *J Biol Chem* **275**, 41447-41457, doi:10.1074/jbc.M006951200 (2000).

172 Wright, P. T. *et al.* Partial Mechanical Unloading of the Heart Disrupts L-Type Calcium Channel and Beta-Adrenoceptor Signaling Microdomains. *Front Physiol* **9**, 1302, doi:10.3389/fphys.2018.01302 (2018).

173 Beavo, J. A. & Brunton, L. L. Cyclic nucleotide research -- still expanding after half a century. *Nat Rev Mol Cell Biol* **3**, 710-718, doi:10.1038/nrm911 (2002).

174 Shi, Q. *et al.* Heterologous desensitization of cardiac beta-adrenergic signal via hormone-induced betaAR/arrestin/PDE4 complexes. *Cardiovasc Res* **113**, 656-670, doi:10.1093/cvr/cvx036 (2017).

175 Zaccolo, M. & Pozzan, T. Discrete microdomains with high concentration of cAMP in stimulated rat neonatal cardiac myocytes. *Science* **295**, 1711-1715, doi:10.1126/science.1069982 (2002).

176 Zaccolo, M., Magalhaes, P. & Pozzan, T. Compartmentalisation of cAMP and Ca(2+) signals. *Curr Opin Cell Biol* **14**, 160-166, doi:10.1016/s0955-0674(02)00316-2 (2002).

177 Yang, P. C. *et al.* A Computational Modeling and Simulation Approach to Investigate Mechanisms of Subcellular cAMP Compartmentation. *PLoS*

Comput Biol **12**, e1005005, doi:10.1371/journal.pcbi.1005005 (2016).

178 Penela, P. *et al.* Mechanisms of regulation of G protein-coupled receptor kinases (GRKs) and cardiovascular disease. *Cardiovasc Res* **69**, 46-56, doi:10.1016/j.cardiores.2005.09.011 (2006).

179 Danner, S. & Lohse, M. J. Regulation of beta-adrenergic receptor responsiveness modulation of receptor gene expression. *Rev Physiol Biochem Pharmacol* **136**, 183-223, doi:10.1007/BFb0032325 (1999).

180 Lohse, M. J., Benovic, J. L., Caron, M. G. & Lefkowitz, R. J. Multiple pathways of rapid beta 2-adrenergic receptor desensitization. Delineation with specific inhibitors. *J Biol Chem* **265**, 3202-3211 (1990).

181 Lohse, M. J., Engelhardt, S. & Eschenhagen, T. What is the role of beta-adrenergic signaling in heart failure? *Circ Res* **93**, 896-906, doi:10.1161/01.RES.0000102042.83024.CA (2003).

182 Patel, P. A., Tilley, D. G. & Rockman, H. A. Beta-arrestin-mediated signaling in the heart. *Circ J* **72**, 1725-1729, doi:10.1253/circj.cj-08-0734 (2008).

183 Carr, R., 3rd *et al.* beta-arrestin-biased signaling through the beta2-adrenergic receptor promotes cardiomyocyte contraction. *Proc Natl Acad Sci U S A* **113**, E4107-4116, doi:10.1073/pnas.1606267113 (2016).

184 Wright, P. T. *et al.* Cardiomyocyte Membrane Structure and cAMP Compartmentation Produce Anatomical Variation in beta2AR-cAMP Responsiveness in Murine Hearts. *Cell Rep* **23**, 459-469, doi:10.1016/j.celrep.2018.03.053 (2018).

185 Groenewegen, A., Rutten, F. H., Mosterd, A. & Hoes, A. W. Epidemiology of heart failure. *Eur J Heart Fail* **22**, 1342-1356, doi:10.1002/ejhf.1858 (2020).

186 Triposkiadis, F. *et al.* The sympathetic nervous system in heart failure physiology, pathophysiology, and clinical implications. *Journal of the American College of Cardiology* **54**, 1747-1762, doi:10.1016/j.jacc.2009.05.015 (2009).

187 Ciccarelli, M., Santulli, G., Pascale, V., Trimarco, B. & Iaccarino, G. Adrenergic receptors and metabolism: role in development of cardiovascular disease. *Front Physiol* **4**, 265, doi:10.3389/fphys.2013.00265 (2013).

188 Soto, P. F. *et al.* Impact of aging on myocardial metabolic response to dobutamine. *Am J Physiol Heart Circ Physiol* **285**, H2158-2164, doi:10.1152/ajpheart.00086.2003 (2003).

189 Koitabashi, N. & Kass, D. A. Reverse remodeling in heart failure--mechanisms and therapeutic opportunities. *Nat Rev Cardiol* **9**, 147-157, doi:10.1038/nrcardio.2011.172 (2011).

190 Reiken, S. *et al.* Beta-blockers restore calcium release channel function and improve cardiac muscle performance in human heart failure. *Circulation* **107**, 2459-2466, doi:10.1161/01.CIR.0000068316.53218.49 (2003).

191 Jayasinghe, I. *et al.* Shining New Light on the Structural Determinants of Cardiac Couplon Function: Insights From Ten Years of Nanoscale Microscopy. *Front Physiol* **9**, 1472, doi:10.3389/fphys.2018.01472 (2018).

192 Jayasinghe, I. *et al.* True Molecular Scale Visualization of Variable Clustering Properties of Ryanodine Receptors. *Cell Rep* **22**, 557-567, doi:10.1016/j.celrep.2017.12.045 (2018).

193 Bristow, M. R. *et al.* Beta 1- and beta 2-adrenergic-receptor subpopulations in nonfailing and failing human ventricular myocardium: coupling of both receptor subtypes to muscle contraction and selective beta 1-receptor down-regulation in heart failure. *Circ Res* **59**, 297-309, doi:10.1161/01.res.59.3.297 (1986).

194 Bristow, M. R. & Ginsburg, R. Beta 2 receptors on myocardial cells in human ventricular

myocardium. *Am J Cardiol* **57**, 3F-6F, doi:10.1016/0002-9149(86)90880-5 (1986).

195 Bristow, M. R. *et al.* Decreased catecholamine sensitivity and beta-adrenergic-receptor density in failing human hearts. *N Engl J Med* **307**, 205-211, doi:10.1056/NEJM198207223070401 (1982).

196 Ungerer, M., Bohm, M., Elce, J. S., Erdmann, E. & Lohse, M. J. Altered expression of beta-adrenergic receptor kinase and beta 1-adrenergic receptors in the failing human heart. *Circulation* **87**, 454-463, doi:10.1161/01.cir.87.2.454 (1993).

197 Sarnago, S., Elorza, A. & Mayor, F., Jr. Agonist-dependent phosphorylation of the G protein-coupled receptor kinase 2 (GRK2) by Src tyrosine kinase. *J Biol Chem* **274**, 34411-34416, doi:10.1074/jbc.274.48.34411 (1999).

198 Gurevich, V. V. & Gurevich, E. V. Targeting arrestin interactions with its partners for therapeutic purposes. *Adv Protein Chem Struct Biol* **121**, 169-197, doi:10.1016/bs.apcsb.2019.11.011 (2020).

199 Koch, W. J. *et al.* Cardiac function in mice overexpressing the beta-adrenergic receptor kinase or a beta ARK inhibitor. *Science* **268**, 1350-1353, doi:10.1126/science.7761854 (1995).

200 Cannavo, A. *et al.* GRK2 as a therapeutic target for heart failure. *Expert Opin Ther Targets* **22**, 75-83, doi:10.1080/14728222.2018.1406925 (2018).

201 Rengo, G. *et al.* Reduction of lymphocyte G protein-coupled receptor kinase-2 (GRK2) after exercise training predicts survival in patients with heart failure. *Eur J Prev Cardiol* **21**, 4-11, doi:10.1177/2047487313491656 (2014).

202 Rengo, G. *et al.* Targeting the beta-adrenergic receptor system through G-protein-coupled receptor kinase 2: a new paradigm for therapy and prognostic evaluation in heart failure: from bench to bedside. *Circ Heart Fail* **5**, 385-391, doi:10.1161/CIRCHEARTFAILURE.112.966895 (2012).

203 Rengo, G., Lymperopoulos, A., Leosco, D. & Koch, W. J. GRK2 as a novel gene therapy target in heart failure. *J Mol Cell Cardiol* **50**, 785-792, doi:10.1016/j.yjmcc.2010.08.014 (2011).

204 Raake, P. W. *et al.* G protein-coupled receptor kinase 2 ablation in cardiac myocytes before or after myocardial infarction prevents heart failure. *Circ Res* **103**, 413-422, doi:10.1161/CIRCRESAHA.107.168336 (2008).

205 Madamanchi, A. Beta-adrenergic receptor signaling in cardiac function and heart failure. *Mcgill J Med* **10**, 99-104 (2007).

206 Seeland, U. *et al.* Interstitial remodeling in beta1-adrenergic receptor transgenic mice. *Basic Res Cardiol* **102**, 183-193, doi:10.1007/s00395-006-0635-y (2007).

207 Engelhardt, S., Hein, L., Wiesmann, F. & Lohse, M. J. Progressive hypertrophy and heart failure in beta1-adrenergic receptor transgenic mice. *Proc Natl Acad Sci U S A* **96**, 7059-7064, doi:10.1073/pnas.96.12.7059 (1999).

208 Tevaearai, H. T. *et al.* Myocardial gene transfer and overexpression of beta2-adrenergic receptors potentiates the functional recovery of unloaded failing hearts. *Circulation* **106**, 124-129, doi:10.1161/01.cir.0000020220.79105.fd (2002).

209 Eckhart, A. D., Ozaki, T., Tevaearai, H., Rockman, H. A. & Koch, W. J. Vascular-targeted overexpression of G protein-coupled receptor kinase-2 in transgenic mice attenuates beta-adrenergic receptor signaling and increases resting blood pressure. *Mol Pharmacol* **61**, 749-758, doi:10.1124/mol.61.4.749 (2002).

210 Du, X. J. *et al.* Age-dependent cardiomyopathy and heart failure phenotype in mice overexpressing beta(2)-adrenergic receptors in the heart. *Cardiovasc Res* **48**, 448-454, doi:10.1016/s0008-6363(00)00187-5 (2000).

211 Du, X. J., Vincan, E., Percy, E. & Woodcock, E. A. Enhanced negative chronotropy by inhibitory receptors in transgenic heart overexpressing

beta(2)-adrenoceptors. *J Auton Nerv Syst* **79**, 108-116, doi:10.1016/s0165-1838(00)00070-9 (2000).

212 Nguyen, M. N. *et al.* Spontaneous ventricular tachyarrhythmias in beta2-adrenoceptor transgenic mice in relation to cardiac interstitial fibrosis. *Am J Physiol Heart Circ Physiol* **309**, H946-957, doi:10.1152/ajpheart.00405.2015 (2015).

213 Black, J. W. Ahlquist and the development of beta-adrenoceptor antagonists. *Postgrad Med J* **52 Suppl 4**, 11-13 (1976).

214 Black, J. W. & Stephenson, J. S. Pharmacology of a new adrenergic beta-receptor-blocking compound (Nethalide). *Lancet* **2**, 311-314, doi:10.1016/s0140-6736(62)90103-4 (1962).

215 Wang, J., Gareri, C. & Rockman, H. A. G-Protein-Coupled Receptors in Heart Disease. *Circ Res* **123**, 716-735, doi:10.1161/CIRCRESAHA.118.311403 (2018).

216 Weber, P. C., Scherer, B., Siess, W., Held, E. & Schnermann, J. Possible significance of renal prostaglandins for renin release and blood pressure control. *Adv Prostaglandin Thromboxane Res* **7**, 1067-1077 (1980).

217 Kakoki, M. *et al.* Effects of hypertension, diabetes mellitus, and hypercholesterolemia on endothelin type B receptor-mediated nitric oxide release from rat kidney. *Circulation* **99**, 1242-1248, doi:10.1161/01.cir.99.9.1242 (1999).

218 Pal, P. K. Guidelines for management of essential tremor. *Ann Indian Acad Neurol* **14**, S25-28, doi:10.4103/0972-2327.83097 (2011).

219 Ostman-Smith, I. Beta-Blockers in Pediatric Hypertrophic Cardiomyopathies. *Rev Recent Clin Trials* **9**, 82-85, doi:10.2174/1574887109666140908125158 (2014).

220 Vogele, A. *et al.* Effectiveness and safety of beta blockers in the management of hypertension in older adults: a systematic review to help reduce inappropriate prescribing. *BMC Geriatr* **17**, 224, doi:10.1186/s12877-017-0575-4 (2017).

221 Thal, D. M. *et al.* Paroxetine is a direct inhibitor of g protein-coupled receptor kinase 2 and increases myocardial contractility. *ACS Chem Biol* **7**, 1830-1839, doi:10.1021/cb3003013 (2012).

222 Powell, J. M., Ebin, E., Borzak, S., Lymperopoulos, A. & Hennekens, C. H. Hypothesis: Paroxetine, a G Protein-Coupled Receptor Kinase 2 (GRK2) Inhibitor Reduces Morbidity and Mortality in Patients With Heart Failure. *J Cardiovasc Pharmacol Ther* **22**, 51-53, doi:10.1177/1074248416644350 (2017).

223 Waldschmidt, H. V. *et al.* Structure-Based Design of Highly Selective and Potent G Protein-Coupled Receptor Kinase 2 Inhibitors Based on Paroxetine. *J Med Chem* **60**, 3052-3069, doi:10.1021/acs.jmedchem.7b00112 (2017).

224 Salazar, N. C. *et al.* GRK2 blockade with betaARKct is essential for cardiac beta2-adrenergic receptor signaling towards increased contractility. *Cell Commun Signal* **11**, 64, doi:10.1186/1478-811X-11-64 (2013).

225 Sato, P. Y., Chuprun, J. K., Schwartz, M. & Koch, W. J. The evolving impact of g protein-coupled receptor kinases in cardiac health and disease. *Physiol Rev* **95**, 377-404, doi:10.1152/physrev.00015.2014 (2015).

226 Mozaffarian, D. Natural trans fat, dairy fat, partially hydrogenated oils, and cardiometabolic health: the Ludwigshafen Risk and Cardiovascular Health Study. *European heart journal* **37**, 1079-1081, doi:10.1093/eurheartj/ehv595 (2016).

227 Ladapo, J. A. *et al.* Changes in Medical Therapy and Lifestyle After Anatomical or Functional Testing for Coronary Artery Disease. *J Am Heart Assoc* **5**, doi:10.1161/JAHA.116.003807 (2016).

228 De Nunzio, C. *et al.* Metabolic abnormalities linked to an increased cardiovascular risk are associated with high-grade prostate cancer: a single biopsy cohort analysis. *Prostate Cancer*

Prostatic Dis **19**, 35-39, doi:10.1038/pcan.2015.45 (2016).

229 Matthews, K. A., Gump, B. B. & Owens, J. F. Chronic stress influences cardiovascular and neuroendocrine responses during acute stress and recovery, especially in men. *Health Psychol* **20**, 403-410 (2001).

230 Zimmermann, T., Rietdorf, J. & Pepperkok, R. Spectral imaging and its applications in live cell microscopy. *FEBS Lett* **546**, 87-92, doi:10.1016/s0014-5793(03)00521-0 (2003).

231 Eggeling, C. *et al.* Direct observation of the nanoscale dynamics of membrane lipids in a living cell. *Nature* **457**, 1159-1162, doi:10.1038/nature07596 (2009).

232 Eggeling, C., Widengren, J., Rigler, R. & Seidel, C. A. Photobleaching of Fluorescent Dyes under Conditions Used for Single-Molecule Detection: Evidence of Two-Step Photolysis. *Anal Chem* **70**, 2651-2659, doi:10.1021/ac980027p (1998).

233 Henderson, J. N., Ai, H. W., Campbell, R. E. & Remington, S. J. Structural basis for reversible photobleaching of a green fluorescent protein homologue. *Proc Natl Acad Sci U S A* **104**, 6672-6677, doi:10.1073/pnas.0700059104 (2007).

234 Betzig, E. *et al.* Imaging intracellular fluorescent proteins at nanometer resolution. *Science* **313**, 1642-1645, doi:10.1126/science.1127344 (2006).

235 Song, L., Hennink, E. J., Young, I. T. & Tanke, H. J. Photobleaching kinetics of fluorescein in quantitative fluorescence microscopy. *Biophys J* **68**, 2588-2600, doi:10.1016/S0006-3495(95)80442-X (1995).

236 Calebiro, D. & Koszegi, Z. The subcellular dynamics of GPCR signaling. *Mol Cell Endocrinol* **483**, 24-30, doi:10.1016/j.mce.2018.12.020 (2019).

237 Calebiro, D., Sungkaworn, T. & Maiellaro, I. Real-time monitoring of GPCR/cAMP signalling by FRET and single-molecule microscopy. *Hormone and metabolic research = Hormon- und Stoffwechselforschung = Hormones et metabolisme* **46**, 827-832, doi:10.1055/s-0034-1384523 (2014).

238 Lerner, E. *et al.* Toward dynamic structural biology: Two decades of single-molecule Forster resonance energy transfer. *Science* **359**, 288-+, doi:ARTN eaan113310.1126/science.aan1133 (2018).

239 Gales, C. *et al.* Real-time monitoring of receptor and G-protein interactions in living cells. *Nat Methods* **2**, 177-184, doi:10.1038/nmeth743 (2005).

240 Petrin, D., Robitaille, M. & Hebert, T. E. Real-time BRET assays to measure G protein/effector interactions. *Methods in molecular biology (Clifton, N.J.)* **756**, 245-261, doi:10.1007/978-1-61779-160-4_13 (2011).

241 Machleidt, T. *et al.* NanoBRET--A Novel BRET Platform for the Analysis of Protein-Protein Interactions. *ACS Chem Biol* **10**, 1797-1804, doi:10.1021/acschembio.5b00143 (2015).

242 Coulon, V. *et al.* Subcellular imaging of dynamic protein interactions by bioluminescence resonance energy transfer. *Biophys J* **94**, 1001-1009, doi:10.1529/biophysj.107.117275 (2008).

243 Albizu, L. *et al.* Time-resolved FRET between GPCR ligands reveals oligomers in native tissues. *Nat Chem Biol* **6**, 587-594, doi:10.1038/Nchembio.396 (2010).

244 Masuho, I., Martemyanov, K. A. & Lambert, N. A. Monitoring G Protein Activation in Cells with BRET. *Methods in molecular biology (Clifton, N.J.)* **1335**, 107-113, doi:10.1007/978-1-4939-2914-6_8 (2015).

245 Sun, S., Yang, X., Wang, Y. & Shen, X. J. I. j. o. m. s. In vivo analysis of protein–protein interactions with bioluminescence resonance energy transfer (BRET): progress and prospects. **17**, 1704 (2016).

246 Thomsen, A. R. B. *et al.* GPCR-G Protein-beta-Arrestin Super-Complex Mediates Sustained G

Protein Signaling. *Cell* **166**, 907-919, doi:10.1016/j.cell.2016.07.004 (2016).

247 Wan, Q. *et al.* Mini G protein probes for active G protein-coupled receptors (GPCRs) in live cells. *J Biol Chem* **293**, 7466-7473, doi:10.1074/jbc.RA118.001975 (2018).

248 Peach, C. J. *et al.* Real-Time Ligand Binding of Fluorescent VEGF-A Isoforms that Discriminate between VEGFR2 and NRP1 in Living Cells. *Cell Chem Biol* **25**, 1208-1218 e1205, doi:10.1016/j.chembiol.2018.06.012 (2018).

249 O'Brien, S. L. *et al.* BRET-based assay to monitor EGFR transactivation by the AT1R reveals Gq/11 protein-independent activation and AT1R-EGFR complexes. *Biochem Pharmacol* **158**, 232-242, doi:10.1016/j.bcp.2018.10.017 (2018).

250 Hill, R. *et al.* The novel mu-opioid receptor agonist PZM21 depresses respiration and induces tolerance to antinociception. *Br J Pharmacol* **175**, 2653-2661, doi:10.1111/bph.14224 (2018).

251 Calebiro, D. *et al.* Persistent cAMP-signals triggered by internalized G-protein-coupled receptors. *PLoS Biol* **7**, e1000172, doi:10.1371/journal.pbio.1000172 (2009).

252 Lohse, M. J., Nuber, S. & Hoffmann, C. Fluorescence/bioluminescence resonance energy transfer techniques to study G-protein-coupled receptor activation and signaling. *Pharmacol Rev* **64**, 299-336, doi:10.1124/pr.110.004309 (2012).

253 Sungkaworn, T. *et al.* Single-molecule imaging reveals receptor-G protein interactions at cell surface hot spots. *Nature* **550**, 543-547, doi:10.1038/nature24264 (2017).

254 Ha, T. *et al.* Probing the interaction between two single molecules: fluorescence resonance energy transfer between a single donor and a single acceptor. *Proc Natl Acad Sci U S A* **93**, 6264-6268, doi:10.1073/pnas.93.13.6264 (1996).

255 Roy, R., Hohng, S. & Ha, T. A practical guide to single-molecule FRET. *Nat Methods* **5**, 507-516, doi:10.1038/nmeth.1208 (2008).

256 Peleg, G., Ghanouni, P., Kobilka, B. K. & Zare, R. N. Single-molecule spectroscopy of the beta(2) adrenergic receptor: observation of conformational substates in a membrane protein. *Proc Natl Acad Sci U S A* **98**, 8469-8474, doi:10.1073/pnas.151239698 (2001).

257 Lamichhane, R. *et al.* Single-molecule view of basal activity and activation mechanisms of the G protein-coupled receptor beta2AR. *Proc Natl Acad Sci U S A* **112**, 14254-14259, doi:10.1073/pnas.1519626112 (2015).

258 Gregorio, G. G. *et al.* Single-molecule analysis of ligand efficacy in β2AR–G-protein activation. *Nature*, doi:10.1038/nature22354 (2017).

259 Jamshad, M. *et al.* G-protein coupled receptor solubilization and purification for biophysical analysis and functional studies, in the total absence of detergent. *Biosci Rep* **35**, doi:10.1042/BSR20140171 (2015).

260 Wheatley, M. *et al.* GPCR-styrene maleic acid lipid particles (GPCR-SMALPs): their nature and potential. *Biochem Soc Trans* **44**, 619-623, doi:10.1042/BST20150284 (2016).

261 Grime, R. L. *et al.* Single molecule binding of a ligand to a G-protein-coupled receptor in real time using fluorescence correlation spectroscopy, rendered possible by nano-encapsulation in styrene maleic acid lipid particles. *Nanoscale* **12**, 11518-11525, doi:10.1039/d0nr01060j (2020).

262 Routledge, S. J. *et al.* Ligand-induced conformational changes in a SMALP-encapsulated GPCR. *Biochim Biophys Acta Biomembr* **1862**, 183235, doi:10.1016/j.bbamem.2020.183235 (2020).

263 Hegener, O. *et al.* Dynamics of beta2-adrenergic receptor-ligand complexes on living cells. *Biochemistry* **43**, 6190-6199, doi:10.1021/bi035928t (2004).

264 Briddon, S. J., Kilpatrick, L. E. & Hill, S. J. Studying GPCR Pharmacology in Membrane Microdomains: Fluorescence Correlation Spectroscopy Comes of Age. *Trends Pharmacol Sci* **39**, 158-174, doi:10.1016/j.tips.2017.11.004 (2018).

265 Goulding, J. *et al.* The use of fluorescence correlation spectroscopy to monitor cell surface beta2-adrenoceptors at low expression levels in human embryonic stem cell-derived cardiomyocytes and fibroblasts. *FASEB J* **35**, e21398, doi:10.1096/fj.202002268R (2021).

266 Lanoiselee, Y. & Grebenkov, D. S. Unraveling intermittent features in single-particle trajectories by a local convex hull method. *Phys Rev E* **96**, 022144, doi:10.1103/PhysRevE.96.022144 (2017).

267 Calebiro, D. *et al.* Single-molecule analysis of fluorescently labeled G-protein-coupled receptors reveals complexes with distinct dynamics and organization. *Proc Natl Acad Sci U S A* **110**, 743-748, doi:10.1073/pnas.1205798110 (2013).

268 Hirschfeld, T. Optical microscopic observation of single small molecules. *Appl Opt* **15**, 2965-2966, doi:10.1364/AO.15.002965 (1976).

269 Moerner, W. E. & Kador, L. Optical detection and spectroscopy of single molecules in a solid. *Phys Rev Lett* **62**, 2535-2538, doi:10.1103/PhysRevLett.62.2535 (1989).

270 Walter, N. G., Huang, C. Y., Manzo, A. J. & Sobhy, M. A. Do-it-yourself guide: how to use the modern single-molecule toolkit. *Nat Methods* **5**, 475-489, doi:10.1038/nmeth.1215 (2008).

271 Keppler, A. *et al.* A general method for the covalent labeling of fusion proteins with small molecules in vivo. *Nat Biotechnol* **21**, 86-89, doi:10.1038/nbt765nbt765 (2003).

272 Gautier, A. *et al.* An engineered protein tag for multiprotein labeling in living cells. *Chemistry & biology* **15**, 128-136, doi:10.1016/j.chembiol.2008.01.007 (2008).

273 Klein, T. *et al.* Live-cell dSTORM with SNAP-tag fusion proteins. *Nat Methods* **8**, 7-9, doi:10.1038/nmeth0111-7b (2011).

274 Wolter, S. *et al.* rapidSTORM: accurate, fast open-source software for localization microscopy. *Nat Methods* **9**, 1040-1041, doi:10.1038/nmeth.2224 (2012).

275 Szalai, A. M. *et al.* A fluorescence nanoscopy marker for corticotropin-releasing hormone type 1 receptor: computer design, synthesis, signaling effects, super-resolved fluorescence imaging, and in situ affinity constant in cells. *Phys Chem Chem Phys* **20**, 29212-29220, doi:10.1039/c8cp06196c (2018).

276 Siddig, S. *et al.* Super-resolution imaging reveals the nanoscale organization of metabotropic glutamate receptors at presynaptic active zones. *Sci Adv* **6**, eaay7193, doi:10.1126/sciadv.aay7193 (2020).

277 Scarselli, M., Annibale, P. & Radenovic, A. Cell type-specific beta2-adrenergic receptor clusters identified using photoactivated localization microscopy are not lipid raft related, but depend on actin cytoskeleton integrity. *J Biol Chem* **287**, 16768-16780, doi:10.1074/jbc.M111.329912 (2012).

278 Rivolta, C. Airy disk diffraction pattern: comparison of some values of f/No. and obscuration ratio. *Appl Opt* **25**, 2404, doi:10.1364/ao.25.002404 (1986).

279 Sekar, R. B. & Periasamy, A. Fluorescence resonance energy transfer (FRET) microscopy imaging of live cell protein localizations. *J Cell Biol* **160**, 629-633, doi:10.1083/jcb.200210140 (2003).

280 Sezgin, E. *et al.* Polarity-Sensitive Probes for Superresolution Stimulated Emission Depletion Microscopy. *Biophys J* **113**, 1321-1330, doi:10.1016/j.bpj.2017.06.050 (2017).

281 Ambrose, E. J. A surface contact microscope for the study of cell movements. *Nature* **178**, 1194, doi:10.1038/1781194a0 (1956).

282 Axelrod, D. Cell-substrate contacts illuminated by total internal reflection fluorescence. *J Cell Biol* **89**, 141-145, doi:10.1083/jcb.89.1.141 (1981).

283 Jaqaman, K. *et al.* Robust single-particle tracking in live-cell time-lapse sequences. *Nat Methods* **5**, 695-702, doi:10.1038/nmeth.1237 (2008).

284 Murase, K. *et al.* Ultrafine membrane compartments for molecular diffusion as revealed by single molecule techniques. *Biophys J* **86**, 4075-4093, doi:10.1529/biophysj.103.035717 (2004).

285 Kusumi, A. *et al.* Paradigm shift of the plasma membrane concept from the two-dimensional continuum fluid to the partitioned fluid: high-speed single-molecule tracking of membrane molecules. *Annu Rev Biophys Biomol Struct* **34**, 351-378, doi:10.1146/annurev.biophys.34.040204.144637 (2005).

286 Kusumi, A., Suzuki, K. G., Kasai, R. S., Ritchie, K. & Fujiwara, T. K. Hierarchical mesoscale domain organization of the plasma membrane. *Trends Biochem Sci* **36**, 604-615, doi:10.1016/j.tibs.2011.08.001 (2011).

287 Suzuki, K., Ritchie, K., Kajikawa, E., Fujiwara, T. & Kusumi, A. Rapid hop diffusion of a G-protein-coupled receptor in the plasma membrane as revealed by single-molecule techniques. *Biophys J* **88**, 3659-3680, doi:10.1529/biophysj.104.048538 (2005).

288 Insel, P. A. *et al.* Compartmentation of G-protein-coupled receptors and their signalling components in lipid rafts and caveolae. *Biochem Soc Trans* **33**, 1131-1134, doi:10.1042/BST20051131 (2005).

289 Insel, P. A. *et al.* Caveolae and lipid rafts: G protein-coupled receptor signaling microdomains in cardiac myocytes. *Ann N Y Acad Sci* **1047**, 166-172, doi:10.1196/annals.1341.015 (2005).

290 Simons, K. & Ikonen, E. Functional rafts in cell membranes. *Nature* **387**, 569, doi:10.1038/42408 (1997).

291 Simons, K. & Toomre, D. Lipid rafts and signal transduction. *Nat Rev Mol Cell Biol* **1**, 31-39, doi:10.1038/35036052 (2000).

292 MacDougall, D. A. *et al.* Caveolae compartmentalise beta 2-adrenoceptor signals by curtailing cAMP production and maintaining phosphatase activity in the sarcoplasmic reticulum of the adult ventricular myocyte. *J Mol Cell Cardiol* **52**, 388-400 (2012).

293 Munro, S. Lipid Rafts. *Cell* **115**, 377-388, (2003).

294 Eggeling, C. Super-resolution optical microscopy of lipid plasma membrane dynamics. *Essays in biochemistry* **57**, 69-80, doi:10.1042/bse0570069 (2015).

295 Oksche, A. *et al.* Late endosomal/lysosomal targeting and lack of recycling of the ligand-occupied endothelin B receptor. *Mol Pharmacol* **57**, 1104-1113 (2000).

296 Shenoy, S. K. *et al.* beta-arrestin-dependent, G protein-independent ERK1/2 activation by the beta2 adrenergic receptor. *J Biol Chem* **281**, 1261-1273, doi:10.1074/jbc.M506576200 (2006).

297 Fu, Q. & Xiang, Y. K. Trafficking of beta-Adrenergic Receptors: Implications in Intracellular Receptor Signaling. *Progress in molecular biology and translational science* **132**, 151-188, doi:10.1016/bs.pmbts.2015.03.008 (2015).

298 Lanoiselee, Y. & Grebenkov, D. S. Revealing nonergodic dynamics in living cells from a single particle trajectory. *Phys Rev E* **93**, 052146, doi:10.1103/PhysRevE.93.052146 (2016).

299 Witzel, P. *et al.* Heterogeneities Shape Passive Intracellular Transport. *Biophys J* **117**, 203-213, doi:10.1016/j.bpj.2019.06.009 (2019).

300 Kusumi, A. *et al.* Membrane mechanisms for signal transduction: the coupling of the meso-scale raft domains to membrane-skeleton-

induced compartments and dynamic protein complexes. *Semin Cell Dev Biol* **23**, 126-144, doi:10.1016/j.semcdb.2012.01.018 (2012).

301 Michalet, X. Mean square displacement analysis of single-particle trajectories with localization error: Brownian motion in an isotropic medium. *Phys Rev E Stat Nonlin Soft Matter Phys* **82**, 041914, doi:10.1103/PhysRevE.82.041914 (2010).

302 Hern, J. A. *et al.* Formation and dissociation of M1 muscarinic receptor dimers seen by total internal reflection fluorescence imaging of single molecules. *Proc Natl Acad Sci U S A* **107**, 2693-2698, doi:0907915107 10.1073/pnas.0907915107 (2010).

303 Kasai, R. S. *et al.* Full characterization of GPCR monomer-dimer dynamic equilibrium by single molecule imaging. *J Cell Biol* **192**, 463-480, doi:jcb.201009128 10.1083/jcb.201009128 (2011).

304 Pin, J. P. *et al.* International Union of Basic and Clinical Pharmacology. LXVII. Recommendations for the recognition and nomenclature of G protein-coupled receptor heteromultimers. *Pharmacol Rev* **59**, 5-13, doi:10.1124/pr.59.1.5 (2007).

305 White, J. H. Heterodimerization is required for the formation of a functional GABAB receptor. *Nature* **396**, 679-682 (1998).

306 Pin, J. P., Kniazeff, J., Prézeau, L., Liu, J. F. & Rondard, P. GPCR interaction as a possible way for allosteric control between receptors. *Mol Cell Endocrinol* **486**, 89-95, doi:10.1016/j.mce.2019.02.019 (2019).

307 Tabor, A. *et al.* Visualization and ligand-induced modulation of dopamine receptor dimerization at the single molecule level. *Sci Rep* **6**, 33233, doi:10.1038/srep33233 (2016).

308 Kasai, R. S., Ito, S. V., Awane, R. M., Fujiwara, T. K. & Kusumi, A. The Class-A GPCR Dopamine D2 Receptor Forms Transient Dimers Stabilized by Agonists: Detection by Single-Molecule Tracking. *Cell Biochem Biophys* **76**, 29-37, doi:10.1007/s12013-017-0829-y (2018).

309 Irannejad, R. *et al.* Functional selectivity of GPCR-directed drug action through location bias. *Nat Chem Biol* **13**, 799-806, doi:10.1038/nchembio.2389 (2017).

310 Irannejad, R. *et al.* Conformational biosensors reveal GPCR signalling from endosomes. *Nature* **495**, 534-538, doi:10.1038/nature12000 (2013).

311 Kim, H. R. *et al.* Structural mechanism underlying primary and secondary coupling between GPCRs and the Gi/o family. *Nat Commun* **11**, 3160, doi:10.1038/s41467-020-16975-2 (2020).

312 Van Eps, N. *et al.* Gi- and Gs-coupled GPCRs show different modes of G-protein binding. *Proc Natl Acad Sci U S A* **115**, 2383-2388, doi:10.1073/pnas.1721896115 (2018).

313 Touhara, K. K. & MacKinnon, R. Molecular basis of signaling specificity between GIRK channels and GPCRs. *Elife* **7**, doi:10.7554/eLife.42908 (2018).

314 Hein, P., Frank, M., Hoffmann, C., Lohse, M. J. & Bünemann, M. Dynamics of receptor/G protein coupling in living cells. *EMBO J* **24**, 4106-4114, doi:7600870 [10.1038/sj.emboj.7600870 (2005).

315 Eichel, K. *et al.* Catalytic activation of beta-arrestin by GPCRs. *Nature* **557**, 381-386, doi:10.1038/s41586-018-0079-1 (2018).

316 Valentine, C. D. & Haggie, P. M. Confinement of beta(1)- and beta(2)-adrenergic receptors in the plasma membrane of cardiomyocyte-like H9c2 cells is mediated by selective interactions with PDZ domain and A-kinase anchoring proteins but not caveolae. *Mol Biol Cell* **22**, 2970-2982, doi:10.1091/mbc.E11-01-0034 (2011).

317 Bathe-Peters, M. *et al.* Visualization of beta-adrenergic receptor dynamics and differential localization in cardiomyocytes. *Proc Natl Acad Sci U S A* **118**, doi:10.1073/pnas.2101119118 (2021).

318 Nenasheva, T. A. *et al.* Abundance, distribution, mobility and oligomeric state of M(2) muscarinic acetylcholine receptors in live cardiac muscle. *J Mol Cell Cardiol* **57**, 129-136, doi:10.1016/j.yjmcc.2013.01.009 (2013).

319 Lohse, M. J., Benovic, J. L., Codina, J., Caron, M. G. & Lefkowitz, R. J. beta-Arrestin: a protein that regulates beta-adrenergic receptor function. *Science* **248**, 1547-1550, doi:10.1126/science.2163110 (1990).

320 Lane, J. R., May, L. T., Parton, R. G., Sexton, P. M. & Christopoulos, A. A kinetic view of GPCR allostery and biased agonism. *Nat Chem Biol* **13**, 929-937, doi:10.1038/nchembio.2431 (2017).

321 Calebiro, D. & Sungkaworn, T. Single-Molecule Imaging of GPCR Interactions. *Trends Pharmacol Sci* **39**, 109-122, doi:10.1016/j.tips.2017.10.010 (2018).

322 Alvarez-Curto, E. *et al.* Targeted Elimination of G Proteins and Arrestins Defines Their Specific Contributions to Both Intensity and Duration of G Protein-coupled Receptor Signaling. *J Biol Chem* **291**, 27147-27159, doi:10.1074/jbc.M116.754887 (2016).

323 Baker, J. G. *et al.* Synthesis and characterization of high-affinity 4,4-difluoro-4-bora-3a,4a-diaza-s-indacene-labeled fluorescent ligands for human beta-adrenoceptors. *J Med Chem* **54**, 6874-6887, doi:10.1021/jm2008562 (2011).

324 Nuber, S. *et al.* beta-Arrestin biosensors reveal a rapid, receptor-dependent activation/deactivation cycle. *Nature* **531**, 661-664, doi:10.1038/nature17198 (2016).

325 Kilpatrick, L. E. *et al.* Complex Formation between VEGFR2 and the beta2-Adrenoceptor. *Cell Chem Biol* **26**, 830-841 e839, doi:10.1016/j.chembiol.2019.02.014 (2019).

326 White, C. W., Vanyai, H. K., See, H. B., Johnstone, E. K. M. & Pfleger, K. D. G. Using nanoBRET and CRISPR/Cas9 to monitor proximity to a genome-edited protein in real-time. *Sci Rep* **7**, 3187, doi:10.1038/s41598-017-03486-2 (2017).

327 Cocucci, E., Aguet, F., Boulant, S. & Kirchhausen, T. The first five seconds in the life of a clathrin-coated pit. *Cell* **150**, 495-507, doi:10.1016/j.cell.2012.05.047 (2012).

328 Labun, K. *et al.* CHOPCHOP v3: expanding the CRISPR web toolbox beyond genome editing. *Nucleic Acids Res* **47**, W171-W174, doi:10.1093/nar/gkz365 (2019).

329 Ackers-Johnson, M. *et al.* A Simplified, Langendorff-Free Method for Concomitant Isolation of Viable Cardiac Myocytes and Nonmyocytes From the Adult Mouse Heart. *Circ Res* **119**, 909-920, doi:10.1161/CIRCRESAHA.116.309202 (2016).

330 Tsunoyama, T. A. *et al.* Super-long single-molecule tracking reveals dynamic-anchorage-induced integrin function. *Nat Chem Biol* **14**, 497-506, doi:10.1038/s41589-018-0032-5 (2018).

331 Gustafsson, N. *et al.* Fast live-cell conventional fluorophore nanoscopy with ImageJ through super-resolution radial fluctuations. *Nat Commun* **7**, 12471, doi:10.1038/ncomms12471 (2016).

332 Lanoiselee, Y., Moutal, N. & Grebenkov, D. S. Diffusion-limited reactions in dynamic heterogeneous media. *Nat Commun* **9**, 4398, doi:10.1038/s41467-018-06610-6 (2018).

333 Lanoiselee, Y., Grimes, J., Koszegi, Z. & Calebiro, D. Detecting Transient Trapping from a Single Trajectory: A Structural Approach. *Entropy (Basel)* **23**, doi:10.3390/e23081044 (2021).

334 Cherstvy, A. G., Thapa, S., Mardoukhi, Y., Chechkin, A. V. & Metzler, R. Time averages and their statistical variation for the Ornstein-Uhlenbeck process: Role of initial particle distributions and relaxation to stationarity. *Phys Rev E* **98**, 022134, doi:10.1103/PhysRevE.98.022134 (2018).

335 Cherstvy, A. G., Nagel, O., Beta, C. & Metzler, R. Non-Gaussianity, population heterogeneity, and transient superdiffusion in the spreading dynamics of amoeboid cells. *Phys Chem Chem*

Phys **20**, 23034-23054, doi:10.1039/c8cp04254c (2018).

336 Richardson, W. Bayesian-Based Iterative Method of Image Restoration. *Journal of the Optical Society of America* **vol. 62, issue 1, p.55** (1972).

337 Lucy, L. An iterative technique for the rectification of observed distributions. *Astronomical Journal* **Vol. 79, p. 745** (1974).

338 Fiser, A., Do, R. K. & Sali, A. Modeling of loops in protein structures. *Protein Sci* **9**, 1753-1773, doi:10.1110/ps.9.9.1753 (2000).

339 Sali, A. & Blundell, T. L. Comparative protein modelling by satisfaction of spatial restraints. *J Mol Biol* **234**, 779-815, doi:10.1006/jmbi.1993.1626 (1993).

340 Zhan, X., Gimenez, L. E., Gurevich, V. V. & Spiller, B. W. Crystal structure of arrestin-3 reveals the basis of the difference in receptor binding between two non-visual subtypes. *J Mol Biol* **406**, 467-478, doi:10.1016/j.jmb.2010.12.034 (2011).

341 Symons, J. L. *et al.* Lipidomic atlas of mammalian cell membranes reveals hierarchical variation induced by culture conditions, subcellular membranes, and cell lineages. *Soft Matter* **17**, 288-297, doi:10.1039/d0sm00404a (2021).

342 Dwivedi-Agnihotri, H. *et al.* Distinct phosphorylation sites in a prototypical GPCR differently orchestrate beta-arrestin interaction, trafficking, and signaling. *Sci Adv* **6**, doi:10.1126/sciadv.abb8368 (2020).

343 Grimm, J. B. *et al.* A general method to fine-tune fluorophores for live-cell and in vivo imaging. *Nat Methods* **14**, 987-994, doi:10.1038/nmeth.4403 (2017).

344 Shukla, A. K., Singh, G. & Ghosh, E. Emerging structural insights into biased GPCR signaling. *Trends Biochem Sci* **39**, 594-602, doi:10.1016/j.tibs.2014.10.001 (2014).

345 Shiina, T., Kawasaki, A., Nagao, T. & Kurose, H. Interaction with beta-arrestin determines the difference in internalization behavor between beta1- and beta2-adrenergic receptors. *J Biol Chem* **275**, 29082-29090, doi:10.1074/jbc.M909757199 (2000).

346 Kumari, P. *et al.* Core engagement with beta-arrestin is dispensable for agonist-induced vasopressin receptor endocytosis and ERK activation. *Mol Biol Cell* **28**, 1003-1010, doi:10.1091/mbc.E16-12-0818 (2017).

347 Kumari, P. *et al.* Functional competence of a partially engaged GPCR-beta-arrestin complex. *Nat Commun* **7**, 13416, doi:10.1038/ncomms13416 (2016).

348 Boltz, H. H. *et al.* The Impact of Membrane Protein Diffusion on GPCR Signaling. *Cells* **11**, doi:10.3390/cells11101660 (2022).

349 Lee, Y. *et al.* Molecular basis of beta-arrestin coupling to formoterol-bound beta1-adrenoceptor. *Nature* **583**, 862-866, doi:10.1038/s41586-020-2419-1 (2020).

350 Sente, A. *et al.* Molecular mechanism of modulating arrestin conformation by GPCR phosphorylation. *Nat Struct Mol Biol* **25**, 538-545, doi:10.1038/s41594-018-0071-3 (2018).

351 Nobles, K. N. *et al.* Distinct phosphorylation sites on the beta(2)-adrenergic receptor establish a barcode that encodes differential functions of beta-arrestin. *Sci Signal* **4**, ra51, doi:10.1126/scisignal.2001707 (2011).

352 Lorenz, K., Rosner, M. R., Brand, T. & Schmitt, J. P. Raf kinase inhibitor protein: lessons of a better way for beta-adrenergic receptor activation in the heart. *J Physiol* **595**, 4073-4087, doi:10.1113/JP274064 (2017).

353 Jung, S. R. & Hille, B. Optical approaches for visualization of arrestin binding to muscarinic receptor. *Methods Cell Biol* **149**, 1-18, doi:10.1016/bs.mcb.2017.11.001 (2019).

354 Godbole, A., Lyga, S., Lohse, M. J. & Calebiro, D. Internalized TSH receptors en route to the TGN induce local Gs-protein signaling and gene transcription. *Nat Commun* **8**, 443, doi:10.1038/s41467-017-00357-2 (2017).

355 Schobesberger, S. *et al.* T-tubule remodelling disturbs localized beta2-adrenergic signalling in rat ventricular myocytes during the progression of heart failure. *Cardiovasc Res* **113**, 770-782, doi:10.1093/cvr/cvx074 (2017).

356 Vernall, A. J. *et al.* Conversion of a non-selective adenosine receptor antagonist into A3-selective high affinity fluorescent probes using peptide-based linkers. *Org Biomol Chem* **11**, 5673-5682, doi:10.1039/c3ob41221k (2013).

357 Soave, M., Briddon, S. J., Hill, S. J. & Stoddart, L. A. Fluorescent ligands: Bringing light to emerging GPCR paradigms. *Br J Pharmacol* **177**, 978-991, doi:10.1111/bph.14953 (2020).

358 Soave, M., Stoddart, L. A., Brown, A., Woolard, J. & Hill, S. J. Use of a new proximity assay (NanoBRET) to investigate the ligand-binding characteristics of three fluorescent ligands to the human beta1-adrenoceptor expressed in HEK-293 cells. *Pharmacol Res Perspect* **4**, e00250, doi:10.1002/prp2.250 (2016).

359 Stoddart, L. A. *et al.* Development of novel fluorescent histamine H1-receptor antagonists to study ligand-binding kinetics in living cells. *Sci Rep* **8**, 1572, doi:10.1038/s41598-018-19714-2 (2018).

360 Guthrie, D. A. *et al.* Novel Fluorescent Ligands Enable Single-Molecule Localization Microscopy of the Dopamine Transporter. *ACS Chem Neurosci* **11**, 3288-3300, doi:10.1021/acschemneuro.0c00397 (2020).

361 Loudet, A. & Burgess, K. BODIPY dyes and their derivatives: syntheses and spectroscopic properties. *Chem Rev* **107**, 4891-4932, doi:10.1021/cr078381n (2007).

362 Beija, M., Afonso, C. A. & Martinho, J. M. Synthesis and applications of Rhodamine derivatives as fluorescent probes. *Chem Soc Rev* **38**, 2410-2433, doi:10.1039/b901612k (2009).

363 Zhang, X. F. & Feng, N. Attaching naphthalene derivatives onto BODIPY for generating excited triplet state and singlet oxygen: Tuning PET-based photosensitizer by electron donors. *Spectrochim Acta A Mol Biomol Spectrosc* **189**, 13-21, doi:10.1016/j.saa.2017.08.005 (2018).

364 Ji, Y. *et al.* A novel BODIPY-based fluorescent probe for selective detection of hydrogen sulfide in living cells and tissues. *Talanta* **181**, 104-111, doi:10.1016/j.talanta.2017.12.067 (2018).

365 Zhang, T., Zhang, W., Zheng, M. & Xie, Z. Near-infrared BODIPY-paclitaxel conjugates assembling organic nanoparticles for chemotherapy and bioimaging. *J Colloid Interface Sci* **514**, 584-591, doi:10.1016/j.jcis.2017.12.074 (2018).

366 Atlas, D., Melamed, E. & Lahav, M. beta-Adrenergic receptors in rat kidney: direct localization by a fluorescent beta-blocker. *Lab Invest* **36**, 465-468 (1977).

367 Melamed, E., Atlas, D. & Lahav, M. Direct evidence for absence of beta-adrenergic receptors in rat cerebral vessels histochemical study with a fluorescent beta-blocker. *Stroke* **8**, 261-263, doi:10.1161/01.str.8.2.261 (1977).

368 Rademaker, B., Kramer, K., van Ingen, H., Kranendonk, M. & Timmerman, H. Non-specific binding of the fluorescent beta-adrenergic receptor probe alprenolol-NBD. *J Recept Res* **5**, 121-131, doi:10.3109/10799898509041874 (1985).

369 Rademaker, B., Kramer, K., Bast, A. & Timmerman, H. Irreversible binding of the fluorescent beta-adrenoceptor probes alprenolol-NBD and pindolol-NBD to specific and non-specific binding sites. *Res Commun Chem Pathol Pharmacol* **60**, 147-159 (1988).

370 Ma, Z. *et al.* Discovery of the First Environment-Sensitive Near-Infrared (NIR) Fluorogenic Ligand for alpha1-Adrenergic Receptors Imaging in Vivo. *J Med Chem* **59**, 2151-2162, doi:10.1021/acs.jmedchem.5b01843 (2016).

371 Alcobia, D. C. *et al.* Visualizing Ligand Binding to a GPCR In Vivo Using NanoBRET. *iScience* **6**, 280-288, doi:10.1016/j.isci.2018.08.006 (2018).

372 Bilski, A. J., Halliday, S. E., Fitzgerald, J. D. & Wale, J. L. The pharmacology of a beta 2-selective adrenoceptor antagonist (ICI 118,551). *J Cardiovasc Pharmacol* **5**, 430-437, doi:10.1097/00005344-198305000-00013 (1983).

373 Bond, R. A. *et al.* Physiological effects of inverse agonists in transgenic mice with myocardial overexpression of the beta 2-adrenoceptor. *Nature* **374**, 272-276, doi:10.1038/374272a0 (1995).

374 Azzi, M. *et al.* Allosteric effects of G protein overexpression on the binding of beta-adrenergic ligands with distinct inverse efficacies. *Mol Pharmacol* **60**, 999-1007, doi:10.1124/mol.60.5.999 (2001).

375 Wacker, D. *et al.* Conserved binding mode of human beta2 adrenergic receptor inverse agonists and antagonist revealed by X-ray crystallography. *J Am Chem Soc* **132**, 11443-11445, doi:10.1021/ja105108q (2010).

376 Gong, H. *et al.* Specific beta(2)AR blocker ICI 118,551 actively decreases contraction through a G(i)-coupled form of the beta(2)AR in myocytes from failing human heart. *Circulation* **105**, 2497-2503, doi:10.1161/01.cir.0000017187.61348.95 (2002).

377 Goulding, J. *et al.* Subtype selective fluorescent ligands based on ICI 118,551 to study the human beta2-adrenoceptor in CRISPR/Cas9 genome-edited HEK293T cells at low expression levels. *Pharmacol Res Perspect* **9**, e00779, doi:10.1002/prp2.779 (2021).

378 Nikolaev, V. O., Bunemann, M., Schmitteckert, E., Lohse, M. J. & Engelhardt, S. Cyclic AMP imaging in adult cardiac myocytes reveals far-reaching beta1-adrenergic but locally confined beta2-adrenergic receptor-mediated signaling. *Circ Res* **99**, 1084-1091, doi:10.1161/01.RES.0000250046.69918.d5 (2006).

379 Plouffe, B., Thomsen, A. R. B. & Irannejad, R. Emerging Role of Compartmentalized G Protein-Coupled Receptor Signaling in the Cardiovascular Field. *ACS Pharmacol Transl Sci* **3**, 221-236, doi:10.1021/acsptsci.0c00006 (2020).

380 Ostrom, R. S., Post, S. R. & Insel, P. A. Stoichiometry and compartmentation in G protein-coupled receptor signaling: implications for therapeutic interventions involving G(s). *J Pharmacol Exp Ther* **294**, 407-412 (2000).

381 Ostrom, R. S., Violin, J. D., Coleman, S. & Insel, P. A. Selective enhancement of beta-adrenergic receptor signaling by overexpression of adenylyl cyclase type 6: colocalization of receptor and adenylyl cyclase in caveolae of cardiac myocytes. *Mol Pharmacol* **57**, 1075-1079 (2000).

382 Hatakeyama, H., Nakahata, Y., Yarimizu, H. & Kanzaki, M. J. M. b. o. t. c. Live-cell single-molecule labeling and analysis of myosin motors with quantum dots. **28**, 173-181 (2017).

383 Briddon, S. J., Kellam, B. & Hill, S. J. Design and use of fluorescent ligands to study ligand-receptor interactions in single living cells. *Methods in molecular biology (Clifton, N.J.)* **746**, 211-236, doi:10.1007/978-1-61779-126-0_11 (2011).

384 Gentzsch, C. *et al.* Selective and Wash-Resistant Fluorescent Dihydrocodeinone Derivatives Allow Single-Molecule Imaging of mu-Opioid Receptor Dimerization. *Angew Chem Int Ed Engl* **59**, 5958-5964, doi:10.1002/anie.201912683 (2020).

385 Wisler, J. W., Xiao, K., Thomsen, A. R. & Lefkowitz, R. J. Recent developments in biased agonism. *Curr Opin Cell Biol* **27**, 18-24, doi:10.1016/j.ceb.2013.10.008 (2014).

386 Wisler, J. W. *et al.* A unique mechanism of beta-blocker action: carvedilol stimulates beta-arrestin signaling. *Proc Natl Acad Sci U S A* **104**, 16657-16662, doi:10.1073/pnas.0707936104 (2007).

387 Kondrashov, A. *et al.* Simplified Footprint-Free Cas9/CRISPR Editing of Cardiac-Associated Genes in Human Pluripotent Stem Cells. *Stem*

Cells Dev **27**, 391-404, doi:10.1089/scd.2017.0268 (2018).

388 Denning, C. *et al.* Cardiomyocytes from human pluripotent stem cells: From laboratory curiosity to industrial biomedical platform. *Biochim Biophys Acta* **1863**, 1728-1748, doi:10.1016/j.bbamcr.2015.10.014 (2016).

389 Knollmann, B. C. *et al.* Familial hypertrophic cardiomyopathy-linked mutant troponin T causes stress-induced ventricular tachycardia and Ca2+-dependent action potential remodeling. *Circ Res* **92**, 428-436, doi:10.1161/01.RES.0000059562.91384.1A (2003).

390 Ghosh, E. *et al.* A synthetic intrabody-based selective and generic inhibitor of GPCR endocytosis. *Nat Nanotechnol* **12**, 1190-1198, doi:10.1038/nnano.2017.188 (2017).

391 Carr, R., 3rd *et al.* Development and characterization of pepducins as Gs-biased allosteric agonists. *J Biol Chem* **289**, 35668-35684, doi:10.1074/jbc.M114.618819 (2014).